UNIVERSITY OF SOUTHAMPTON

FACULTY OF ENGINEERING AND APPLIED SCIENCE

INSTITUTE OF SOUND AND VIBRATION RESEARCH

A STUDY OF THE PHYSICAL PROPERTIES OF MID-RANGE LOUDSPEAKER HORNS AND THEIR RELATIONSHIP TO PERCEIVED SOUND QUALITY

by

Keith Robert Holland

A dissertation submitted for the degree of
Doctor of Philosophy

1992

UNIVERSITY OF SOUTHAMPTON

ABSTRACT

FACULTY OF ENGINEERING AND APPLIED SCIENCE

INSTITUTE OF SOUND AND VIBRATION RESEARCH

Doctor of Philosophy

A STUDY OF THE PHYSICAL PROPERTIES OF MID-RANGE LOUDSPEAKER HORNS AND THEIR RELATIONSHIP TO PERCEIVED SOUND QUALITY

by Keith Robert Holland

The objective of this work is to establish relationships between the measurable physical properties and perceived sound quality of loudspeaker horns intended for use as the mid-frequency drive-units in studio monitor systems. It has often been reported that horn loudspeakers impart a colouration to reproduced sounds which allows them to be identified as horns. The physical properties of horns that are responsible for this characteristic sound are investigated via objective measurements and a subjective listening test.

The results of measurements on a variety of sample horns are compared to theoretical predictions based on mathematical models of idealised horn behaviour, and any departures from ideal behaviour are explained in terms of the physical construction of the horn flares. It is concluded that horns in which the acoustic field can be described in a one-parameter manner perform better than those whose behaviour departs from this ideal. Obstructions and discontinuities within or at the mouth of a horn flare are found to have undesirable effects on the performance of a horn for studio monitoring applications. In an investigation into nonlinear horn behaviour, it is concluded that nonlinear distortion is not responsible for any characteristic horn sound.

A study of the subjectively perceived similarity or otherwise, between horn and conventional direct-radiating loudspeakers is described. It is concluded from the results of this test and those of the objective measurements that reflections from the mouth discontinuity of horns greater than about 350mm in length are responsible for a characteristic horn sound, and that horns having lengths shorter than this tend not to sound like horns.

ACKNOWLEDGEMENTS

Official.

The research presented in this thesis was supported financially by Mr P. R. Newell and was carried out by the author at the Institute of Sound and Vibration Research (ISVR) under the supervision of Professor F. J. Fahy.

Personal.

I wish to thank Philip Newell for supporting this work, not only financially, but through innumerable hours of discussion, encouragement and hard work. I am particularly grateful to him for sharing his wealth of practical knowledge and experience in the field. Philip has since become a valued friend.

The task of supervising this work cannot have been an easy one! I am very grateful to Professor Frank Fahy for the guidance, inspiration and understanding which he has shown, during the research period and the subsequent writing of this thesis. I also wish to thank him for the contribution that he has made to the academic part of this work. I have enormous regard for his knowledge in the field of engineering acoustics and have learned a great deal from him.

I also owe thanks to Dr Christopher Morfey for supervision of the work on horn non-linearity and to Dr Ian Flindell for guidance concerning the listening test. Thanks also go to Dr Tonni Johansen for his cooperation and for planting the seeds of thought on axial symmetry.

The experimental parts of this work would not have been possible without the help of Dennis Howell. I wish to thank him, not only for the considerable technical support that he gave me, but also for endless patience while part of his laboratory was taken over!

I am also grateful to Tony Rogerson and Mike Tudor-Pole for help in the anechoic chamber, Dave Goldsworthy for making the prototype horns, Mike Bartlett for the construction of the impedance tube and Dave Edwards, Andy Giles and Simon Klitz for making life a lot easier while I was writing this.

Finally, I would like to express my gratitude to my parents for their kindness and support during this work, and especially to my girlfriend, Sharon, for her patience, understanding and encouragement; I dedicate this work to her.

CONTENTS

Chapter 6 The Listening Test

GLOSSARY OF TERMS

Relating to Loudspeaker Horns.

Area Profile. A graph of the cross-sectional area of a horn flare as a function of axial distance along the horn. The area profile may also refer to the area of curved wave-front surfaces within a horn flare.

Baffle. A flat, hard surface, assumed to be infinite in extent, in which the mouth of a horn may be mounted.

Driver. Electrodynamic transducer (usually moving-coil) for generating acoustic power at the throat of a horn.

Flare. The waveguide part of a horn with a cross-sectional area which expands with increasing distance along the horn.

Flare-rate. The rate of expansion of cross-sectional or wavefront area with increasing distance along a horn.

Lips. Curved extensions to the mouth of a horn flare beyond the baffle flange.

Mouth. The end of the horn having the largest cross-sectional area from which sound is radiated into the far-field.

Throat. The end of the horn having the smallest cross-sectional area to which the driver is attached.

Wave-front. A surface over which the phase of the acoustic pressure is uniform.

General.

Control Room. A room within a recording studio which houses the monitor loudspeaker system(s), mixing console and recording equipment.

Directivity. The pattern of sound radiation from a loudspeaker as a function of angle from the loudspeaker axis.

LIST OF SYMBOLS

A Amplitude of forward travelling wave.

a Impedance tube radius (m).

B Amplitude of backward travelling wave.

c_o Ambient speed of sound (m/s).

c_{ph} Phase speed (m/s).

f Frequency (Hz).

h Finite-difference model step-size (m).

k Acoustic free-field wave-number (m^{-1}).

l Finite-element model element length (m).

m Flare-rate (m^{-1}).

N Number of elements.

n Mode number.

P_o Ambient atmospheric pressure (N/m^2).

p Acoustic pressure (N/m^2).

q Acoustic volume velocity (m^3/s).

R_p Pressure reflection coefficient.

R Modulus of R_p.

R_T Non-dimensional throat resistance.

r Radial distance (m).

S Area (m^2).

T Pressure / pressure transfer function and distortion time advance (s).

t Time (s).

u Acoustic particle velocity (m/s).

X_T Non-dimensional throat reactance.

x Axial distance(m).

Z_T Non-dimensional throat impedance.

α Real part of R_p.

β Imaginary part of R_p.

γ Propagation coefficient and ratio of specific heats.

ϕ Phase of R_p.

ρ_o Ambient density of propagating medium (kg/m^3).

ξ Displacement (m).

ω Radial frequency.

The presence of a ^ over a variable shows that it represents a complex quantity.

Chapter 1
INTRODUCTION

1.1 BACKGROUND TO RESEARCH

The following thesis is the result of three years of research into various aspects of the measurable physical properties of mid-range loudspeaker horns for use in recording studio monitoring systems, and the relationship that these properties may have to perceived sound quality.

Modern recording studio practice can place high demands on a monitor loudspeaker system. Music is increasingly being created using electronic equipment, with the result that many musicians prefer to 'perform' in the control room rather than the studio, and use the monitor loudspeakers as an extension of their instruments. During multi-track recording sessions, instruments such as drums need to be reproduced individually at high levels to enable spurious noise from 'rattles' or 'squeaks' to be detected. The control rooms in which the monitors are housed can be very large and acoustically 'dead', requiring a large amount of acoustic power to generate sufficiently high sound levels. The loudspeakers therefore need to be capable of producing high acoustic power output but at the same time be robust and reliable; wasted recording studio time whilst loudspeaker diaphragms are replaced can be expensive. To allow a recording engineer to make valid judgements concerning a recording, it is desirable that the sound heard is a close analogue of the recording; thus as well as being powerful, a monitoring system also needs to be very 'accurate' over the entire audible frequency range. Figure 1.1 shows a view of the inside of a modern recording studio control room. The room is actually larger than it looks due to approximately 1m of acoustic treatment between the soft visible walls and ceiling and the hard outer walls.

A conventional 'direct-radiating' loudspeaker, consisting of a diaphragm, cone or dome mounted in a baffle, suffers from a poor radiation efficiency at frequencies where the acoustic wavelength greatly exceeds the length of the diaphragm perimeter. To overcome this problem the diaphragm must be large and if rigidity problems are to be avoided, heavy, resulting in a reduction in output at higher frequencies. This compromise between size and mass limits the bandwidth of a conventional loudspeaker drive-unit and sets an upper limit on electro-acoustic efficiency to a mere few percent. If a diaphragm could be made large enough for efficient radiation at low frequencies and light enough for high frequencies, severe directivity problems would be apparent at high frequencies due to interference between the sound radiated from different parts of the diaphragm. For the efficient

reproduction of the entire audible bandwidth, it is therefore necessary to divide the electrical input signal into different frequency bands using a set of filters known as a cross-over network; the low frequencies then being reproduced by loudspeaker drive-units with large diaphragms, and the high frequencies by loudspeaker drive-units with small diaphragms.

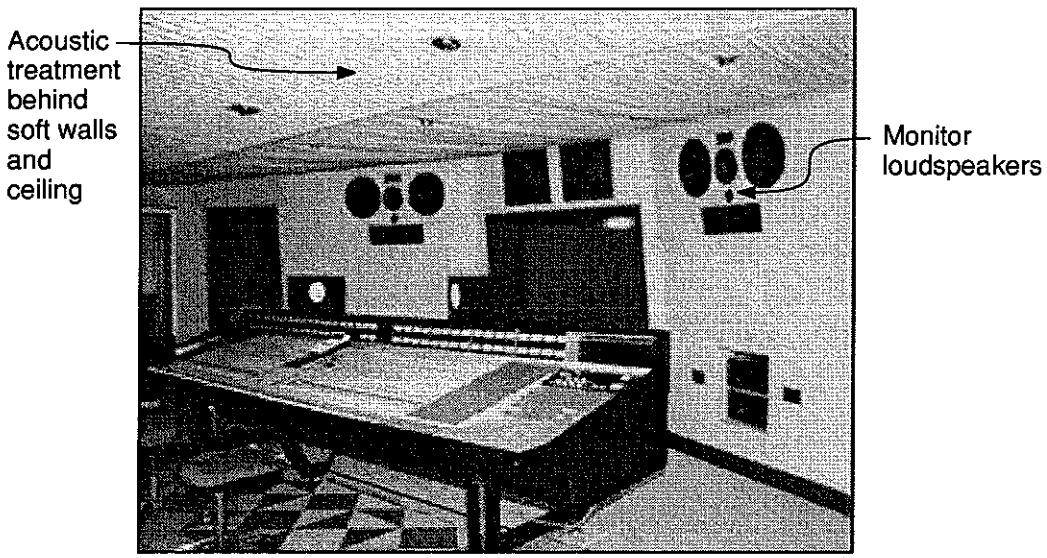

Figure 1.1 The control room of a modern recording studio.

Because of the inherent low electro-acoustic efficiency of conventional direct-radiating drive-units, the electrical inputs needed to reproduce the high sound levels required of a large monitor loudspeaker generate voice-coil temperatures beyond the capability of currently available materials, so more than one of each size of drive-unit is required in each loudspeaker. At low frequencies, the acoustic wavelengths are sufficiently large that the use of two or more diaphragms gives a useful increase in sound power output and interference between the sound radiated from the separate drive-units is not a problem, but at mid- and high frequencies, the interference causes directivity problems. These problems can be overcome by the use of horn loudspeakers for the reproduction of mid- and high frequencies.

Horn loudspeakers combine the high radiation efficiency of a large diaphragm with the low mass of a small diaphragm in a single unit. This is achieved by coupling a small diaphragm to a large radiating area via a gradually tapering flare. This arrangement can result in electro-acoustic efficiencies of ten to fifty percent and hence a sound power output capability from a single drive-unit in excess of the

requirements for studio monitoring. For the reproduction of low frequencies, multiple direct-radiating drive-units are used as effective low-frequency horns are prohibitively large. Figure 1.2 shows an example of a large studio monitor loudspeaker. The bandwidth is divided into four bands; the very low frequencies are reproduced by two fifteen inch diameter direct-radiating drive-units, the lower mid frequencies by a single ten inch direct-radiating drive-unit and the upper mid- and high frequencies by horn loudspeakers.

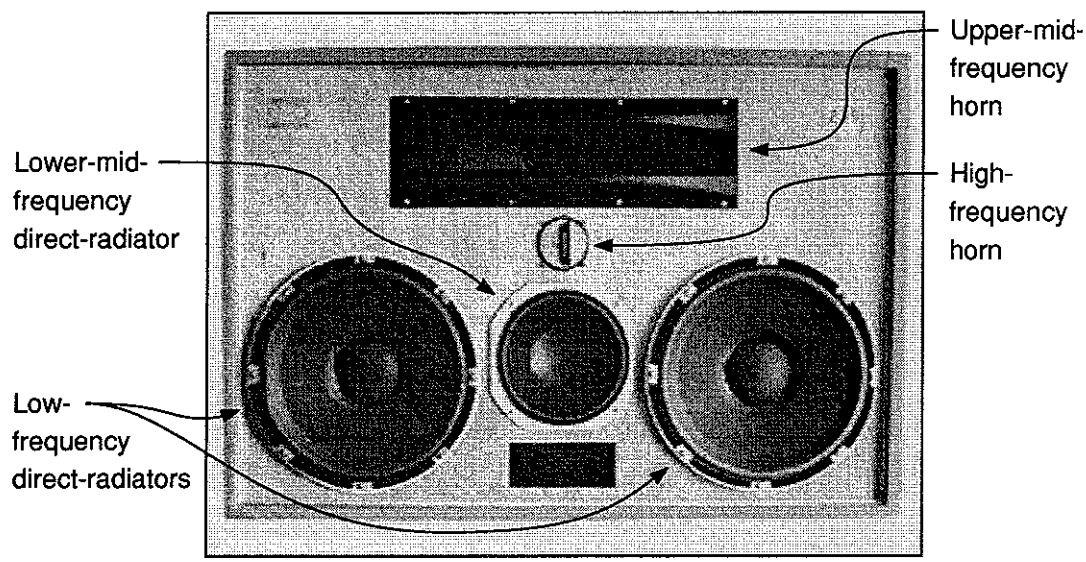

Figure 1.2 A Large Monitor Loudspeaker using a combination of Direct-Radiating Drive-Units and Horns.

Mid- and high-frequency horn loudspeakers have been used successfully in studio monitor systems for some time, particularly in the larger recording studios in the US. Opinions on the perceived sound quality of such systems are generally polarised on two extremes. On the one hand there are people for whom horn loudspeakers are capable of the very highest sound quality with an "immediacy" or "clarity" unobtainable with other systems. On the other hand there are people who actively dislike the reproduction of sound over horn loudspeakers and claim that horns have a characteristic sound, often described as "honky" or "quacky", which allows a horn to be identified as a horn by sound alone.

During the development of a range of studio monitor loudspeaker systems, Philip Newell quickly realised the limitations of conventional drive-units for mid- and high-frequency use in larger systems, and found that horn loudspeakers offered

the only realistic alternative [1]. The choice of high-frequency horn was not difficult as readily available units offered a quality of sound reproduction that appeared to be acceptable to most people, but a suitable mid-frequency horn proved more difficult to find. A thorough search of available mid-range horn units revealed a bewildering variety of shapes and sizes of horn flare, all seemingly designed to perform the same task. Newell acquired a number of different horns and mounted each one in turn in a monitor system and listened to the reproduction of a range of music and speech. It came as no surprise that as well as looking different, the horns all sounded different, even when attached to the same driver. Some of the horns were found to be capable of acceptably good sound reproduction whilst others added very distinct character to the sound. Newell was unable to find any published literature on the perceived sound quality of horn loudspeakers, and approached ISVR for answers to his questions.

1.2 A BRIEF HISTORY OF HORN ANALYSIS

A thorough literature study on the analysis of horns up to 1967 is contained in a paper by Eisner [2], in which over 200 references are listed. In the following, some of the important 'landmarks' in this history are outlined, along with some more recent developments. A bibliography of papers and books on various aspects of the analysis, design and use of acoustic horns is listed in chapter 9.

For centuries, horns of some form or another have been used to amplify the human voice and as terminations for musical instruments. These horns were designed more or less by 'trial and error' but some examples bear a remarkable similarity to modern designs. The history of theoretical horn development dates back to the eighteenth century when Bernoulli [3] and Lagrange [4] carried out theoretical studies of the vibration of tapered solid structures, but it was not until the beginning of this century that the analysis of acoustic horns began through interest in the development of the phonograph. At this time, Lord Rayleigh [5] and Webster [6] presented independent derivations of the so called 'Webster Horn Equation' and many papers have since been written on the application of this equation to acoustic horn analysis and design, with the most notable contributions made by Hall in 1932, Salmon in 1945 and Keele in 1973. Hall [7] discusses the assumptions made in the derivation of the horn equation and its use, and presents results of the measurement of the pressure field within conical and exponential horns. In [8], Salmon derives a reduced form of the

horn equation based on the conservation of energy, and shows the calculation of the admittance of a horn from details of the wall profile, and the calculation of the wall profile from a given admittance. In [9], he defines a 'family' of horn profiles ranging from conical through exponential to hyperbolic. Keele [10] shows that, by matching the radiation impedance at the mouth of a horn with the characteristic impedance within the flare, an optimum mouth size, and hence length, exists for minimum reflection from the mouth of a horn. More recently, Geddes [11] and [12] derives a form of the horn equation for horn profiles defined in the oblate spheroidal coordinate system. This form of horn profile allows "diffractionless" waves to propagate from a plane source at the horn throat to spherical waves at the mouth.

A complete analysis of the field within horns, taking into account higher modes of propagation, was presented by Stevenson [13] and [14] in 1951. Although the first paper is concerned primarily with electromagnetic waves, Stevenson points out in the second that the equations describing the field within acoustic horns are similar, but simpler than those for electromagnetic horns. The analysis results in an infinite set of simultaneous differential equations which describe the exact field within a horn as a set of coupled modes. In a paper written in 1974, Benade and Jansson [15] discuss the shape of the wave-fronts in flaring horns and compare the resonant behaviour of a "trombone-like" horn assuming the propagation of plane waves, with that assuming spherical waves. Comparison with experimental data shows that the 'true' wave-front shape lies "somewhere inbetween".

More recently, with the advent of more powerful and freely available computers, numerical methods have been used to aid the study of horn behaviour. In 1972, Alfredson [16] modelled a horn of arbitrary profile as a series of finite 'steps'; the modes of propagation either side of each step are matched and summed yielding an accurate representation of the field within, and the radiation from, an exponential horn. In two papers published in 1982, Morita et al [17] and [18] used the finite-element method to predict the field within a horn, with the mouth termination and radiation calculated analytically. In 1988 [19], 1989 [20], and 1991 [21], Johansen modelled the walls of a horn as a thin screen and used the integral equation method to yield accurate predictions of the sound field within the flare of the horn and that radiated into the far-field in a thorough study of the directivity properties of horns (see section 1.3).

1.3 SCOPE OF RESEARCH

The main objective of this research is to find relationships between the measurable physical properties and the subjectively perceived sound quality of horn loudspeakers. The results of the research can then be used as tools for the development of a mid-range loudspeaker for use in studio monitoring systems which possesses the high efficiency of current horn loudspeakers without the characteristic 'horn sound'. The term 'quality' here does not strictly refer to 'the pursuit of perfection', but is used to describe the particular 'sound' of a loudspeaker in much the same way as the word 'timbre' is used in music; although the former is perhaps the ultimate goal, being the absence of any 'quality'.

In order that this objective be approached, a large number of measurements have to be made of the physical properties of a wide variety of horn loudspeakers. In all, eighteen different horns were made available for detailed study and the sum of all of the measurements on all of the horns represents an enormous amount of data. To keep the size of this thesis down to practical (readable) limits, measurements are only presented for five horns that either possessed properties thought representative of the other horns in the range, or clearly demonstrated important aspects of design or performance. Despite this, much of the research project is concerned with the measurement of horns and the following chapters necessarily contain many measurement results.

In order that the measured results be interpreted, it is necessary to understand the physics of horn behaviour. To this end, chapter 2 is concerned with the development of 'simple' models of idealised horn behaviour, the results of which are compared to measurements in chapter 3 so that any differences can be attributed to departures from this idealised behaviour. This approach was preferred to the pursuit of an accurate horn model, such as the numerical models above, as these are essentially design tools which can be useful for parametric studies of horn behaviour, but do not give as much insight into the physics.

Chapter 4 is concerned with the departures from idealised behaviour found in chapter 3. In this chapter, the radiation of sound from the horn mouths into the far field is measured and discussed. During the project, the author was fortunate to collaborate with Dr. T. F. Johansen at the University of Trondheim, Norway. Dr. Johansen was developing a method for predicting the directivity properties of horns using

numerical techniques. His main interest lay in the development of controlled-directivity horns for public address applications, and our respective projects were arranged to complement each other rather than overlap to any great extent. Thus, the measurement and discussion of the directivity properties of horns in chapter 4 are limited to the effect that these may have on the performance of the horns in a studio monitoring environment. Unlike the case of horns intended for use in public address applications, the control of directivity is not a main requirement for horns intended for studio monitoring; the recording engineers are almost always in the optimum position (usually on-axis) and only hear the off-axis radiation via reflections. The rooms in which the monitors are used are usually fairly acoustically 'dead', but some reflection of the off-axis sound from the monitors will occur due to the necessary inclusion in the room of equipment, a mixing desk and a floor. The only directivity requirements for a studio monitor loudspeaker therefore, are that the on-axis sound 'covers' an angle of something like 60 degrees horizontally and 30 degrees vertically, and that any radiation outside these angles varies 'smoothly' with frequency so that any reflections are not unduly 'coloured'.

One criticism of the reproduction of sound by horn loudspeakers that is often cited is that the sounds changes in character as the level of reproduction is changed; comments such as "they sound hard when you turn them up" being typical. This property must be due to non-linear behaviour in the horn system, as the effect appears to be level dependent. Possible sources of non-linearity include the electro-mechanical / electro-magnetic 'motor' in the horn driver, and 'air overload' within the horn. As the former is common to all similar electro-magnetic loudspeakers, this property which is peculiar to horns must be due to the latter. In chapter 5, the non-linear behaviour of propagating waves within horn flares is studied with the development of a theoretical horn model that takes into account finite amplitude acoustic waves, along with experimental verification and some measurements of the harmonic distortion generated by horn loudspeakers.

Chapter 6 is concerned with the perceived sound quality of horns. To investigate which of the available horns have a characteristic horn sound and which do not, and to find the physical cause of this colouration, a listening test was set up in the large anechoic chamber at ISVR. The people taking part in the test were not asked to judge the reproduction of sound from the horns in any absolute sense, as all of the horns are mid-range units and thus have a limited bandwidth; instead, they were asked to judge which of four reference loudspeakers sounded most similar to the

loudspeaker under test. Twelve questionnaires were completed by twenty people for nine sounds reproduced by sixteen test loudspeakers, three of which are of the direct-radiating type and thirteen are horns. Statistical analysis is performed on the test results and on measurements of the on-axis frequency response of the loudspeakers. Conclusions are drawn from the results of these analyses and the physical properties of the loudspeakers.

The theoretical and measured physical properties of the horns and the results of the listening test are discussed in chapter 7.

1.4 TECHNICAL NOTES

Unless otherwise stated, all sound pressure measurements were taken using Brüel and Kjær half inch microphones type 4133 or 4134, connected via a Brüel and Kjær pre-amplifier type 2619 to a Brüel and Kjær power supply type 2804. Transfer function measurements were taken using a Solartron 1200 dual channel FFT analyser connected to a BBC B microcomputer via an IEEE standard interface.

All of the analysis contained herein uses, where appropriate, the harmonic time dependence vector represented by $e^{i\omega t}$.

Chapter 2
MODELLING ONE-PARAMETER BEHAVIOUR

2.1 INTRODUCTION.

Some of the work presented in this, and the following chapter has been published in references [22] and [23].

Webster's Horn Equation, which can be written (assuming that the sound speed and density remain constant along the length of the horn),

$$\frac{1}{c_o^2}\frac{\partial^2 \hat{p}}{\partial t^2} - \frac{\partial^2 \hat{p}}{\partial x^2} - \left\{\frac{1}{S}\frac{dS}{dx}\right\}\frac{\partial \hat{p}}{\partial x} = 0 \qquad (2.1)$$

where $\hat{p} = \hat{p}\ (x,t)$ is acoustic pressure and $S = S(x)$ is the cross-sectional area of the horn, describes the quasi-one-dimensional sound field in a duct which has a cross-sectional area that varies along its length ($S(x)$ will herein be called the 'area profile' of the horn; it can refer to the area of curved wave-front surfaces within a horn - see section 2.4). Analytic solutions of this equation exist for only a few area profiles (see Morse [24]), so the equation can only be used in the design or analysis of horns with area profiles that take one of these forms. The multiplying factor in the right-most term in equation (2.1), represents the ratio of the rate of change of area with distance to the area and is termed the flare-rate ($m(x)$) of the horn. If a value of zero is substituted for the flare-rate, equation (2.1) becomes the one-dimensional wave equation for plane waves; a waveguide supporting these has, by definition, zero flare. The next simplest solution of equation (2.1) results from the substitution of an exponential area profile, as the flare-rate is then constant along the length of the horn. A horn possessing an exponential area profile (an exponential horn) can then be defined as $S(x) = S(0)e^{mx}$, where $S(0)$ is the area of the throat and m the flare-rate of the horn. Appendix 1 shows a derivation of Webster's Horn Equation, and its solution for an exponential area profile. An exponential horn has the most desirable properties for loudspeaker horns, as a high radiation efficiency is maintained down to a low frequency (see Olson [25]), so many horn loudspeaker designs have taken this form. In using this equation for the design of an exponential horn, the flare rate can be decided from consideration of the lowest frequency to be generated and the mouth size can be optimised for maximum coupling to the free field and minimum reflection of the sound back down the flare.

Most of the horns mentioned in section 1.1 are designed using this equation, with an exponential area profile and broadly similar compromises between overall size, frequency range and mouth area. So why are there such wide differences in

appearance? The reason is the one-dimensional nature of the equation, requiring only the area profile to be defined, leaving the cross sectional shape of the horn to the imagination of the designer. It should be noted here that the area profile can refer to the area of curved surfaces within a horn.

Horn loudspeakers are used extensively in large-scale sound reproduction applications, such as public address and larger cinemas. The reason for their wide-spread use is that as well as being more efficient than conventional loudspeakers, horns have more clearly defined and controllable directivity properties allowing the sound to be 'pointed' only where it is needed. Often it is desirable to have different horizontal and vertical directivity patterns, so horns can be arranged in clusters with different array properties along the two different axis; alternatively, the mouth of a single horn can be shaped to the same effect. The former method, by driving the cluster from a single drive unit is used in 'multicellular' designs (figure 2.1).

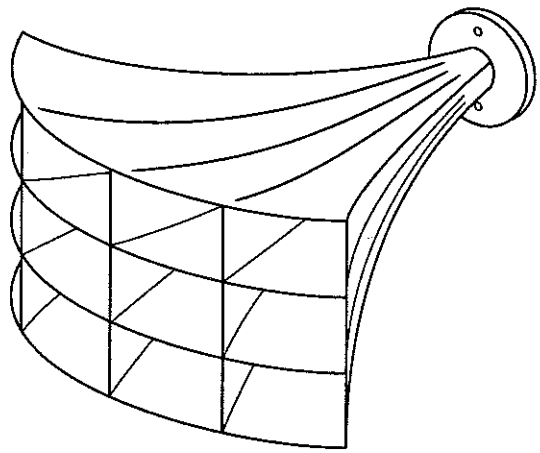

Figure 2.1 A Multicellular Horn

Some horns have a flare in both directions and are referred to as 'exponential' horns (figure 2.2). Others require very tight directivity constraints along one axis and have two straight sides set to the required directivity angle, with the other two contoured to maintain a desirable area profile. These are referred to as 'sectoral' or 'radial' horns (figure2.3). Recently a new family of rectangular horn has been developed whereby the directivity is optimised along both axis at the expense of some efficiency at low frequencies. This is achieved by constructing the flare from a number of short straight sided sections with rapid and slow flare alternating in the two axis (see Keele [26] and Long [27]). These horns are referred to as 'constant directivity' horns (figure 2.4).

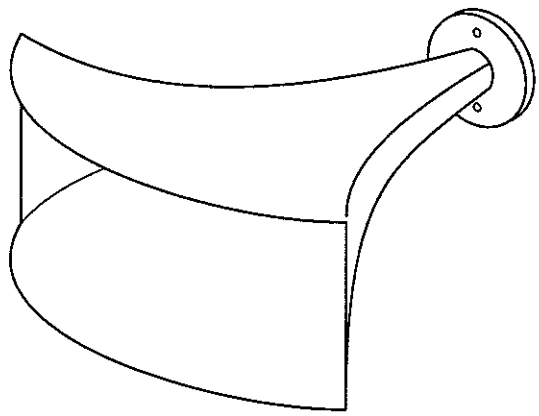

Figure 2.2 An Exponential Horn

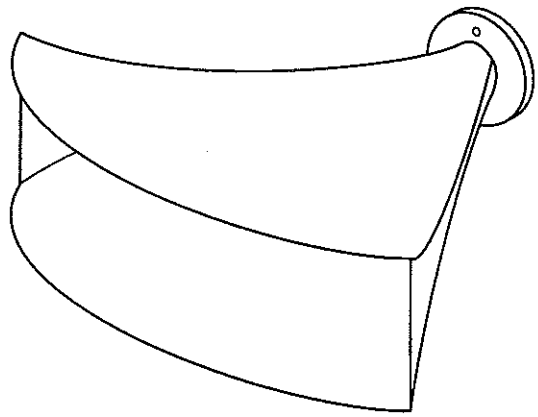

Figure 2.3 A Sectoral Horn

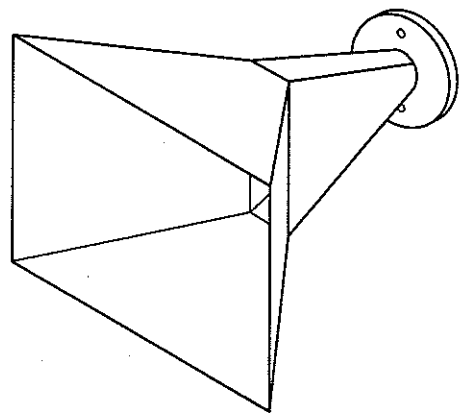

Figure 2.4 A Constant Directivity Horn

Within each of these horn catagories there can be wide variations, for example a horn may be flat fronted or it may have 'lips' to continue the flare in two dimensions only (figure 2.5).

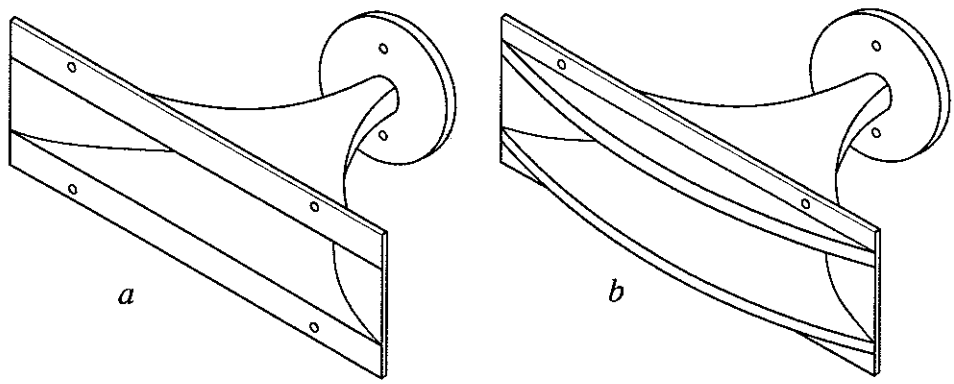

Figure 2.5 A Rectangular Horn with a: Flat Front and b: Lips

The underlying assumption made in the design of most loudspeaker horns is that the actual three-dimensional shape of a horn only affects directivity, and the one-parameter behaviour of a horn can be modelled by substitution of the cross-sectional area profile into Webster's one-dimensional horn equation regardless of the cross-sectional shape of the horn. It is the purpose of the investigation in this and the next chapter to find to what extent this is true and to what extent aspects of the performance of real horns can be modelled in a quasi-one-dimensional manner.

Many real horns do not have area profiles for which an analytical solution of equation (2.1) exists. The one-parameter analysis of such horns therefore requires a model for horns of any arbitrary area profile. The following is a description of the development of a semi-numerical model for this purpose.

2.2 DEVELOPMENT OF MODELS.

The development of two mathematical models is described below; the first, named 'Model A', uses numerical methods to solve a reflection coefficient version of equation (2.1), and the second, named 'Model B' uses finite-length exponential elements, within which the solution of equation (2.1) is expressible in closed analytical form (see appendix 1). The development of Model B was the logical

result of a consideration of the assumed shape of the horn between the steps used in Model A.

Both models were programmed in BBC BASIC V on an Acorn Archimedes microcomputer and all calculations were carried out using standard precision (5 byte) real numbers.

2.2.1 Model A.

Starting with the one-parameter momentum and continuity equations:

$$\frac{\partial \hat{q}}{\partial t} = \frac{-S}{\rho_o} \frac{\partial \hat{p}}{\partial x} \quad \text{and} \quad \frac{\partial \hat{q}}{\partial x} = \frac{-S}{\rho_o c_o^2} \frac{\partial \hat{p}}{\partial t} \quad , \tag{2.2}$$

where $\hat{q} = \hat{q}(x,t)$ is acoustic volume velocity, a complex pressure reflection coefficient version of equation (2.1) can be derived for simple harmonic time dependence (see Appendix 2):

$$\frac{d\hat{R}_p(x)}{dx} = 2ik\hat{R}_p(x) + \frac{1}{2}\left(1 - \hat{R}_p(x)^2\right) \frac{d}{dx} \ln\left(\frac{S}{\rho_o c_o}\right) \quad , \tag{2.3}$$

where $\hat{R}_p(x)$ is the complex pressure reflection coefficient and is equal to $(\hat{Z}(x)-1)/(\hat{Z}(x)+1)$ where $\hat{Z}(x)$ is the acoustic impedance. It can be reasonably assumed for practical horns that the characteristic acoustic impedance $\rho_o c_o$ of the medium within the horn will be independent of length, so that equation (2.3) becomes

$$\frac{d\hat{R}_p(x)}{dx} = 2ik\hat{R}_p(x) + \frac{m(x)}{2}\left(1 - \hat{R}_p(x)^2\right) \quad , \tag{2.4}$$

where

$$m(x) = \frac{1}{S(x)} \frac{dS(x)}{dx} \quad . \tag{2.5}$$

For an exponential horn, the cross-sectional area is defined by

$$S(x) = S(0)e^{mx} \quad , \tag{2.6}$$

so $m(x)$ becomes the so called 'flare-rate' (m) of the horn, and an analytic solution of equation (2.4) exists. For any arbitrary area profile however, approximate numerical integration methods are necessary, requiring the use of a computer for practical results.

Numerical solutions of the first order differential equation (2.4) are generally less involved than those of the second order Webster equation (2.1), but as equation (2.4) is complex, the simultaneous solution of differential equations for either the real and imaginary parts or the modulus and phase of $\hat{R}_p$ is necessary. These two pairs of

equations take on the following forms:

$$\frac{dR(x)}{dx} = \frac{m(x)}{2}\left(1 - R(x)^2\right)\cos(\phi(x)) \quad , \tag{2.7a}$$

and

$$\frac{d\phi(x)}{dx} = 2k - \frac{m(x)}{2}\left\{\frac{1}{R(x)} + R(x)\right\}\sin(\phi(x)) \quad , \tag{2.7b}$$

where

$$\hat{R}_p(x) = R(x)e^{i\phi(x)} \quad ,$$

or with $\hat{R}_p(x)$ written as $\alpha(x) + i\beta(x)$,

$$\frac{d\alpha(x)}{dx} = \frac{m(x)}{2}\left(1 - \alpha(x)^2 - \beta(x)^2\right) - 2k\beta(x) \quad , \tag{2.8a}$$

and

$$\frac{d\beta(x)}{dx} = 2k\alpha(x) - m(x)\alpha(x)\beta(x) \quad . \tag{2.8b}$$

The solutions of either of these sets of equations can be used to determine the value of $\hat{R}_p$ at the throat of a horn, and hence its power transmission quantities, given the area profile ($S(x)$) defined at a number of values of x, and the value of $\hat{R}_p$ at the mouth of the horn (from radiation conditions).

Both of these sets of equations were programmed into a microcomputer and various numerical differentiation and integration techniques were used to solve the equations. The performance of the two sets of equations and the different numerical techniques were then assessed and compared.

2.2.2 Model B.

During the development of model A, it became clear that because it was necessary to specify the area profile of the horn at finite 'steps' along its length (both for the numerical techniques, and also to define an arbitrary area profile), the value of $m(x)$ remained necessarily constant over one of these steps. As mentioned above, a horn of which the value of $m(x)$ was a constant in x was in fact an exponential horn, indicating that each step between adjacent values of $S(x)$ in the above model had been treated as exponential in shape. This being the case, a 'one-parameter finite element' type model using exponential elements (see figure 2.1) was developed to compare with the 'one-parameter finite difference' type model discussed above.

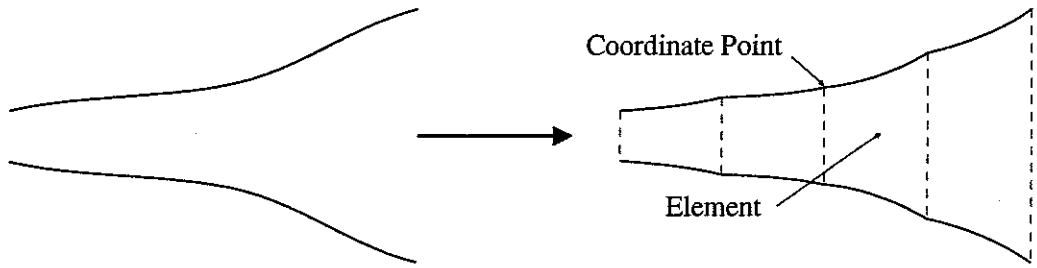

Figure 2.6 Division of Arbitrary Horn into Exponential Elements.

The solution of equation (2.1) for a finite exponential horn is shown in appendix 1 and can be written as follows:

$$\hat{p} = \hat{A}e^{\hat{\gamma}^+} + \hat{B}e^{\hat{\gamma}^-} \quad , \tag{2.9}$$

where

$$\hat{\gamma} = \frac{-m \pm \sqrt{m^2 - 4k^2}}{2} \quad . \tag{2.10}$$

$\hat{A}$ and $\hat{B}$ represent the complex amplitudes of the forward and backward travelling waves respectively, k is the free field wave number (ω/c_o) and m is the flare-rate of the horn. Using this solution, equations for the acoustic impedance at the throat and the transfer function of the horn in terms of the acoustic impedance at the mouth can be derived.

Consider a single exponential horn element with an area profile defined by $S(x) = S(0)e^{mx}$. The normalised acoustic impedance at a position x along the element can be written

$$\hat{Z}(x) = \frac{\hat{p}}{\rho_o c_o \hat{u}} = -ik\hat{p} \; / \; \frac{\partial \hat{p}}{\partial x} \quad .$$

Substitution of equation (2.9) yields

$$\hat{Z}(x) = -ik\left\{ \frac{\hat{A}e^{\hat{\gamma}^+ x} + \hat{B}e^{\hat{\gamma}^- x}}{\hat{\gamma}^+\hat{A}e^{\hat{\gamma}^+ x} + \hat{\gamma}^-\hat{B}e^{\hat{\gamma}^- x}} \right\} \quad .$$

By first substituting a value of $x = 0$, and then a value of $x = l$, where l is the length of the element, a pair of equations expressing the impedances at the two end of the element can be written:

$$\hat{Z}(0) = -ik\left\{ \frac{\hat{A} + \hat{B}}{\hat{\gamma}^+\hat{A} + \hat{\gamma}^-\hat{B}} \right\} \quad \text{and} \quad \hat{Z}(l) = -ik\left\{ \frac{\hat{A}e^{\hat{\gamma}^+ l} + \hat{B}e^{\hat{\gamma}^- l}}{\hat{\gamma}^+\hat{A}e^{\hat{\gamma}^+ l} + \hat{\gamma}^-\hat{B}e^{\hat{\gamma}^- l}} \right\} \quad .$$

Substitution of the second equation into the first yields

$$\hat{Z}(0) = -ik\left\{\frac{\left(\hat{Z}(l)\hat{\gamma}^{-} + ik\right)e^{\hat{\gamma}^{-}l} - \left(\hat{Z}(l)\hat{\gamma}^{+} + ik\right)e^{\hat{\gamma}^{+}l}}{\hat{\gamma}^{+}\left(\hat{Z}(l)\hat{\gamma}^{-} + ik\right)e^{\hat{\gamma}^{-}l} - \hat{\gamma}^{-}\left(\hat{Z}(l)\hat{\gamma}^{+} + ik\right)e^{\hat{\gamma}^{+}l}}\right\} .$$

This impedance transformation equation expresses the impedance at the 'throat' of an element ($x = 0$), in terms of the impedance at the 'mouth' ($x = l$) and the two complex propagation coefficients (γ). As shown in appendix 1 (equations (A.1.9) and (A.1.10)), the propagation coefficients take different forms depending on whether the frequency of interest is above or below the cut-off frequency of the exponential element. Two equations are therefore required for computation; the choice of which equation is used being made subject to the result of a comparison between the cut-off frequency and the frequency of interest. These equations can be used to find the 'throat' impedance of the first element given the mouth impedance of the horn: this throat impedance then becomes the mouth impedance of the next element and so on until the throat of the horn is reached. In this method, the use of the numerical differentiation and integration routines is avoided.

2.3 PERFORMANCE OF MODELS.

2.3.1 Model A.

As mentioned above, several different techniques for numerical solution of both equations (2.7) and (2.8) were tried. These techniques ranged from the simplest, namely

$$\frac{dy(n)}{dx} \approx \frac{y(n) - y(n-1)}{\delta x} \quad \text{and} \quad y(n) \approx y(n-1) + \frac{dy(n)}{dx}\,\delta x \quad ,$$

to the relatively involved Gregory-Newton and fourth order Runge-Kutta methods which require several iterations. The results using the various methods were compared with analytical solutions for exponential and conical horns so that an idea of relative performance could be obtained. As well as accuracy, computer run times and non-dimensional step size/frequency parameters (kh) were recorded.

It came as no surprise that the more advanced numerical methods took longer to run per step, but in their favour, larger values of kh could be used whilst maintaining accuracy. As a rule it was found that for most of the methods tried, the accuracy that could be achieved within a given computer run time was about the same. This meant however that using the simpler methods required specification of the area profile of

the horn at a larger number of steps than with the more advanced methods, so a decision as to how many steps are required to 'accurately' define an arbitrary area profile was necessary. A choice of 20 steps was found to be optimum for most practical horns as a compromise between errors due to the assumed shape of the steps and the tedium of defining (and measuring, if modelling a real horn!) a large number of cross-sectional areas. A choice also had to be made between the polar equations (2.7) and the Cartesian equations (2.8). Although essentially doing the same job, two significant differences in the performance of the programmes containing the two sets of equations were noted. The first concerned the computer run times, and the second the stability of the programmes when $\hat{R}_p$ approached zero. The polar equations took nearly twice as long to run as the Cartesian equations and the programme had a tendency to 'crash' at some frequencies. Reference to equations (2.7) and (2.8) shows that if $\hat{R}_p$ tends to zero, $d\alpha(x)/dx$ remains non zero ($m(x)/2$) whereas $d\beta(x)/dx$ and $dR(x)/dx$ tend to zero and $d\phi(x)/dx$ tends to infinity. This may explain the superior stability of equations (2.8) over equations (2.7) as $\hat{R}_p$ approaches zero.

Taking all of the above results into account, the method using the Cartesian equations (2.8), Gregory-Newton differentiation and fourth order Runge-Kutta integration routines was judged to perform best, with an upper frequency limit for within 1dB accuracy dictated by $kh = 0.6$ ($f_{max} = 2c/l$ for 20 steps).

2.3.2 Model B.

At first glance it may seem as if the equations for model B would require very much longer computer run times than those for model A. However they need to be used only once per element, whereas the numerical integration in the first model requires several iterations. As a result, the run times for this model, for the same number of steps (or elements) and frequencies, are comparable with those of the best for model A. As far as the one-parameter assumptions go, model B should give results for one element which are accurate for a finite exponential horn at all frequencies. This means that there is no upper frequency (kh) limit as found with the model A. The only limit therefore on the minimum number of elements necessary to give accurate results for a given area profile is how close the profile is to being exponential (ie an exponential horn would require only one element for accurate results, but a conical horn, for example, would require many). The 'safe' criterion of 20 steps used with model A therefore needed fresh examination before use with this model. To this end, the results for this model, for a range of numbers of elements,

were compared to the analytical results for a conical horn. As expected, the difference between the two results, which gives an indication of the model error, was seen to decrease as the number of elements was increased, and it was observed that large errors did not occur at either of the frequency extremes even when using only one element.

In order to test the model for errors when simulating the response of other (possibly intricate) shaped horns, an attempt was made to define a 'performance surface' to enable the maximum model errors to be predicted (or pre-defined) for any shape. To do this, the results obtained using a range of numbers of elements were compared to the results obtained using a large number of elements (128), which were assumed to be accurate, for a range of different profile parameters. The parameters considered to have the most influence on the error were length, general rate of flare and rate of change of flare-rate with distance. A set of horn shapes, defined by

$$S(x) = S(0)e^{fx^g} \quad , \quad 0 < x < l \quad , \quad g > 1 \quad , \tag{2.11}$$

were tested for various values of f, g and l so that the general flare-rate is proportional to f and the order of rate of change of flare-rate with distance is proportional to g (ie when $g = 1$, $m(x)$ = constant (exponential); $g = 2$, $\mathrm{d}m(x)/\mathrm{d}x$ = constant; $g = 3$, $\mathrm{d}^2m(x)/\mathrm{d}x^2$ = constant etc.). A large number of these error results for both the real and the imaginary parts of the throat impedance ($R_T + iX_T$) were plotted on logarithmic graph paper and it was discovered that plots of the maximum error in decibels against each of the parameters in turn, closely followed straight line laws. Analysis of this data resulted in two expressions describing five-dimensional performance surfaces linking the maximum dB error, for R_T and X_T, to values of f, g, l and the number of elements N, thus:

$$\text{dB error (max) in } R_T = \frac{fgl^g}{N^{1.25}} \quad , \tag{2.12a}$$

and

$$\text{dB error (max) in } X_T = \left\{\frac{2fl^g(g-1)}{N}\right\}^2 \quad . \tag{2.12b}$$

The values of f and g above obviously only apply to the profiles tested, but they can be approximated for any arbitrary shape as follows:

$$f \approx \frac{m_{ave}}{l^{g-1}} \quad \text{and} \quad g \approx \frac{m_{max}}{m_{ave}} \quad , \tag{2.13}$$

where m_{max} is the maximum flare-rate and m_{ave} is the average flare-rate. Equations (2.12) then become

$$\text{dB error (max) in } R_T \approx \frac{lm_{max}}{N^{1.25}} \quad , \tag{2.14a}$$

and

$$\text{dB error (max) in } X_T \approx \left\{\frac{2l(m_{max} + m_{ave})}{N}\right\}^2 \quad . \tag{2.14b}$$

Values of m_{max} and m_{ave} could either be estimated by inspection of a particular profile, or from a 'trial run' on an error programme with a large number of elements. The latter choice, unfortunately, requires the profile to be defined at a large number of points, but with care, the former method can work. Note, $m_{ave} = \Sigma m / N$ generally, or $m_{ave} = \ln_e(\text{mouth area/throat area}) / l$ for a continually expanding duct. Equations (2.14) were then checked against a variety of 'odd' shapes and proved to be fairly accurate. A graph of predicted error vs. actual error, with number of elements as a third variable over a range of these 'odd' profiles, is shown in figure 2.7. The limitations of the performance surface can be seen by allowing g to equal unity in equations (2.12) or $m_{max} = m_{ave}$ in equations (2.14). This corresponds to an exponential horn and will, by definition of the elements, give zero error, whereas the performance surfaces predict finite errors. This is of course, a trivial case but it shows that when the value of g is only slightly greater than unity, the error predictions are less accurate. However, the errors will be very small in these cases and so would be of little concern. Another limitation, which was taken into account in the assembly of the error data, is when the results are very close to zero. In these cases, which occur mostly with the imaginary part of the result at certain frequencies, the dB errors can be very large but misrepresentative of the accuracy of the model. Errors for $X_T < 0.05$ were therefore ignored in the definition of the error surface. It can be seen in figure 2.7 that the real part errors are more predictable than those for the imaginary part so a 'safe' factor of 5 may be applied to equation 2.14b if required.

The analysis of the performance of the two models showed the exponential element model to be the better of the two. For a given computer run time it proved more accurate and more robust over a wider frequency range than the first model so its development for practical usage was favoured. Because numerical procedures are avoided, the model allows the length of each element to be defined separately. This means that a few large elements can be used to model parts of an area profile that are essentially exponential, with many small elements to model any intricate parts. Equations (2.14) could therefore be applied only to the 'troublesome' parts of the profile for error estimation.

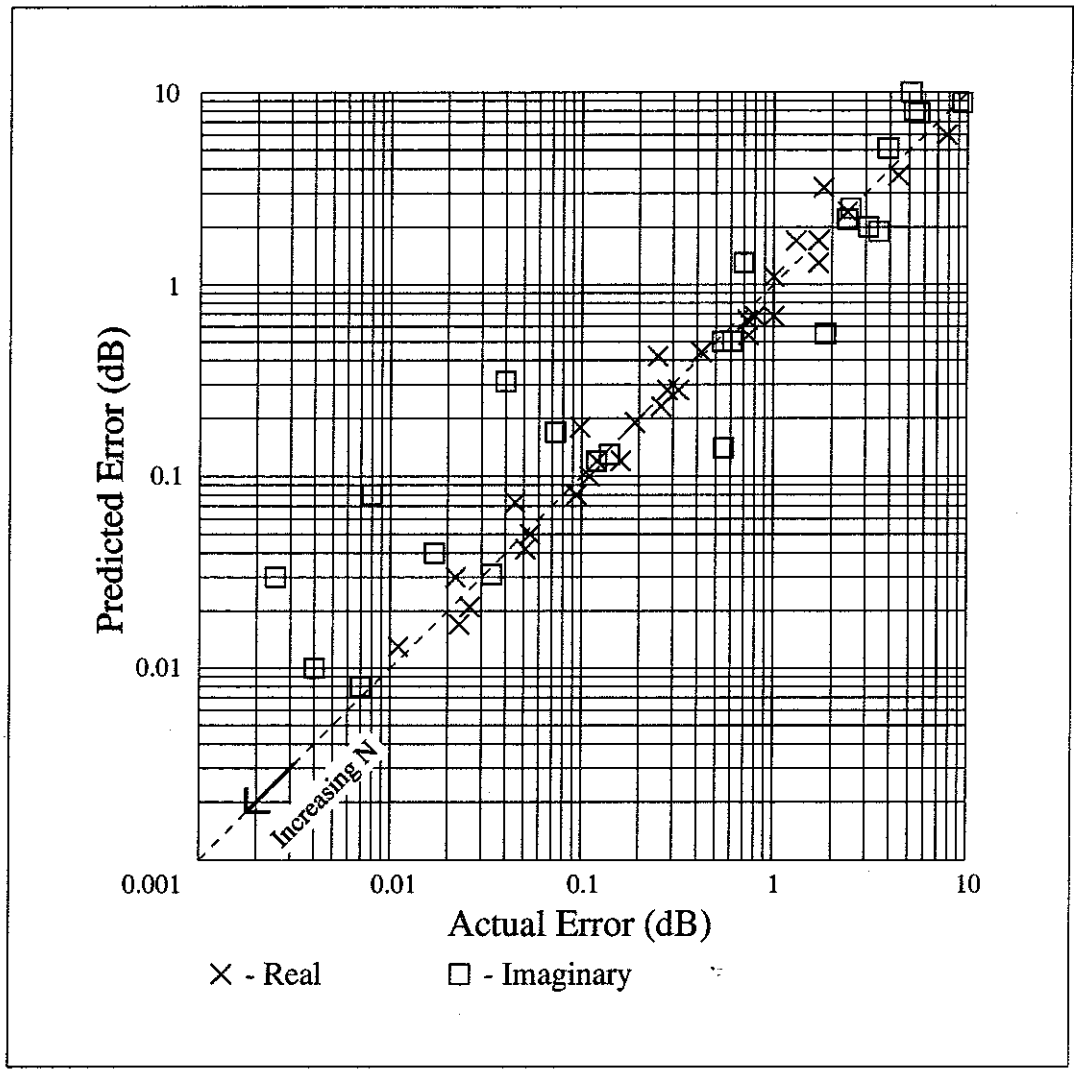

Figure 2.7 Predicted Error Verses Actual Error Against Number of Elements for a Variety of Shapes.

The model first requires the area profile to be defined at intervals along the length of the horn, then the length of each element, the speed of sound and the mouth impedance.

2.3.3 Model Output.

The model is capable of calculating a number of one-parameter horn properties. Each property, the significance of which are outlined below, is calculated at 256 linearly spaced frequencies.

2.3.3.1 Throat Impedance. A knowledge of the acoustic impedance presented by a horn flare to a velocity source, such as a diaphragm, placed at the throat is vital for

assessing the performance of a horn. The power output of the horn for a given velocity input is proportional to the real part of this impedance (R_T) and its value over a range of frequencies gives an indication of the smoothness of the frequency response as well as the low frequency limit and efficiency of the horn. The imaginary part (X_T) shows the reactive load presented to the source by the horn. The values calculated are normalised to the characteristic air impedance $\rho_o c_o$.

2.3.3.2 Transfer Impedance. The major assumption made in the derivation of the one-parameter horn equation used in the above model was that the sound field within a horn was a function of only one parameter, the area profile $S(x)$. The pressure and particle velocity must, therefore be uniform over a chosen wavefront surface (see section 2.4). This being the case, a knowledge of the pressure at the mouth of a horn, along with the defined mouth impedance, is sufficient for calculations of the radiated field. The transfer impedance is proportional to the pressure at the mouth for unit velocity at the throat and can therefore be used to calculate the field radiated by the horn when driven by a perfect diaphragm. The calculated values are again normalised to $\rho_o c_o$.

2.3.3.3 Axial Pressure Distribution. It can be seen from equation (2.9) that the sound field within a horn can take the form of a dispersive standing wave field. This being the case, it can be difficult to decide if and where reflections occur inside a horn from a knowledge of the sound fields at the throat and mouth alone. The axial pressure distribution gives at least a qualitative idea of the nature of these reflections.

2.3.3.4 Transverse Pressure Variations. Due to the assumption of one-parameter behaviour in this model, the pressure across a chosen wavefront surface (see section 2.4) within or outside a horn must be uniform in both amplitude and phase.

2.4 EXTENSION OF MODEL

Because of the one-dimensional form of equation (2.1), the area profile $S(x)$ used to define a horn in the above model, must refer to the area of surfaces which are independent of the other two coordinates of the chosen coordinate system. For example, for an exponential horn defined in cylindrical or Cartesian coordinates, with x as the dependant coordinate, $S(x)$ defines flat surfaces which are normal to the x axis. These surfaces, by definition, define the shape of the wavefronts (or iso-phase

surfaces) within the horn. As these wavefronts must be normal to the walls of the horn at the walls, and therefore curved for a flaring horn, the direct application of equation (2.1) to an exponential horn (or element of) using flat cross-sectional areas would lead to errors with all but the most trivially low flare-rates. The section below is concerned with a physical description of horn behaviour which began as an attempt to answer the frequently asked question "why do horns have a cut-off frequency?". The formulation of an answer has led to a useful extension of the one-parameter model above to include horns with rapid flare.

2.4.1 A Physical Description of Horn Behaviour.

Horns are waveguides that have a cross-sectional area which increases, steadily or otherwise, from a small throat at one end to a large mouth at the other. An acoustic wave within a horn therefore has to expand as it propagates from throat to mouth. The manner in which acoustic waves propagate along a horn is so dependent upon the exact nature of this expansion that the acoustic performance of a horn can be radically changed by quite small changes in flare-shape. It is usually assumed in acoustics that changes in geometry that are small compared to the wavelength of the sound of interest do not have a large effect on the behaviour of the sound waves, so why should horns be any different? A comparison between the propagation of waves in two simple acoustic systems, one in which the wave does not expand as it propagates and one in which it does, may explain the physics of horn behaviour.

Consider first the propagation of a one-dimensional free progressive plane wave such as low frequency sound in an infinite, uniform pipe. A wavefront (defined here as an iso-phase surface) undergoes no change in cross-sectional area as it propagates and the normalised acoustic impedance, at any point along or across the pipe is purely resistive and equal to unity (ignoring losses). A plane velocity source placed anywhere along the pipe therefore has no reactive acoustic loading on it at any frequency, either as added mass or stiffness. Consider second the propagation of a three-dimensional free progressive spherical wave such as sound radiating from a point monopole source. In this case a wavefront continually expands as it propagates and the normalised acoustic impedance at a point is dependent upon both the distance from the source and frequency thus:

$$\hat{Z}(r\,,\,k) = \left\{ \frac{(kr)^2 + ikr}{1 + (kr)^2} \right\} \quad , \tag{2.15}$$

where k is the acoustic wave number (ω/c) and r is the radial distance from the

source. The impedance is seen to approach unity (resistive) at large radii (where it becomes almost a plane wave) and at high frequencies but is reactively dominated at small radii and at low frequencies. At the non-dimensional frequency/size value kr = 1 the resistive and reactive components of the impedance are seen to be equal in magnitude. A spherical velocity source of finite size will therefore have either resistively or reactively dominated acoustic loading on it depending on the size of the source and the frequency of vibration.

The only physical difference between the propagation of waves in these two systems is the expansion and consequent 'stretching' of the spherical wave as it propagates. In the plane wave case, a forward or positive particle velocity is accompanied by a positive increase in pressure at the same point due to the parallel motion of all of the adjacent particles. In the spherical wave case however, because an outward positive velocity causes adjacent particles to move apart, the positive (radiating) pressure is accompanied by a negative "stretching" pressure due to the expansion. This is shown diagramatically in figure 2.8.

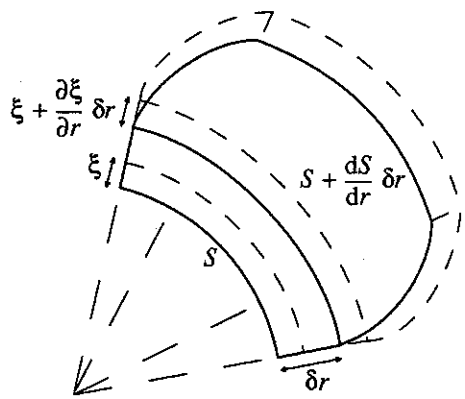

Figure 2.8 Geometry for a Spherical Wave.

This stretching pressure (p_s) can be identified by considering the physics of propagation in the two cases above. In the plane wave case, a positive displacement ξ of a small element of air of length δx gives, according to continuity, an acoustic pressure (p_r) equal to

$$p_r(\xi, x) = -\rho_o c_o^2 \left\{ \frac{S\delta x - S\xi + S(\xi + \partial\xi/\partial x.\delta x) - S\delta x}{S\delta x} \right\}$$

$$= -\rho_o c_o^2 \frac{\partial \xi}{\partial x} \quad . \qquad (2.16)$$

In the spherical wave case (figure 2.8), an outward displacement ξ of a small element

at radius r of thickness δr and area S gives an acoustic pressure equal to

$$p(\xi, r) = -\rho_o c_o^2 \left\{ \frac{S\delta r - S\xi + S(\xi + \partial\xi/\partial r.\delta r)(S + dS/dr.\delta r) - S\delta r}{S\delta r} \right\}$$

$$= -\rho_o c_o^2 \left\{ \frac{\partial \xi}{\partial r} + \frac{2\xi}{r} \right\} \quad , \quad S = 4\pi r^2 \quad . \tag{2.17}$$

The first term in the brackets is, with the substitution of r for x, identical to equation (2.16) above for the propagating plane wave. The second term represents the stretching pressure (p_s). The pressure due to a displacement in a spherical wave is thus the sum of the two; $p = p_r + p_s$. (2.18)

For harmonic waves it can be shown, from momentum considerations, that for a given particle velocity, the plane wave type, propagating pressure p_r is independent of frequency and radius and in-phase with the velocity and that the non-propagating, stretching pressure p_s, being displacement dependent, is inversely proportional to frequency and radius and in quadrature with the velocity. The expansion of a spherical wave, which is responsible for the stretching pressure, thus has the effect of reducing the resistive part of the impedance at low values of kr, replacing it with a positive reactance. Positive reactance is generally associated with inertial effects, and negative reactance with stiffness. However, there is no extra inertia involved in spherical waves compared to plane waves, so this interpretation is inappropriate for the purpose of this discussion; the positive reactance in this case is clearly due to 'negative stiffness' and not added mass. The region where this reactance dominates ($kr << 1$) is known as the hydrodynamic near-field and its extent is frequency dependent. The region outside this ($kr >> 1$) where resistance dominates is known as the far-field.

The concept of a stretching pressure can be applied to horns by considering flare-rate. Flare-rate can be defined as the rate of change of area with distance divided by the area. An exponential horn has a flare-rate that is constant along the length of the horn and a conical horn has a radially dependent flare-rate ($m(r)$) which is given by

$$m(r) = 2 / r \ , \tag{2.19}$$

where r is the distance from the apex of the cone to the point of interest. A spherically radiating source can be thought of as a special case of a conical horn and thus shares the same expression for flare-rate. As mentioned above, in a spherical wave at a given radius, the frequency at which the resistive and reactive parts of the impedance are equal in magnitude occurs at $kr = 1$. The flare-rate at this radius in a conical horn is equal to $2k$ which is identical to the flare-rate in an exponential horn

having this cut-off frequency (see appendix 1). From this it can be seen that with flare-rates below this value, resistive, far-field-type propagation takes place, and with flare-rates above this value, reactive, near-field-type behaviour takes place. The difference in behaviour of the various types of horn can be explained using this physical concept.

The radial dependence of the flare-rate in a conical horn (and a spherical wave) gives rise to a gradual transition from the reactive, near-field dominated behaviour associated with the stretching pressure, to the resistive, radiating, far-field dominated propagation as a wave propagates from throat to mouth. The transition from near- to far-field dominance is gradual with increasing frequency and / or distance from apex, so distinct "zones" of propagation are not clearly evident.

An exponential horn however, with a flare-rate that is constant with distance along the horn, behaves quite differently. At frequencies below $k = m/2$ (cut-off), throughout the entire length of the horn, the reactive, near-field-type propagation dominates and, if the horn is sufficiently long, an almost totally reactive impedance exists everywhere. At frequencies above cut-off, again throughout the entire length of the horn, the far-field-type propagation dominates leading to an almost totally resistive impedance everywhere. Physically, propagation within an exponential horn above cut-off is similar to a spherical wave of large radius, with minimal stretching pressure, and that below cut-off, similar to a spherical wave of small radius, dominated by the stretching pressure. The sharp cut-off phenomenon clearly occurs because the transition from one type of propagation to the other occurs simultaneously throughout the entire length of the horn as the frequency is lowered through cut-off.

2.4.2 Extension of One-parameter Model.

By considering the physical description of wave propagation within horns above, it is possible to extend the application of the finite exponential element technique to the accurate prediction of the throat impedance of horns of any shape, and to a lesser extent, the internal pressure distributions. It is reasonable to assume that the parameter that most affects the behaviour of waves within a horn is the rate of change of area of the wavefronts as they propagate. In the one-parameter model, as the cross-sectional area of the horn is used to define the elements, these wavefronts are assumed to be plane. As stated above, this cannot be the case in a rigid-walled, flaring waveguide as it is necessary for the wavefront to intercept the walls at right

angles. In equation (2.1), the pressure field is a function of $S(x)$ which does not specify any particular coordinate system. The wavefronts can therefore take any shape or area as a function of x. The extension to this model involves using the area of 'assumed' wavefronts to define the elements. These areas (and their influence on the element lengths) are calculated using a set of empirical rules based on measurements of wavefront shapes in real horns.

Figures 4.1.5a and 4.1.5b show plots of the measured pressure distribution along a straight line across the mouth of a circular cross-section axi-symmetric horn (horn type 2 described in appendix 3). From similar measurements within and outside such horns, where a microphone was moved until a comparison of the pressure at two points gave a horizontal phase plot on a dual channel FFT analyser, it was discovered that the wave front shapes in axi-symmetric horns take the form of 'flattened spherical caps'. These findings accord with those of Voigt [28] with the development of his "Tractrix" horns, and Benade [15] in the study of musical instrument horns. It was discovered from these measurements that the area of such wavefronts, and the end correction to an element length due to the curvature (see figure 2.9), could be approximated by the arithmetic mean of that of the plane cross-section and that of a spherical cap normal to the horn walls.

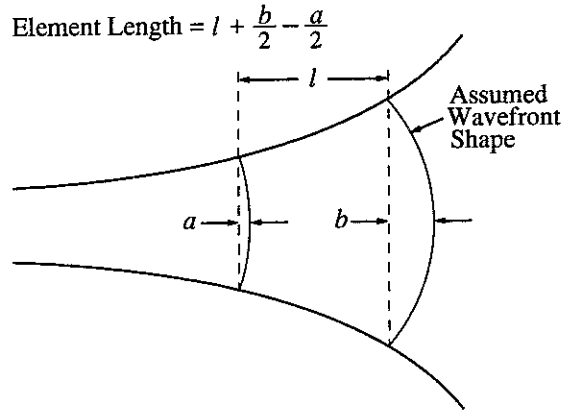

Figure 2.9 Element Length End Correction.

Figures 4.1.4a and 4.1.4b show plots of the measured pressure distribution across the mouth of a rectangular horn with lips in an arc following the lips. From similar measurements, it was discovered that, unlike those in axi-symmetric horns, the wavefronts in the measured rectangular horns take the form of circular arcs normal to the horn walls. The areas of the wavefronts within a rectangular horn could be approximated by the product of the arc length across one dimension and the arc

length across the other at the position of the arc of the first. The element end correction could be approximated as the sum of the axial heights of the two arcs. A problem occurs however, with rectangular horns with flat fronts, or those without 'full' lips (circular arcs normal to the horn walls at the mouth) with different flares in the two dimensions. When defining wavefronts near the mouth, the larger circular arc passes outside the horn preventing the calculation of an arc length across the other dimension. Measurements outside such horns showed that the wavefronts effectively 'fold' around the mouth to form a spherical cap on the horn baffle with the radius of the large arc and a height approximately the same as if the horn were continued (see figure 2.10). The corrected wavefront area is then taken as the sum of the area of this cap and the truncated wavefront within the horn.

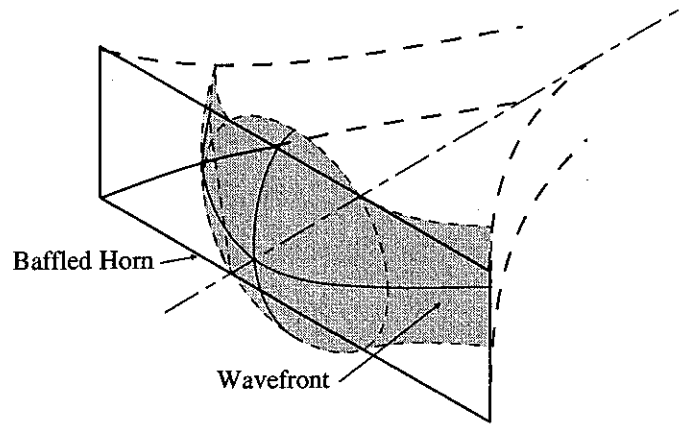

Figure 2.10 Wavefront near mouth of rectangular horn.

To allow for expansion of the wavefront at the mouth as it propagates out of the horn, an additional mouth element is defined using the stretching pressure argument above for expansion. This mouth element is defined as having as its 'throat' the mouth of the last element within the horn and as its 'mouth' a large hemispherical surface about the centre of the horn mouth which is given the radiation impedance of a sphere. With the addition of this mouth element, the above extensions allow the modelling of both axi-symmetric and rectangular horns, with or without lips provided the horn can be considered mounted in an infinite, flat baffle. An alternative mouth correction and element could be developed for un-baffled horns. Apart from the shape of the wavefronts, the main assumption (by default) made in this model is that the magnitude of the pressure is uniform over the entire wavefront surface. In most cases, particularly at the mouths of horns, this will not be so due to beaming etc. This makes the prediction of the far-field radiated by a horn impossible using this model (the hemispherical shape of the mouth element would lead to every horn being omni-directional). These transverse pressure distributions, apart from

being the mechanism by which the wavefronts expand in any non-spherical manner, are assumed to have little effect on throat impedance, this being one-dimensional by definition. The throat impedance should therefore be fairly accurately modelled using this method.

Chapter 3
MEASUREMENT OF ONE-PARAMETER BEHAVIOUR

3.1 INTRODUCTION

In order to test the validity of the model described in chapter 2, measurements are made of the throat and transfer impedances and of the axial pressure variations of a variety of real horns and compared with the model predictions. Figure 3.1 shows some of the eighteen horns that were made available for these tests. Although measurements were taken of many of these horns, only the results for five horns which exhibit 'interesting' behaviour will be presented here. Because the one-parameter model does not take account of any directivity properties that a horn may possess, no attempt has been made to model the far-field response of the horns. The physical significance of the various measurements is outlined in chapter 2 (section 2.3.3).

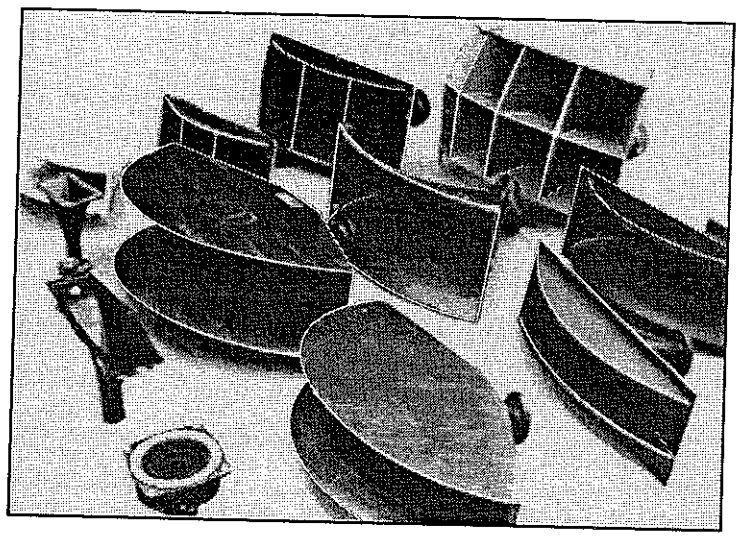

Figure 3.1 A Sample of the Variety of Horns Made Available for Testing.

3.2 THROAT IMPEDANCE

3.2.1 Measurement Method.

Various different methods were considered for the measurement of the throat impedance of horns. These included :-

a) The measurement of pressure near the throat of a horn due to the calibrated or measured velocity of a diaphragm at the throat.

b) A similar method utilising acoustic reciprocity.

c) Measurement of far field pressure in a calibrated reverberation chamber.

d) Measurement of the standing wave field in a pipe attached to the throat of a horn.

Methods **a** and **b** suffer from two problems. First, the throats of most of the horns available for measurement had diameters of only one inch, requiring the use of a very small microphone for the throat pressure measurement. Second, it would be difficult to attach a diaphragm to the horn throats which could be relied upon to remain as a pure piston (i.e. with axial vibration only) over a wide range of frequencies. These methods would also require the accurate calibration of both the velocity source and microphone. Method **a** has however, been successfully used by Merhaut [29], who measures the impulse response of a horn throat using an electrostatic source and miniature microphone. Method **c** would only give results for the real part of the throat impedance and would suffer the diaphragm problems of the former methods. Method **d** suffers none of these problems however and so its development for this task was favoured.

The principle behind method **d** is that of the standing-wave tube. It is an adaptation of an established technique for the measurement of the absorption coefficient of sound absorbing materials. A sample of the material, of which the surface acoustic properties are required, is placed at one end of a long, rigid tube. The air in the tube is excited at the frequency of interest by a driver mounted at the other end, and the resultant standing wave field is sampled at two known positions along the tube. The acoustic impedance of the sample can then be calculated from the measured transfer function between the pressures at the two positions and the distances from the two positions to the surface of the sample thus :

$$\hat{Z} = i\left\{\frac{\sin(kl_2) - \hat{T}\sin(kl_1)}{\hat{T}\cos(kl_1) - \cos(kl_2)}\right\} \quad , \quad \left(\hat{T} = \frac{\hat{p}_2}{\hat{p}_1}\right) \quad , \tag{3.1}$$

where suffices $_1$ and $_2$ refer to the positions nearest and farthest from the sample respectively (see appendix 4 for derivation). To measure the impedance at the throat of a horn using this method, the tube needs to be of the same diameter as the throat, so that when a horn is mounted at the end of the tube, the throat becomes a 'virtual surface' allowing its impedance to be measured in the same way as for an absorptive sample.

Traditionally, these measurements are carried out at one frequency at a time. To build up a picture of the variations in impedance over a range of frequencies, to compare with the 256 frequencies calculated by the model, would obviously take a prohibitive amount of time so an adaptation, using a dual channel FFT analyser, developed by Fahy [30], was used. This adaptation involved the use of a probe

microphone which is moved, instead of two separate microphones, to avoid matching problems, and excitation of the tube with pseudo-random noise (PRBS). Transfer functions are then measured between the probe output at both positions and the driving signal. The transfer function for position 2 is then divided by that for position 1 in the analyser and the result fed into a computer which calculates the impedance at 500 frequencies. The complete process takes only minutes - a considerable saving in time over the traditional method. A diagram of the apparatus used and details of the tube are shown in figures 3.2 and 3.3 respectively.

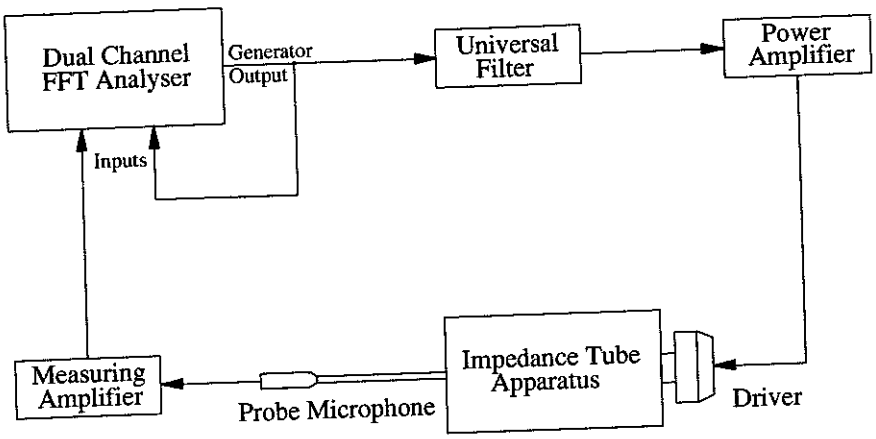

Figure 3.2 Throat Impedance Measurement Apparatus.

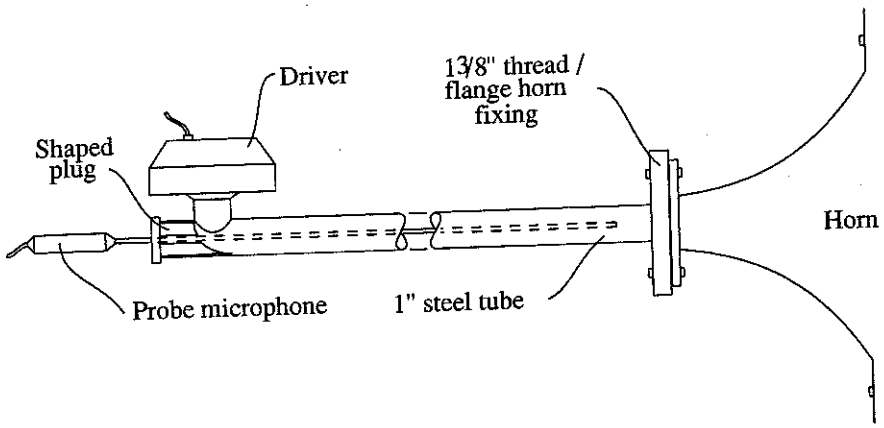

Figure 3.3 Impedance Tube Details.

Various precautions are taken to minimise any errors in the measurements :-

♦ The use of one microphone which is moved instead of two fixed microphones to eliminate the need for microphone matching or calibration.

♦ The reference of the microphone output at the two positions to the driving signal before calculation of the transfer function to improve coherence.

♦ Care in the choice of microphone positions and spacing. These were optimised for minimum error over a frequency range of 200 to 5000Hz, to distances of 30 and 55mm from the throat by testing on the open, unbaffled tube end, the impedance of which has been well researched [31].

♦ The microphone probe is made as small as is practically possible (3mm dia.) to minimise any effect of its movement on the sound field within the tube. Initially, it was hoped that a miniature (6mm diameter) electret microphone could be used instead of a probe microphone, but the position of this microphone was found to influence the pressure field elsewhere in the tube to an unacceptable degree; the small probe microphone however, was shown to have negligible effect on the sound field within the tube.

♦ Pseudo-random noise is used as a source signal to provide an overall flat spectrum with a low crest-factor to reduce driver headroom problems. Because this type of signal does not have a flat spectrum within one FFT analysis time window, an average of greater than 500 measurements of each transfer function is taken within the analyser to reduce random noise errors.

♦ The insertion of a variable filter in the signal path to the driver to correct for its bandwidth limitations and hence improve the signal to noise ratio at the frequency extremes.

♦ The air temperature close to the tube is monitored to accurately estimate the speed of sound for use in the calculations.

As impedance is by definition a one-dimensional quantity, the upper frequency limit for such measurements is determined by the radius of the tube and its corresponding plane wave limit, given by ka=1.83, where a is the radius of the tube. With the one inch tube used, this gives an upper frequency limit of about 8000Hz, so 5000Hz is considered to be a 'safe' maximum. The horn to be measured is mounted in a sub-baffle which is mounted in a 'window' between two isolated rooms (see figures 3.4). To simulate infinite baffle loading and free-field radiation conditions, the receiving room is made anechoic over the frequency range of interest with foam wedges on all surfaces except the baffle wall.

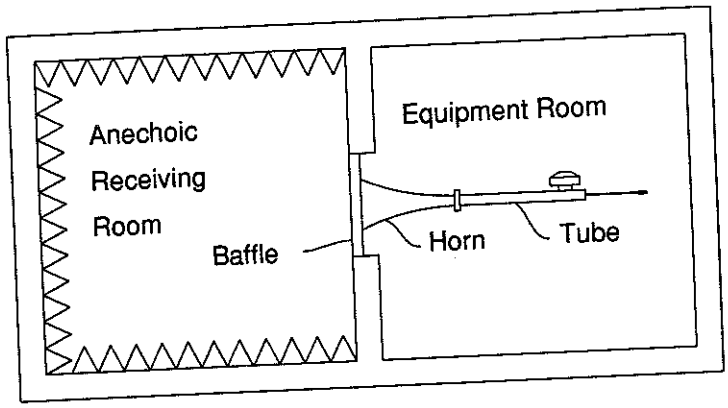

Figure 3.4a Diagram of Impedance Measurement Rooms.

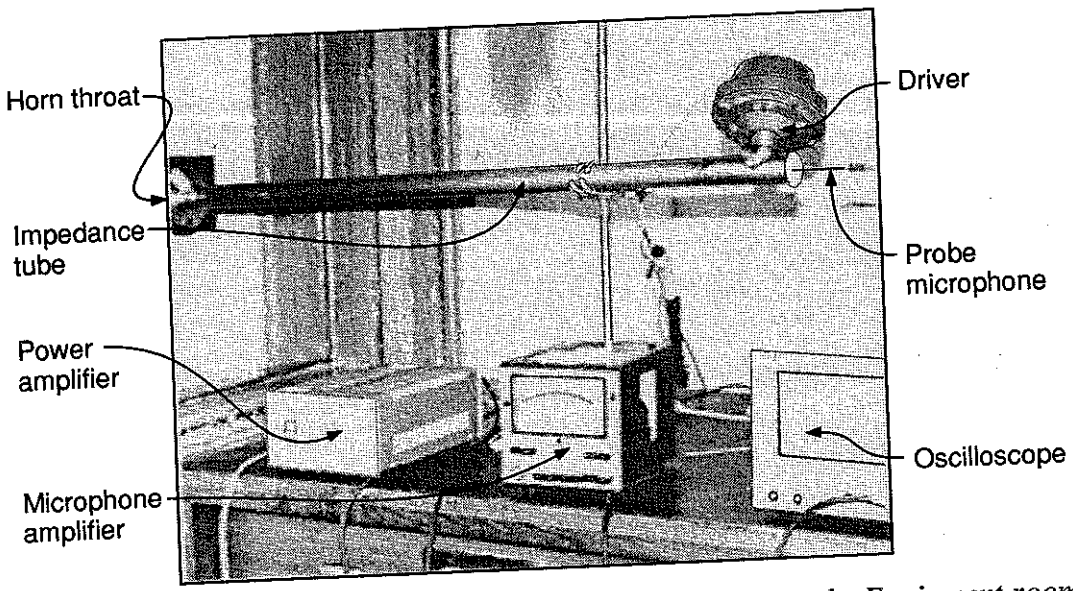

Figure 3.4b The Impedance Measurement Set-up Viewed from the Equipment room.

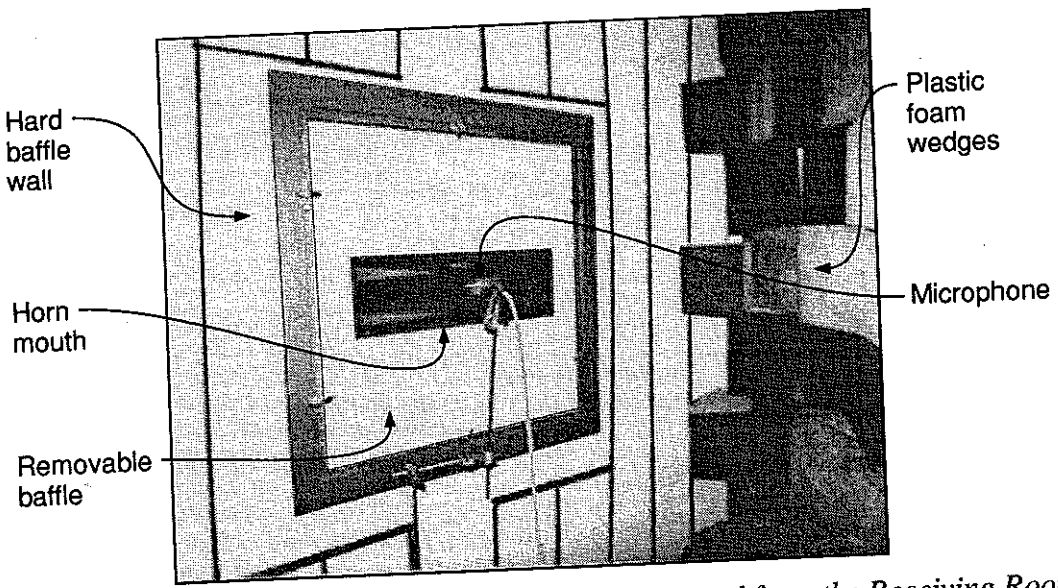

Figure 3.4c The Impedance Measurement Set-up Viewed from the Receiving Room.

3.2.2 Comparison between Theoretical and Measured Results.

Figures 3.5.1a to 3.5.5a show the theoretical throat impedances of the horns described in appendix 3. In order to calculate the throat impedance, the theoretical model requires, as input, the physical dimensions of the horns. The physical dimensions of rectangular horns are measured by inserting gauges of various known widths into the flare until they contacted the horn wall; the axial distance from the top of the gauge to a reference point on the horn is then recorded. The two axi-symmetric horns were constructed around moulds, the dimensions of which are easily measured using vernier calipers. Figures 3.5.1b to 3.5.5b show the measured throat impedances corresponding to the theoretical predictions. The 'horn type' numbers refer to the horn descriptions in appendix 3.

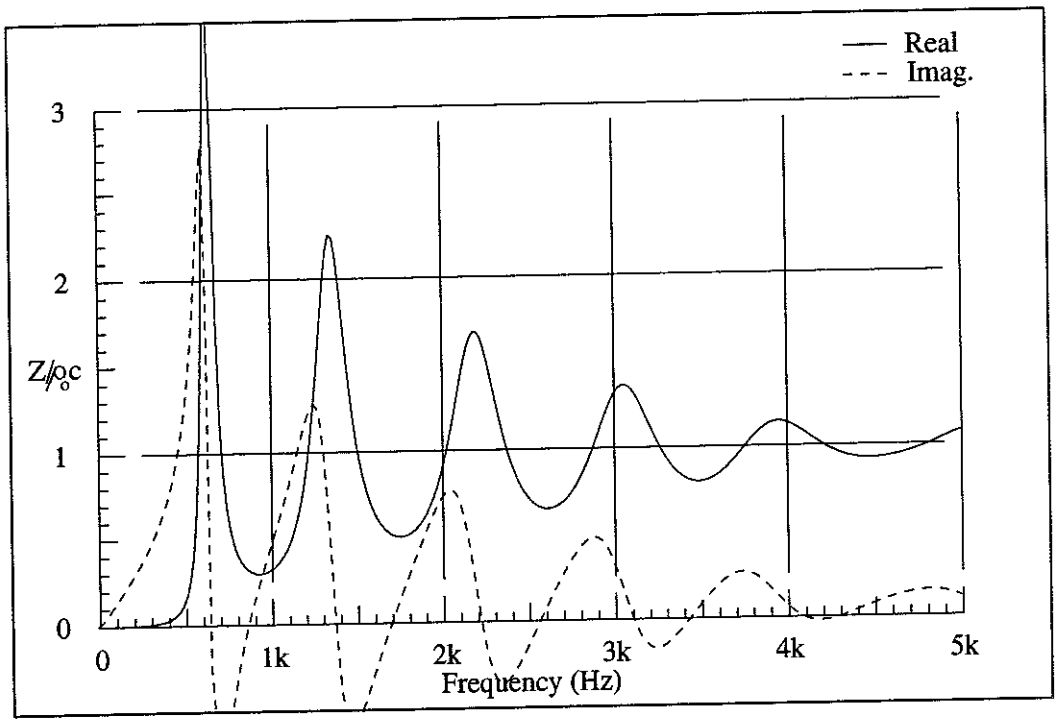

Figure 3.5.1a Theoretical Normalised Throat Impedance: Horn type 1; Small Axisymmetric (AX1).

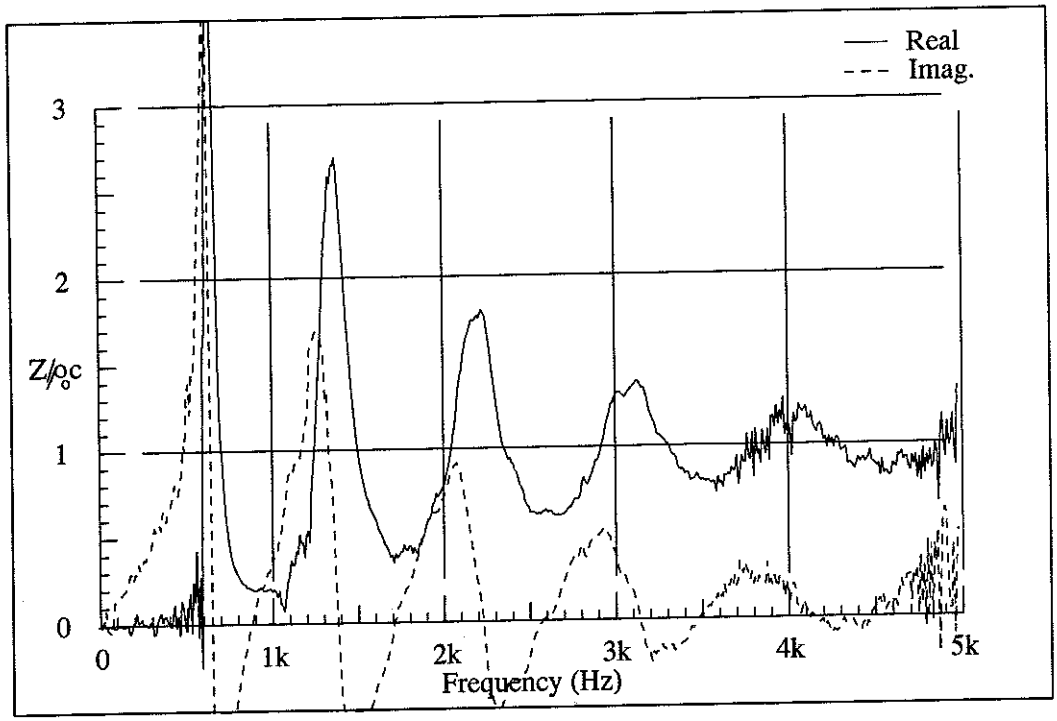

Figure 3.5.1b Measured Normalised Throat Impedance: Horn type 1; Small Axisymmetric (AX1).

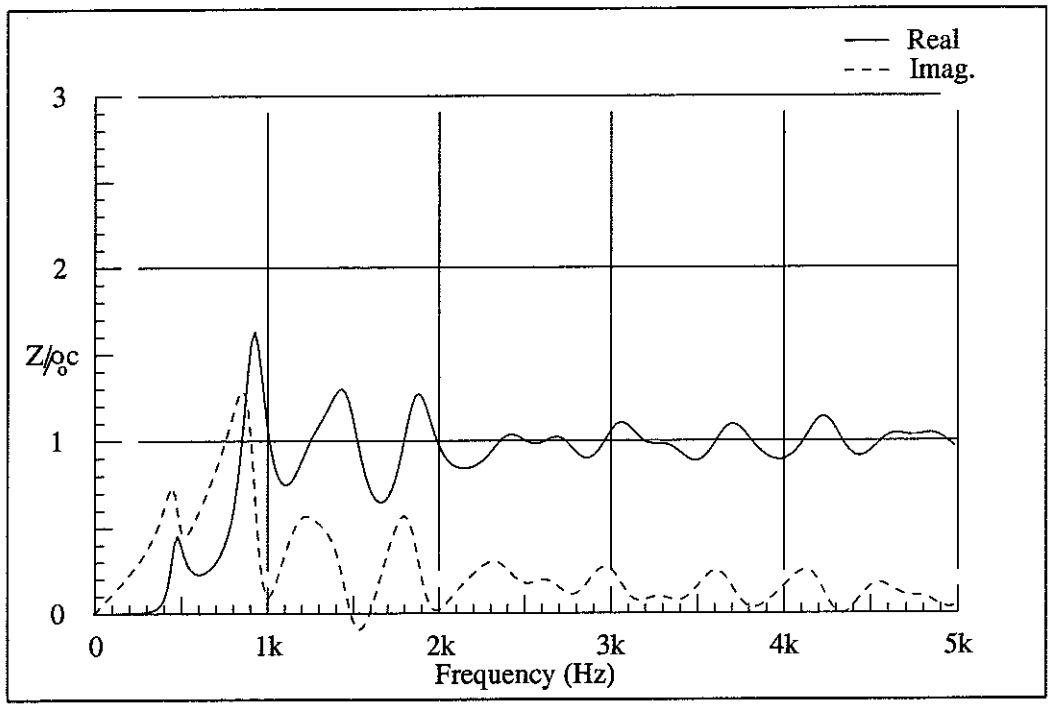

Figure 3.5.2a Theoretical Normalised Throat Impedance: Horn type 2; Reflexion Arts Rectangular.

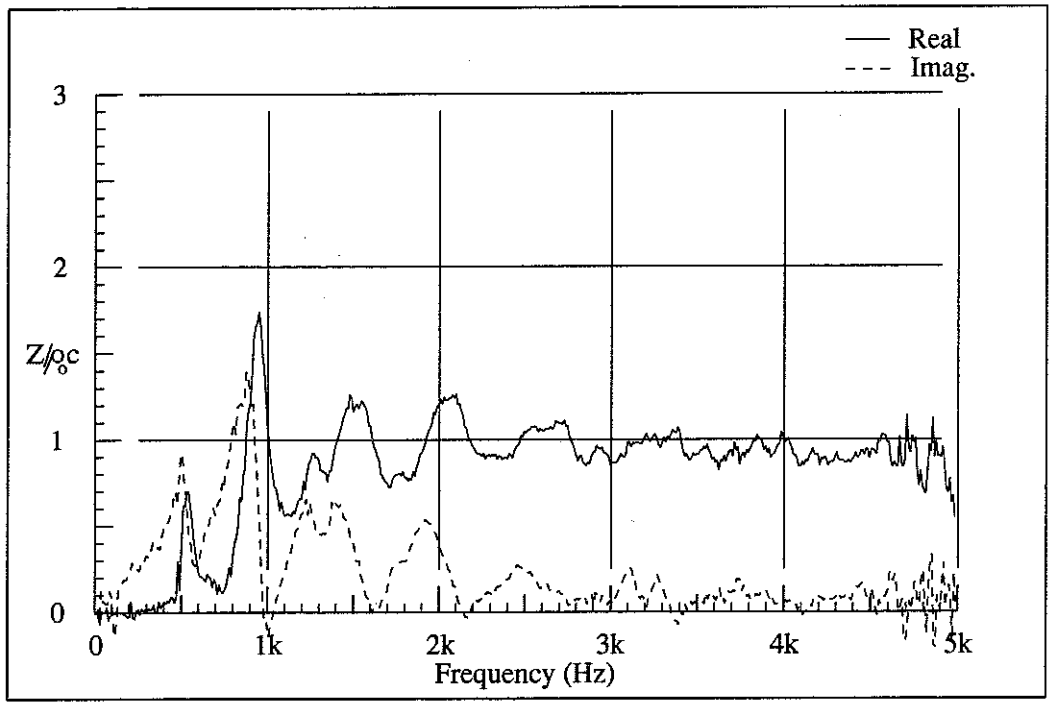

Figure 3.5.2b Measured Normalised Throat Impedance: Horn type 2; Reflexion Arts Rectangular.

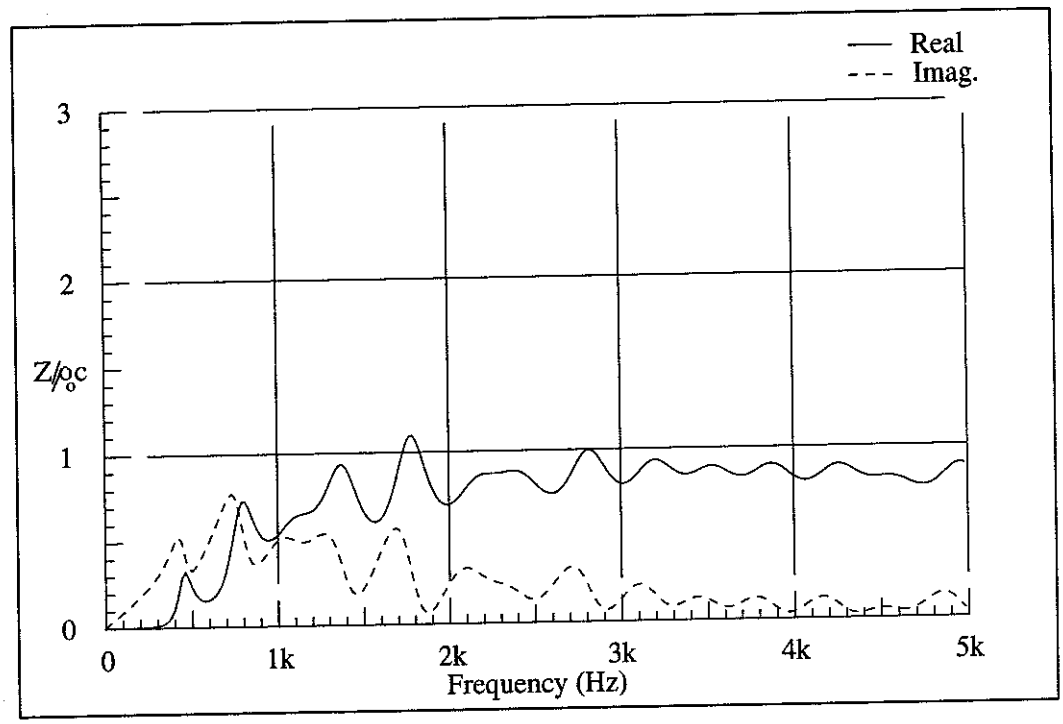

Figure 3.5.3a Theoretical Normalised Throat Impedance: Horn type 3; Vitavox Rectangular.

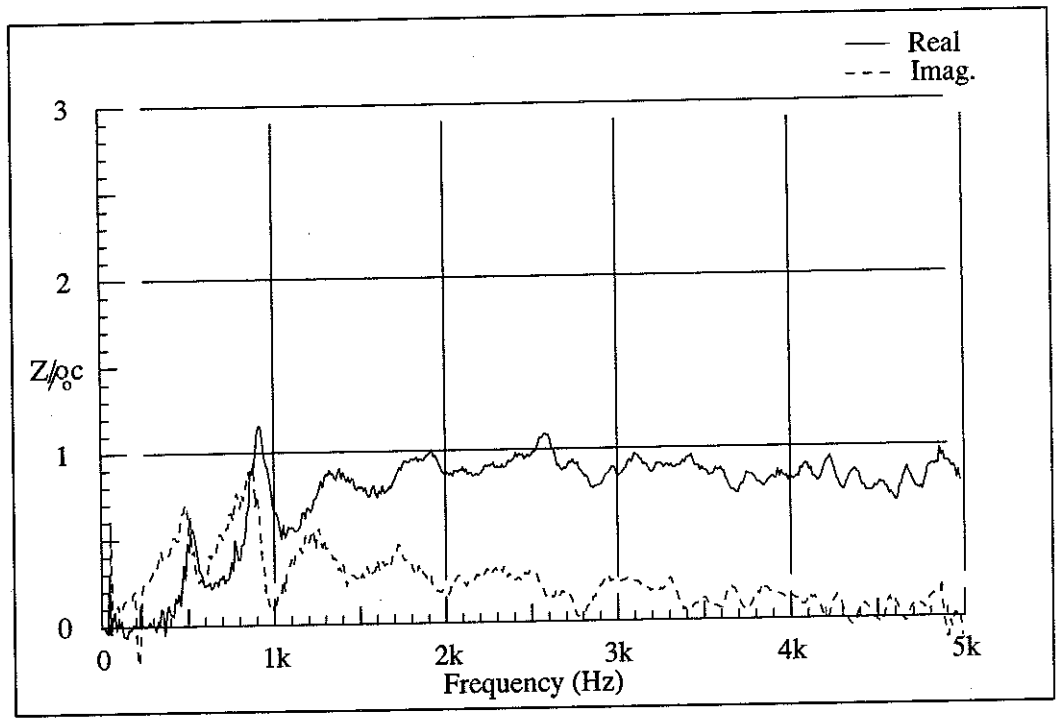

Figure 3.5.3b Measured Normalised Throat Impedance: Horn type 3; Vitavox Rectangular.

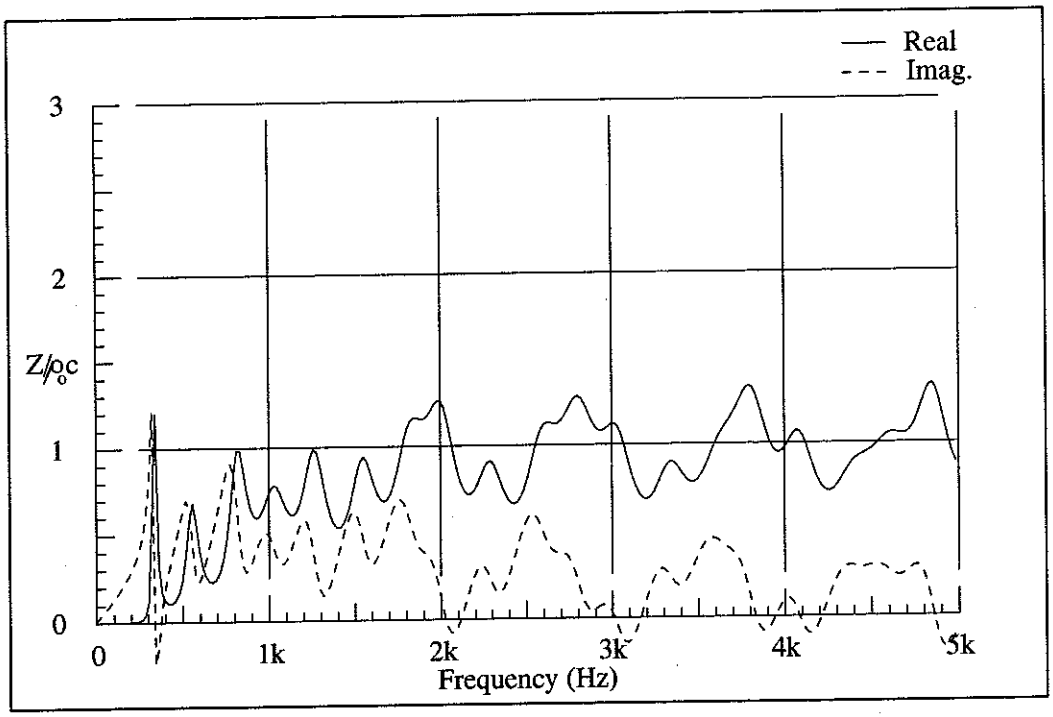

Figure 3.5.4a Theoretical Normalised Throat Impedance: Horn type 4; Fostex Sectoral.

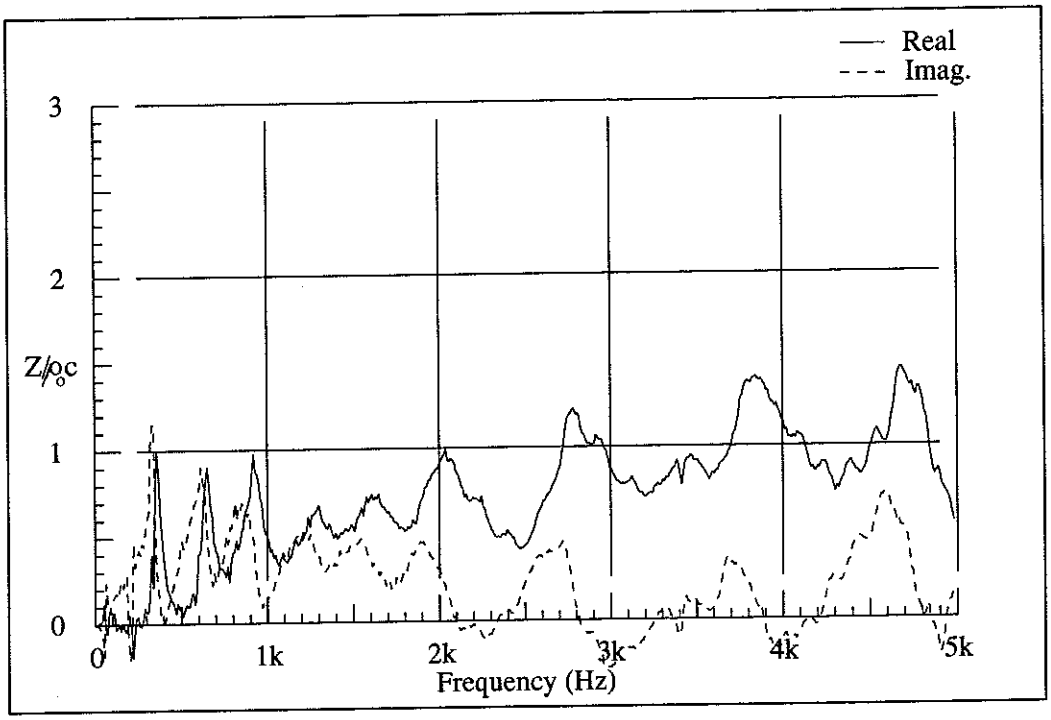

Figure 3.5.4b Measured Normalised Throat Impedance: Horn type 4; Fostex Sectoral.

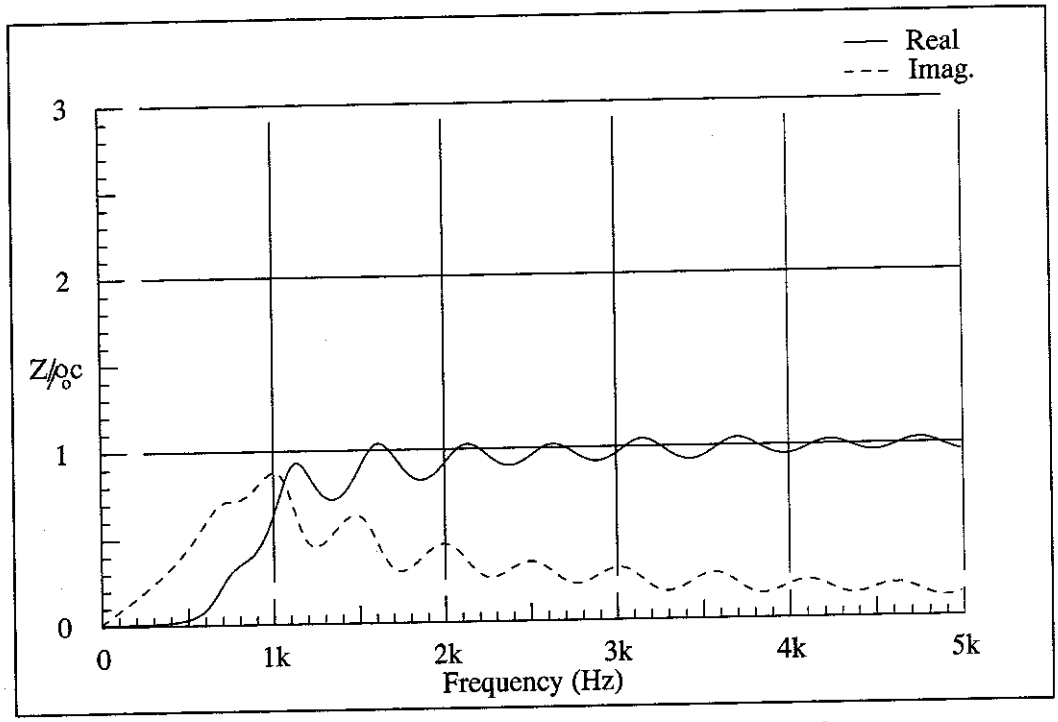

Figure 3.5.5a Thoretical Normalised Throat Impedance: Horn type 5; Large Axisymmetric (AX2).

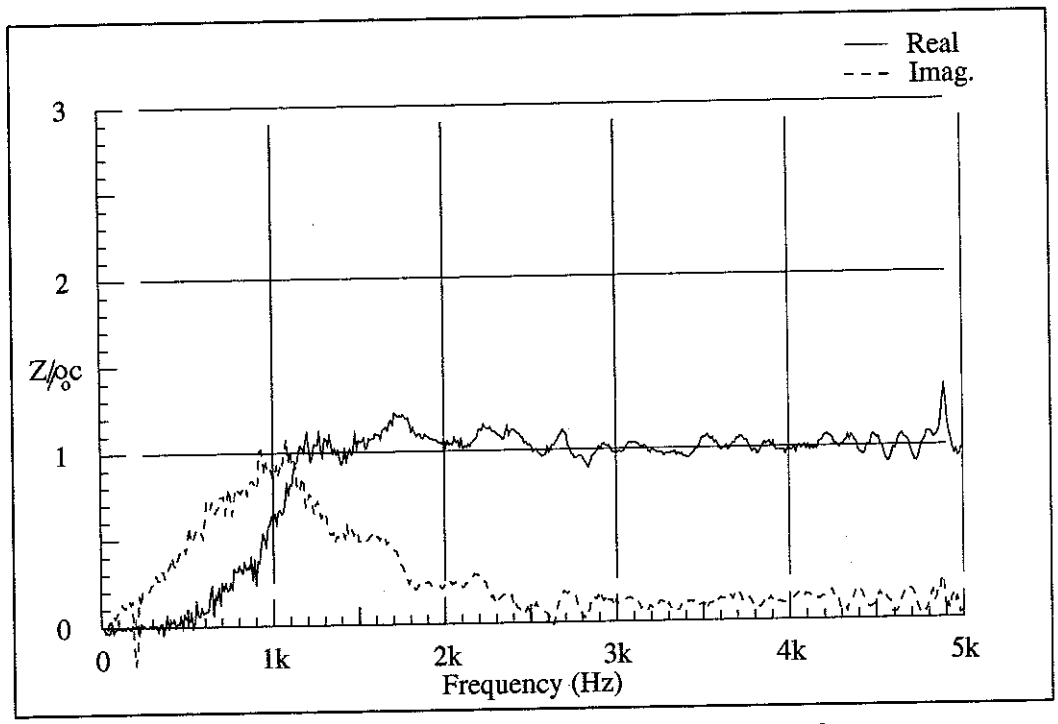

Figure 3.5.5b Measured Normalised Throat Impedance: Horn type 5; Large Axisymmetric (AX2).

3.3 TRANSFER IMPEDANCE

3.3.1 Measurement Method.

Calculation of the transfer impedance of a horn requires a knowledge of the pressure at the mouth (or in the far field) and the particle velocity at the throat. The former is straightforward, but the latter cannot easily be measured directly due to the problems mentioned above. To overcome this problem, the probe microphone used for the throat impedance measurements was extended to reach the mouth of the horns. Using this probe, measurements of pressure are taken at the throat and the mouth, each being referenced to the driving signal as above. The division of these measurements yields the pressure transfer function and subsequent multiplication by the previously measured throat impedance gives the transfer impedance.

3.3.2 Comparison between Theoretical and Measured Results.

Figures 3.6.1a and b to 3.6.5a and b show the theoretical and measured transfer impedances respectively for the horns described in appendix 3. The modulus of the transfer impedance is plotted in decibels as 20 Log($|Z_{tr}|$), and the phase as $\angle Z_{tr}$.

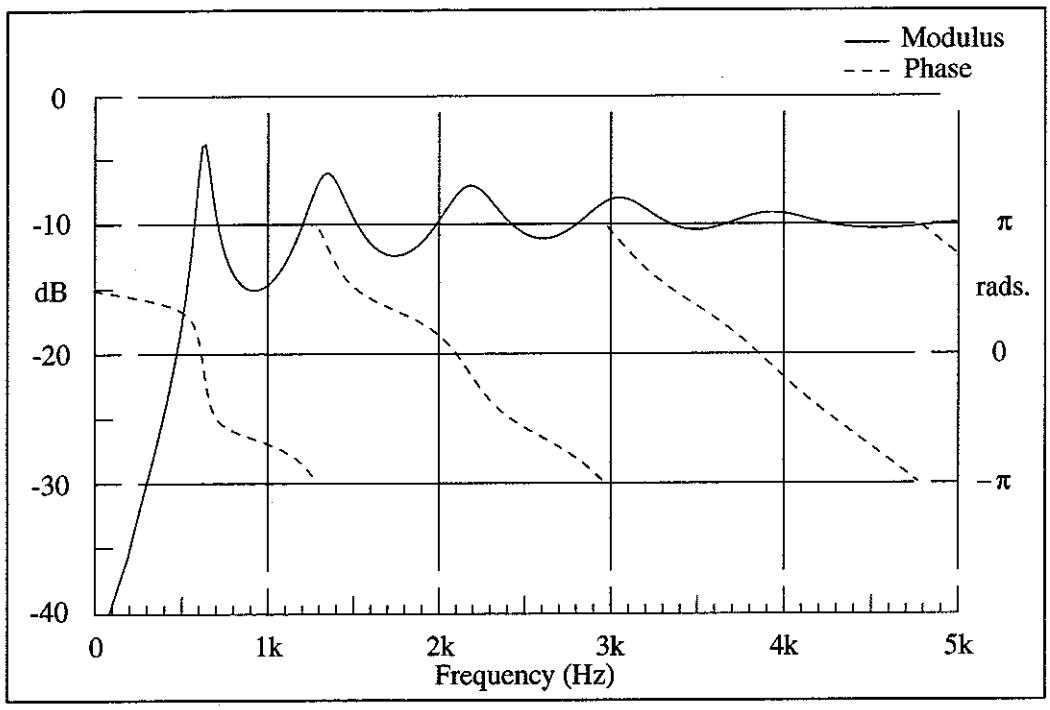

Figure 3.6.1a Theoretical Normalised Transfer Impedance: Horn type 1; Small Axisymmetric (AX1).

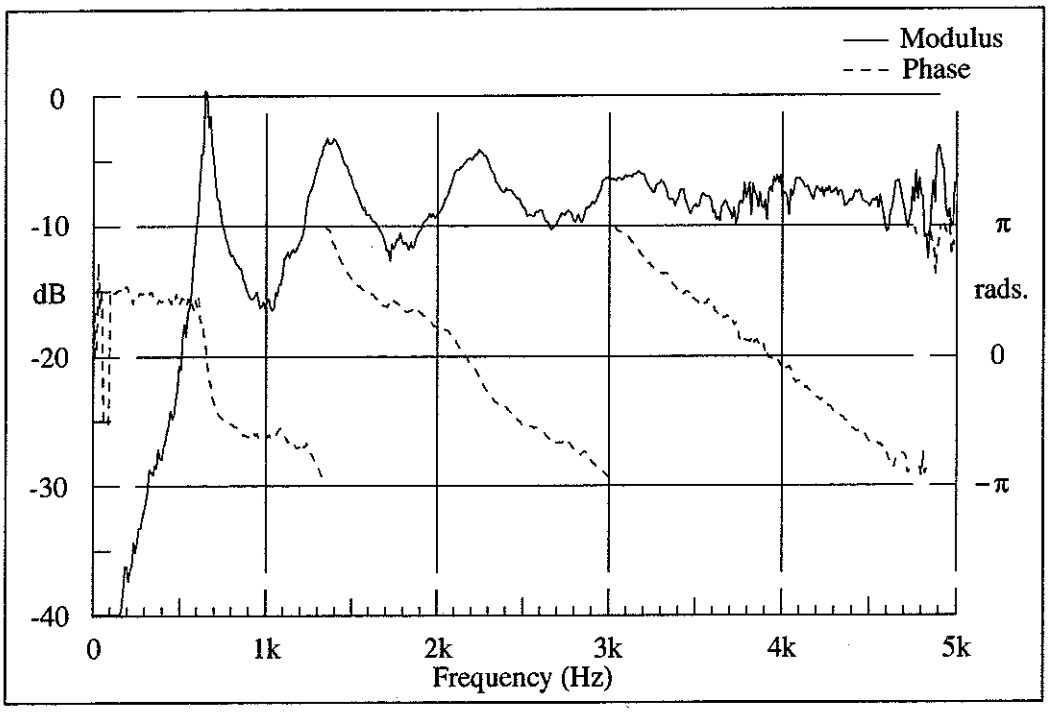

Figure 3.6.1b Measured Normalised Transfer Impedance: Horn type 1; Small Axisymmetric (AX1).

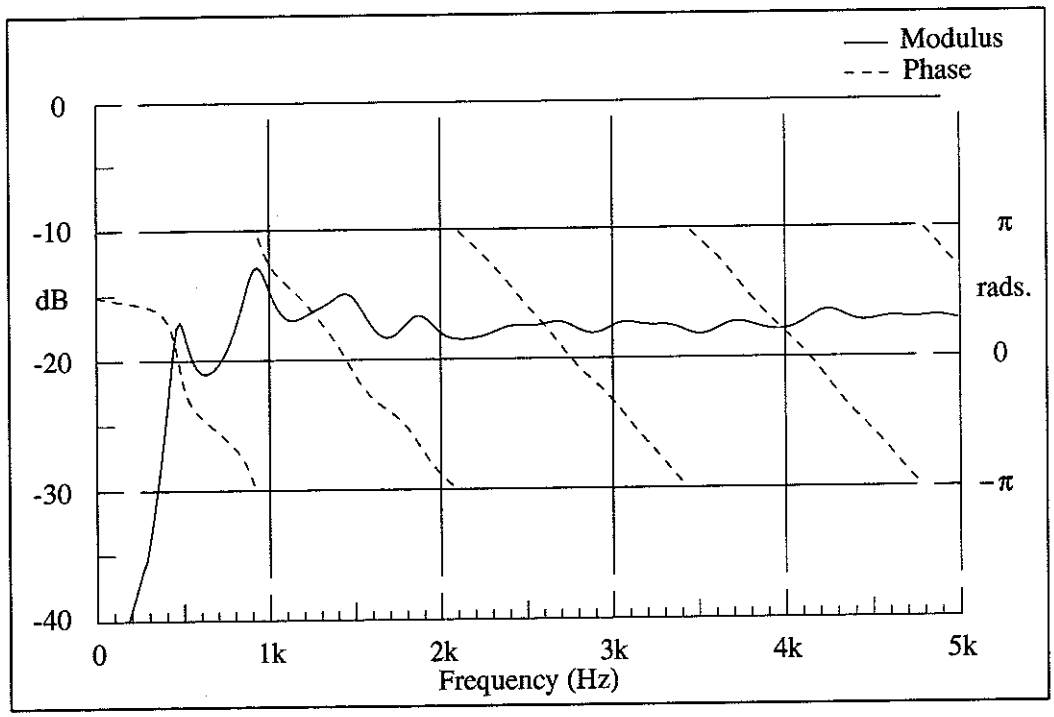

Figure 3.6.2a Theoretical Normalised Transfer Impedance: Horn type 2; Reflexion Arts Rectangular.

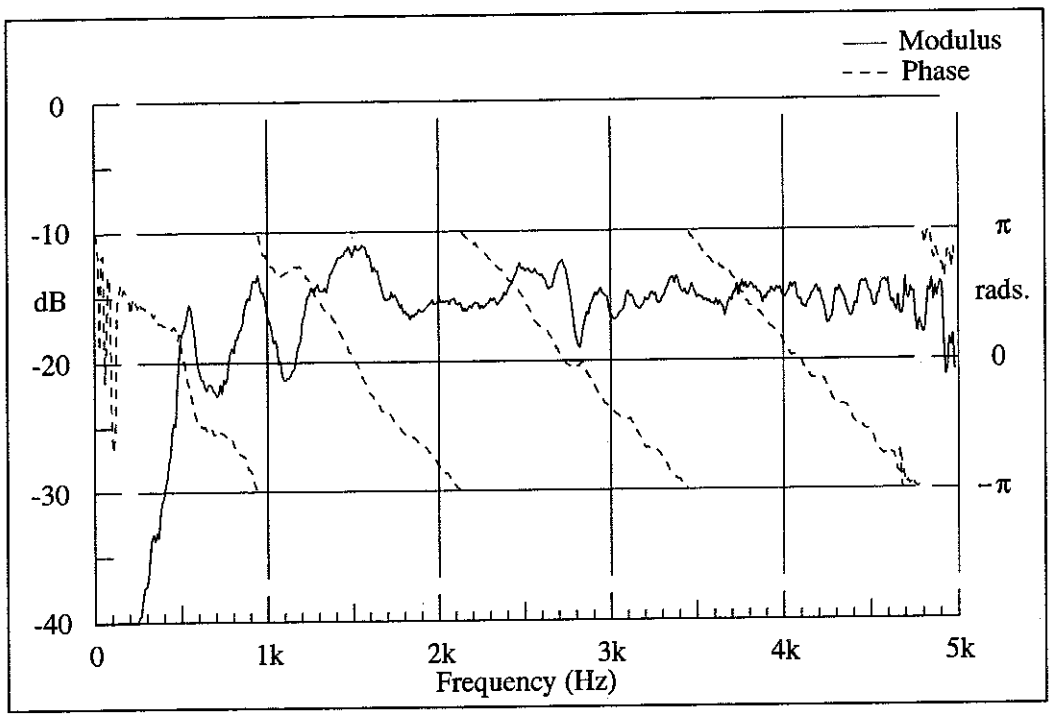

Figure 3.6.2b Measured Normalised Transfer Impedance: Horn type 2; Reflexion Arts Rectangular.

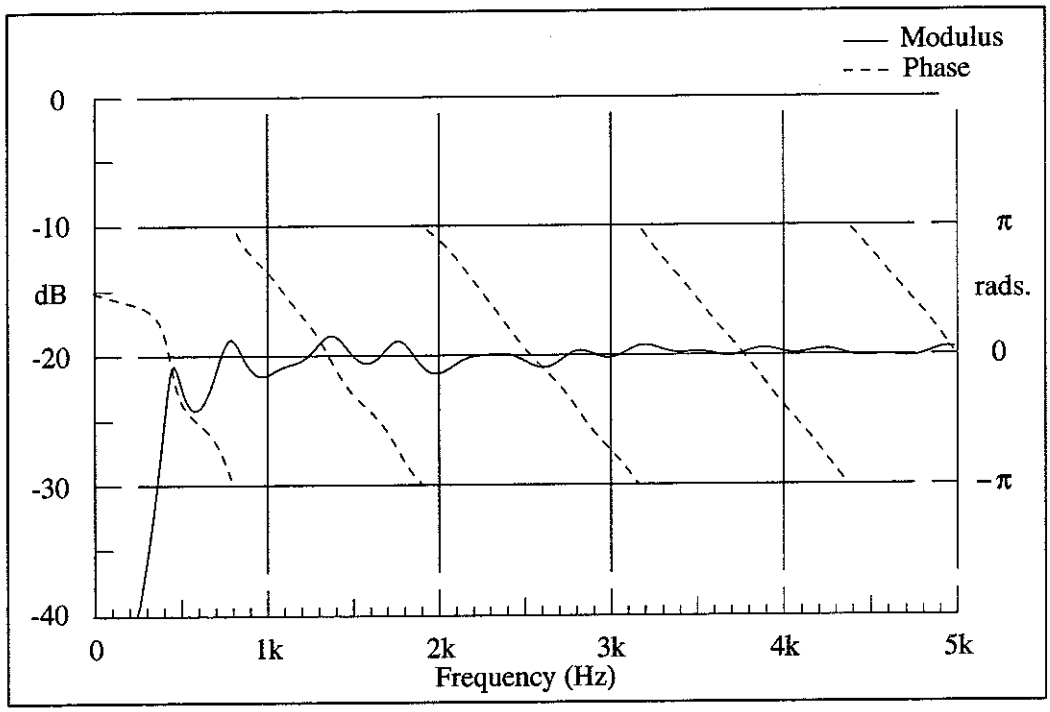

Figure 3.6.3a Theoretical Normalised Transfer Impedance: Horn type 3; Vitavox Rectangular.

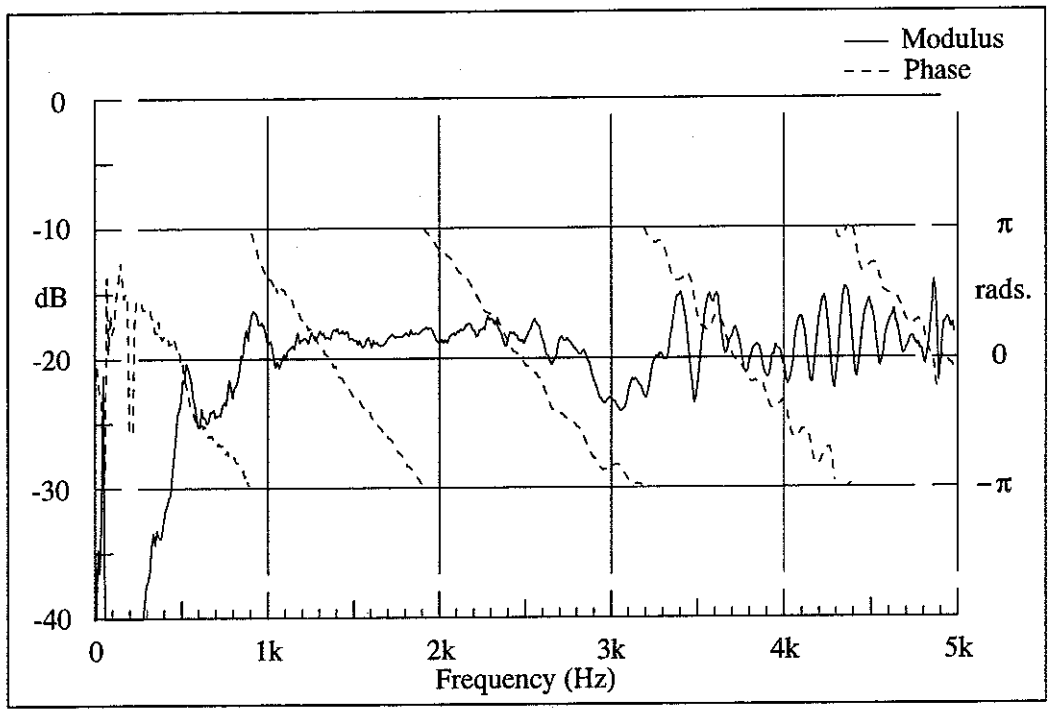

Figure 3.6.3b Measured Normalised Transfer Impedance: Horn type 3; Vitavox Rectangular.

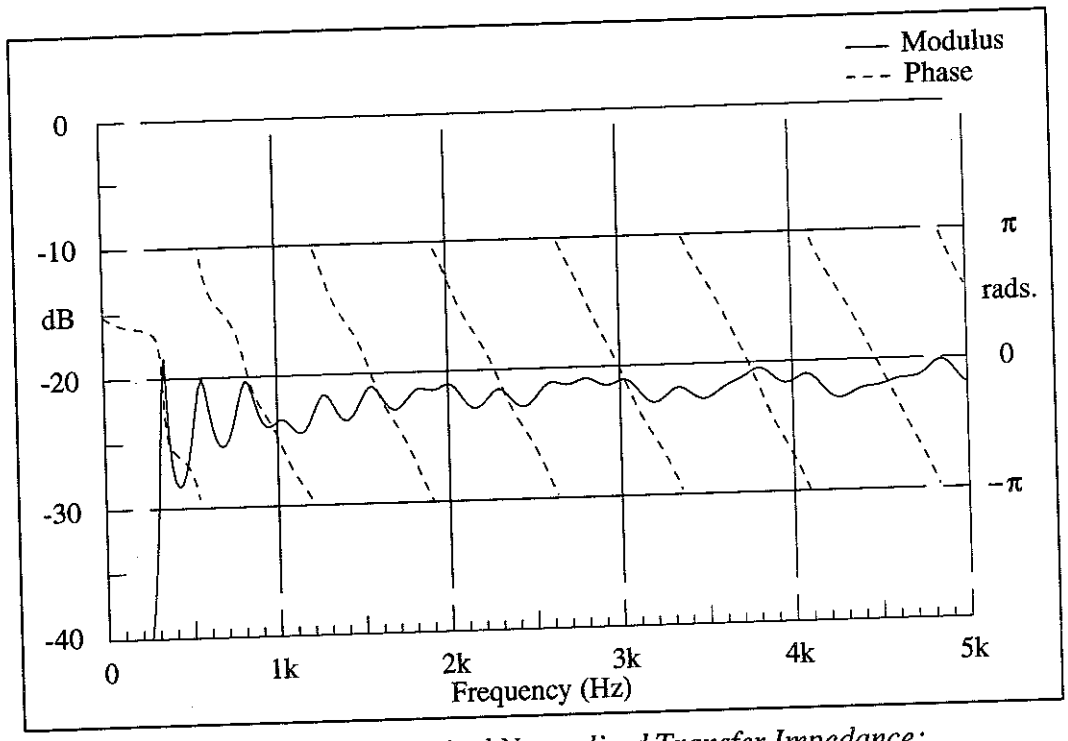

Figure 3.6.4a Theoretical Normalised Transfer Impedance: Horn type 4; Fostex Sectoral.

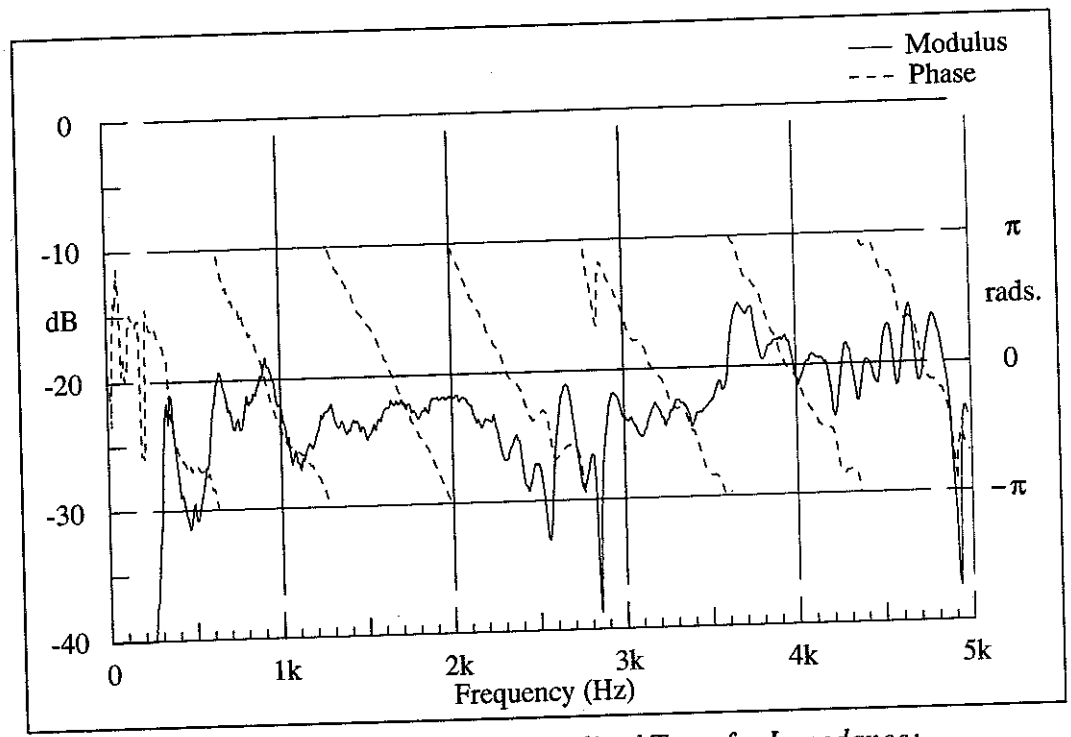

Figure 3.6.4b Measured Normalised Transfer Impedance: Horn type 4; Fostex Sectoral.

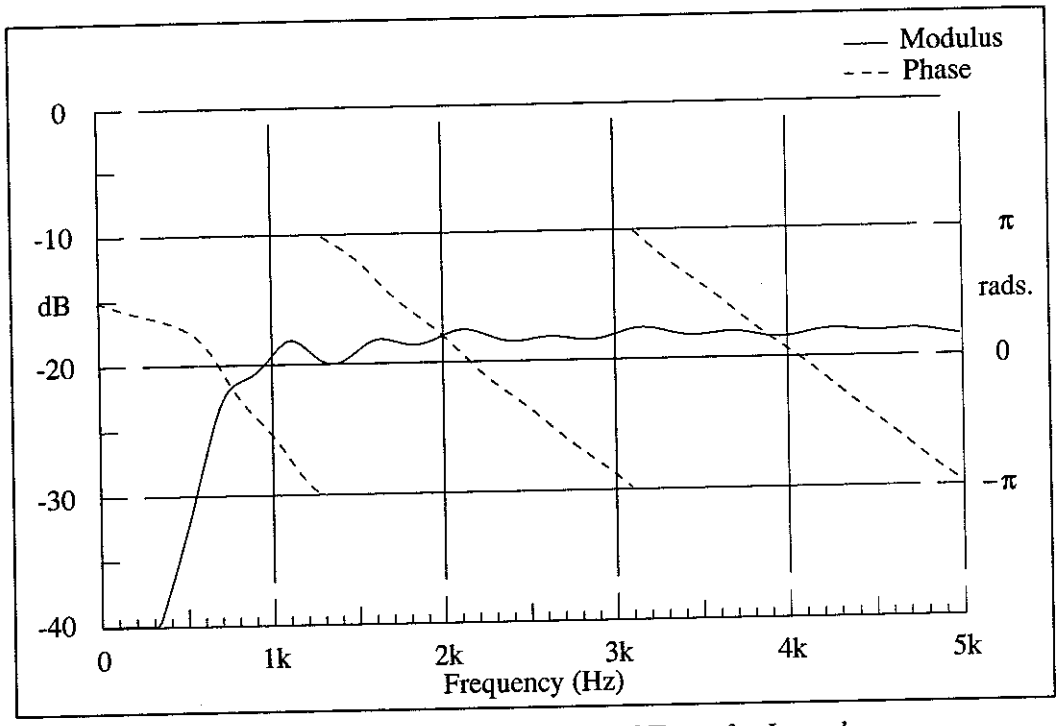

Figure 3.6.5a Theoretical Normalised Transfer Impedance: Horn type 5; Large Axisymmetric (AX2).

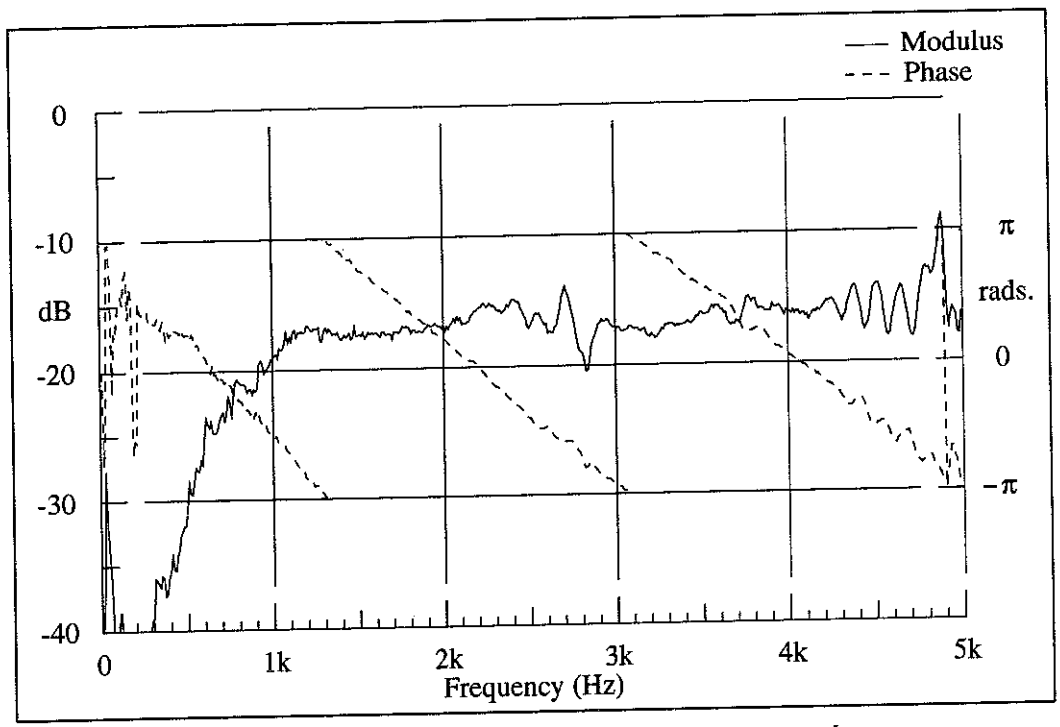

Figure 3.6.5b Measured Normalised Transfer Impedance: Horn type 5; Large Axisymmetric (AX2).

3.4 AXIAL PRESSURE DISTRIBUTION

3.4.1 Measurement Method.

The extension to the microphone probe mentioned above makes possible the measurement of the axial pressure distribution within the horn. Measurements are taken of the transfer functions between various points along the axis and the throat in a similar manner to that for the transfer impedance above.

3.4.2 Comparison between Theoretical and Measured Results.

Figures 3.7.1a, b, c and d to 3.7.5a, b, c and d show the modulus and phase of the theoretical and measured axial pressure distributions respectively for the horns described in appendix 3. To ease interpretation, the phase plots are normalised at each frequency by the distance travelled at the speed of sound.

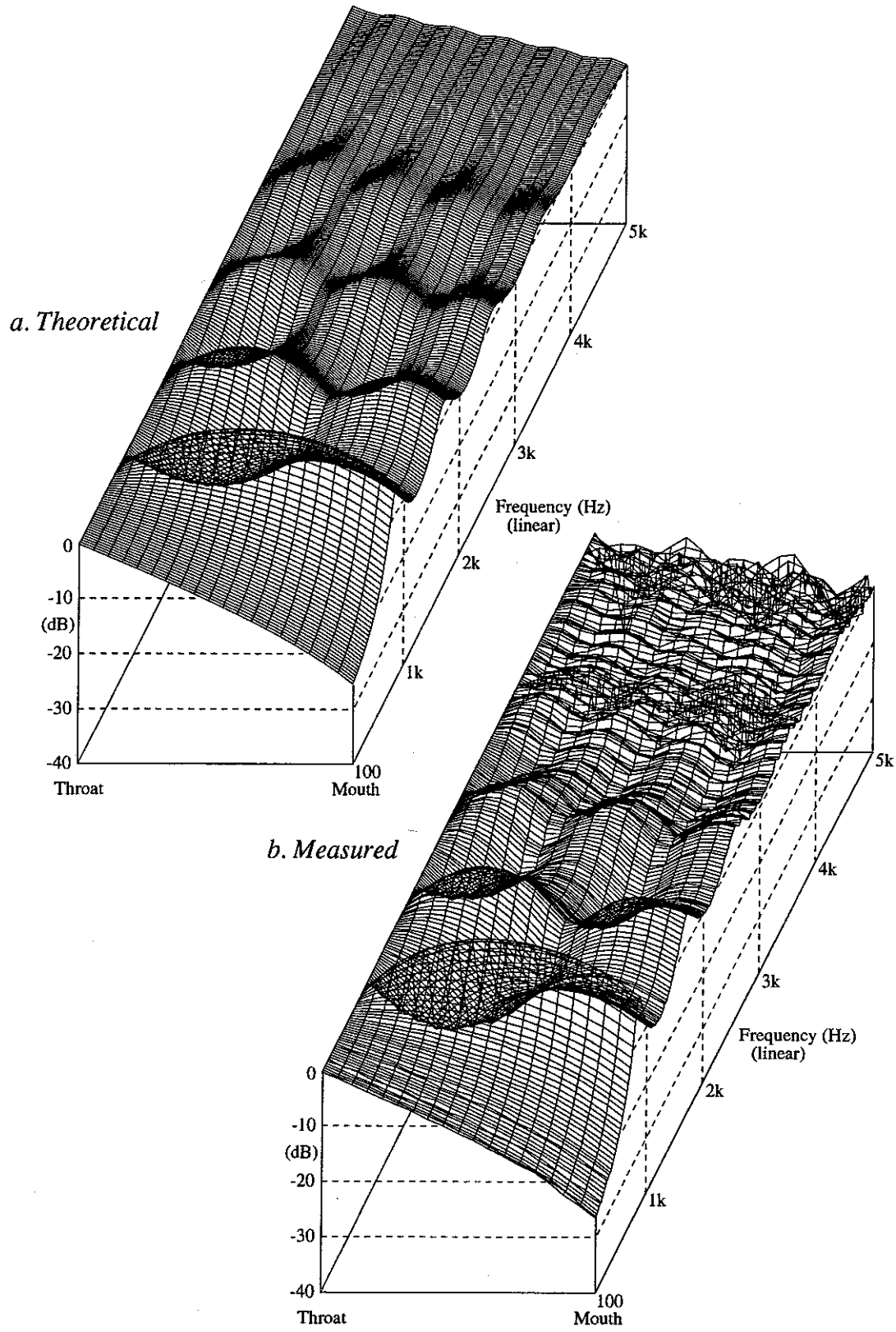

Figures 3.7.1 Modulus of Axial Pressure Distribution: Horn type 1; Small Axisymmetric (AX1).

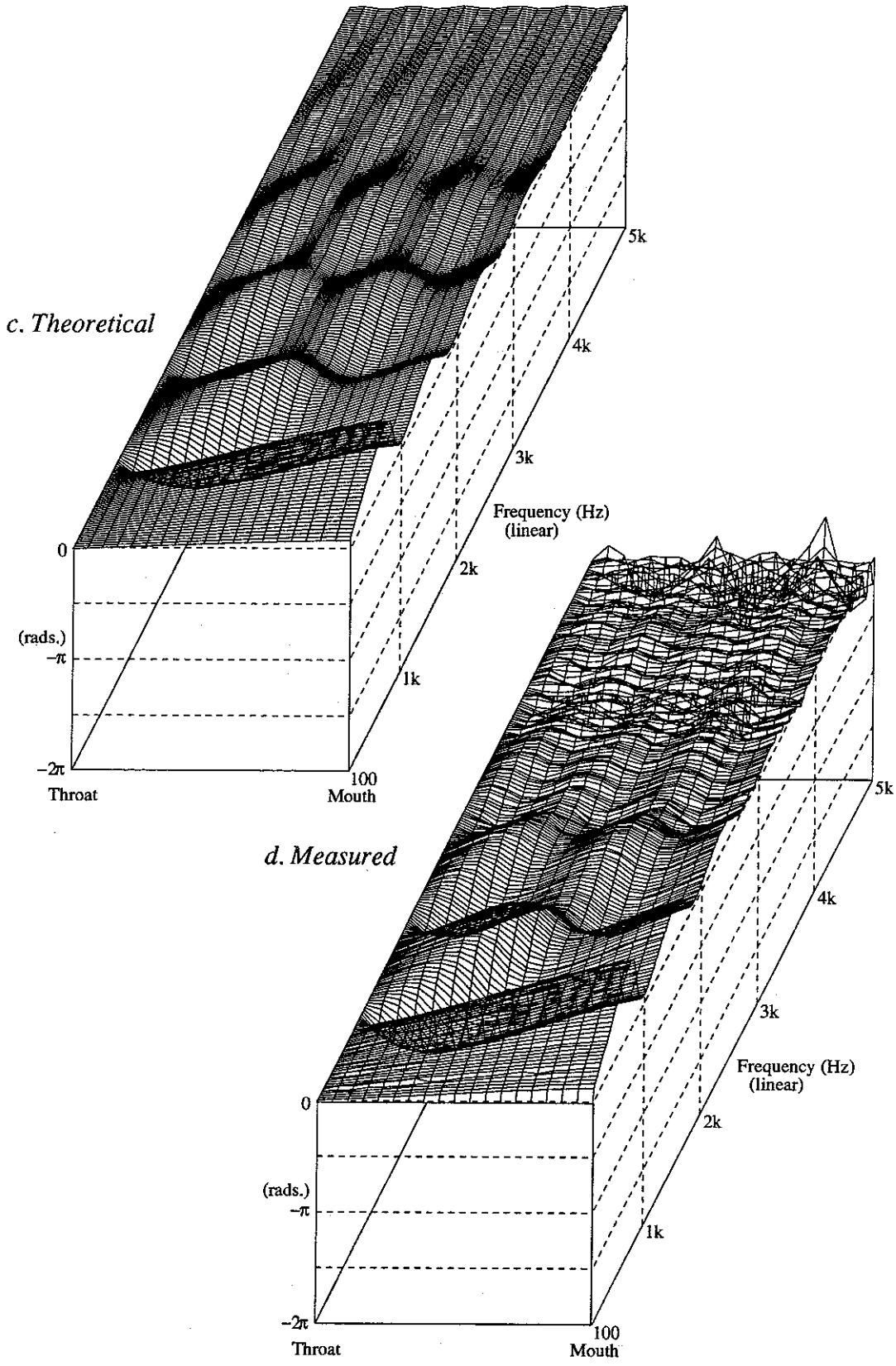

Phase of Axial Pressure Distribution:
Horn type 1; Small Axisymmetric (AX1).

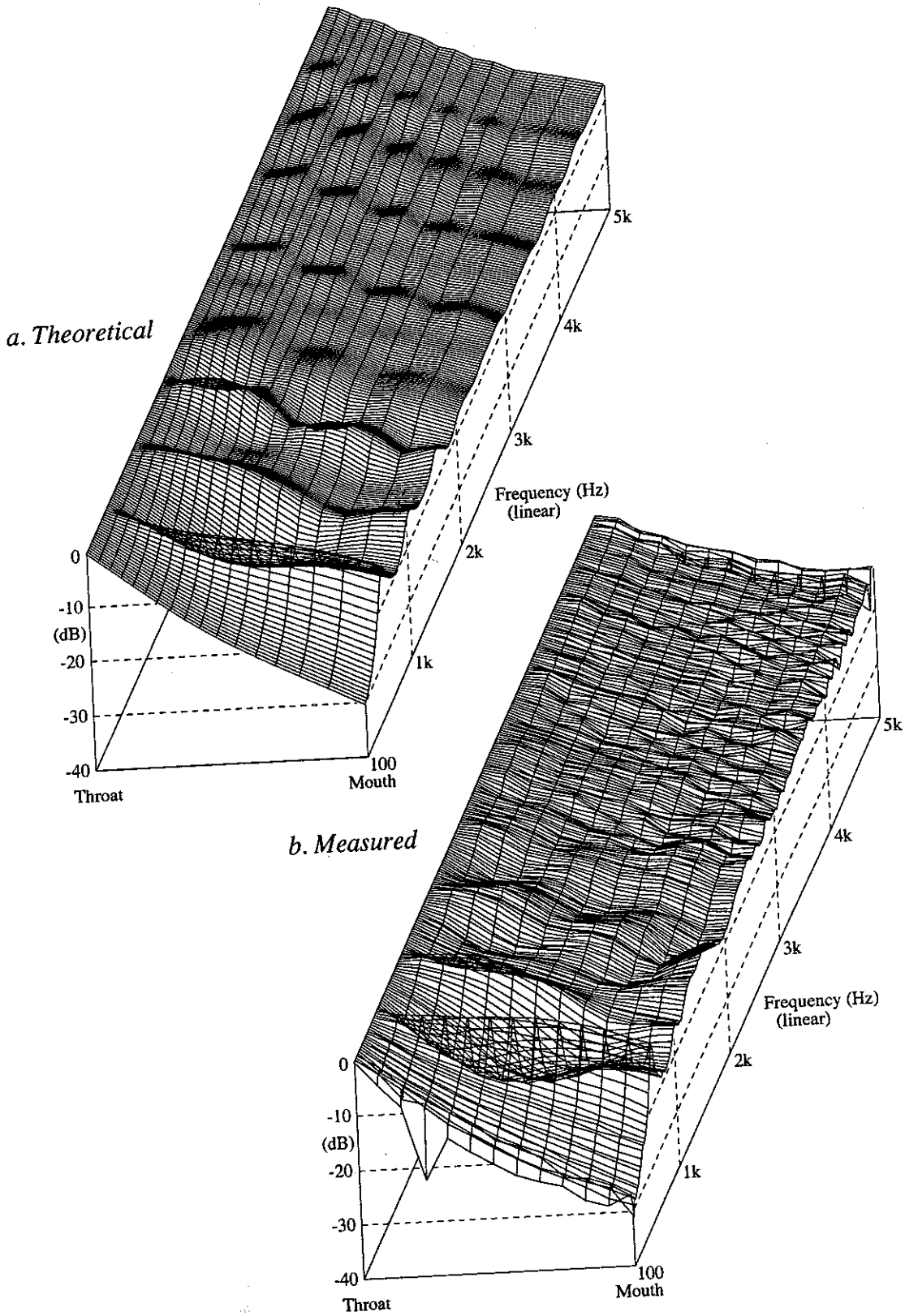

Figure 3.7.2 Modulus of Axial Pressure Distribution: Horn type 2; Reflexion Arts Rectangular.

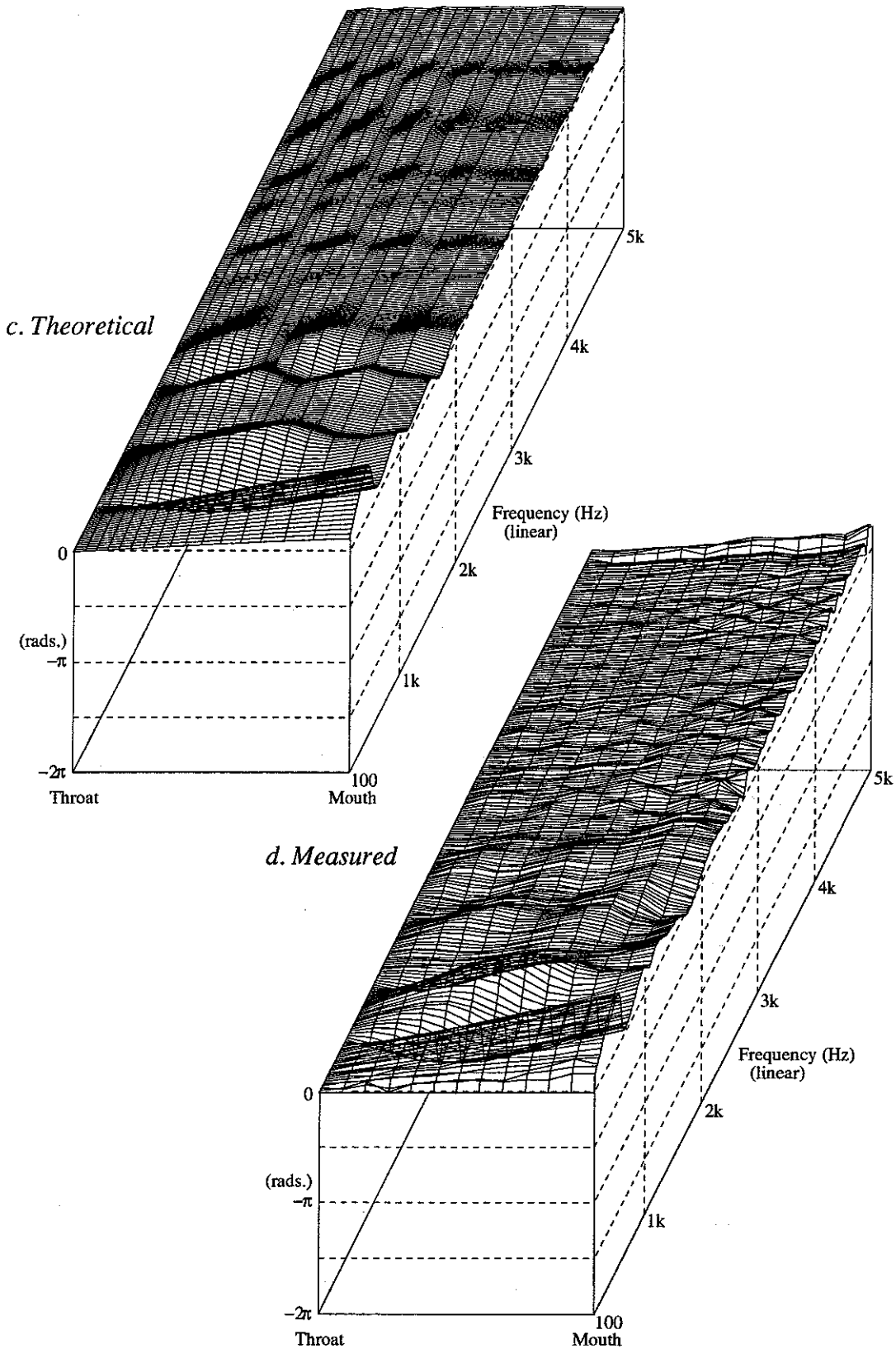

Phase of Axial Pressure Distribution:
Horn type 2; Reflexion Arts Rectangular.

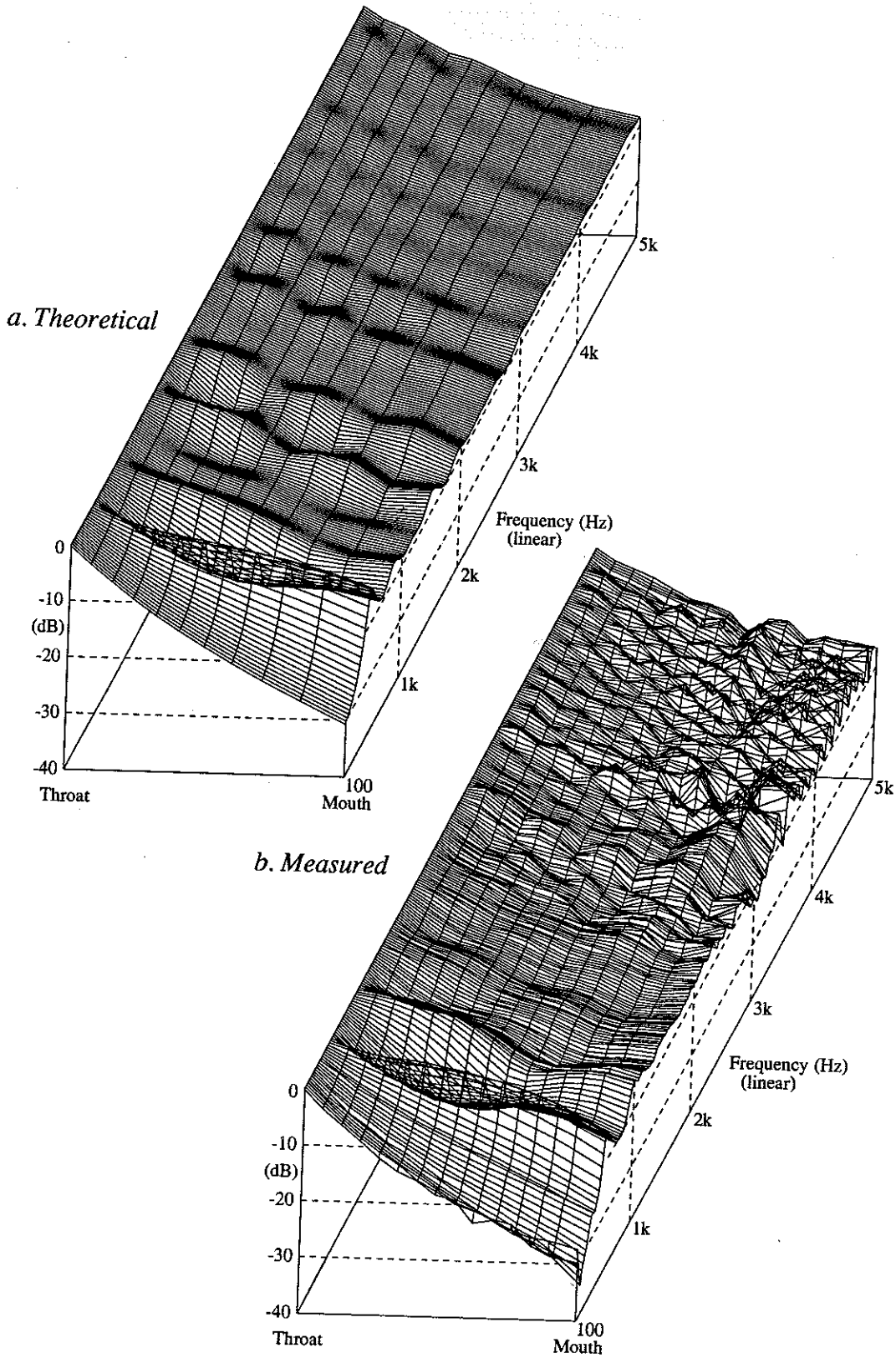

Figure 3.7.3 Modulus of Axial Pressure Distribution: Horn type 3; Vitavox Rectangular.

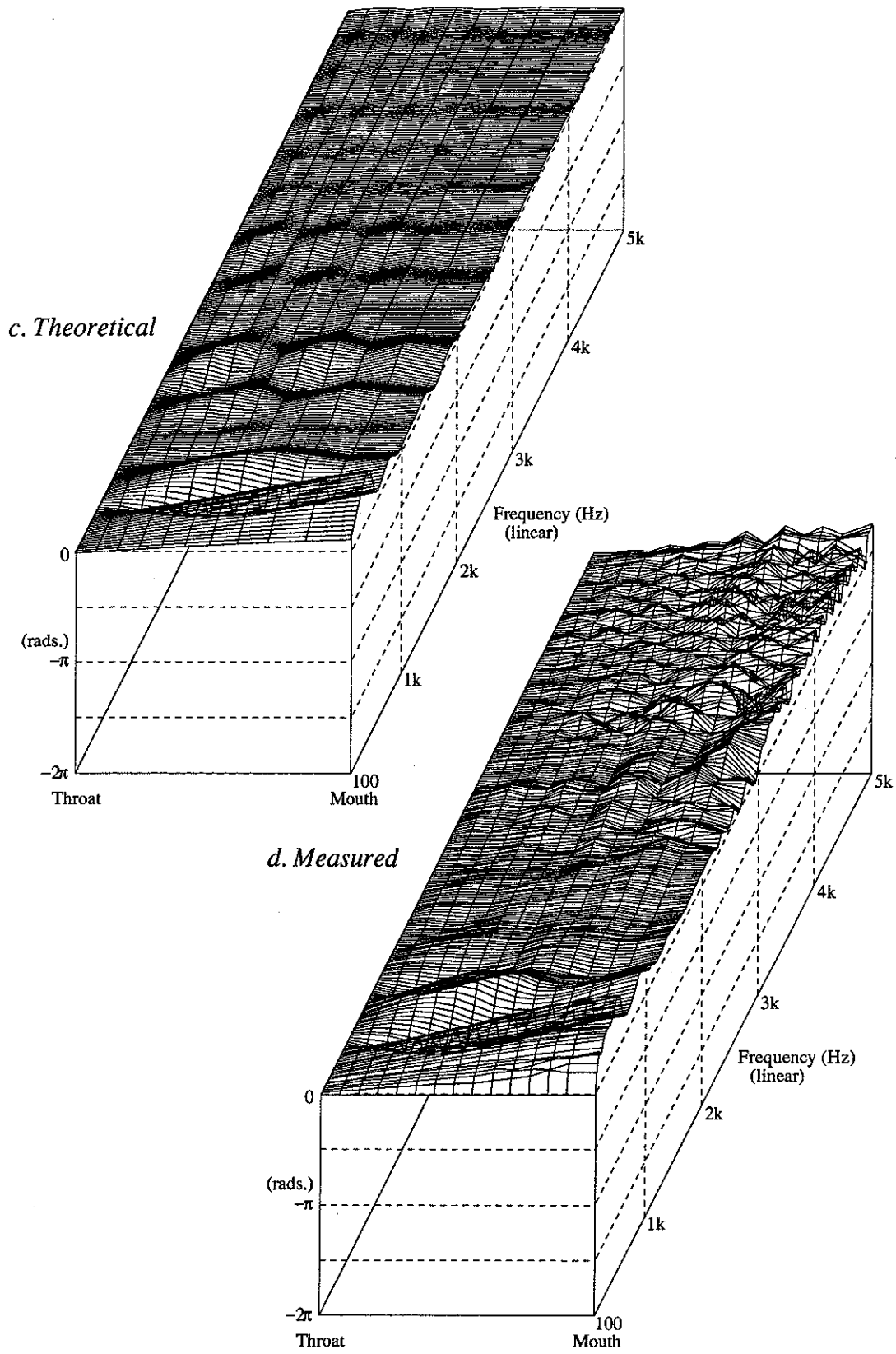

Phase of Axial Pressure Distribution:
Horn type 3; Vitavox Rectangular.

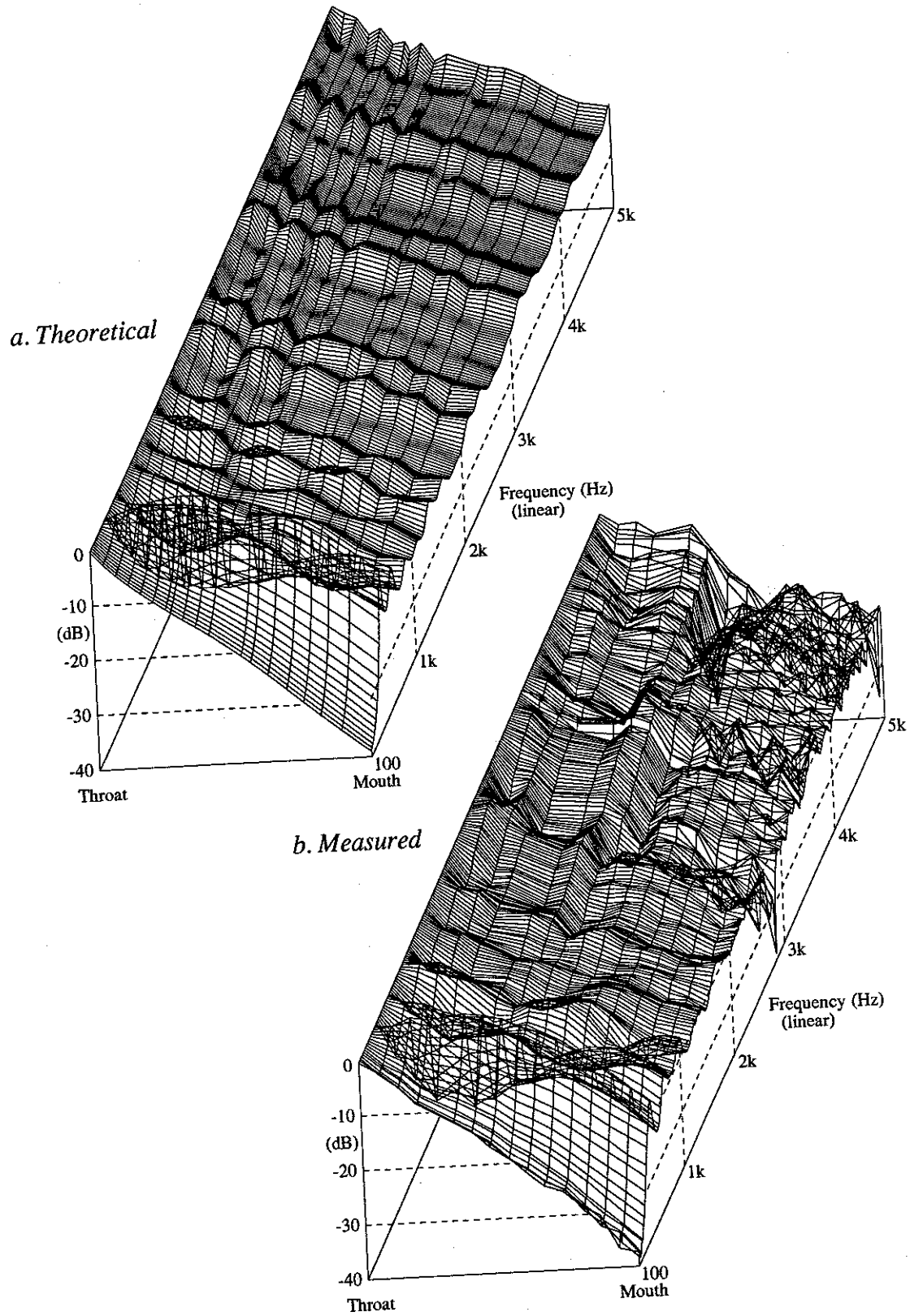

Figure 3.7.4 Modulus of Axial Pressure Distribution: Horn type 4; Fostex Rectangular.

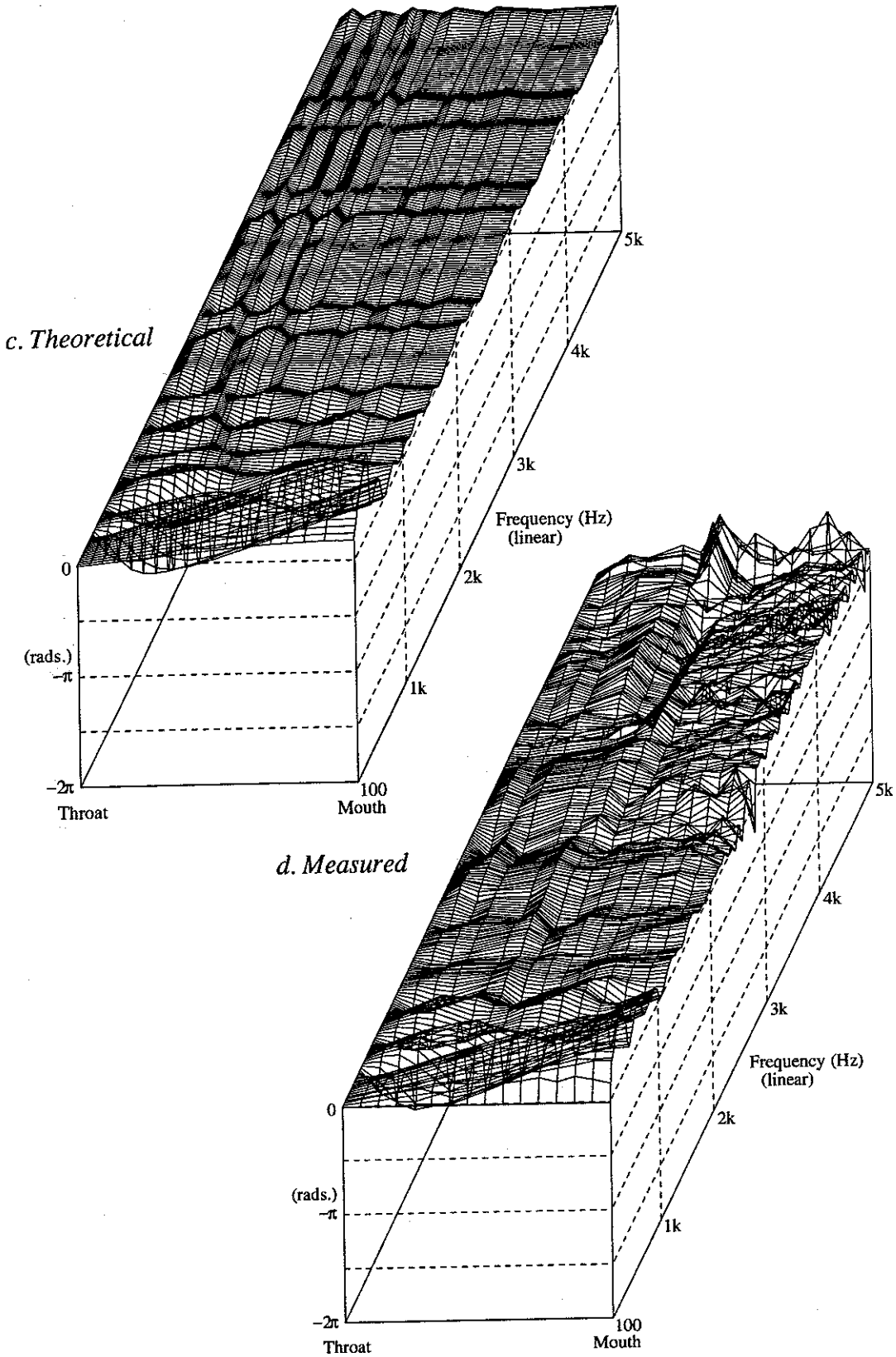

Phase of Axial Pressure Distribution:
Horn type 4; Fostex Rectangular.

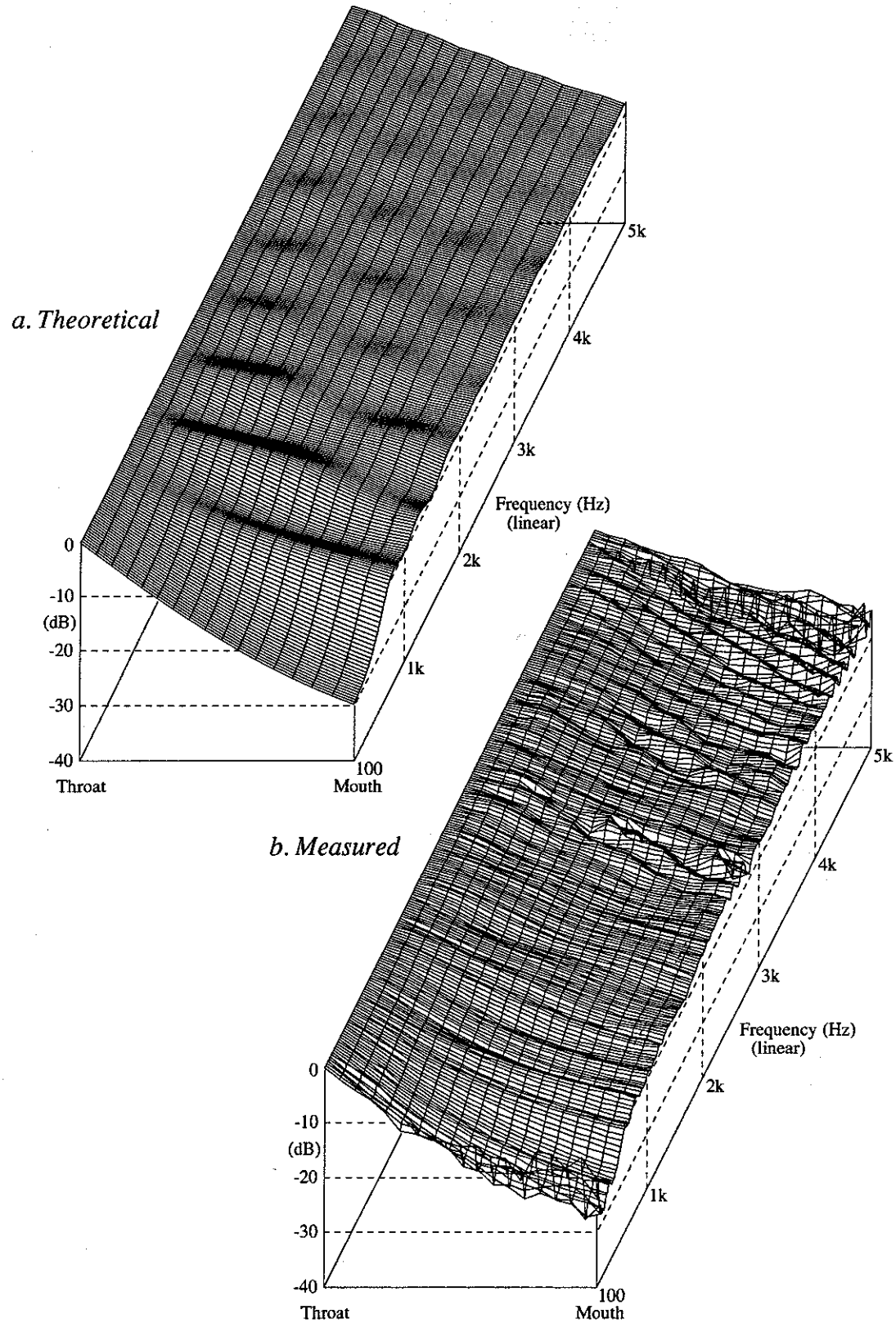

Figure 3.7.5 Modulus of Axial Pressure Distribution: Horn type 5; Large Axisymmetric (AX2).

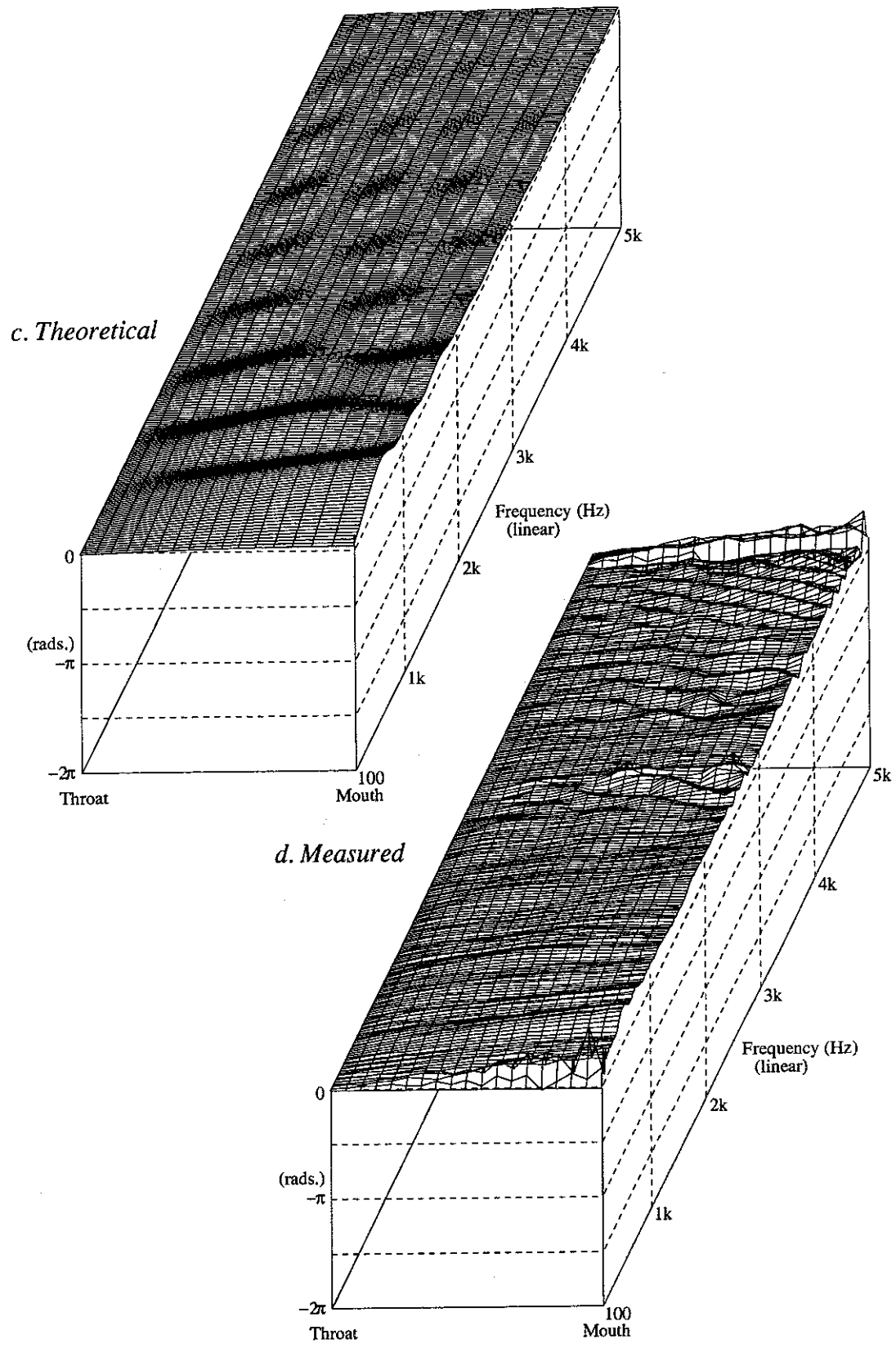

Phase of Axial Pressure Distribution:
Horn type 5; Large Axisymmetric (AX2).

3.5 COMPARISON BETWEEN THEORETICAL AND MEASURED RESULTS

The following discussion refers to the plots shown in figures 3.5 to 3.7, it is divided into three main sections; Throat Impedance, Transfer Impedance and Axial Pressure Distribution.

3.5.1 Throat Impedance.

For all of the throat impedance measurements, the narrow small amplitude peaks at high frequencies are due to reflections from the imperfect anechoic walls of the receiving room, and the 'noise' present on the measurement of horn type 1 at the frequency extremes is due to driver bandwidth limitations causing a poor signal to noise ratio (this measurement was taken before the filter was fitted in the driving circuit). A severe 'dip' in the output response of the impedance tube driver at about 2800Hz which could not be corrected by filtering (response is near zero) also causes some problems in the measurements at that frequency.

Figures 3.5.1a and b show the theoretical and measured throat impedance for horn type 1; the small axi-symmetric (AX1). Because of the low flare rate of this horn, fairly accurate modelling of the throat impedance was possible without the need for the wavefront area extension to the model, taking the mouth impedance to be that of a baffled piston, although all of the results shown have been calculated using the extension. The presence of gross reflections from the small mouth of the horn causing large peaks and troughs in the impedance curve can be seen in both the theoretical and measured results, with close agreement between them in both frequency and magnitude. The large variations in the real part of the impedance could cause variations in the power output frequency response of this horn which would be undesirable for high quality applications.

Figures 3.5.2a and b show the theoretical and measured throat impedance for horn type 2; the Reflexion Arts rectangular. Because of the rapid horizontal flare rate of this horn, modelling without considering the wavefront areas led to gross errors; indeed including the lips was impossible. With the inclusion of the model extension however, good agreement can be seen between the theoretical (figure 3.5.2a) and measured (figure 3.5.2b) throat impedances. The power frequency response of this horn can be seen to be very much smoother than that for the small axi-symmetric horn above, indicating better suitability to high quality applications.

Figures 3.5.3a and b show the theoretical and measured throat impedance for horn type 3; the Vitavox rectangular. Fair agreement can be seen between the theoretical throat impedance and the measurement. The higher peaks in the measured impedance at low frequencies indicate poorer impedance matching between the mouth and the free field than predicted. The real part of the impedance can be seen to be assymptotic to a value less than one as frequency is increased. This is due to a short (approx. 1 mm) section of rapid expansion at the throat of the horn. The general smoothness of the power frequency response would indicate that this horn could be suitable for high quality applications.

Figures 3.5.4a and b show the theoretical and measured throat impedance for horn type 4; the Fostex sectoral. As described in appendix 3, this horn is strengthened by three pillars of about 12 mm diameter between the top and bottom surfaces. Correction in the modelling for the presence of the pillars in the flare was achieved by calculating the reduction in area of the wavefront at positions where it intersected the pillars. The broad peaks and troughs in impedance seen in both the theoretical and measured impedances from about 1500 Hz upwards are due to reflections set up by the pillars, which are encountered by a curved wavefront at the same position as the change in cross-sectional shape of the horn. The narrow peaks at low frequencies are due to reflections from the mouth. The low value of the real part of the impedance at low frequencies indicates poor efficiency and is due to the approximately conical flare of the horn near the throat. Because of the reflections from the pillars and the consequent uneven power frequency response, and poor loading at low frequencies for the size of the horn, this horn would appear to be unsuitable for high quality applications.

Figures 3.5.5a and b show the theoretical and measured throat impedances for horn type 5; the large axi-symmetric (AX2). This horn was designed, using the one-parameter model, to have as good a throat impedance characteristic as was possible within size constraints. The lack of peaks and troughs in both the theoretical and measured impedances shows that this exercise was a success; indeed, the measured impedance shows an even smoother characteristic than the theoretical prediction. The relative lack of peaks and troughs in the impedance shows that the transition between the horn mouth and the free-field is very gradual for this design, and the gentle roll-off below cut-off indicates an apparent transition from an exponential-type flare at the throat of the horn to a more conical-type flare at the mouth. Figure 3.8 shows a comparison between the effective radial profile for this horn assuming

plane-waves and that for curved wavefronts as calculated by the model. It can be seen that the flare near the mouth of the horn is indeed nearly conical when the curved wavefront areas are taken into account. The very smooth power frequency response of this horn would indicate that it could be ideal for high quality applications.

One of the major sources of error in the predictions of the throat impedance of these horns is the difficulty in accurately measuring the dimensions of the horn. This is important, and also most difficult, in the narrow regions of the horn near the throat where the model results, and indeed those for real horns, are very sensitive to small changes in geometry.

It can be seen from these plots that the close agreement between predictions and measurements indicates that both are reasonably accurate and that the one-parameter model can be used with confidence to predict the one-parameter behaviour of a horn.

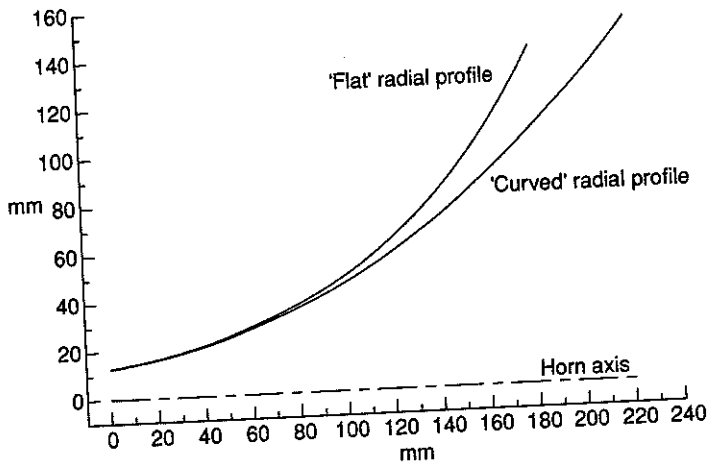

Figure 3.8 Comparison between Effective Radial Profile of Horn Type 5 to Plane and Curved Wavefronts.

3.5.2 Transfer Impedance.

Because the transfer impedance is derived from the product of the throat impedance and the pressure transfer function from one end of the horn to the other, the measurement errors described above with reference to the throat impedance measurements are also apparent here, along with a further 'comb-filtering' at high frequencies due to the close proximity of the probe microphone to the imperfect measurement room boundaries when measuring the pressure at the mouth of the horns.

Figures 3.6.1a and b show the theoretical and measured transfer impedances for horn type 1. Fair agreement can be seen between the two plots but the amplitude of the measured peaks is greater than the model predicts. The measured transfer impedance can be seen to be two or three dB higher than the theoretical at high frequencies. This is probably due to on-axis 'beaming' which cannot be taken into account in a one-parameter model.

Figures 3.6.2a and b show the theoretical and measured transfer impedance for horn type 2. 2 or 3dB of beaming can again be seen at high frequencies. The dip in response at 2.8kHz is due to the driver problem mentioned above. The measurement shows a broad peak in transfer impedance at around 1.5kHz and a narrow peak at 2.5kHz which are not present in the theoretical prediction, and cannot be explained from the throat impedance results (see section 4.2).

Figures 3.6.3a and b show the theoretical and measured transfer impedances for horn type 3. Beaming is slight but the uneven response at and around 3.1kHz indicates the presence of severe resonant transverse pressure variations. This behaviour is probably due to a pronounced mechanical 'ring' of the structure of the horn noticed during measurements (see section 4.2).

Figures 3.6.4a and b show the theoretical and measured transfer impedances for horn type 4. Gross transverse pressure variations can be seen between 2 and 4kHz. This may be due to the one-parameter behaviour of the horn being upset by the presence of the pillars.

Figures 3.6.5a and b show the theoretical and measured transfer impedances for horn type 5. Good agreement can be seen with only a small amount of beaming and very little transverse pressure variation evident.
These plots clearly indicate the limitations of the one-parameter model for the prediction of the performance of a horn when the design of the horn disturbs in some way the clean propagation of waves from throat to mouth. Comparison between one-parameter predictions and measurements can however prove valuable for determining the causes of this type of behaviour.

3.5.3 Axial Pressure Distributions.

Figures 3.7.1a to d show the amplitude and phase of the theoretical and measured axial pressure distributions for horn type 1. As expected from the reasonably good

transfer impedance results, there is close agreement between the theoretical results and the measurements due to the essentially one-parameter behaviour of this horn. The phase dispersion associated with horn cut-off can be seen by the rising phase response with frequency below cut-off. The rise is due to the plots having been corrected for the distance propagated as if only a plane progressive wave existed within the horn. The uncorrected phase response would be almost flat below cut-off followed by a rapid fall as frequency is raised and distance along the horn is increased. The almost pure standing wave field set up by reflections from the mouth is clearly seen in both sets of plots.

Figures 3.7.2a to d show the amplitude and phase of the theoretical and measured axial pressure distributions for horn type 2. The cut-off phenomenon is again clearly shown in both sets of results and good agreement is evident between them. The regular pattern of peaks and troughs from throat to mouth indicate that the standing wave field is almost entirely due to mouth reflections.

Figures 3.7.3a to d show the amplitude and phase of the theoretical and measured axial pressure distributions for horn type 3. The standing wave field can be seen to be less 'pure' than for the horns above, due to the presence of transverse pressure variations which extend from within the horn out to the mouth.

Figures 3.7.4a to d show the amplitude and phase of the theoretical and measured axial pressure distributions for horn type 4. The most notable feature in both the theoretical and measured results is the standing wave field near the throat set up by the pillars. The disruptive effect that the pillars have on the one-parameter behaviour of the horn can be seen by comparing the two distributions "downstream" of the pillars. The presence of the gross transverse pressure variations near the mouth of the horn can clearly be seen. Note: the 'missing' set of points about one quarter the way along the horn in the measured result is due to one of the pillars being on axis preventing a probe measurement at that point.

Figures 3.7.5a to d show the amplitude and phase of the theoretical and measured axial pressure distributions for horn type 5. Very little evidence of a standing wave field can be seen in both sets of results and the shallow cut-off is apparent from the relatively flat phase response at low frequencies.

3.5.4 Cepstral Analysis of Results.

In order to further identify any reflections that occur at the mouth or within the flare of a horn, a form of power cepstrum is calculated from the modulus of the measured throat impedance. In this analysis, the frequency domain representation of the modulus of the throat impedance is treated as a spectrum; the power cepstrum then being calculated from this spectrum using Fourier transforms. Cepstral analysis is useful for identifying echoes or reflections and pin-pointing them in time. Such reflections show up on the equivalent spectrum as 'comb filtering' or a series of peaks and troughs regularly spaced in frequency, but when more than one reflection is present, interpretation can be difficult; each reflection shows as an individual 'spike' on a cepstrum so the reflections are thus more easily separated and identified. The cepstrum plot has an *x*-axis with units of time, so with a knowledge of the speed of sound, the distance from the throat to the reflection can be estimated. Figures 3.9.1 to 3.9.5 show the cepstra calculated from the measured throat impedance of horn types 1 to 5 respectively. The plots have two *x*-axis scales, one of time and one of axial distance to a reflection calculated using the speed of sound at the time the measurements were taken; thus a reflection from the mouth of a horn should show as a spike shifted along the *x*-axis to a point roughly corresponding to the length of the horn. These distances can only be approximate due to the phase dispersion effects of the horn cut-off and will be 'smeared' in time by any complex, frequency dependent reflection coefficients. Note: to aid clarity, the log impedance spectra were scaled to have an average value of zero; the '0 seconds' spike on the cepstra thus has a value of zero. The arrow on the 'distance' scale of each plot indicates the physical length of the horn flare.

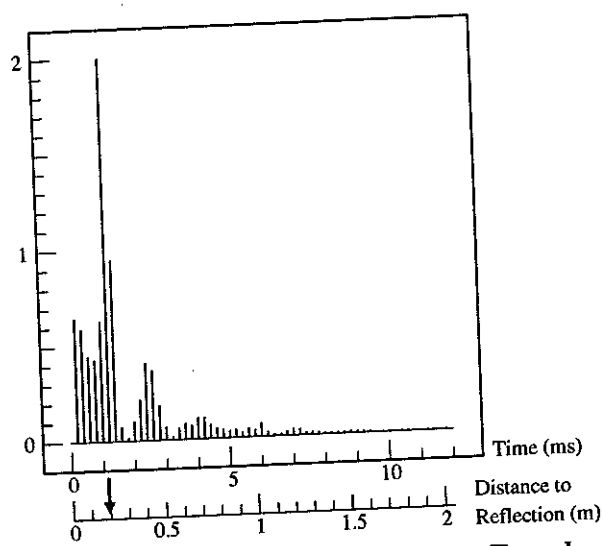

Figure 3.9.1 Power Cepstrum: Horn Type 1.

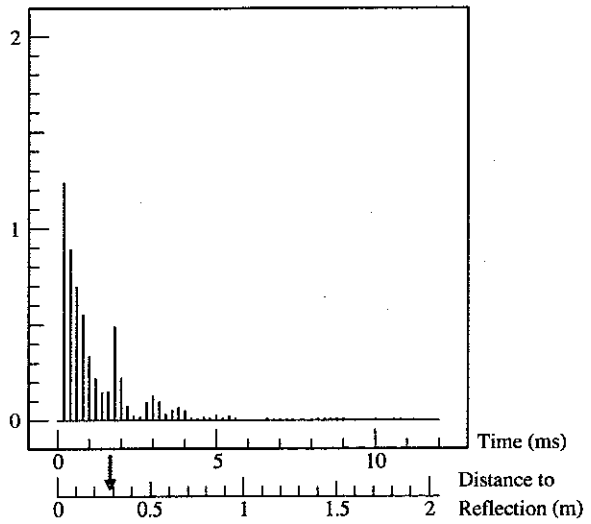

Figure 3.9.2 Power Cepstrum: Horn Type 2.

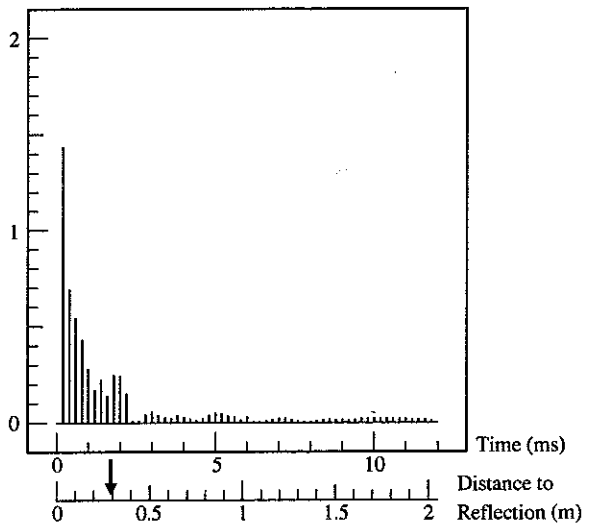

Figure 3.9.3 Power Cepstrum: Horn Type 3.

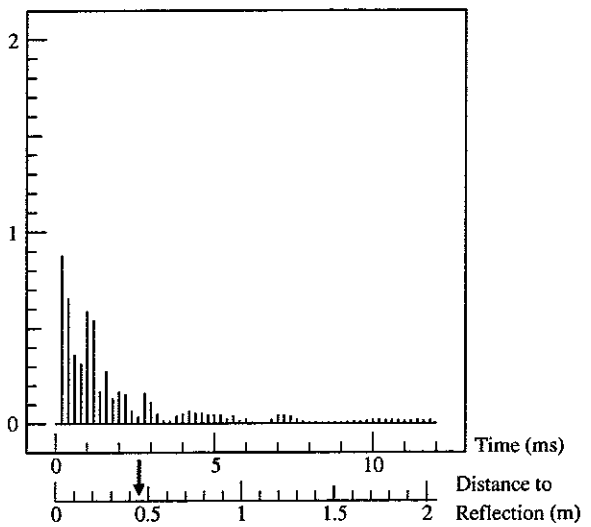

Figure 3.9.4 Power Cepstrum: Horn Type 4.

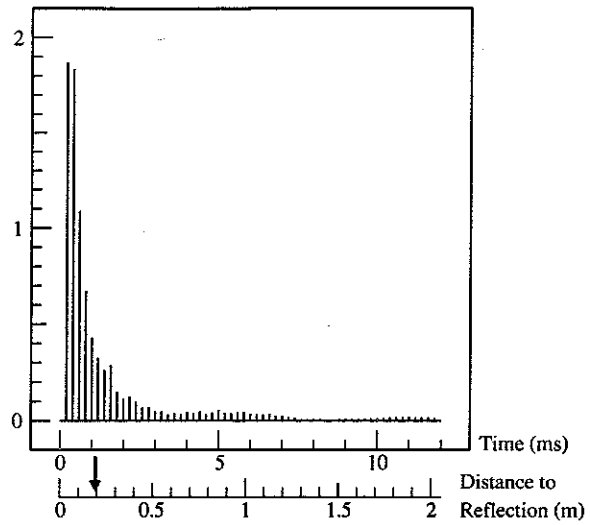

Figure 3.9.5 Power Cepstrum: Horn Type 5.

Because all of the horns tested have a cut-off towards the lower end of the measurement bandwidth, the absence of reflections does not result in a 'perfect', single-spike cepstrum; the cepstrum of an exponential horn with no flare discontinuities takes the form of a roughly exponentially decaying plot, with the cut-off frequency determining the height of the plot (the higher the cut-off frequency, the higher the plot).

Figure 3.9.1 shows the power cepstrum for horn type 1. The most significant feature of this plot is the large spike at around 1.2ms, which corresponds to a gross reflection at a distance of about 0.2m from the horn throat. This horn has a length of 0.18m from throat to mouth; the reflection is clearly due to a discontinuity of flare at the small horn mouth. Because of the severity of the mouth reflection, second and third 'echoes' can be seen on the plot at around 2.4ms and 4ms. These analyses show that the mouth reflection is responsible for the comb filtering in the power frequency response evident from the throat impedance measurement.

Figure 3.9.2 shows the power cepstrum for horn type 2. Again a distinct mouth reflection is evident at around 1.9ms which corresponds to the overall length of this horn at 0.28m. The 'lips' of this horn extend approximately 0.09m beyond the baffle flange, which is 0.19m from the throat; this analysis shows that, due to the curvature of the wavefronts, the flare discontinuity exists at the outer edge of the 'lips' and not at the baffle. Apart from a second 'echo' of the mouth reflection, no other significant reflections are evident.

Figure 3.9.3 shows the power cepstrum for horn type 3. The only significant feature is a slight reflection at about 2ms, which corresponds to the overall length of this horn including 'lips' of 0.29m. The lack of distinct spikes on this cepstrum confirms the smoothness of the power frequency response evident from the impedance measurement.
Figure 3.9.4 shows the power cepstrum for horn type 4. The plot is complicated due to the multiple discontinuities in the flare of this horn. The highest spikes occur at around 1.1ms; these are due to the three pillars and the cross-sectional shape change at about 0.2m from the throat. Also evident is a reflection from the mouth of this horn at about 3ms (overall horn length 0.45m) despite its large size.

Figure 3.9.5 shows the power cepstrum for horn type 5. As expected from the exceptionally smooth impedance measurement, the cepstrum for this horn shows very little evidence of any reflections either at the mouth of the horn (0.18m from throat) or within the flare. The exponential-type decay of the plot is actually smoother than that for an infinite length exponential horn due to the gentle roll-off of the impedance below the cut-off frequency. The overall height of the plot, relative to those for the other horns, is due to the high cut-off frequency of approximately 1kHz.

3.6 DISCUSSION

3.6.1 Model performance.

The fairly close agreement between the theoretical and measured throat impedances indicates that the one-parameter model can effectively predict the one-parameter behaviour of a horn. The use of the empirically derived wavefront shapes allows the throat impedance of horns with axi-symmetric or rectangular cross-sectional shape to be modelled, including horns with 'lips' extending beyond the baffle. Figure 3.10 shows the throat impedance of horn type 2 modelled assuming plane cross-sections; a comparison with figures 3.5.2 shows the improvement in accuracy that the wavefront shape approximation yields.

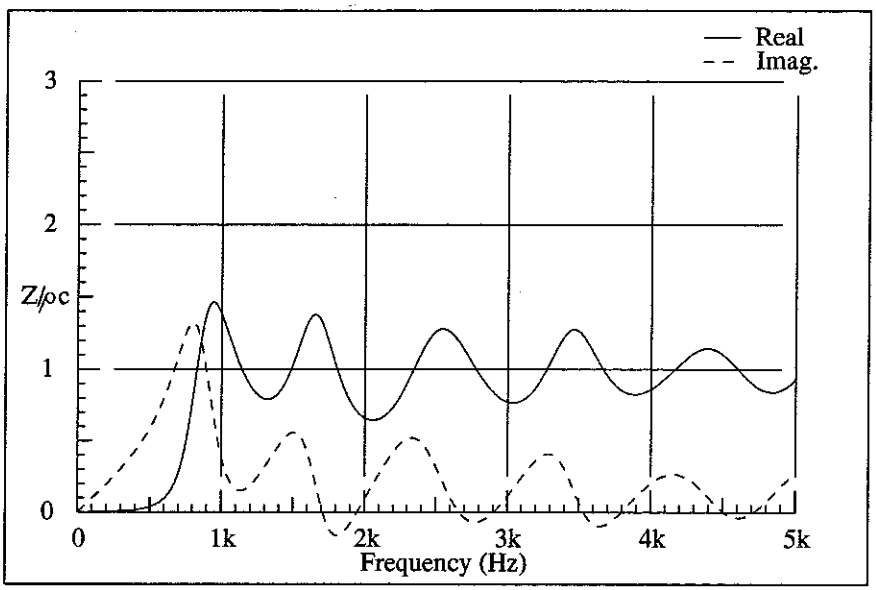

Figure 3.10 Theoretical Throat Impedance of Horn Type 2, Modelled Assuming Plane Cross-sections (compare with figures 3.5.2).

Generally, the model tends to underestimate the effect of flare discontinuities on the throat impedance. The comparisons between the theoretical and measured transfer impedances and axial pressure distributions show clearly that the model cannot take into account any departure from one-parameter behaviour such as beaming or transverse pressure variations. These departures from one-parameter behaviour are likely to be undesirable in a high-quality horn, and the comparisons between the theoretical, one-parameter results and the measurements help to highlight these effects. The results also show that the departures from one-parameter behaviour have little or no effect on the throat impedance, and hence sound power output of a horn; at least in the frequency range for which only plane-waves can exist at the throat (the concept of a throat impedance at higher frequencies is a dubious one as impedance is one-dimensional by definition).

The one-parameter model can serve two purposes: a diagnostic tool when the performance of a horn shows departures from an ideal, and a tool to assist in the design of high-quality horns. The accurate measurement of the physical dimensions of a horn is a potential source of error when using the model as a diagnostic tool, particularly near the throat where small changes in cross-sectional area can have large effects on throat impedance. The same is true of manufacture when the model is used as a design tool. To illustrate this, figure 3.11 shows the effect on the real

part of the throat impedance of a change† in radius of 18mm ± 1mm near the throat of a typical exponential horn.

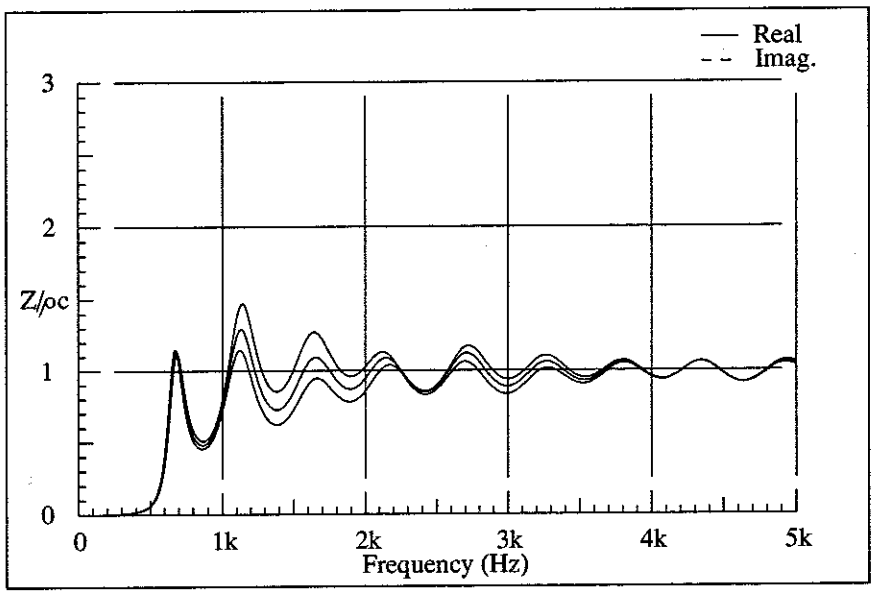

Figure 3.11 The effect on the real part of the throat impedance of a change† in radius of 18mm ± 1mm near the throat of a typical horn.

3.6.2 Performance of Horns.

Horn type 1, the small axi-symmetric, was designed using the one-parameter model to have gross mouth reflections to enable these reflections to be investigated. This was achieved by a combination of low flare-rate and small mouth, and the results above show that this was successful. The axial pressure distributions clearly show a dispersive, standing-wave field within the horn and the position of the reflective discontinuity shows up clearly using cepstral analysis.

The throat impedance results and associated cepstra for horn type 2, the Reflexion Arts rectangular, show that although the mouth of the horn is quite large, with an effective radius of 120mm, significant mouth reflection exists. This must be due to the narrow rectangular shape of the mouth, with the shallow flare in the vertical plane leading to a sharp discontinuity at the mouth, despite the presence of the 'lips'. The transfer impedance and axial pressure distribution results show that the field within the flare is essentially one-parameter, despite the rapid horizontal flare, except for a small degree of beaming and some evidence of transverse pressure variations. This is because the walls of the horn are constructed of heavily-braced mineral-loaded fibreglass and are smooth, with no sharp angles or flare discontinuities.

†*Note: the 'change' here refers to three values of the radius of the horn at a distance of 20mm from the throat: 17mm, 18mm and 19mm; the flare of the horn remaining continuous.*

Horn type 3, the Vitavox rectangular, has a mouth with an effective radius of 136mm, only slightly larger than horn type 2, but does not suffer any significant mouth reflection. This is because the mouth has a much larger vertical dimension and nearly full 'radial lips', leading to less of a discontinuity. The transfer impedance and axial pressure distribution results show that the sound field within the flare departs markedly from one-parameter behaviour at about 3kHz. During the measurements, a pronounced 'ring' was heard from behind the horn in response to the random excitation from the driver. The frequency of the ring was estimated to be about 3kHz and disappeared when the horn flare was tightly clamped by the arms (see chapter 4, section 4.4). The horn is of cast aluminium construction with quite thick, heavy walls and substantial stiffener / waveguide plates near the mouth, so a lot of damping material would be required to significantly reduce the severity of the resonance.

Horn type 4, the Fostex sectoral, is of cast aluminium construction with thinner walls than horn type 3, but with three stiffening pillars between the top and bottom walls near the throat. The throat impedance and associated cepstrum show that this horn has severe reflections from these pillars which are placed close to a sharp discontinuity in the flare, as well as some mouth reflection. The transfer impedance and axial pressure distribution results show that the presence of these flare discontinuities severely disrupt the passage of wavefronts from throat to mouth, setting up large transverse pressure variations in the rest of the flare.

Horn type 5, the large axi-symmetric, was designed to have as 'smooth' a power frequency response as possible in the frequency range of interest (1kHz to 6kHz), within reasonable size constraints. The throat impedance and cepstrum results show that this has been achieved, with little or no evidence of reflections within the flare or at the mouth. The area profile, being near exponential to flat cross-sections, becomes almost conical near the mouth to curved wavefronts (see figure 3.8), which results in a gentle roll-off below a relatively high cut-off frequency. The transfer impedance and axial pressure distribution results show that this horn behaves in an essentially one-parameter manner, except for a small amount of beaming.

Chapter 4 deals with the departures from one-parameter behaviour found in many horn examples and considers directivity and the radiated sound field.

Chapter 4
DEPARTURE FROM ONE-PARAMETER BEHAVIOUR

4.1 INTRODUCTION

Some of the work described in this chapter has been published in reference [32].

The model of horn behaviour described in chapter 2 relies on the assumption that the amplitude and phase of the pressure field within a horn flare is even over a chosen wavefront surface. Using this assumption, it is possible to model the behaviour of any horn in a one-parameter manner providing some simple, empirically derived rules concerning the shape of the wavefronts are followed. Comparisons between the measured behaviour of real horns and the theoretical model output (chapter 3), indicates that the behaviour of some of the horns tested is more complicated than the one-parameter model would suggest, especially at or near the horn mouth. In this chapter, these departures from one-parameter behaviour, and the effect that they have on the radiated sound field are investigated.

4.2 MOUTH PRESSURE DISTRIBUTIONS

To aid the investigation of the nature and causes of these departures from one-parameter behaviour, measurements were taken of the distribution of pressure across the mouths of the horns tested over a range of frequencies. This is achieved by measuring the transfer function between the pressure at a number of positions across the horn mouth and the pressure at the horn throat. For those horns having flat fronts, the measurements were taken along a straight line, and for those horns with 'lips' the measurement positions follow the curve of the lips. Figures 4.1.2a to 4.1.4a show the distribution of pressure phase across the mouths of horn types 2,3 and 4 in the horizontal (large dimension) plane. As these horns have mouths with 'lips', the distributions are plotted relative to arcs equivalent to the curvature of the mouths. The phase responses are converted to equivalent propagation distances at the speed of sound at the time of measurement and plotted on the same scale as the horn mouth arcs, the distributions then represent approximations to the shape of the wavefronts at the mouths of the horns. Figures 4.1.2b to 4.1.4b show the distribution of pressure amplitude across the mouths of horn types 2, 3 and 4, again plotted relative to the horn mouth arcs. The pressure distributions across the smaller vertical dimensions of the horn mouths were also measured but are not plotted as these measurements contain only limited information. Figures 4.1.5a and 4.1.5b show the distribution of pressure phase and amplitude across the mouth of the axisymmetric horn type 5. As

the mouth of this horn is flat, the distributions are plotted relative to a straight line of length equivalent to the mouth diameter. As horn type 1 has a very shallow flare and small mouth diameter, the wavefronts at the mouth are near plane, thus the mouth pressure distributions for this horn are very flat and are not shown.

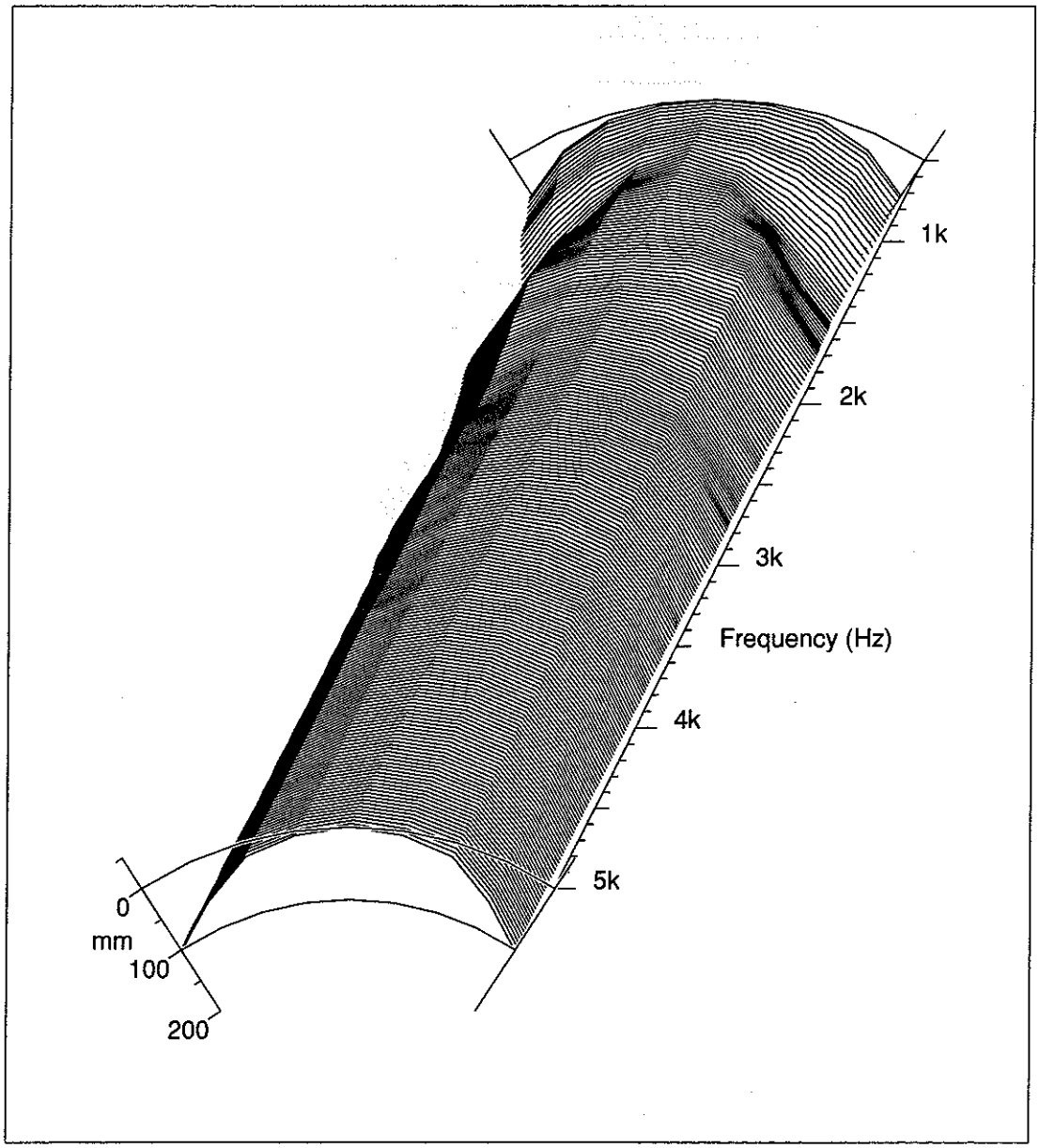

Figure 4.1.2a Distribution of Pressure Phase across the Mouth of Horn Type 2, converted to Equivalent Propagation Distances.

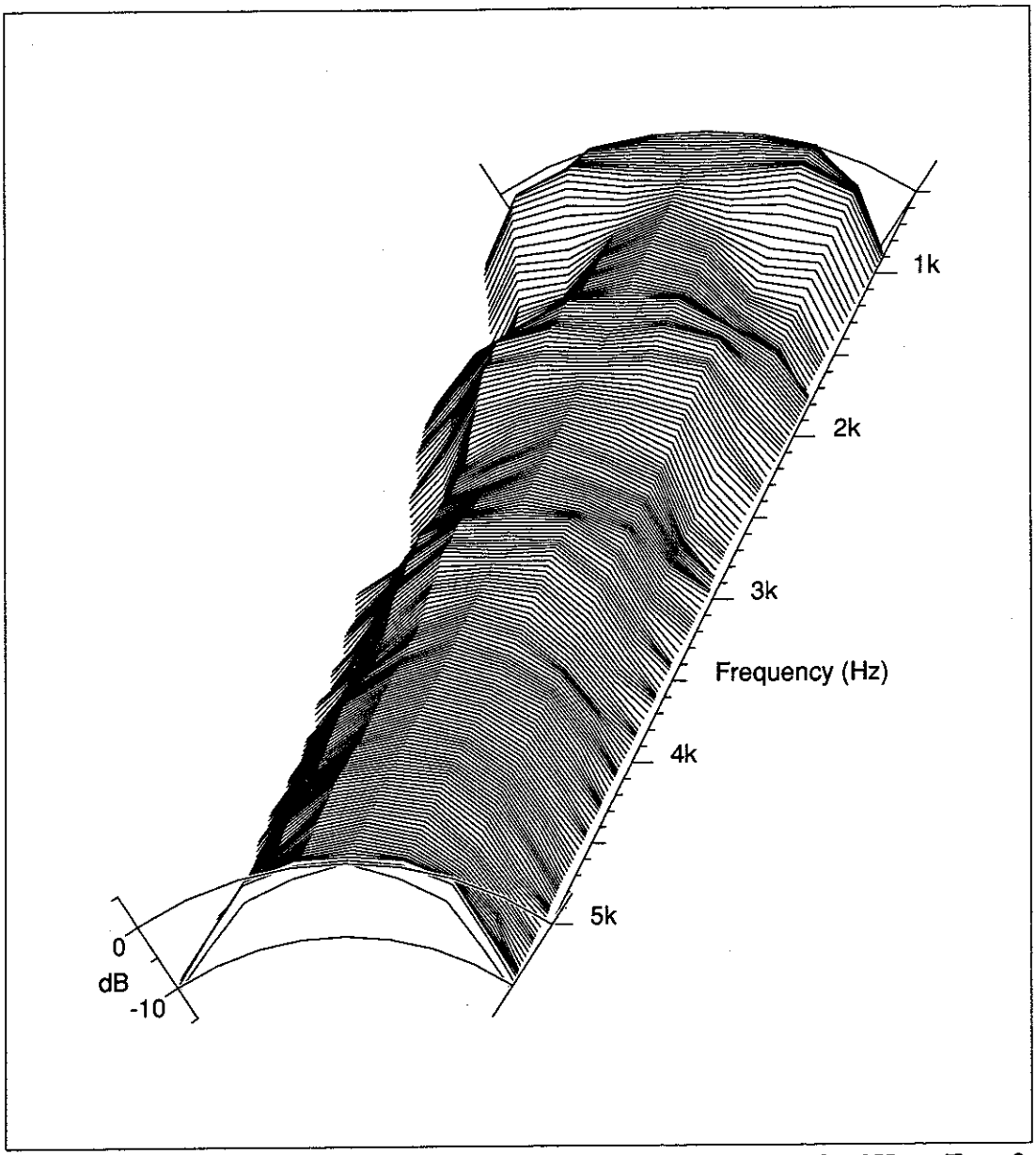

Figure 4.1.2b Distribution of Pressure Amplitude across the Mouth of Horn Type 2.

Figures 4.1.2a and b show the pressure distribution across the mouth of horn type 2. Figure 4.1.2a shows circular-arc wavefront shapes at all frequencies above 2kHz with a curvature greater than that of the horn mouth. This is due to the lips on the mouth of this horn being shallower than a circular arc normal to the very rapidly flaring horn walls, and is responsible for the on-axis beaming at higher frequencies mentioned in the discussion of the transfer impedance results (section 3.5.2); the wavefronts reach the centre of the mouth before the edges, by which time further expansion, and hence reduction in pressure, has taken place. A set of resonant transverse pressure 'modes' can be seen in figure 4.1.2b as alternate 'narrow' sections

where the pressure is higher on the horn axis and broad sections, where it is lower on-axis. The frequencies at which the 'narrowing' occurs are 600Hz, 1.5kHz and 2.5kHz, with wavelengths of approximately 570mm, 200mm and 140mm. The mouth of this horn has a width of 570mm, so the lowest frequency 'mode' occurs when the wavelength is equal to the mouth width ('mode' n=1), and the highest when the wavelength is equal to a quarter of the mouth width ('mode' n=4). The wavelength at 1.5kHz does not bear a simple relationship to the mouth width. The higher values of measured transfer impedance compared to the one-parameter prediction at around 1.5kHz and 2.5kHz can be seen to be due to the two higher frequency transverse pressure 'modes' causing high pressures on the axis of the horn; the reduction in wavefront curvature seen in figure 4.1.2a at the n=1 frequency prevents this 'mode' showing as a peak in the transfer impedance results as the edges of the wavefront contact the walls at a wider part of the flare causing an overall reduction in pressure due to the larger area. A broadening of the plot occurs at 1.2kHz, with a wavelength of approximately 285mm which is half of the width of the horn ('mode' n=2). These transverse pressure 'modes' are not real modes, but are due to the shallow mouth lips; the reflections due to the flare discontinuity at the mouth affect different parts of a wavefront at different times, leading to a complex, non-one-parameter interference pattern near the mouth of the horn.

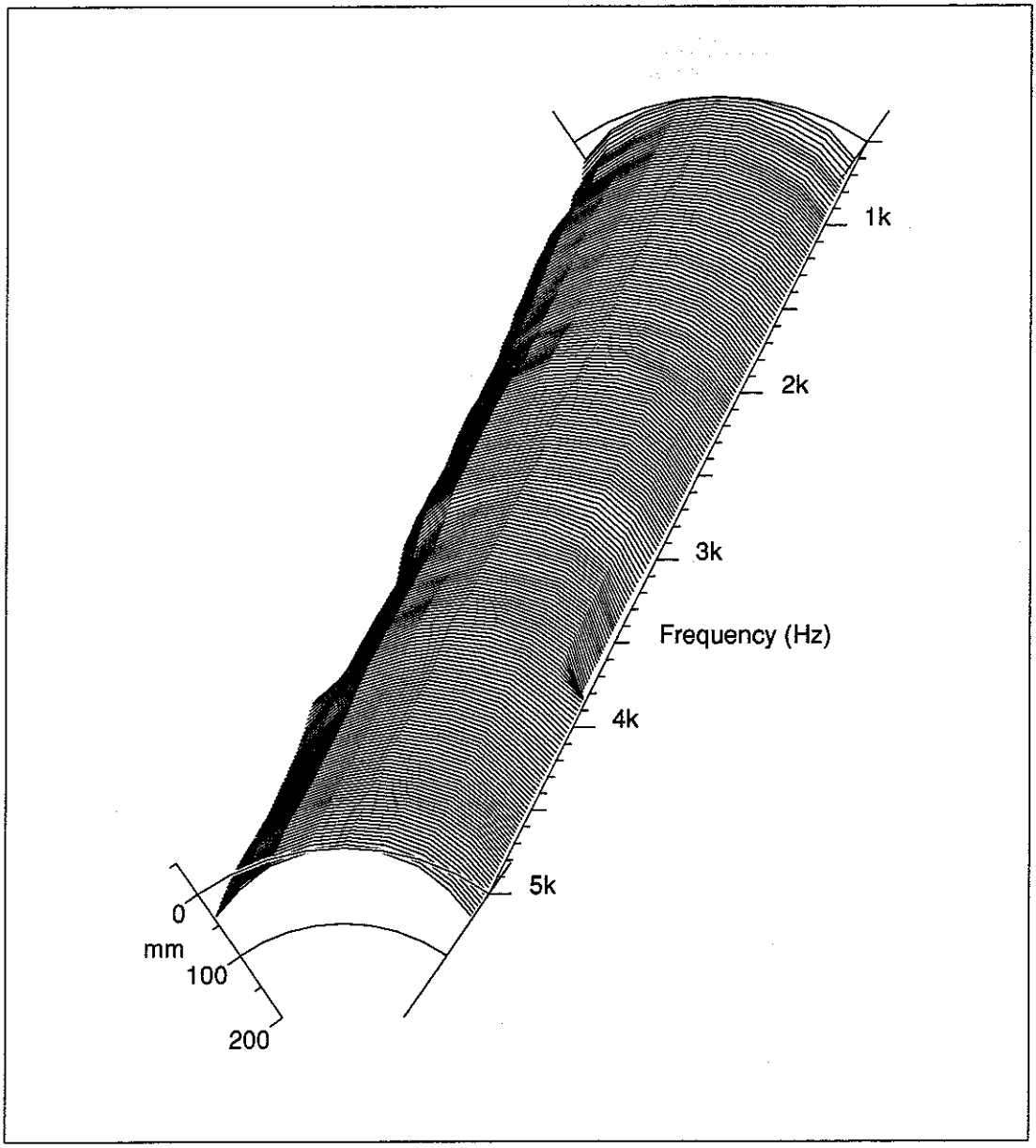

Figure 4.1.3a Distribution of Pressure Phase across the Mouth of Horn Type 3, converted to Equivalent Propagation Distances.

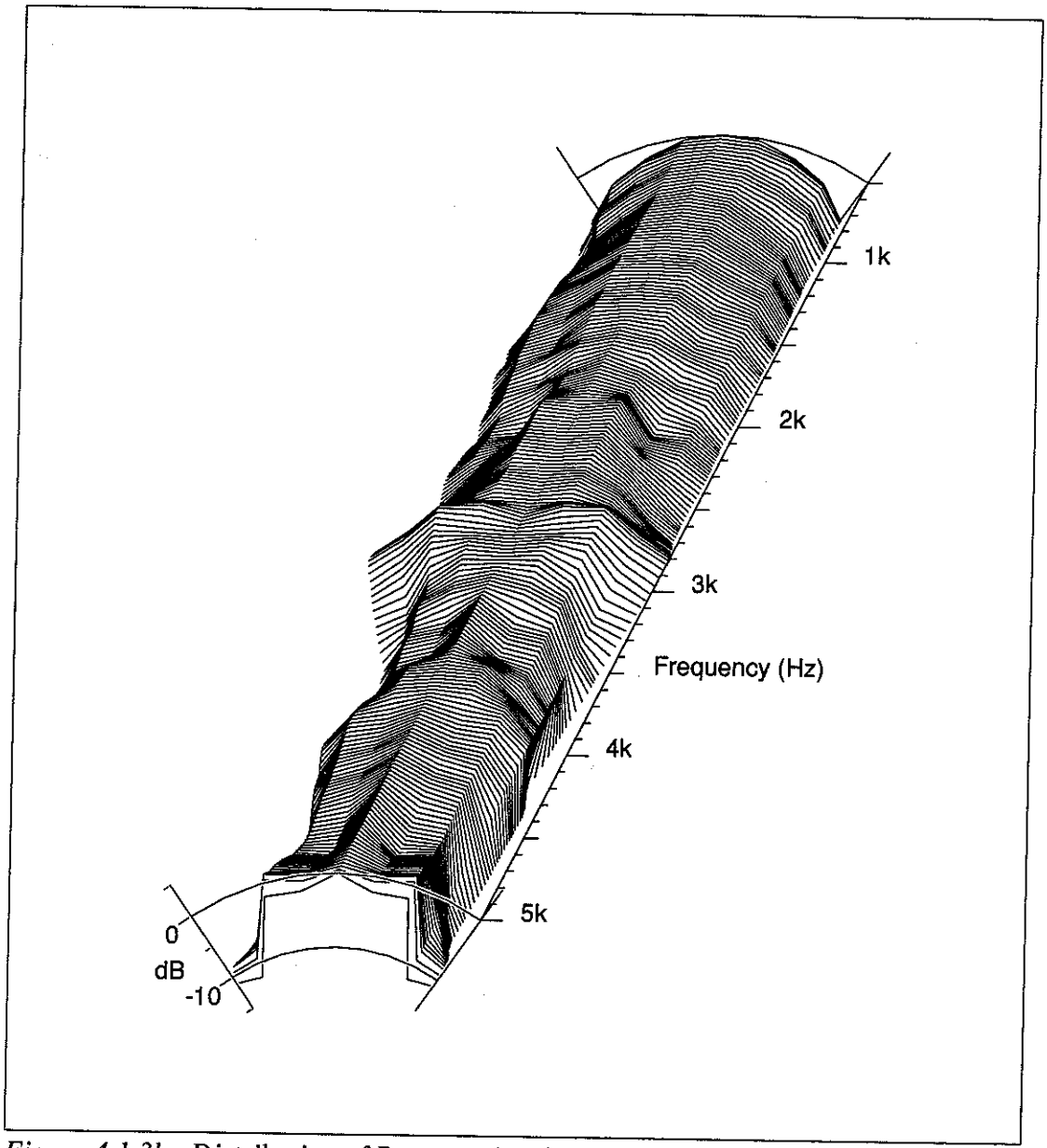

Figure 4.1.3b Distribution of Pressure Amplitude across the Mouth of Horn Type 3.

Figure 4.1.3a shows that the distribution of pressure phase across the mouth of horn type 3 is even, with circular-arc wavefront shapes with a slightly greater curvature than the mouth lips at all frequencies. A slight increase in curvature is seen between 3kHz and 4kHz. The pressure amplitude distribution however (figure 4.1.3b) can be seen to be a very complex function of frequency, with strong evidence of transverse variations at all frequencies above about 2kHz. The width of the mouth of this horn is 390mm so resonant 'modes', equivalent to those in the results for horn type 2 may be expected at about 900Hz, 1.8kHz and 3.6kHz. There is little or no evidence of the presence of these modes as the 'lips' at the mouth of this horn have only slightly

shallower curvature than circular arcs normal to the horn walls, so the complex reflection interference patterns are not set up. Significant 'broadening' of the amplitude distribution can be seen in figure 4.1.3b at 3kHz. This coincides with the 'dip' in measured transfer impedance at 3kHz seen in figure 3.6.3b. Figure 4.1.3c shows the distribution of vibrational velocity amplitude around the edge of the 'lips' of this horn. It can be seen that a strong vibrational resonance is set up at 3kHz, with maximum velocity in line with the horn axis. This vibrational resonance, which was noticed as a distinct 'ring' during measurements, is almost certainly the cause of the departure of this horn from one-parameter behaviour at 3kHz. Substantial beaming is evident at all frequencies above 3kHz, with very low pressure amplitude at the edges of the horn mouth. This may be due to the presence of two stiffener / waveguide plates near the horn mouth creating 'shadows' and channelling the high frequency sound though the central third of the mouth.

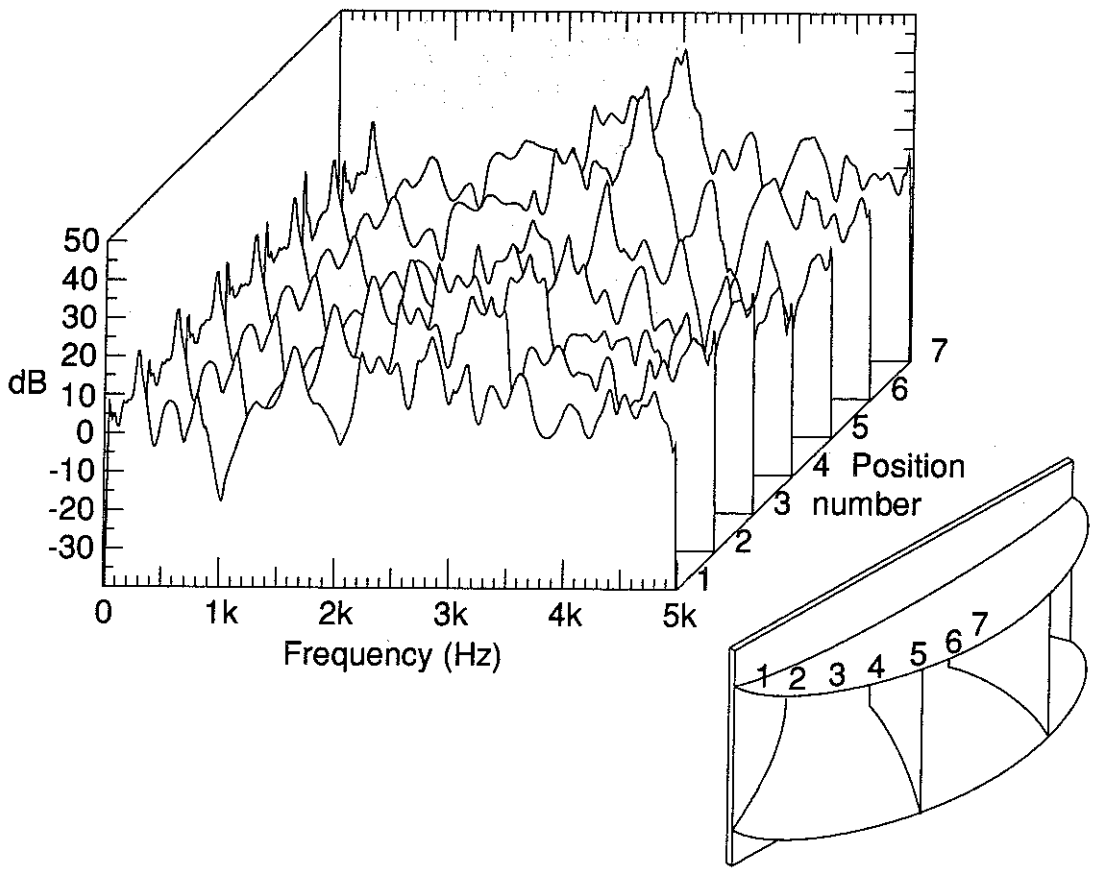

Figure 4.3.1c Distribution of Vibrational Velocity along edge of 'Lips' at Mouth of Horn Type 3.

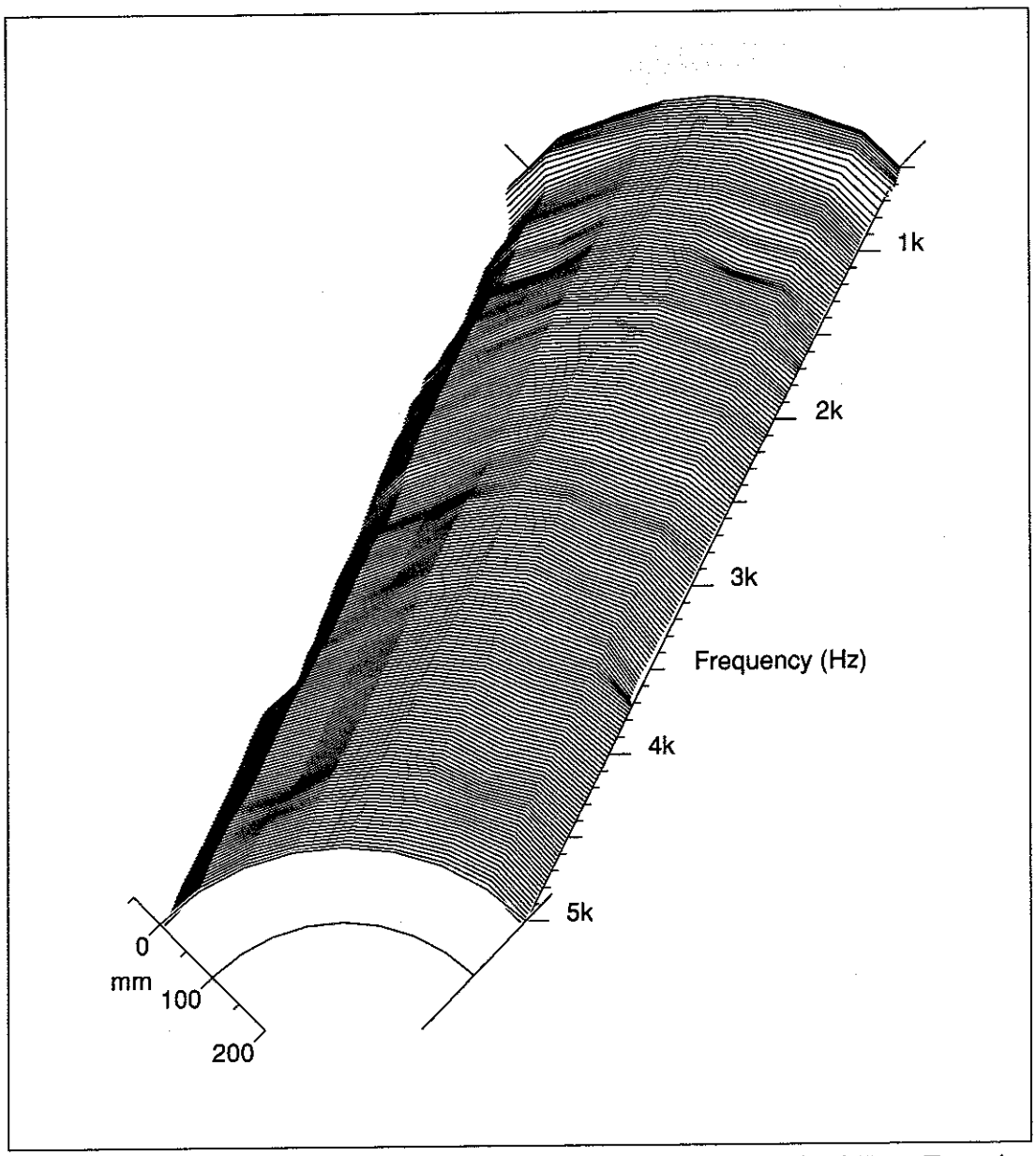

Figure 4.1.4a Distribution of Pressure Phase across the Mouth of Horn Type 4 converted to Equivalent Propagation Distances.

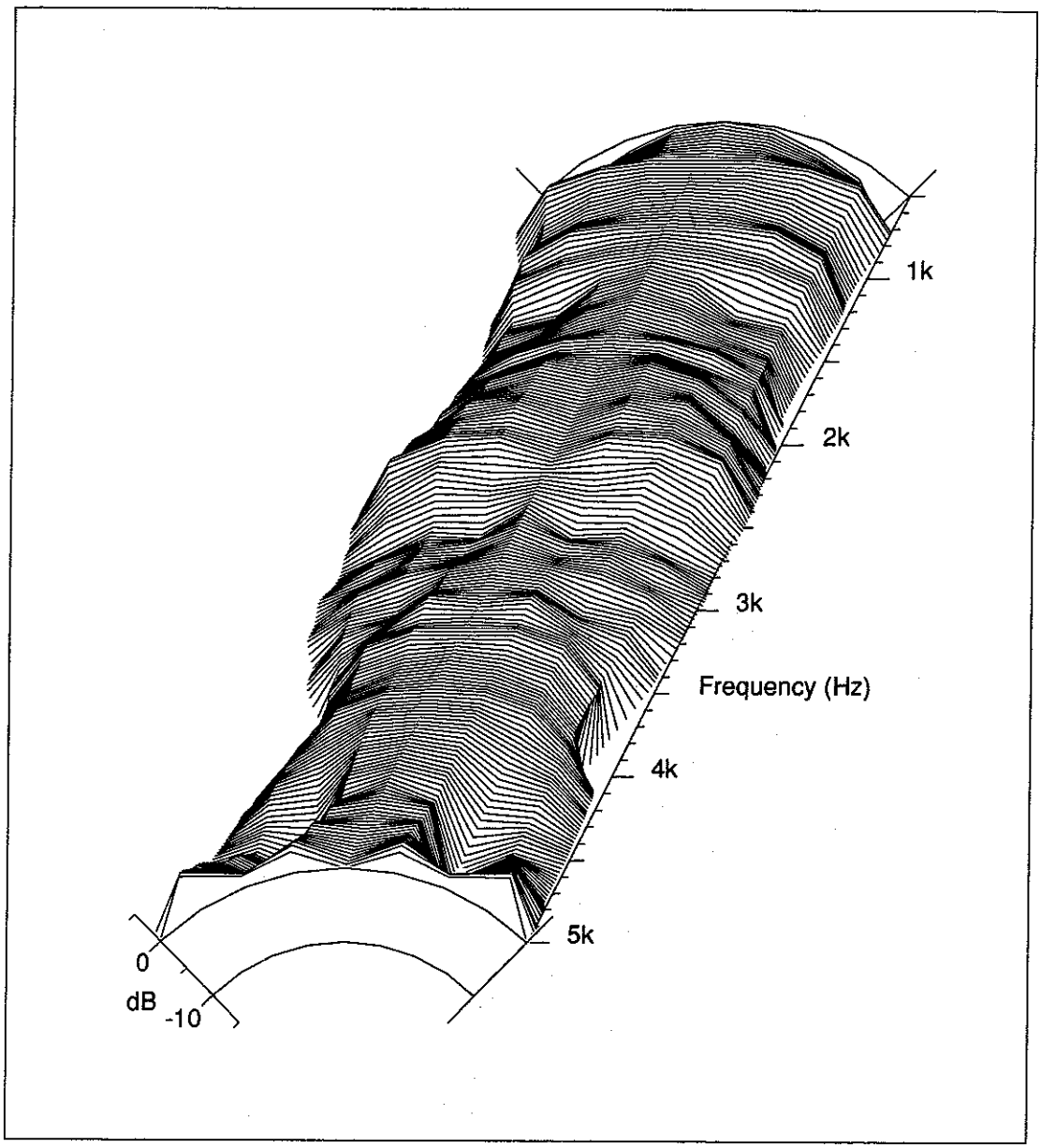

Figure 4.1.4b Distribution of Pressure Amplitude across the Mouth of Horn Type 4.

Figure 4.1.4a shows that for horn type 4, the wavefront shapes follow the curvature of the horn mouth 'lips' at all frequencies above about 800Hz. This horn is a sectoral design and thus has straight-sided vertical walls and 'lips' that form a circular arc normal to these walls; the wavefronts clearly follow this arc. Figure 4.1.4b shows strong transverse pressure variations at all frequencies. The horn mouth has a width of 490mm so the 'modes', equivalent to those in the results for horn type 2, may be expected at around 700Hz, 1.4kHz and 2.8kHz. Some evidence is present for all three modes, although modes can be found at many frequencies inbetween. The broad dip in the measured transfer impedance results between 2 and 3kHz (figure

3.6.4b) can be seen in figure 4.1.4b as a 'broadening' of the plot due to the pressure either side of the axis being higher than that on-axis. This effect is due to the presence of the strengthening pillars, one of which is on-axis, creating a 'shadow' at this frequency. The peak in the measured transfer impedance at 3.7kHz can be seen to be due to beaming which may occur because of the other pillars. The shadow effect of these three pillars can clearly be seen at around 5kHz, with a reduction in pressure on-axis and half-way between the axis and the horn walls. Most, if not all, of the transverse pressure variations present in this horn are due to the pillars disrupting the smooth expansion of the wavefronts from throat to mouth exciting many transverse 'modes' at the mouth.

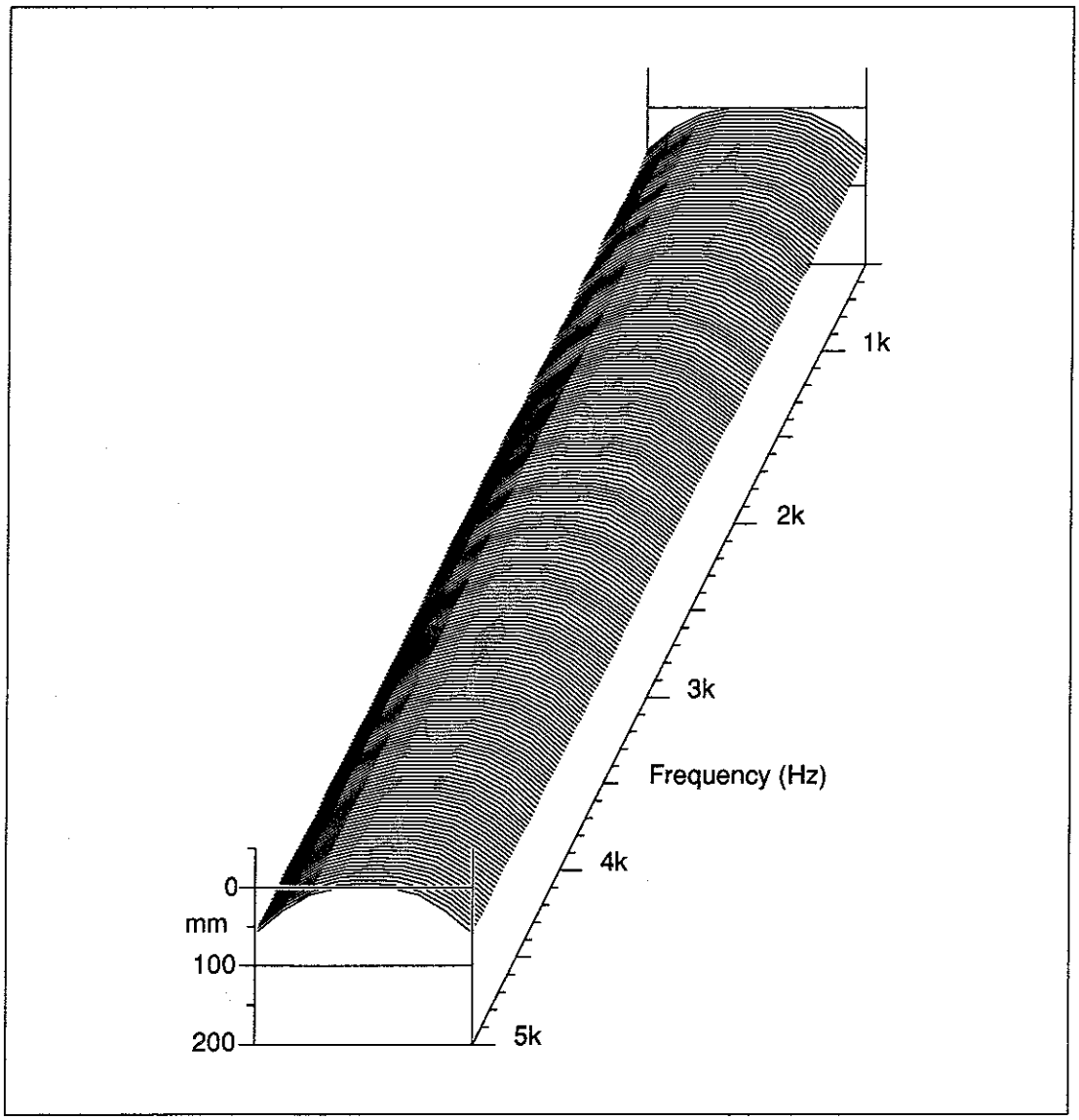

Figure 4.1.5a Distribution of Pressure Phase across the Mouth of Horn Type 5, converted to Equivalent Propagation Distances.

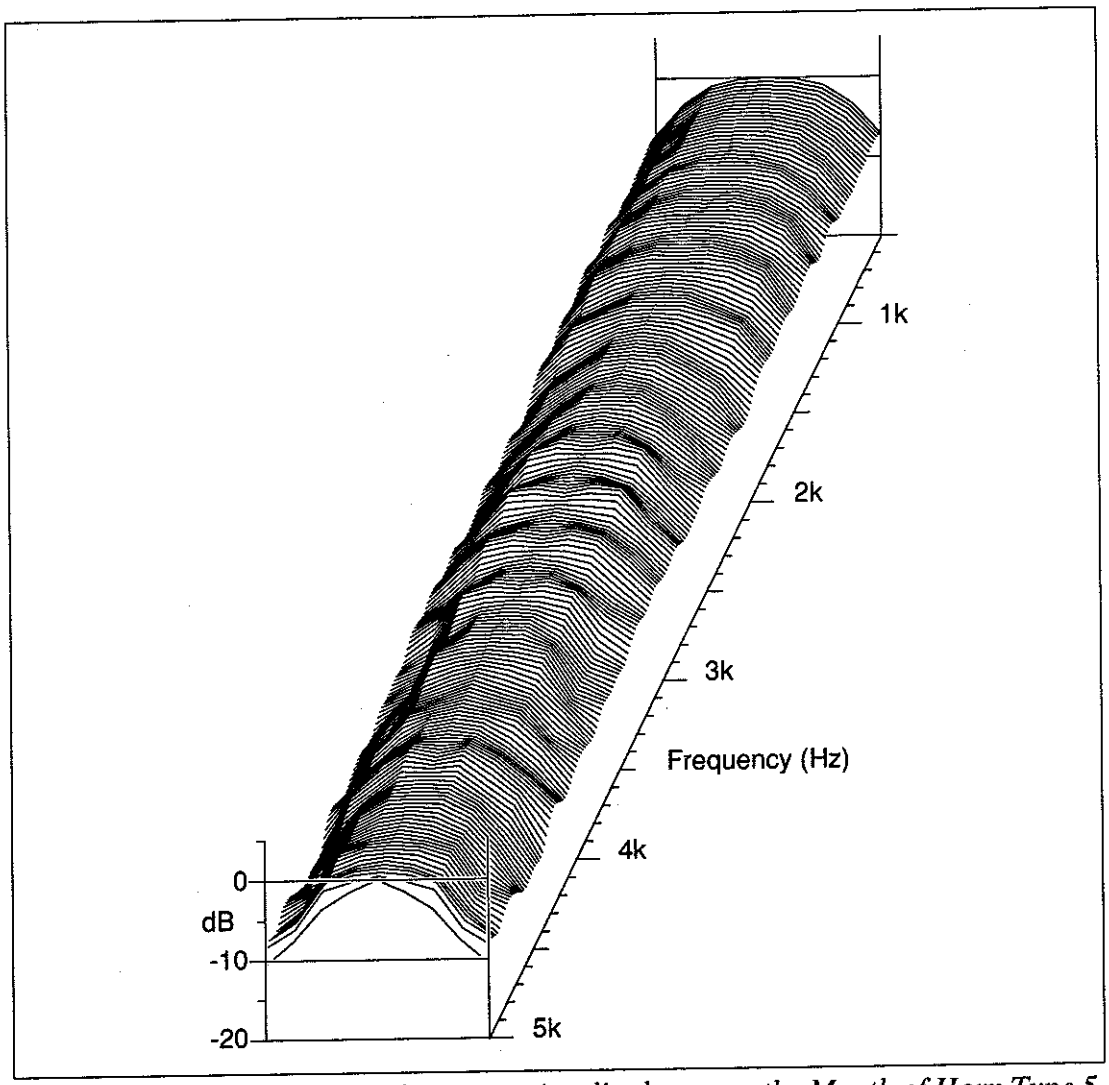

Figure 4.1.5b Distribution of Pressure Amplitude across the Mouth of Horn Type 5.

Figures 4.1.5a and b show the pressure distribution across the mouth of horn type 5. Due to the axisymmetric shape of this horn, the mouth is flat, and the pressure distributions are representative of those along any diametric line across the horn mouth. The 'flattened spherical cap' shape of the wavefronts, used in the extension of the one-parameter model, can be seen in figure 4.1.5a, with little variation in this shape at any frequency. Figure 4.1.5b shows that the pressure amplitude distribution is even over these wavefronts throughout the whole frequency range. The slight 'ripple' in the amplitude distribution is due to reflections from the imperfectly anechoic walls of the measurement room (present on the plots for the other horns but masked by the transverse pressure variations). Clearly, hardly any transverse pressure variations are present at the mouth of this horn as indicated by the agreement between the transfer impedance measurements and the one-parameter predictions.

4.3 DIRECTIVITY

The one-parameter model described in chapter 2 cannot predict the pressure field radiated by a horn into the far-field, only the total sound power. Indeed, the assumption of one-parameter behaviour and the use of a hemi-spherical mouth element would lead to all horns being omni-directional. The main application for mid-range loudspeaker horns is public address systems, and one of the the most important properties that these horns need to possess is good directivity control; the wide variety of shapes and sizes of the horns tested is largely due to the different approaches adopted by the horn designers to achieve this aim. In a studio monitoring situation, a horn may not have to possess a wide directivity pattern or one that remains 'constant' with frequency, but the radiated sound should vary smoothly with angle and frequency, so that the on-axis frequency response remains smooth and that any reflections from the floor or equipment in the control room are not unduly altered in spectral content.

To find out whether the departures from one-parameter behaviour discussed above have any effect on the directivity of the horns tested, measurements were taken of the sound field radiated by the horns in the large anechoic chamber at ISVR. Each horn was mounted on a rectangular baffle of approximately 1.2m high and 0.69m wide, thought representative of the front of a large studio monitoring cabinet, which was fixed to a turntable such that the axis of rotation passed through the point where the horn axis crosses the baffle plane. Transfer functions were measured between the output from a microphone at 2m distance and the voltage input to a compression driver mounted at the throat of the horn, at five degree intervals from on-axis around a 90 degree arc. The rectangular horns were mounted both with the large dimension oriented horizontally and then vertically, allowing the directivity to be measured in both planes.

Figures 4.3.2ha, b and c to 4.3.4ha, b and c show the directivity of the rectangular horn types 2, 3 and 4 in the horizontal plane, figures 4.3.2va, b and c to 4.3.4va, b and c show the directivity of these horns in the vertical plane and figures 4.3.5a, b and c show the directivity of the axisymmetric horn type 5. The directivity properties of horn type 1, being of limited interest, were not measured. Because of the amount of data contained in these measurements, the results for each horn are plotted three different ways. Plots 'a' show the amplitudes of the measured transfer functions and are useful for determining the frequency and level of any directivity features. Plots 'b' show equi-pressure contours derived from the measured transfer

function amplitudes. These plots enable the directivity at angles close to the axis to be studied in detail; the 'coverage angle' of the horn, usually defined as the angle at which the response is -6dB compared to the response on-axis, can be read directly from these plots at the frequency of interest. Plots 'c' show polar diagrams, derived from the measured transfer function amplitudes, distributed along a frequency axis. These plots indicate the shape of the directivity pattern over a range of frequencies and are useful for detecting side-lobes in the directivity response. All of the plots show the data normalised to the on-axis transfer function to prevent confusion due to driver power frequency response irregularities. Unlike the impedance measurements and those of the sound field within the horn, these measurements are representative of the frequency response as perceived by a listener and are plotted on a logarithmic frequency scale to accord with established models of hearing (see [33]) and to maintain some compatibility with previously published data.

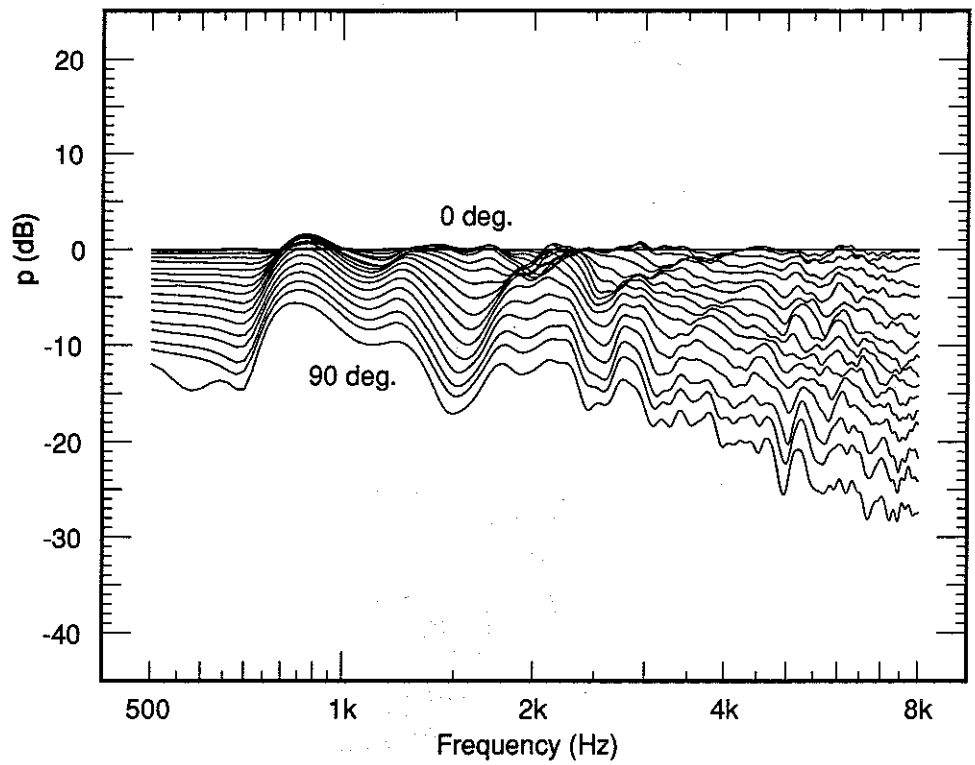

Figure 4.3.2ha Directivity Transfer Functions (Horizontal Plane) for Horn Type 2.

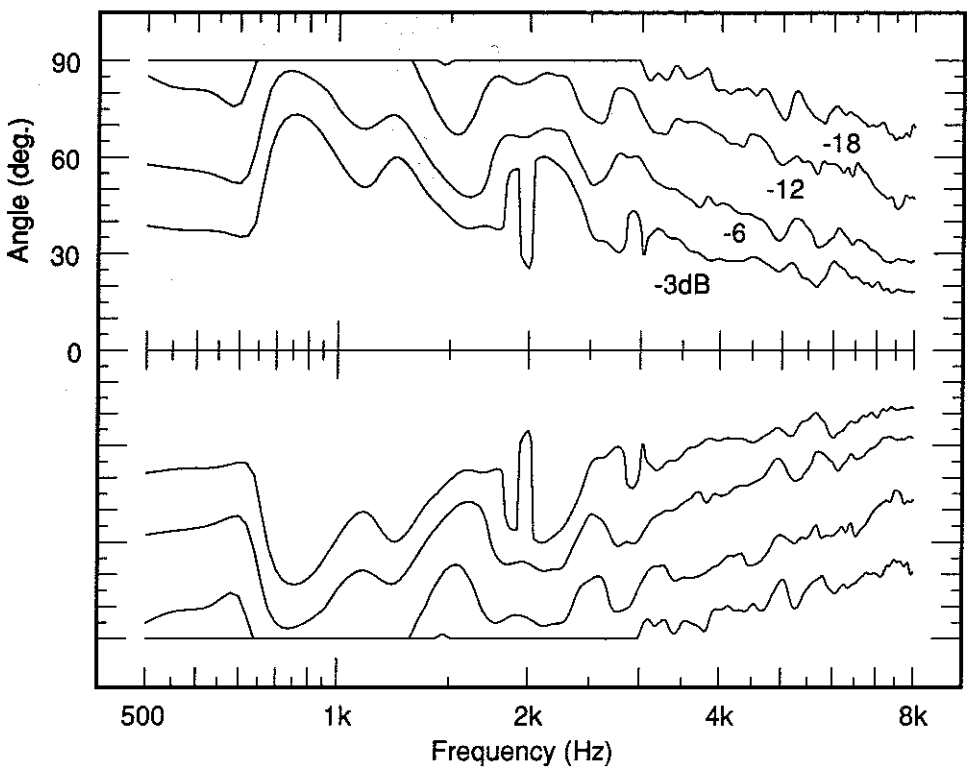

Figure 4.3.2hb Directivity Contours (Horizontal Plane) for Horn Type 2.

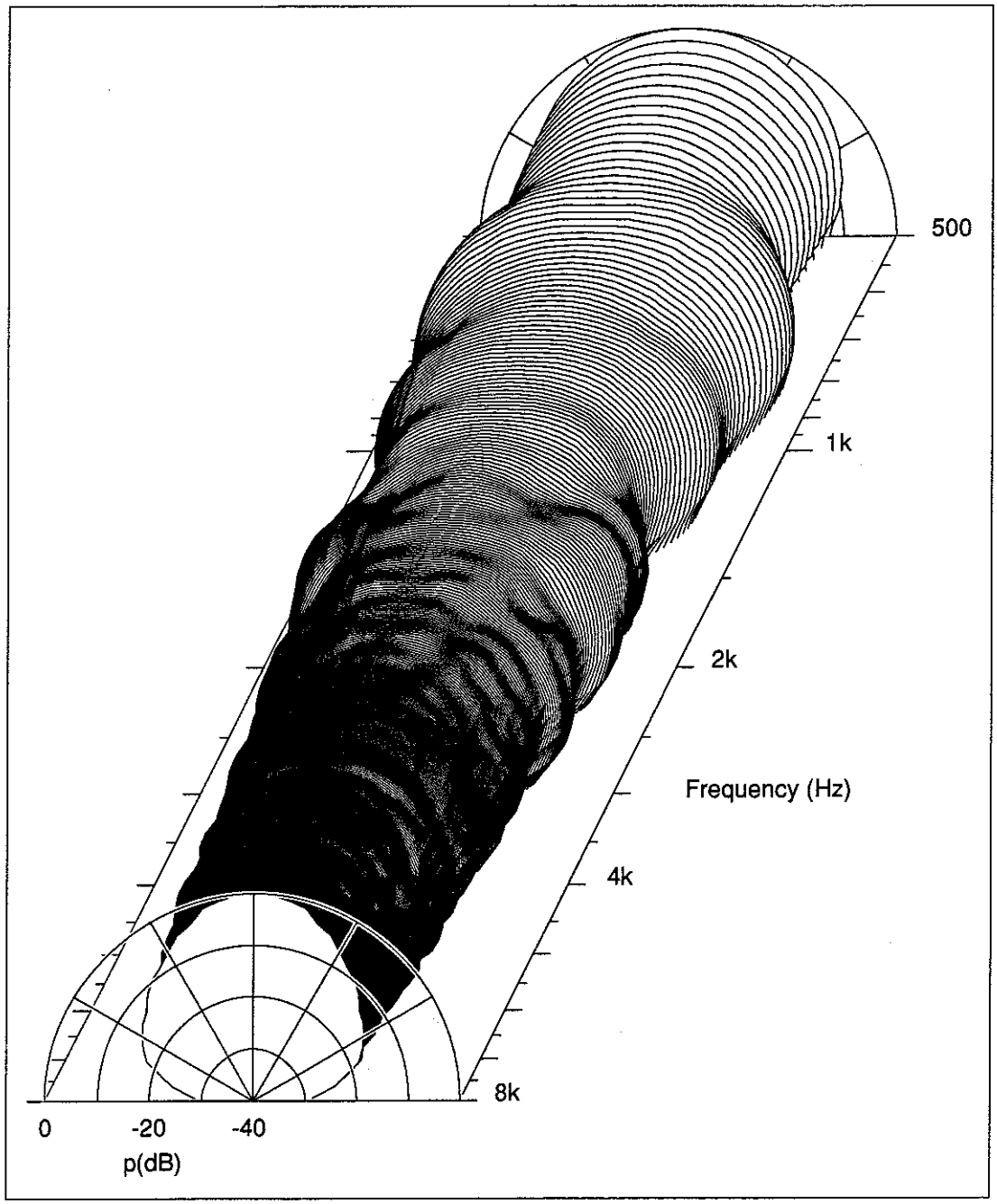

Figure 4.3.2hc Polar Plot Distribution (Horizontal Plane) for Horn Type 2.

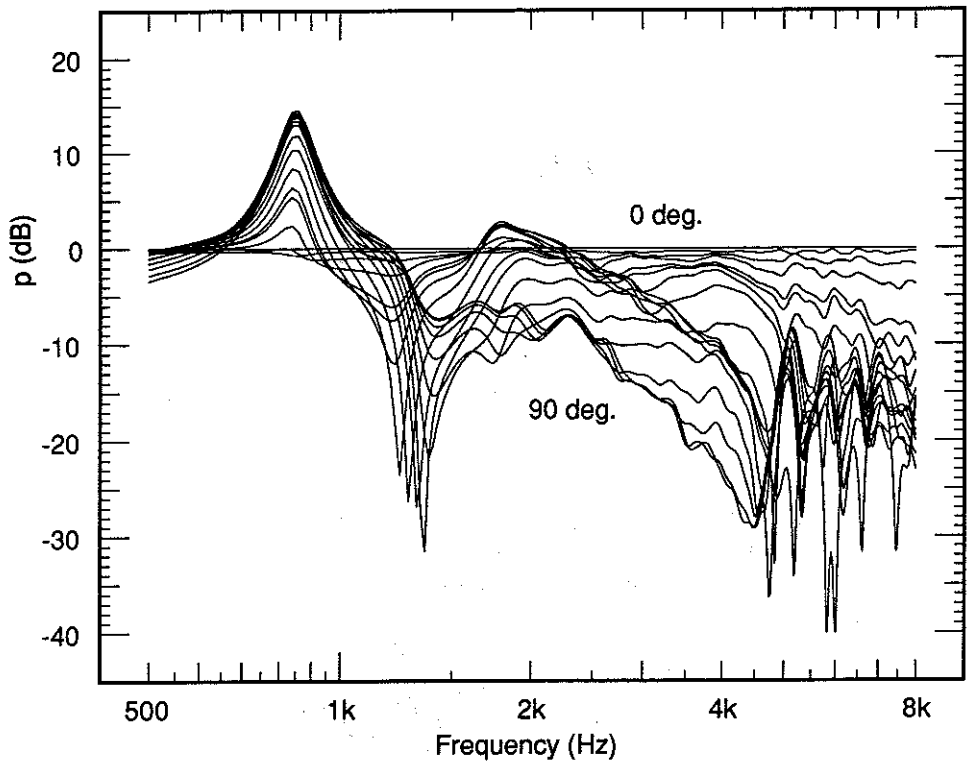

Figure 4.3.2va Directivity Transfer Functions (Vertical Plane) for Horn Type 2.

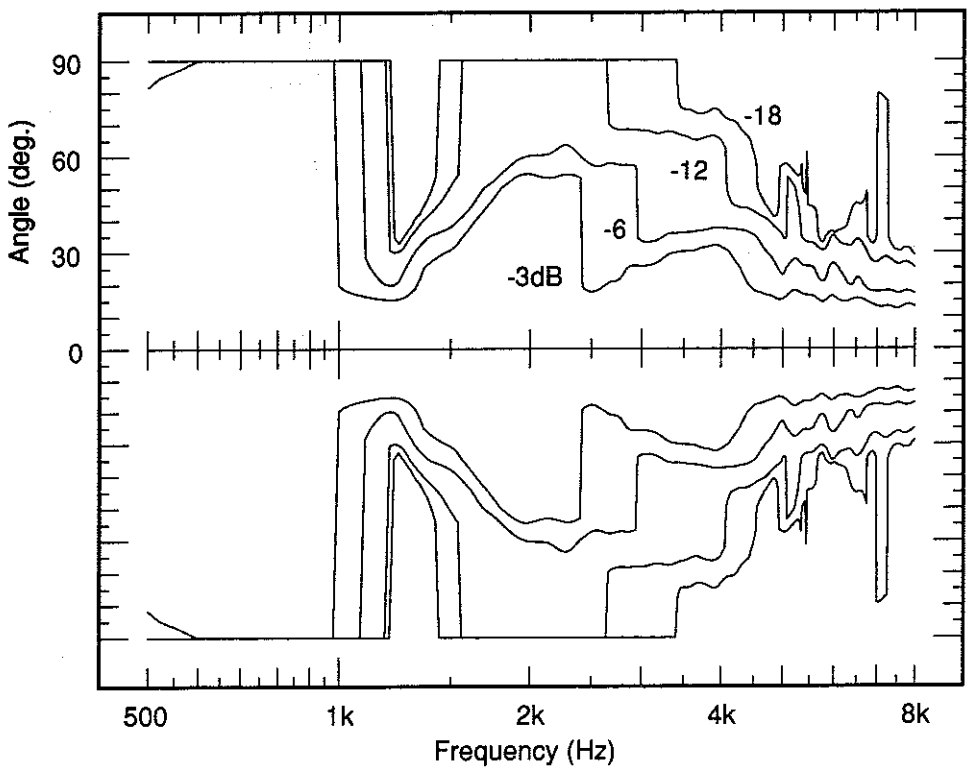

Figure 4.3.2vb Directivity Contours (Vertical Plane) for Horn Type 2.

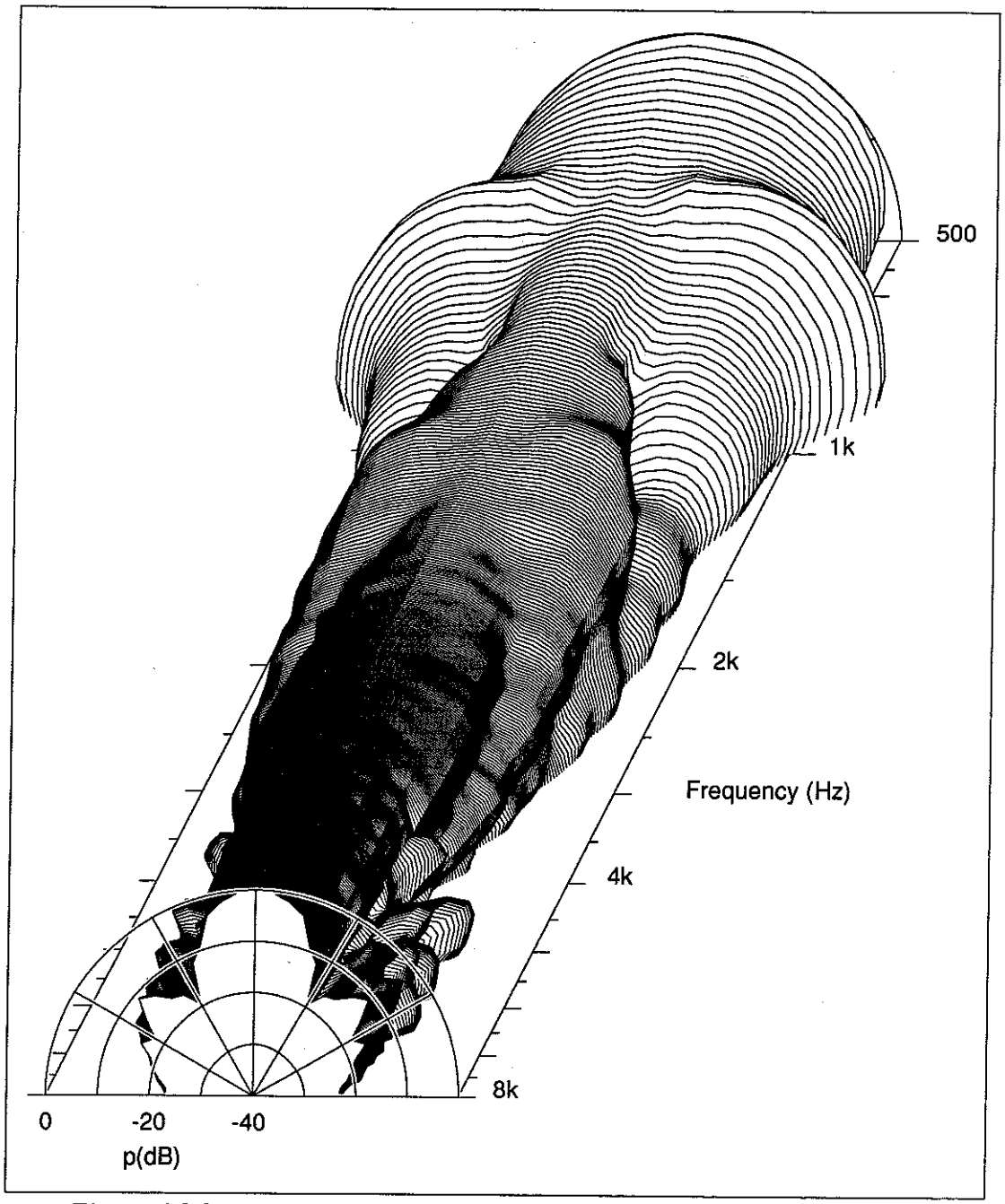

Figure 4.3.2vc Polar Plot Distribution (Vertical Plane) for Horn Type 2.

Figures 4.3.2h show the directivity plots in the horizontal plane for horn type 2. The contour plot shows that the directivity narrows in a controlled manner with increasing frequency above 800Hz with a coverage angle of nearly 180 degrees inclusive, reducing to 55 degrees inclusive at 8kHz. The polar plot shows that the directivity remains smooth at all angles even at high frequencies. A slight broadening of the directivity at about 800Hz can be seen on all of the plots. Figures 4.3.2v show the directivity for this horn in the vertical plane. The polar and transfer function plots show that the broadening at 800Hz is much more severe in this plane with a response at 90 degrees off-axis some 15dB greater than on-axis. No transverse pressure variations were found in the mouth pressure distributions at this frequency, so this broadening of the directivity at this frequency, especially in the vertical plane, is not due to transverse pressure variations at the horn mouth. At 1.2kHz there is a narrowing of the directivity with a response at 45 degrees off-axis which is 30dB lower than on-axis. This frequency coincides with the n=2 'mode' evident from the mouth pressure distributions. A second broadening of directivity can be seen on the contour and transfer function plots at 1.6kHz. This frequency coincides with the n=3 'mode'. these changes in directivity are almost certainly due to the reflection interference pattern 'modes' at the mouth of the horn; the even modes causing a narrowing of vertical directivity and the odd modes a broadening. The polar plot shows that considerable 'lobing' occurs in the vertical plane at wide angles at frequencies above 4kHz and the contour plot shows that the vertical coverage angle narrows to 35 degrees inclusive at high frequencies.

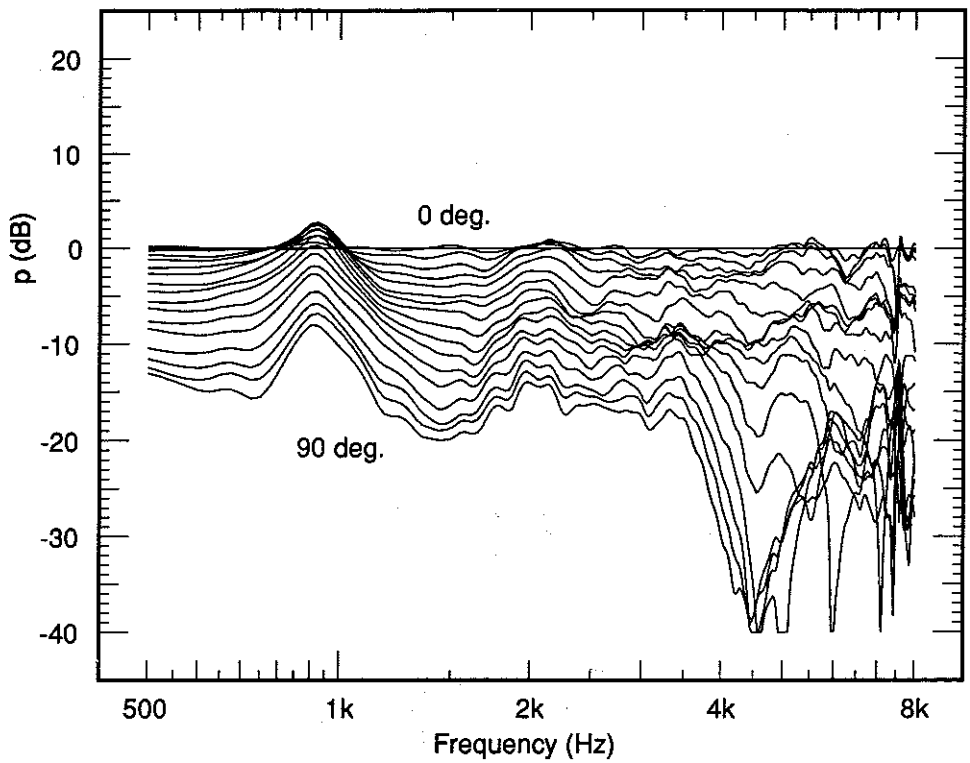

Figure 4.3.3ha Directivity Transfer Functions (Horizontal Plane) for Horn Type 3.

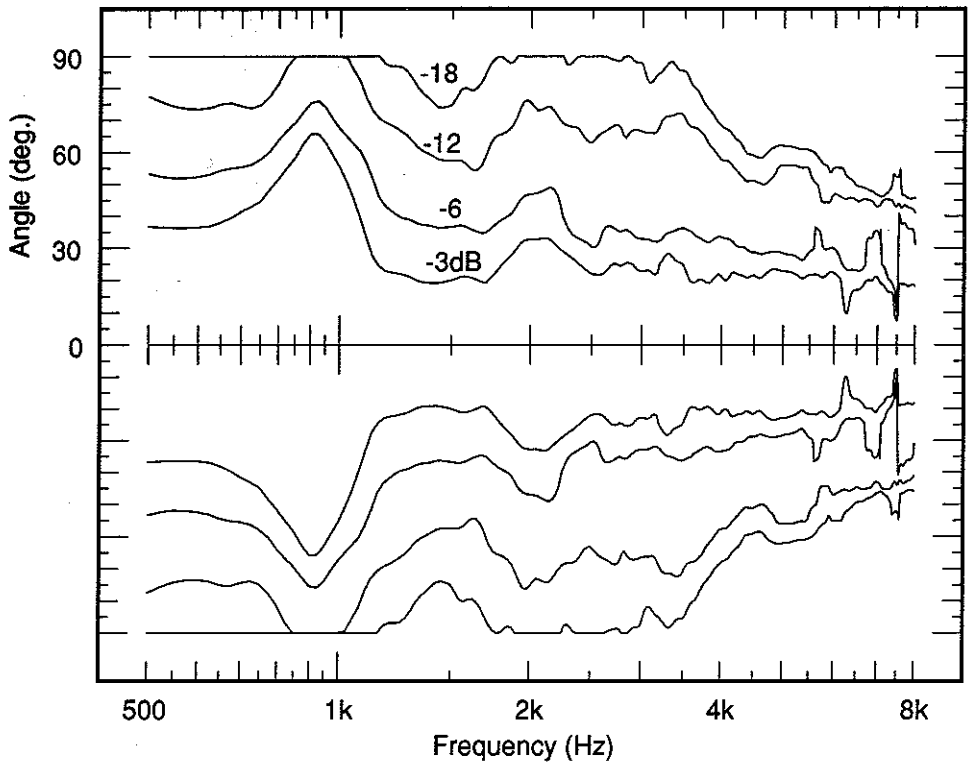

Figure 4.3.3hb Directivity Contours (Horizontal Plane) for Horn Type 3.

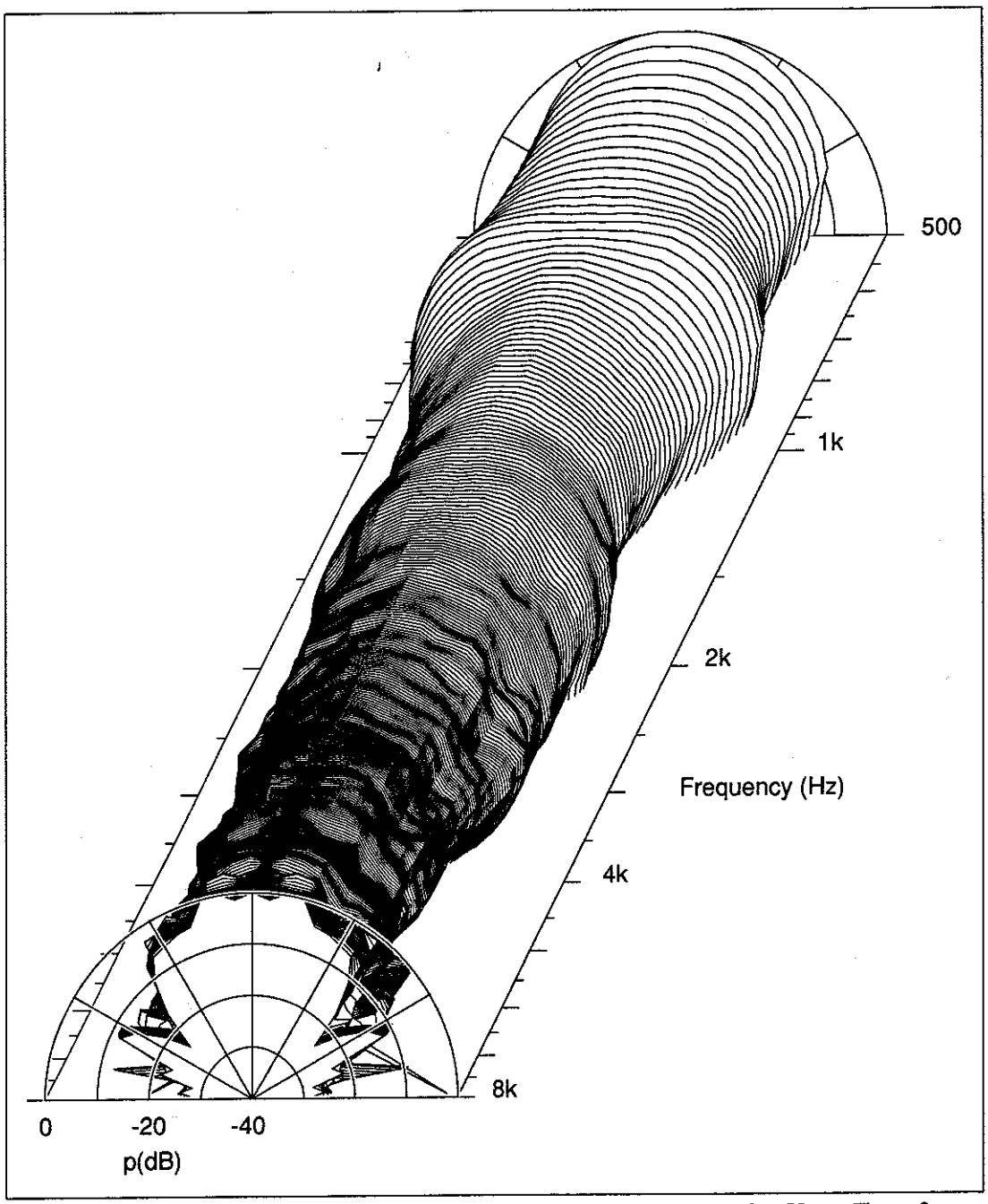

Figure 4.3.3hc Polar Plot Distribution (Horizontal Plane) for Horn Type 3.

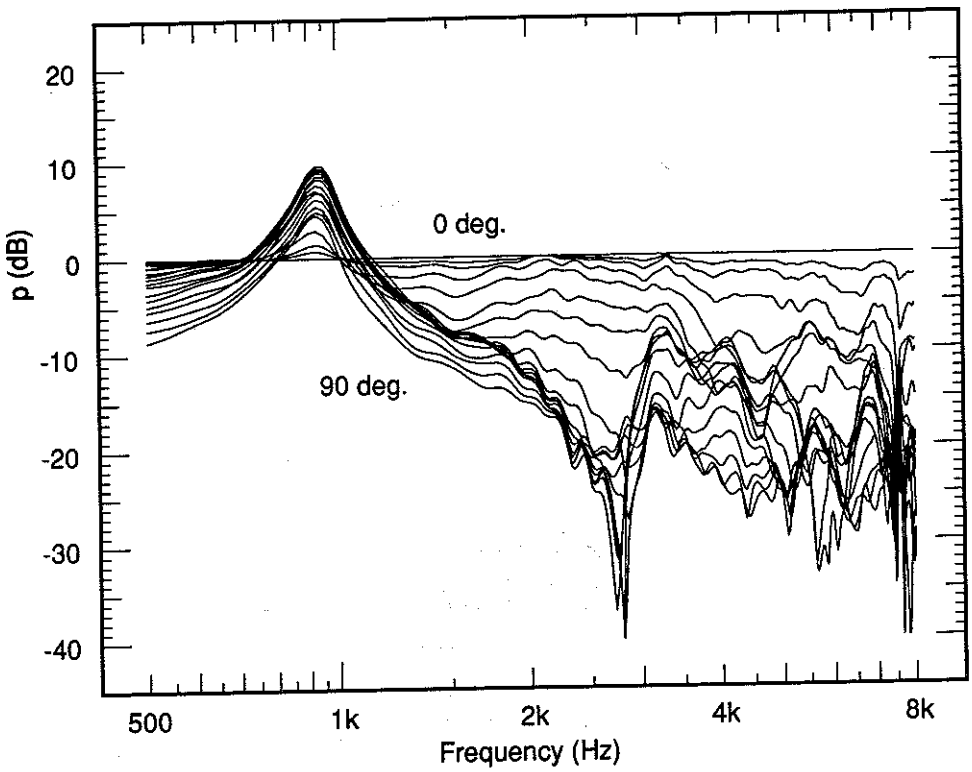

Figure 4.3.3va Directivity Transfer Functions (Vertical Plane) for Horn Type 3.

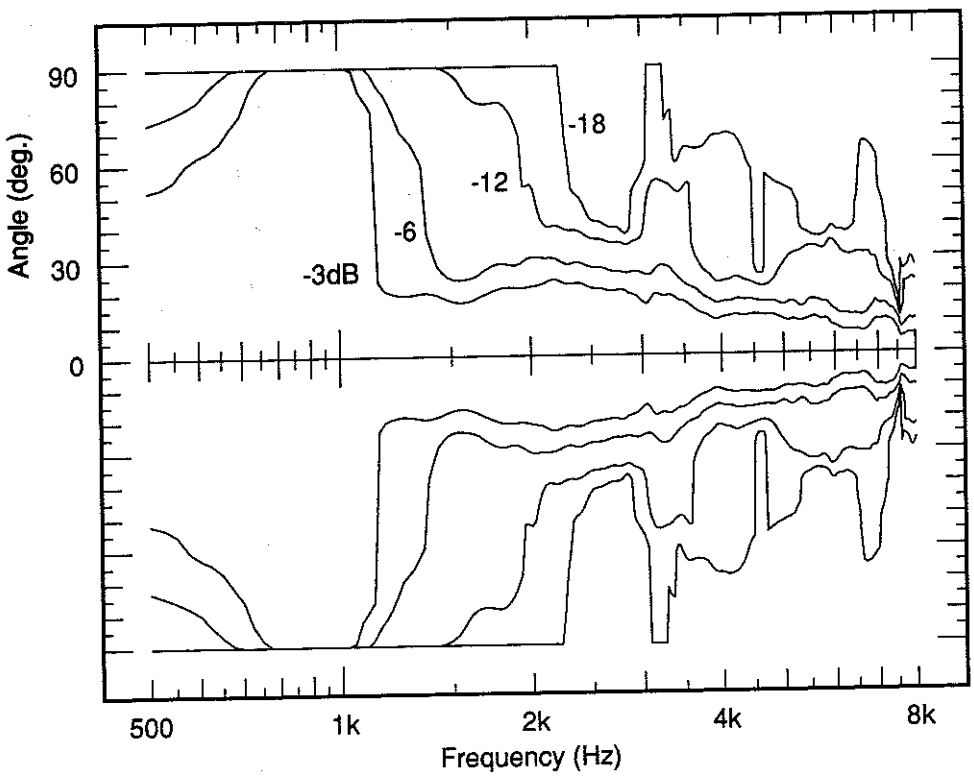

Figure 4.3.3vb Directivity Contours (Vertical Plane) for Horn Type 3.

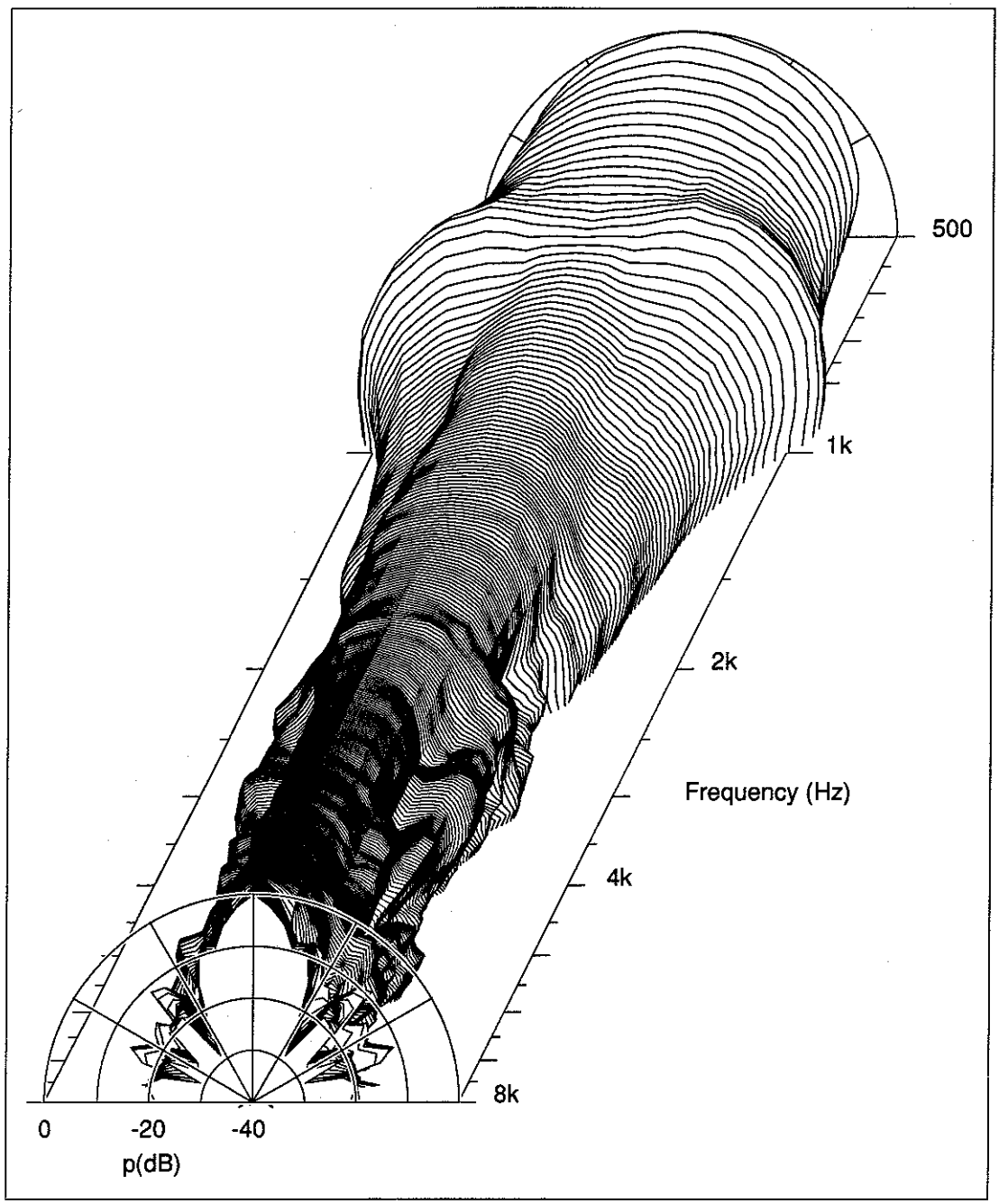

Figure 4.3.3vc Polar Plot Distribution (Vertical Plane) for Horn Type 3.

Figures 4.3.3h show the directivity of horn type 3 in the horizontal plane. The contour plot shows that the directivity at angles near the axis is well controlled above 1.2kHz, with slight broadening of the pattern at 900Hz and a coverage angle of between 50 and 70 degrees inclusive over a frequency range from 1.2kHz to 7kHz. The response at large angles falls off rapidly above 3.5kHz due to the shadowing effect of the waveguide plates at the mouth of the horn. Distinct side-lobes are evident in the polar plot at wide angles above 6kHz. Figures 4.3.3v show the directivity of this horn in the vertical plane. The most significant feature of all of the plots is the broadening of the directivity pattern at 900Hz. This is very similar to the effect noticed in the directivity of horn type 2. The wavelength at 900Hz is about 380mm which is close to the width of the mouth of this horn. As with horn type 2, no significant transverse pressure variations were found at the mouth of this horn at this frequency. The contour plot shows that the vertical directivity of this horn is well controlled at angles near to the axis above 1.2kHz, but that the coverage angle reduces to about 20 degrees inclusive at high frequencies. A severe reduction in output at about 3kHz at large angles is evident from the transfer function plot; this is due to the wall vibration mentioned above. The wall vibration does not appear to affect the horizontal directivity and only has an effect on the vertical directivity at large angles.

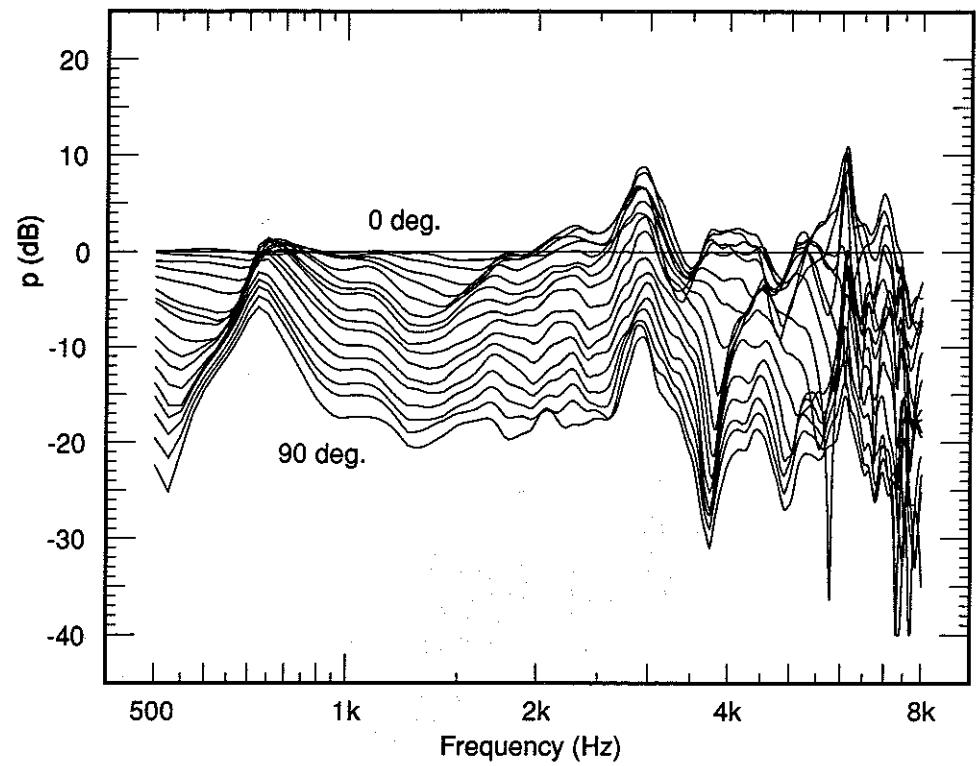

Figure 4.3.4ha Directivity Transfer Functions (Horizontal Plane) for Horn Type 4.

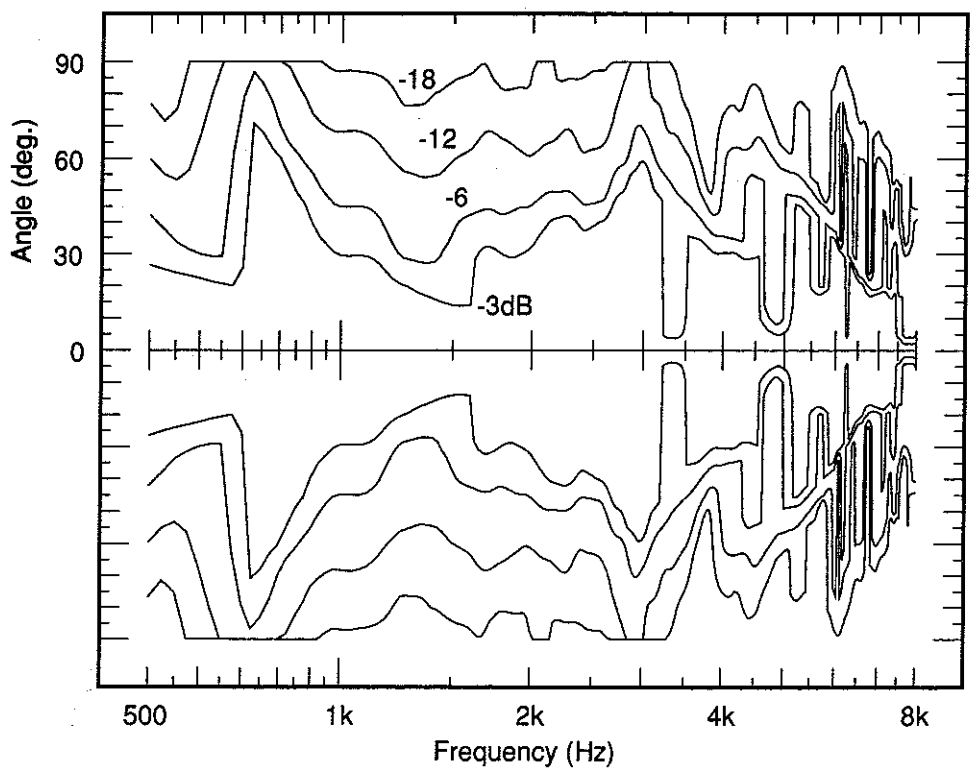

Figure 4.3.4hb Directivity Contours (Horizontal Plane) for Horn Type 4.

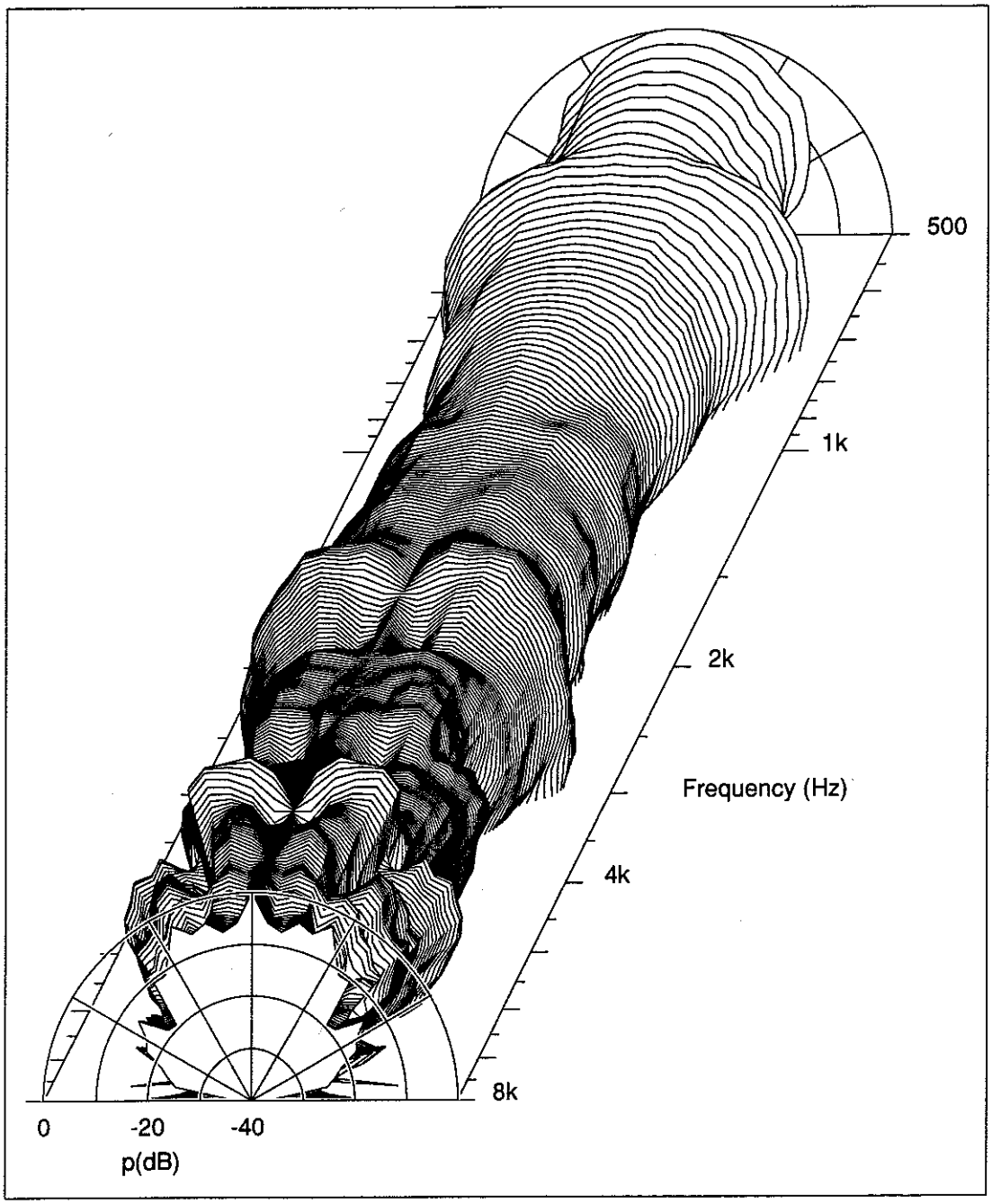

Figure 4.3.4hc Polar Plot Distribution (Horizontal Plane) for Horn Type 4.

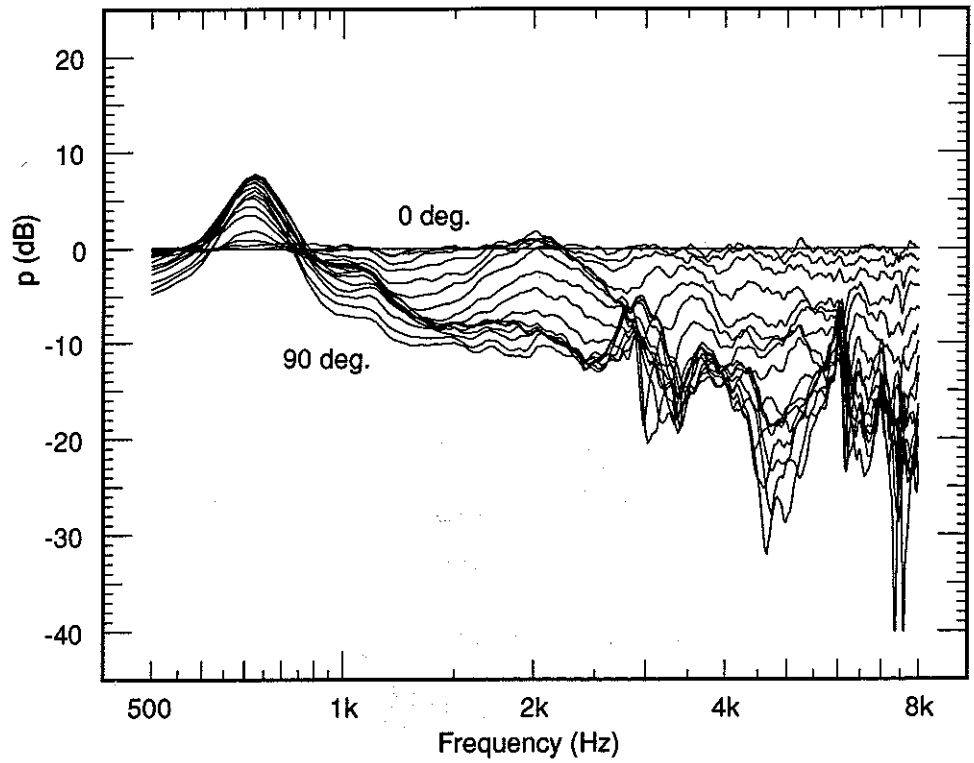

Figure 4.3.4va Directivity Transfer Functions (Vertical Plane) for Horn Type 4.

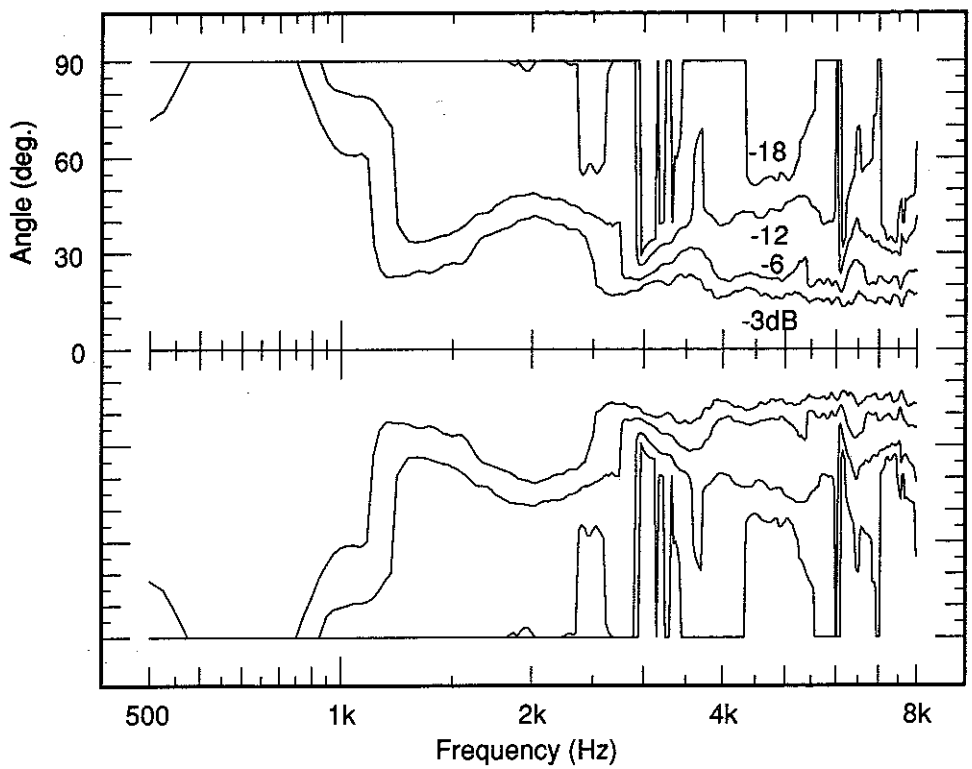

Figure 4.3.4vb Directivity Contours (Vertical Plane) for Horn Type 4.

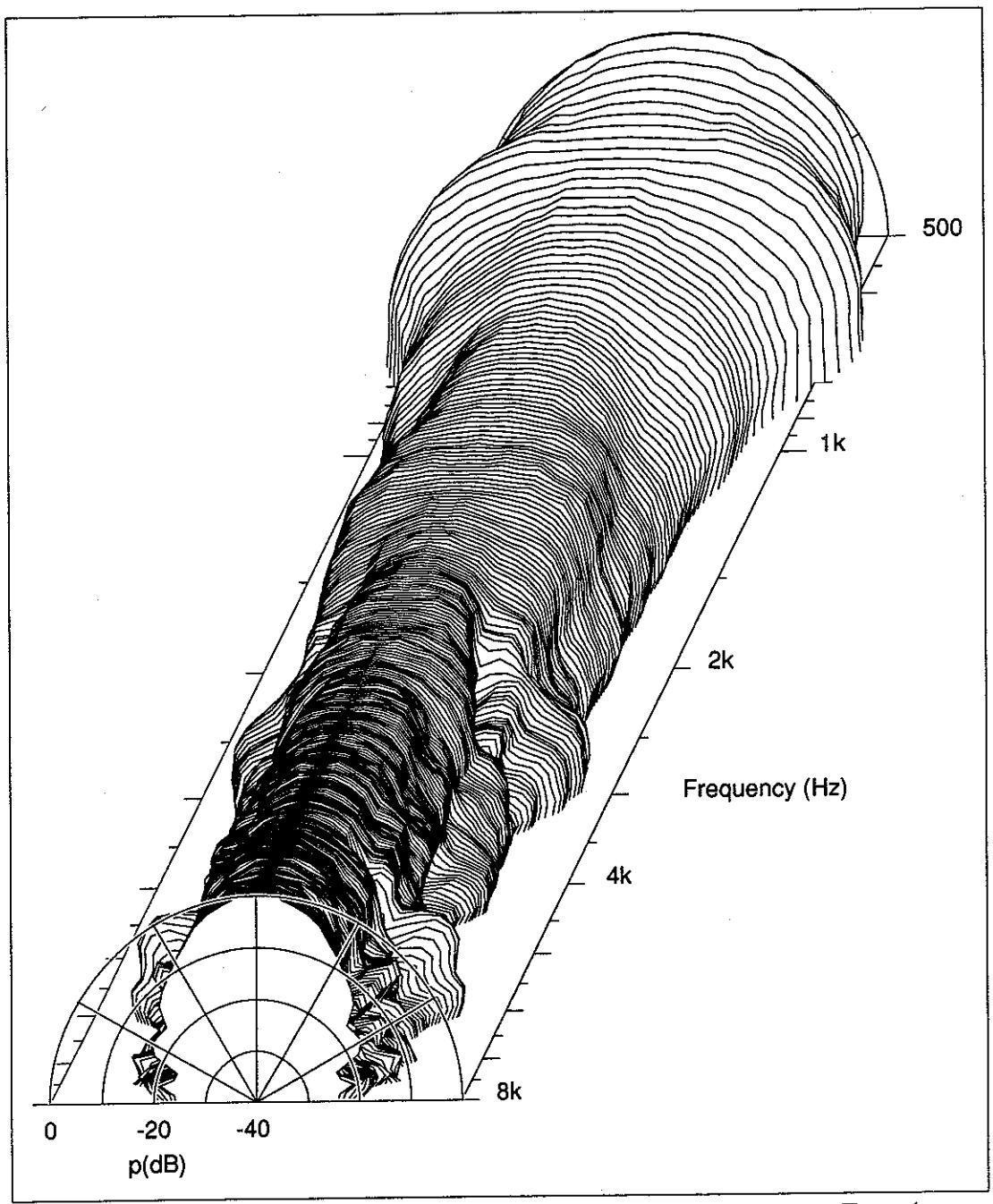

Figure 4.3.4vc Polar Plot Distribution (Vertical Plane) for Horn Type 4.

Figures 4.3.4h show the directivity of horn type 4 in the horizontal plane. All three plots show that this horn has very poor directivity control over most of the frequency range. The horizontal directivity of this horn is severely compromised by the presence of the stiffening pillars which cause shadowing at high frequencies and excitation of transverse modes at low frequencies as seen in the mouth pressure distribution results. As with horn types 2 and 3, a broadening of the directivity pattern is evident at a frequency (750Hz) with a wavelength close to the width of the horn mouth (490mm). Figures 4.3.4v show the directivity of this horn in the vertical plane. The contour plot shows that the directivity is reasonably well controlled at angles close to the horn axis from 1.2kHz with a coverage angle of 70 degrees inclusive to 40 degrees inclusive at 8kHz with a slight broadening to 90 degrees inclusive at 2kHz. Again, the broadening at 750Hz is more evident in the vertical plane than in the horizontal. The pillars do not appear to have affected the directivity in the vertical plane, indeed the vertical directivity of this horn is more controlled and broader than those for the other two rectangular horns tested.

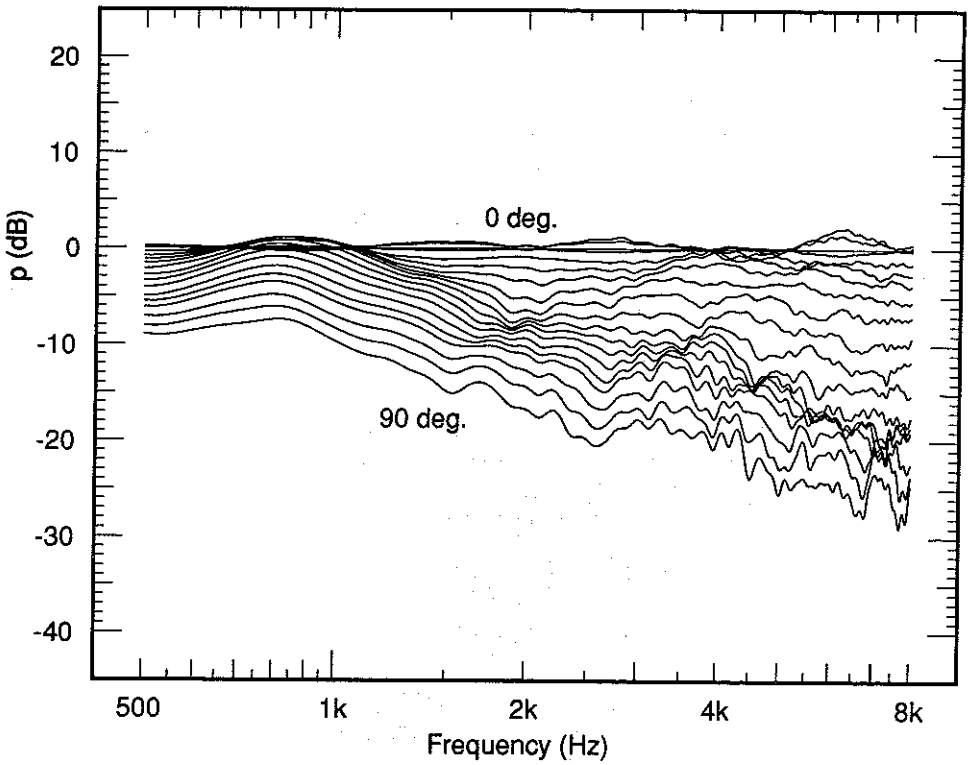

Figure 4.3.5a Directivity Transfer Functions for Horn Type 5.

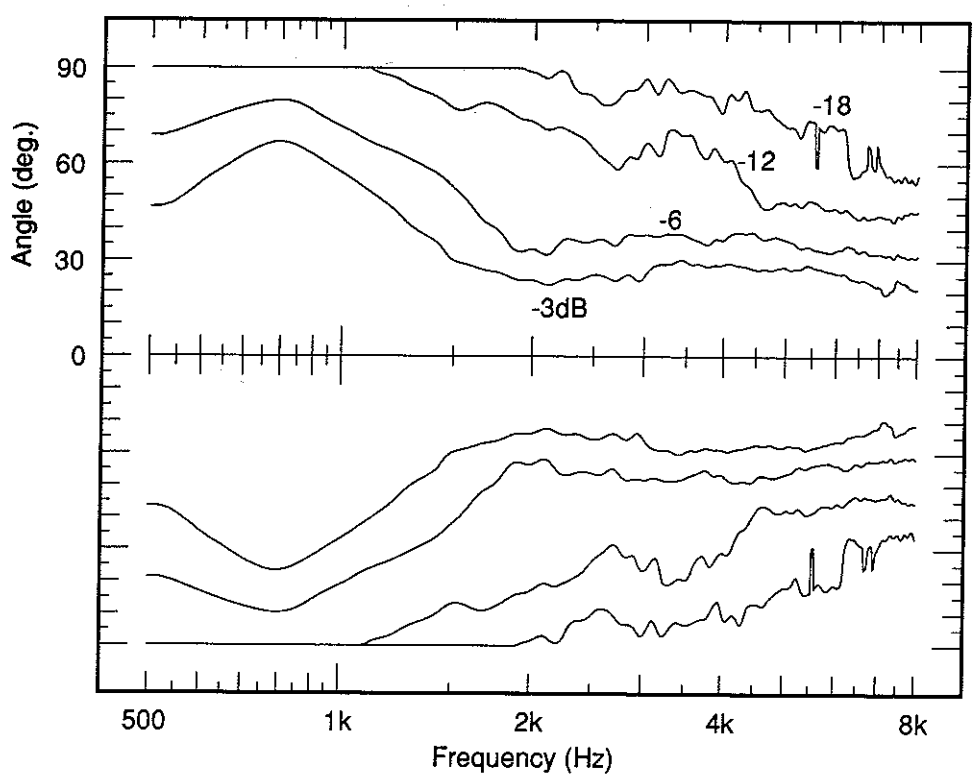

Figure 4.3.5b Directivity Contours for Horn Type 5.

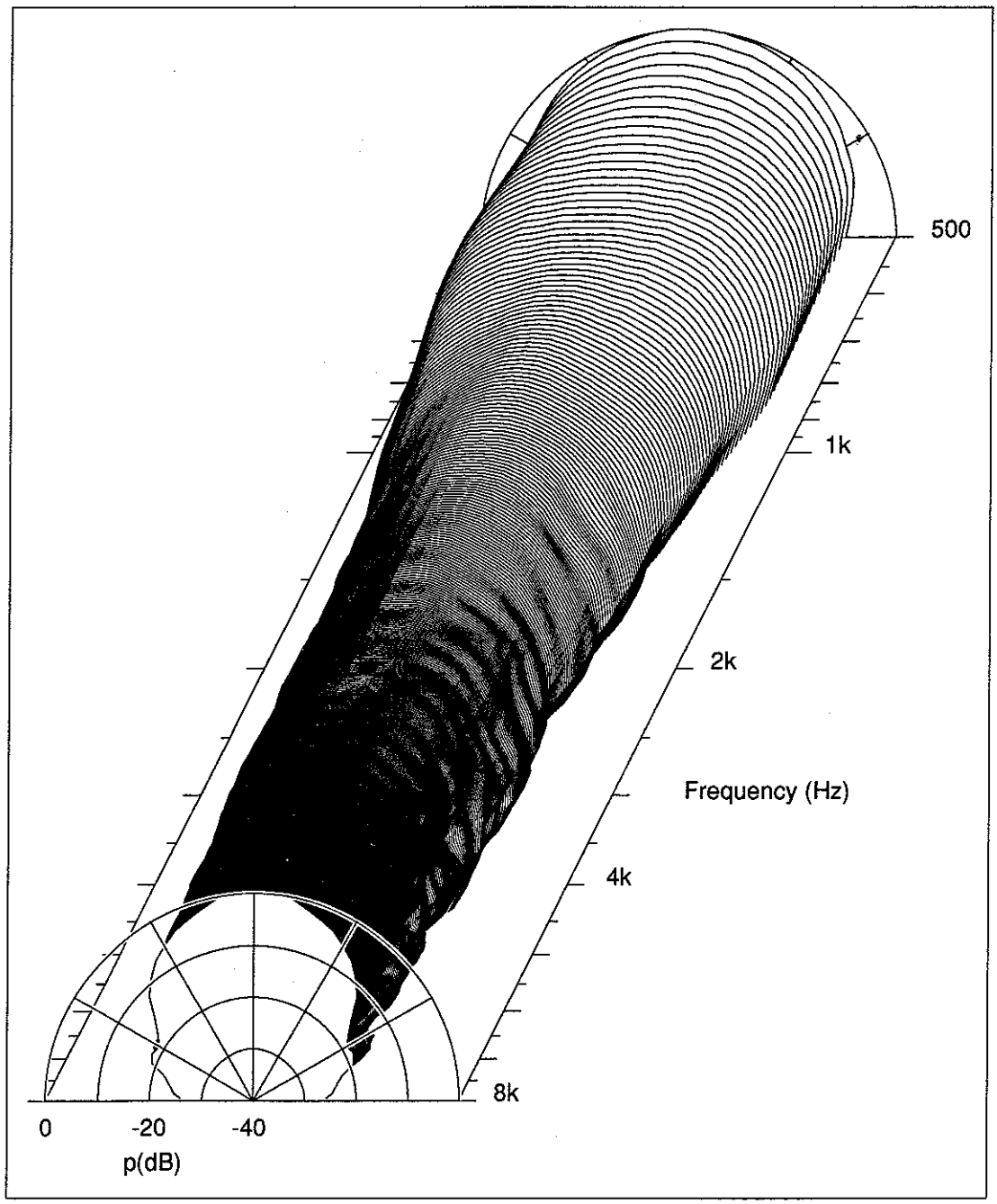

Figure 4.3.5c Polar Plot Distribution for Horn Type 5.

Figures 4.3.5 show the directivity for horn type 5. The contour plot shows that the directivity is widest at 800Hz with a coverage angle of 160 degrees inclusive and narrows to 60 degrees inclusive at 2kHz. The directivity is well controlled at a coverage angle of between 60 and 70 degrees inclusive from 2kHz to 8kHz. The polar plot shows that no significant side-lobes exist at any frequency and that the directivity varies very smoothly with frequency at all angles. Being axisymmetric in shape, the directivity in all planes is the same, so the on-axis frequency response of this horn will be an accurate representation of the total power output above 2kHz, with a gentle tail-off below this frequency. The good directivity control of this horn is due to the adherence of the pressure field within the flare to one-parameter behaviour, the absence of any transverse pressure variations at the mouth and the axisymmetric geometry. The ripple of about 2dB seen in the transfer function plots is due to diffraction from the edge of the horn mouth which affects only the on-axis frequency response (see section 4.4).

4.4 DISCUSSION

The measurements taken of the distribution of pressure phase across the mouths of the horns show that the shape of the wavefronts at the mouths of the rectangular horns are circular arcs normal to the horn walls, and that those for the axisymmetric are 'flattened' spherical caps, over most of the frequency range of the measurements. This shows that the wavefront shape assumptions used in the one-parameter model are valid, as is evident from the agreement between the theoretical and measured throat impedance results (section 3.5.1). The measurements taken of the distribution of pressure amplitude show evidence of departures from one-parameter behaviour in all of the rectangular horns tested. The pressure amplitude distribution for horn type 4 shows that the sound field within the horn is disrupted by the presence of three strengthening pillars within the flare. The effect that these disturbances have on the radiated sound field can be seen in the poor horizontal directivity performance of this horn. The directivity of horn type 3 is better but the mouth pressure distribution is upset by two waveguide plates near the mouth which affect the radiated sound by narrowing the horizontal directivity at high frequencies. The presence of a mechanical resonance in the 'lips' at the mouth of this horn at 3kHz is seen not to affect the horizontal directivity and only affects the vertical directivity at large angles. During the measurements, the sound radiated from the horns was only heard from positions well off-axis or from behind; thus the disturbance of the radiation by

the resonance at wide angles only, explains why the mechanical 'ring' was so audible during the measurements. Despite horn type 2 having no flare discontinuities or other obstructions within the horn, a set of mode-like pressure distributions are present at the mouth due to non-one-parameter reflections from the shallow mouth 'lips'. These 'modes' do not affect the horizontal directivity of the horn, but have a significant effect on the vertical directivity, with the even-order 'modes' causing a reduction in the width of the directivity pattern and the odd-order 'modes' an increase. The mouth pressure distribution results for the axisymmetric horn type 5 show an almost total adherence to one-parameter behaviour. Because of this, and the axisymmetric geometry, the directivity performance is very good, with an almost constant coverage angle above 2kHz in all planes; the changes in response are gradual at all angles throughout the frequency range of the tests.

The gradual narrowing of the coverage angle of horn type 2 with increasing frequency can be a useful asset for a loudspeaker horn as the power response of many horn compression drivers falls off with increasing frequency above the fundamental resonance frequency; the gradual narrowing of the coverage angle of the horn ensures that the on-axis frequency response of the combination remains 'flat' without the need for electronic equalisation. Figure 4.4 shows the on-axis frequency response of this horn in combination with an Emilar EK175 driver. This driver has been used with this horn in a successful monitoring system. The Emilar driver has a power frequency response that peaks at about 1.2kHz and then falls-off at higher frequencies. It can be seen in figure 4.4 that the combination of this falling power response and the decreasing coverage angle of the horn result in a reasonably flat on-axis frequency response. To contrast, figure 4.5 shows the on-axis frequency response of this horn in combination with a TAD TD2001 driver which has a very 'flat' power response from 500Hz to over 20kHz. The on-axis response of this combination rises steadily with increasing frequency. In both responses, the widening of the vertical directivity pattern at 800Hz can be seen as a dip in the on-axis response at that frequency. The peaks at 1.5kHz and 2.5kHz that are common to both responses are due to the peaks in throat impedance shown in figure 3.5.2b, caused by reflections from the horn mouth.

Figure 4.6 shows the on-axis frequency response of horn type 5 in combination with the Emilar EK175 driver and figure 4.7 in combination with the TAD TD2001 driver. This horn has an almost constant coverage angle above 2kHz and a smooth throat impedance, thus the on-axis frequency responses above 2kHz should be

accurate representations of the power response of the drivers. The on-axis response with the Emilar driver can be seen to fall-off above 3kHz due to the falling power response of this driver, and as expected, the on-axis response with the TAD driver is reasonably flat from 1kHz upwards. A ripple of about ±2dB can be seen in both responses above 2kHz. This ripple is due to diffraction from the edge of the axi-symmetric horn mouth which affects the response only very near to on-axis. Figure 4.8 shows the response of the horn type 5 / TAD TD2001 combination at 10 degrees off-axis. The diffraction is seen to have little or no effect at this angle, and the response is almost totally flat from 1kHz upwards. Further measurements revealed that the response of this combination at 10 degrees off-axis remains essentially 'flat' up to 22kHz. Further research is required into methods for reducing the effect of the mouth diffraction on the on-axis response of this horn without compromising either the power response or the directivity.

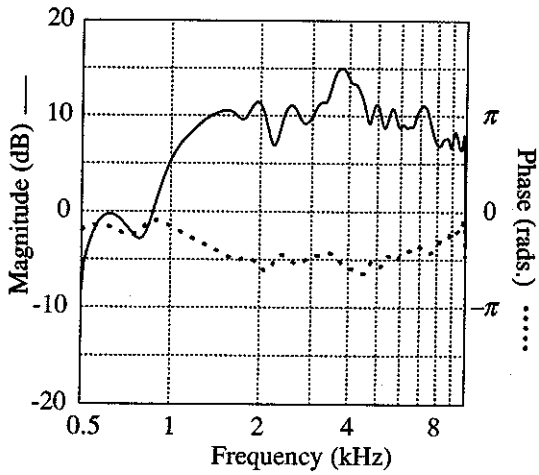

Figure 4.4 On-axis Frequency Response of Horn Type 2 with Emilar EK175 Driver.

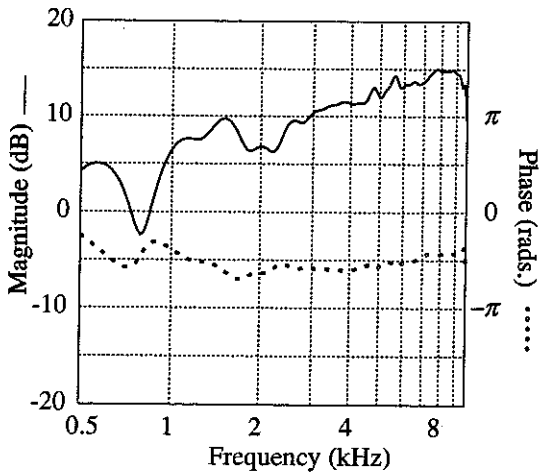

Figure 4.5 On-axis Frequency Response of Horn Type 2 with TAD TD2001 Driver.

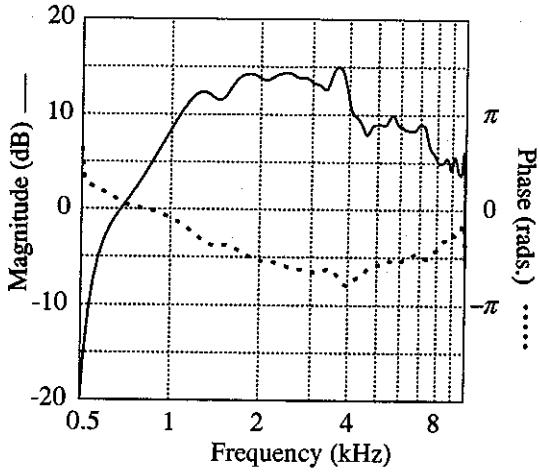

Figure 4.6 On-axis Frequency Response of Horn Type 5 with Emilar EK175 Driver.

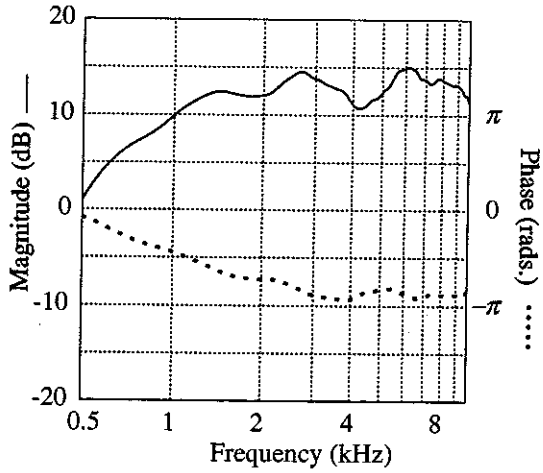

Figure 4.7 On-axis Frequency Response of Horn Type 5 with TAD TD2001 Driver.

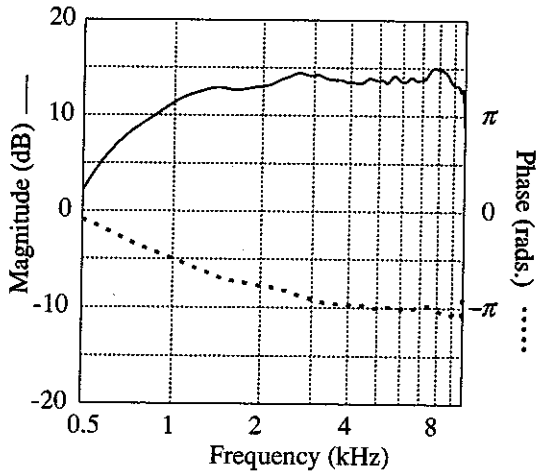

Figure 4.8 Frequency Response of Horn Type 5 at 10 degrees off-axis with TAD TD2001 Driver.

The peak at 3.8kHz seen in the response of both horns when when the Emilar driver is used is due to a mismatch between a rapid flare in the throat section of this driver and the relatively shallow flare at the throats of the horns (see section 6.5.5). The TAD driver has a longer, but much more shallow flare which matches that at the throat of both horns, so a discontinuity at the throat is avoided.

Chapter 5
NON-LINEAR BEHAVIOUR

5.1 INTRODUCTION

Some of the work described in this chapter has been published in references [34] and [35].

The one-parameter finite exponential element model described in chapter 2 was developed using 'Webster's horn equation'. An important assumption inherent in the derivation of this equation (see appendix 1) is that the acoustic pressure and particle velocity have infinitesimal amplitude. This enables the non-linear terms that result from consideration of the thermodynamics of sound propagation to be neglected, resulting in a 'linearised' form of the equation which can be solved analytically. For the study of sound fields where the acoustic pressures are very small fractions of the static pressure (P_o) and the particle velocities, very small fractions of the speed of sound (c_o), this assumption is a valid one, and the resultant linear equations sufficiently accurate. This is the case for many sound fields and indeed, all commonly used linear acoustic theory is based around this assumption.

The high electroacoustic efficiency of horn / compression driver loudspeaker systems leads to their use for the production of high sound pressure levels. This is important when horns are used in public address systems, where propagation over large distances may be required, and is the main reason for their widespread use in this application; even in a studio monitoring environment, if the studio is reasonably large and acoustically 'dead', the loudspeaker system may be called upon to reproduce high peak sound pressure levels, particularly in the mid-frequency range. In order to produce high levels in the far-field, very high acoustic pressures and particle velocities must be present at the small throat of a horn and particularly in the compression driver; a typical high quality compression driver can produce sound pressure levels of over 140dB in a plane-wave tube for an input of 1W of electrical power. The same driver may have a thermally limited maximum power handling of 100W, leading to sound pressure levels in excess of 160dB at the throat of a horn to which it is attached. When a typically 10 or 20:1 compression ratio for the driver is considered, sound pressure levels of 170 to 180dB are possible at the diaphragm. It is clear from the above levels that linear acoustic modelling of the horn and driver is not likely to be valid at high drive levels.

Of the many sources of system non-linearity possible at these levels, three are expected to be predominant. One involves the electro-mechanical limitations of the

5.1 INTRODUCTION

Some of the work described in this chapter has been published in references [34] and [35].

The one-parameter finite exponential element model described in chapter 2 was developed using 'Webster's horn equation'. An important assumption inherent in the derivation of this equation (see appendix 1) is that the acoustic pressure and particle velocity have infinitesimal amplitude. This enables the non-linear terms that result from consideration of the thermodynamics of sound propagation to be neglected, resulting in a 'linearised' form of the equation which can be solved analytically. For the study of sound fields where the acoustic pressures are very small fractions of the static pressure (P_o) and the particle velocities, very small fractions of the speed of sound (c_o), this assumption is a valid one, and the resultant linear equations sufficiently accurate. This is the case for many sound fields and indeed, all commonly used linear acoustic theory is based around this assumption.

The high electroacoustic efficiency of horn / compression driver loudspeaker systems leads to their use for the production of high sound pressure levels. This is important when horns are used in public address systems, where propagation over large distances may be required, and is the main reason for their widespread use in this application; even in a studio monitoring environment, if the studio is reasonably large and acoustically 'dead', the loudspeaker system may be called upon to reproduce high peak sound pressure levels, particularly in the mid-frequency range. In order to produce high levels in the far-field, very high acoustic pressures and particle velocities must be present at the small throat of a horn and particularly in the compression driver; a typical high quality compression driver can produce sound pressure levels of over 140dB in a plane-wave tube for an input of 1W of electrical power. The same driver may have a thermally limited maximum power handling of 100W, leading to sound pressure levels in excess of 160dB at the throat of a horn to which it is attached. When a typically 10 or 20:1 compression ratio for the driver is considered, sound pressure levels of 170 to 180dB are possible at the diaphragm. It is clear from the above levels that linear acoustic modelling of the horn and driver is not likely to be valid at high drive levels.

Of the many sources of system non-linearity possible at these levels, three are expected to be predominant. One involves the electro-mechanical limitations of the

driver, including thermal power compression effects, magnet/gap problems, etc. The second source of non-linearity involves the volumetric changes in the cavity between the diaphragm and the phase plug, and the third involves non-linear propagation within the horn and driver, leading to the possibility of the production of shock waves. The first non-linear mechanism is common to all electro-magnetic loudspeakers and the second is reasonably straightforward to predict; both of these mechanisms have been well researched and documented. The third mechanism has been little researched to date and the following is concerned with the study of this source of non-linearity.

5.2 DESCRIPTION AND IMPLEMENTATION OF THE FINITE AMPLITUDE MODEL

If it could be assumed that the sound field within horns, and that radiated to the far-field, consisted of a single progressive wave from the throat out to infinity, the calculation of the sound field for finite amplitudes, to reasonable accuracy would not be too difficult. However, all practically realizable horns produce, to a greater or lesser extent, reflections from the mouth termination and from discontinuities within the horn flare. Sound propagation within horns is also often dispersive in nature. These complications prevent the prediction of the propagation of finite amplitude waves in such horns by empirical means based on pressure amplitude and propagation distance alone. When dealing with infinitesimal amplitude (linear) waves, it is possible to predict directly the response at one end of a horn due to any input applied at the other, as the presence of a reflected wave does not affect the propagation of an incident wave. Such linear superposition does not apply when dealing with waves of finite amplitude. In this case it is impossible to follow a wave from one end to the other and back again because the forward and backward waves will interact in a complicated manner. It is therefore necessary, under these conditions, to assume that the mouth termination can be characterised by a linear radiation impedance (which is reasonable if the mouth is fairly large) and to model the sound field 'backwards' in time to the input. Pla and Reethof [36] developed a model of the propagation of finite amplitude waves in horns which included boundary layer effects and, because reflections were neglected, they were able to model 'forwards' in time from input to output. The model described below attempts to include reflections and thus predicts the input necessary at the throat of a horn to achieve a desired output at the mouth.

In order to model horns with arbitrary area profiles, it is necessary to split the horn into short exponentially shaped elements, within which the linear standing-wave solution is expressible in closed analytical form, in the same manner as for the linear horn model (see chapter 2). This splitting into elements allows predictions of non-linear behaviour to be implemented in a semi-numerical manner, with the linearly predicted field corrected for finite amplitude distortion over a short distance at the end of each element. This approach involves the calculation of the linear propagation in the frequency domain, and of the non-linear distortion in the time domain; the two sets of calculations being linked by Fourier Transform.

The symbols used in the following description of the model refer to the flow diagram shown in figure 5.1.

5.2.1 Linear Propagation.

The definition of the exponential elements, including the wavefront approximations, and the solutions of equation (2.1) are identical to those for the linear model (see appendix 1).

The linear propagation of an arbitrary waveform along a horn element can best be modelled in the frequency domain, thus the desired starting (horn output) waveform ($p_o(t)$) is transformed into the frequency domain via a Fourier transform. Given the resultant complex pressure spectrum ($p_o(f)$) at the mouth of the element, the flare-rate and length of the element, and the mouth impedance ($Z_o(f)$), the complex amplitudes of the forward and backward propagating pressures at the throat of the element ($p_A(f)$ and $p_B(f)$ respectively) can be calculated from the solutions of equation (2.1):

$$\hat{p}_A(f) = -ik\hat{p}_o(f)\left\{\frac{1 - \hat{\gamma}^-\hat{Z}_o(f)}{(\hat{\gamma}^+ + \hat{\gamma}^-)\hat{Z}_o e^{\hat{\gamma}^+ l}}\right\} \quad \text{and} \quad \hat{p}_B(f) = \frac{\hat{p}_o(f) - \hat{p}_A(f)e^{\hat{\gamma}^+ l}}{e^{\hat{\gamma}^- l}} \quad ,$$

where γ^+ and γ^- are the forward and backward complex propagation coefficients respectively, and l is the length of the element. The complex amplitudes of the forward and backward particle velocities at the throat ($u_A(f)$ and $u_B(f)$ respectively) are then

$$\hat{u}_A(f) = i\left\{\frac{\hat{\gamma}^+\hat{p}_A(f)}{\rho_o c_o k}\right\} \quad \text{and} \quad \hat{u}_B(f) = i\left\{\frac{\hat{\gamma}^-\hat{p}_B(f)}{\rho_o c_o k}\right\} \quad .$$

These separate pressures and particle velocities are then each transformed into the

time domain via inverse Fourier transforms.

5.2.2 Non-linear Waveform Distortion.

The speed of propagation of a sound wave at a point in the horn element is dependent upon the local pressure and particle velocity at that point. At finite amplitudes, this causes a waveform to distort in shape as it propagates. In a free progressive wave, this results in the positive half cycle of the waveform propagating faster than the negative half cycle, giving rise to steepening of sinusoids and eventual shock formation. Because of dispersion and reflections, the characteristic impedance of a wave within an exponential element is usually complex, so the equations for the calculation of waveform steepening in free progressive waves cannot be used. Instead a more universal equation for the local propagation speed ($c(t)$) is necessary:

$$c(t)^{\pm} = c_o \left\{ \frac{P_o + p_T(t)}{P_o} \right\}^{\left(\frac{\gamma-1}{2\gamma}\right)} \pm u_T(t) \quad \text{m/s} \quad ,$$

where c_o is the linear assumed sound speed for the particular static pressure P_o, $p_T(t) = p_A(t) + p_B(t)$ and $u_T(t) = u_A(t) + u_B(t)$ are the instantaneous total acoustic pressure and particle velocity respectively, γ is the ratio of the specific heats of the propagating fluid and $\pm$ refers to calculation for forward and backward waves respectively. The 'time advance' ($T(t)$) of a sample of a waveform compared to its linear propagation can then be calculated:

$$T(t)^{\pm} = \frac{-l}{c_o} \left\{ \frac{c_o}{c(t)^{\pm}} - 1 \right\} \quad \text{secs.} \quad ,$$

where $-l$ is the distance propagated. The concept of a negative propagation distance is introduced to avoid the complications involved with negative time and hence negative velocities. In order to maintain linear spacing between the waveform sample points for subsequent FFT calculations, it is necessary to re-sample each distorted pressure and velocity waveform using linear interpolation between the distorted time points. This distorting and re-sampling process is implemented as follows.

The values of time in seconds for each of the 256 time points (relative to the first time point) and the calculated forward time advances are stored in arrays ($t(t)$ and $T_A(t)$ respectively) along with the forward pressure waveform ($p_A(t)$). The time advance array ($T_A(t)$) is then inspected to find the maximum value of time advance (T_{max}), which is rounded up to an integer number of sample points, and the time array ($t(t)$) is added to $T_A(t)$ so that the time advances become 'distorted' values of

time. Each point (t) in $t(t)$ is then scanned from $t' = t - T_{max}$ to $t' = t + T_{max}$ until $T_A(t) > t(t')$; the distorted pressure waveform ($p_{dA}(t)$) then results from shifting by $t' - t$ points and then interpolating between the points of the un-distorted waveform ($p_A(t)$) thus:

$$p_{dA}(t) = p_A(t' - 1) + \left\{ \frac{\left(p_A(t') - p_A(t' - 1)\right)\left(t(t) - T_A(t' - 1)\right)}{T_A(t') - T_A(t' - 1)} \right\} .$$

This process, shown graphically in figure 5.2, is repeated for the backward pressure waveform (with $p_B(t)$, $T_B(t)$ and $p_{dB}(t)$ in place of $p_A(t)$, $T_A(t)$ and $p_{dA}(t)$), and the two velocity waveforms. As the model cannot handle shock propagation, the time advances are checked to ensure that none of the time points overlap, indicating shock generation.

The two distorted pressure time waveforms are then added ($p_{dT}(t)$) and transformed into the frequency domain for use as the starting waveform for the next element ($p_o(f)$). The particle velocity waveforms are also added ($u_{dT}(t)$) and transformed, and the frequency domain total distorted pressure and particle velocities are used to calculate the impedance for the next element thus:

$$\hat{Z}(f) = \frac{\hat{p}_{dT}(f)}{\rho_o c_o \, \hat{u}_{dT}(f)} .$$

When the throat of the last element is reached, the total distorted pressure or particle velocity waveform can be considered to be that input necessary at the throat of the horn to give the original starting waveform as output at the mouth.

The model as described was programmed in BBC BASIC V on an Acorn Archimedes microcomputer. All of the calculations, including the 256 point FFT and inverse FFT (IFT) routines used for the time / frequency domain transformations, are carried out using standard precision (5 byte) real numbers.

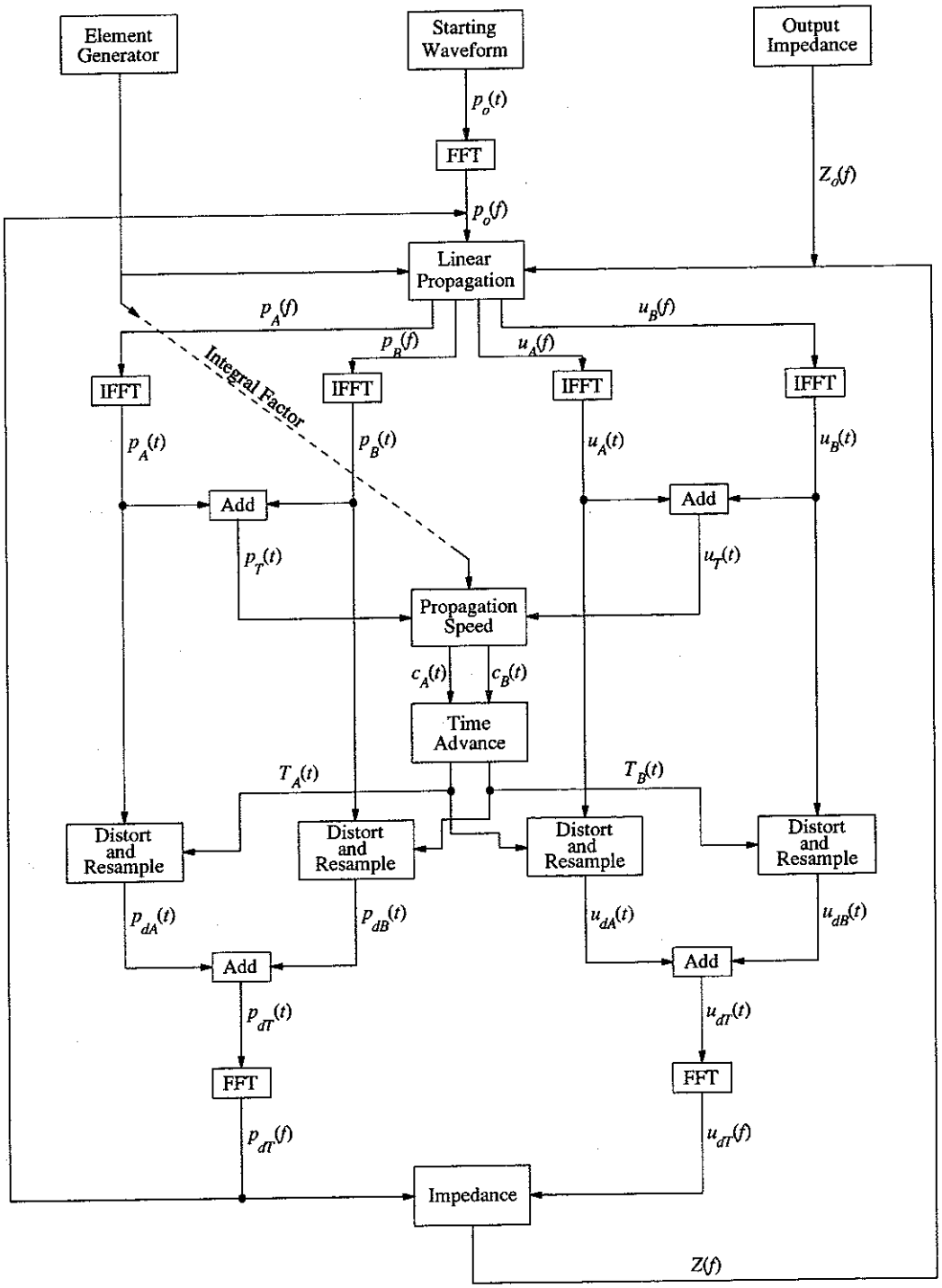

Figure 5.1 Flow Chart for Finite Amplitude Horn Model

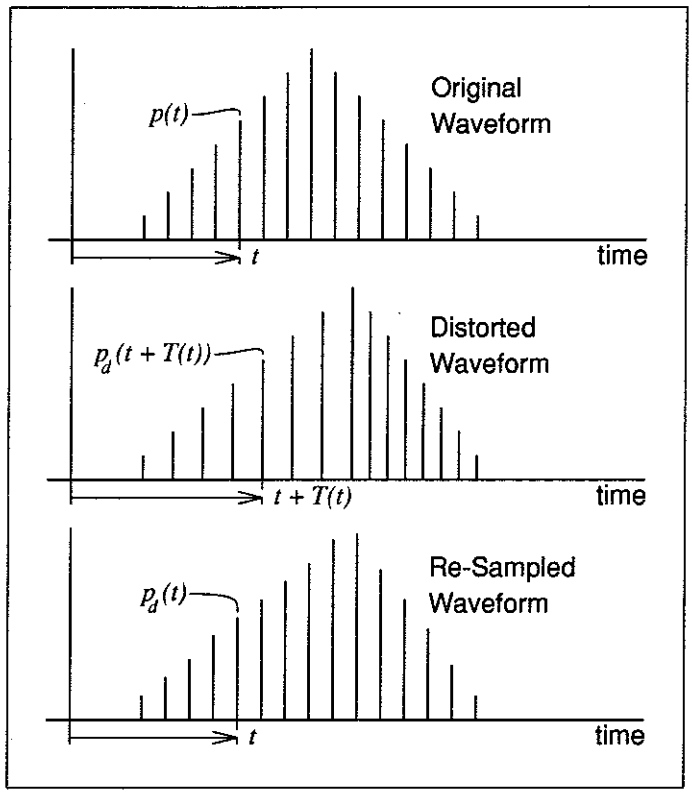

Figure 5.2 Distortion and Re-Sampling of Discrete Waveform.

5.3 TESTING OF THE MODEL

5.3.1 Time Domain Sample Rate.

In order to give maximum resolution in the frequency domain for periodic starting waveforms such as sinusoids, the time domain sample rate is chosen to be an integer division of the time period of the waveform (actually $^1/_{32}$). For transient starting waveforms, a suitable sample rate for the duration and bandwidth of the transient is chosen. A problem became apparent when a large number of elements were used (n>20) and the starting waveform was periodic. It is reasonable to assume that any distortion should appear only as harmonics of the waveform fundamental, however when such a starting waveform was used, spurious frequencies were observed in the spectra after propagation through a large number of elements. This was traced to the lack of any 'signal' at those frequencies, allowing the rounding errors (noise) in the computations to appear as very large numbers in the calculation of impedance at those frequencies (a small number divided by a very small number giving a large number) which after a large number of elements allowed significant values for pressure to appear. A first attempt to overcome this problem was to 'pad' the starting

waveform with a small delta function to give some signal at all frequencies. This resulted in gross amplification at low frequencies, below the cut-off of the horn, (where large amounts of 'input' are necessary at the throat to appear as small outputs on the starting waveform) making the problem worse. Finally it was decided that for sinusoidal starting waveforms, only the harmonics would be calculated in the frequency domain, all other frequencies being held to zero. This technique appears to work well. For transient starting waveforms the problem does not occur and frequency domain calculations are carried out at all frequencies.

5.3.2 Solution Convergence.

The solutions of the linearised horn equation used in the model described in chapter 2 are accurate (within the one-parameter assumptions) for any length of element, and at any frequency, provided the horn area profile is exponential. For this model however, this is not the case as the interactions between the forward and backward waves are likely to vary within the space of one wavelength of the highest frequency of interest. To investigate the effect of varying the number of elements on the model results, an axisymmetric horn having an exponential area profile and poor mouth termination was modelled first using one element and then increasing the number of elements until convergence of the result was apparent. Figure 5.3 shows the results of this modelling in terms of the levels of 2nd, 3rd and 4th harmonics present at the throat of the horn when a sinusoidal starting waveform at a frequency of 1000Hz and a level of 150dB SPL is present at the mouth of the horn. The horn has a cut-off frequency of 150Hz.

As can be seen in figure 5.3, if sufficient elements are not used, the model tends to overestimate the degree of non-linearity compared to the result for a much larger number of elements. This problem was traced to the fact that the total pressure and particle velocity values that are used for the speed of propagation calculations are those that occur at the small end (throat) of each element and, as such, the calculations are always the 'worst case' approximations to the actual degree of non-linearity. To overcome this problem a weighting factor (shown dotted in figure 5.1) was introduced into the calculations by assuming that, for a given forward or backward wave, the product of the pressure and the square root of the area remains constant throughout an element (conservation of power flow). Because of the exponential shape of each element, the integral of this function over an element

appears as a multiplying constant in both the pressure and particle velocity terms:

$$\text{Factor} = \frac{1}{l}\int_0^l e^{\frac{-mx}{2}}\,dx = \frac{2}{ml}\left(1 - e^{\frac{-ml}{2}}\right) ,$$

where l is the length and m is the flare-rate of the element. The only other assumption inherent in this procedure is that the 'distorting effect' varies linearly with pressure and particle velocity over an element; this is reasonable for a short element. After this modification, the convergence test was re-run and the results are shown in figure 5.4. It can be seen that the convergence is now very much more rapid as the number of elements is increased and that more reliable results could be obtained with few elements.

5.3.3 Parametric Study of Model Output.

The following sections deals with some initial investigations into the behaviour of the model when the mouth output sound pressure level and fundamental frequency are varied. In all of these tests the starting waveform is sinusoidal, allowing the degree of non-linearity to be estimated from harmonic distortion figures. The test results are typical example results for a mid-frequency range loudspeaker horn driven at high levels.

Figure 5.5 shows the levels of fundamental, 2nd, 3rd and 4th harmonics present at the throat of the horn for a sinusoidal starting waveform (pressure at mouth) of 150dB SPL over a range of frequencies from 100Hz to 5kHz.

Figure 5.6 shows the levels of fundamental, 2nd, 3rd and 4th harmonics present at the throat of the horn for a sinusoidal starting waveform with a frequency of 1000Hz over a range of levels from 90dB SPL to 170 dB SPL.

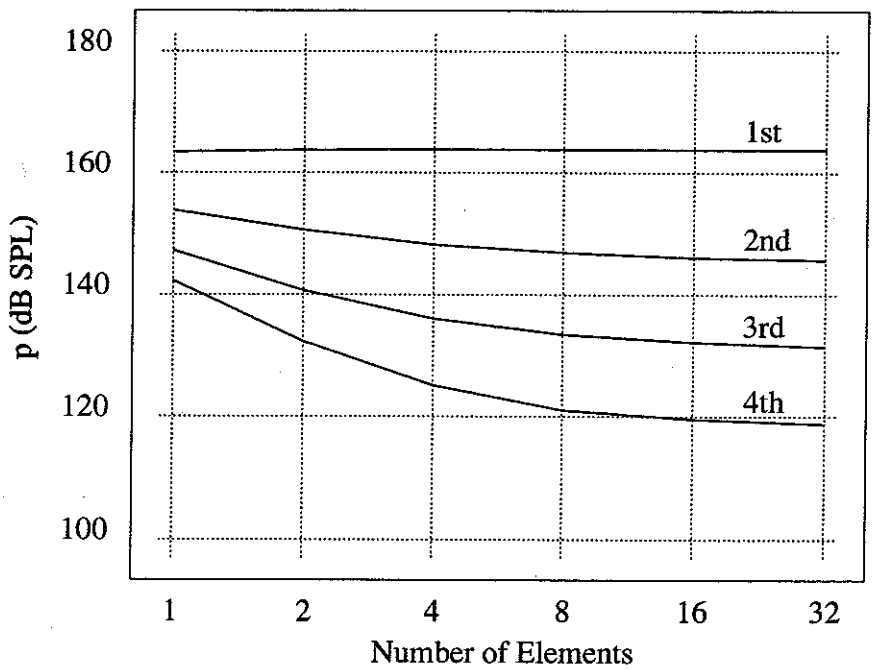

Figure 5.3 Convergence of solution with increasing number of elements

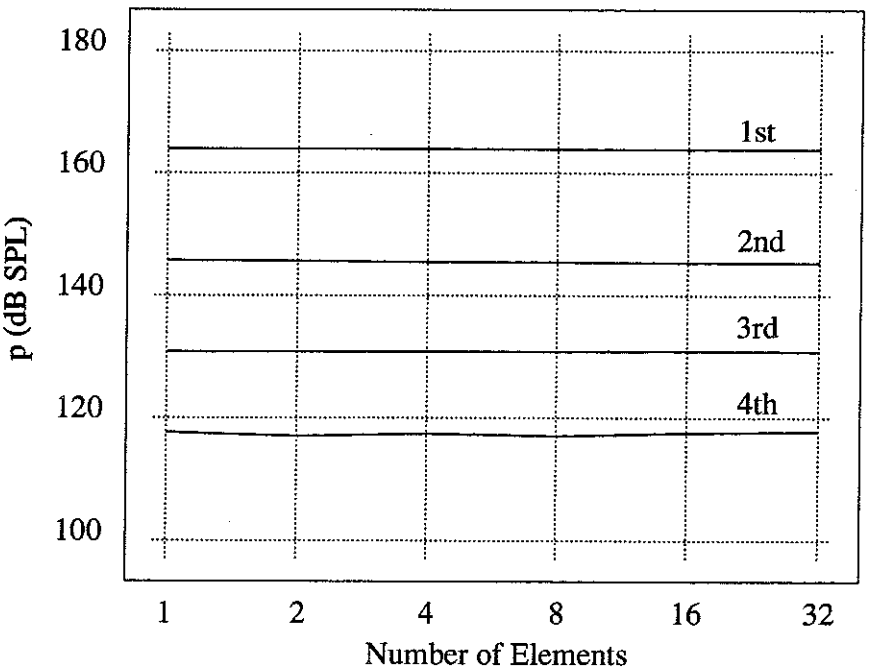

Figure 5.4 As Figure 5.3 with Integrated Factor Correction

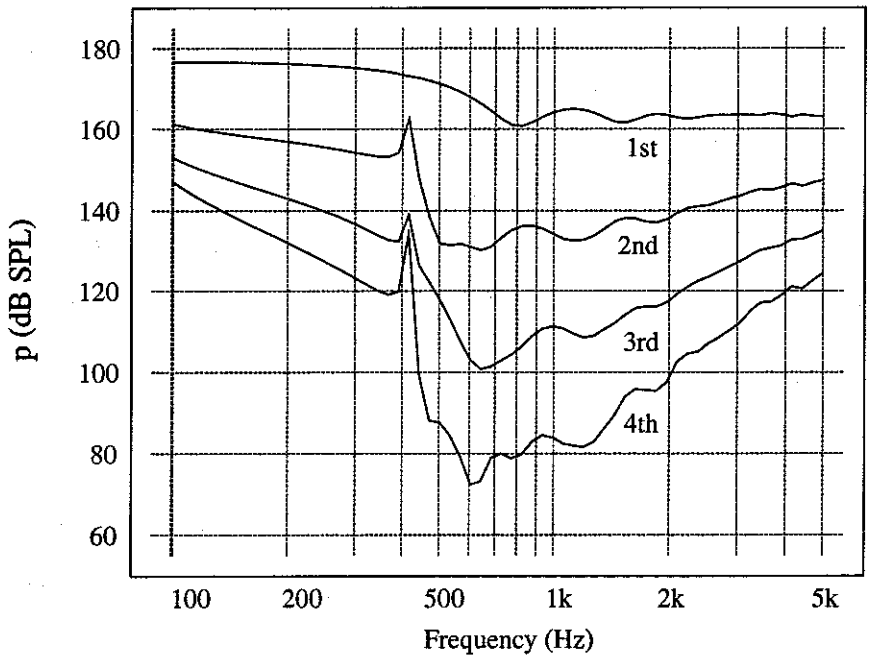

Figure 5.5 Sound Pressure Levels of Harmonics at the Throat of a Horn for a Sinusoidal Mouth Sound Pressure Level of 150dB over a Range of Frequencies.

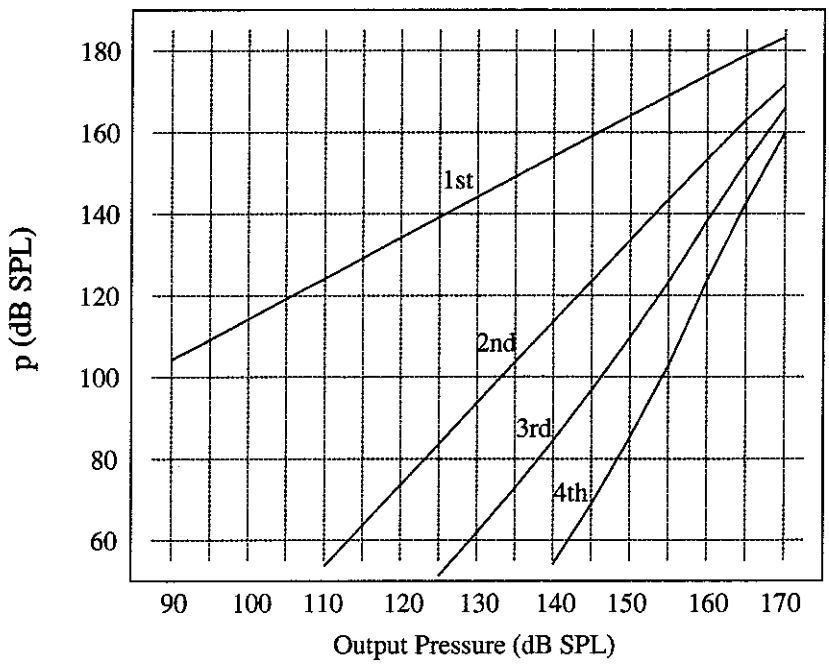

Figure 5.6 Sound Pressure Level of Harmonics at the Throat of a Horn for a Range of Sinusoidal Mouth Sound Pressure Levels at 1kHz.

5.4 EXPERIMENTAL VERIFICATION OF MODEL

In order to verify that the model could reliably predict the the propagation non-linearity in horns, an experiment was set up to measure the performance of a 'real' horn for comparison with the model predictions. The initial intention was to use the model output to drive the horn via a digital-to-analogue converter and then compare the waveform at the mouth of the horn with the sinusoidal starting waveform. This method would have required a great deal of setting up and the system frequency response and inherent non-linearities prior to the horn would have to be taken into account; even if this were done, because of the standing-wave field within the horn, the wave reflected from the mouth would be distorted, so the waveform generated by the driver would not be that of the pressure at the throat (a driver is not a perfect pressure source). Because of these complications and uncertainties, a simpler, essentially self-calibrating, method was preferred. This method involved measuring the amplitude and phase spectra of the harmonics at the mouth of the horn with a sinusoidal input to the driver, then using these measured mouth harmonics to define the starting waveform for the model. Direct comparison could then be made between measurements of the harmonics at the throat and the output from the model.

To reduce as far as possible the effects of errors in the linear part of the modelling, the small axisymmetric horn, which was successfully modelled in chapters 2 and 3, was chosen for the measurements. The small mouth of this horn gives rise to a strong standing-wave field within the flare, and so provided a suitable challenge to this aspect of the modelling. Choice of a suitable means of driving the horn at very high levels was made on the basis of reliability and low inherent source non-linearity, which ruled out the direct connection of available 1" throat drivers. A Community M4 driver, having a 4" throat and an output capability of over 100 acoustic Watts continuous was therefore used. Initial investigations showed that this driver produced harmonics at least 40dB below the fundamental (1% harmonic distortion) at 150dB SPL over the frequency range of 200Hz to 2kHz when driving an ideal load.

The horn was mounted in a baffle between two measurement rooms (see figure 3.4) and the driver clamped to the flange of the horn. Measurements of the sound fields were taken using a Brüel and Kjær 4135 $^1/_4$" measurement microphone connected to a Brüel and Kjær 2032 dual channel FFT analyser set up to measure instantaneous power and phase spectra. A small hole, to fit the microphone was drilled in the horn

to permit measurement of the sound field at the throat. The signal source was a precision sine-wave oscillator connected to the driver via a $^1/_3$rd octave filter set, a manual 'push-on, release-off' button and a Crown DC300 power amplifier. To guard against possible damage to either / or the power amplifier and driver, and to ensure that unwanted sources of non-linearity were kept to a minimum, the output from the power amplifier was monitored on the other channel of the analyser and was observed to produce harmonic distortion at least 70dB below the fundamental throughout the experiment. Measurements were first made of the sound field at the throat of the horn at a number of drive levels and spot frequencies. For each drive condition, The following procedure was followed:

1) Press signal button.
2) Immediately trigger analyser.
3) Release signal button (total duration of signal < 0.5s).
4) Note frequency of signal.
5) Note spectral level and phase of harmonics in microphone output.
6) Check level of harmonics in power amplifier output.
7) Note output voltage from power amplifier.

The microphone was then moved to the mouth of the horn and the measurements repeated but with the drive voltage 'matched' to those for the throat measurements.

The measured amplitude and phase spectra of the harmonics at the mouth were used to define the starting waveform for the modelling of the horn, and the resultant throat harmonics were compared to the measured values. Figure 5.7 shows the measured mouth spectra and the measured and theoretical throat spectra in tabular form; figure 5.8 shows the same in graphical form.

		Measured Mouth Spectra		Throat Spectra dB SPL	
f (Hz)	Harmonic	dB SPL	Degrees	Measured	Theoretical
200	1	134	146	160	159
	2	95	-144	114	116
	3	110	-149	-	127
350	1	112	128	140	135
	2	81	86	92	90
	3	90	19	87	101
350	1	124	89	150	147
	2	95	6	115	98
	3	93	-110	87	104
350	1	135	80	160	158
	2	112	-26	126	125
	3	111	-59	134	122

Continued:-

		Measured Mouth Spectra		Throat Spectra dB SPL	
f (Hz)	Harmonic	dB SPL	Degrees	Measured	Theoretical
600	1	129	63	150	146
	2	94	154	110	108
	3	96	154	96	104
600	1	141	52	160	158
	2	117	159	132	131
	3	104	-50	133	113
800	1	139	18	150	146
	2	99	171	110	113
	3	93	20	100	102
800	1	150	-1	160	157
	2	122	127	132	135
	3	105	-41	134	116
1000	1	131	-75	140	140
	2	89	50	98	98
	3	86	135	-	96
1000	1	141	-88	150	150
	2	108	27	116	117
	3	91	65	104	102
1600	1	140	-156	150	148
	2	106	-99	111	118
	3	-	-	91	87
1600	1	151	-172	158	159
	2	127	-128	139	139
	3	102	-56	128	117
2000	1	129	-19	140	140
	2	92	-126	99	101
2000	1	139	-31	150	150
	2	109	-172	117	119
2400	1	131	150	140	140
	2	94	159	94	106
	3	-	-	89	71
2400	1	141	150	150	150
	2	113	158	114	125
	3	-	-	93	99
3600	1	134	-69	140	143
	2	97	18	104	112
	3	-	-	95	84
3600	1	144	-93	150	153
	2	118	-22	124	133
	3	96	123	103	115
4800	1	134	-135	140	144
	2	91	133	94	108
4800	1	144	-147	150	154
	2	111	116	115	128
	3	92	-156	101	111

Figure 5.7 Comparison between the Measured and Predicted Sound Pressure Levels of Harmonics at the Throat of Test Horn.

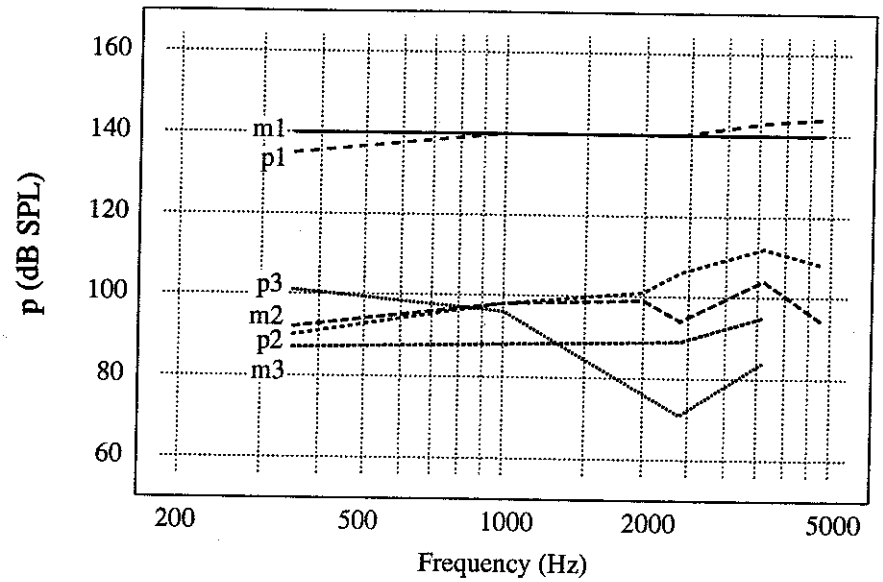

m1 = Measured 1st Harmonic, p1 = Predicted 1st Harmonic etc.

Figure 5.8a Comparison between the Measured and Predicted Sound Pressure Levels of Harmonics at the Throat of Test Horn: Throat Fundamental at 140dB SPL.

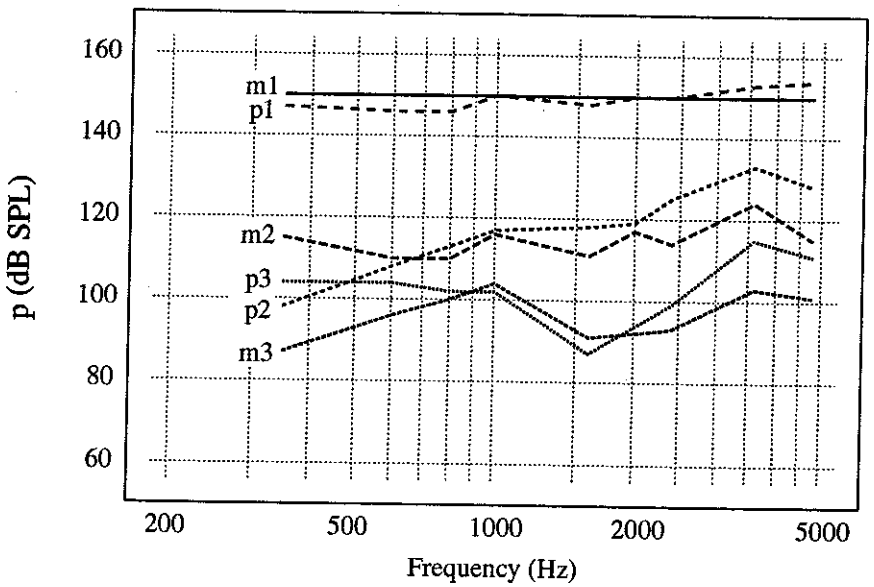

m1 = Measured 1st Harmonic, p1 = Predicted 1st Harmonic etc.

Figure 5.8b Comparison between the Measured and Predicted Sound Pressure Levels of Harmonics at the Throat of Test Horn: Throat Fundamental at 150dB SPL.

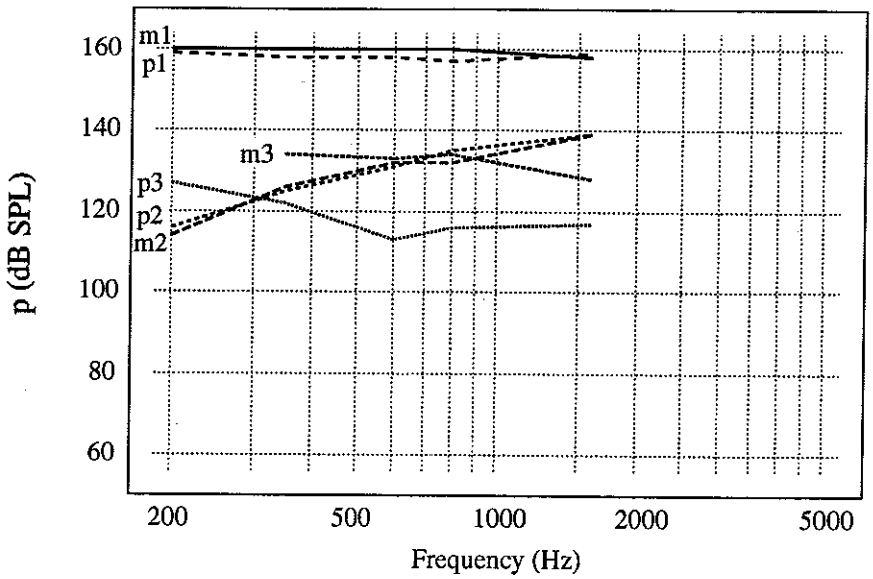

m1 = Measured 1st Harmonic, p1 = Predicted 1st Harmonic etc.

Figure 5.8c Comparison between the Measured and Predicted Sound Pressure Levels of Harmonics at the Throat of Test Horn: Throat Fundamental at 160dB SPL.

5.5 DISCUSSION

5.5.1 Parametric Study of Model Output.

Figure 5.5 shows the levels of fundamental, 2nd, 3rd and 4th harmonics that need to be present at the throat of a typical mid-frequency range loudspeaker horn, to give sinusoidal pressure waveforms of 150dB SPL at the mouth over a range of frequencies (model 'starting waveforms'). The horn has an exponential area profile, a throat diameter of 25mm, a length of 200mm and a cut-off frequency of 420Hz. It can be seen that the levels of the harmonics are high at the frequency extremes, indicating high distortion, with minimum distortion at about 650Hz. A sharp rise in distortion is also evident at the cut-off frequency. Non-linearity in a free propagating wave is characterised by increasing distortion with increasing frequency; this phenomenon can be seen for frequencies above about 650Hz. The rise in distortion at low frequencies is due to the high levels of fundamental necessary at the throat below the cut-off frequency to maintain a mouth pressure of 150dB SPL. The peak in distortion at the cut-off frequency is thought to be due to bad conditioning of the linear equations used to calculate the forward and backward pressure amplitudes when the imaginary part of the propagation coefficient is near zero. At fundamental

frequencies near the cut-off frequency, the reflection coefficient at the mouth of the element is close to -1, so large amplitude forward and backward pressure waves add at the throat of the element to produce a relatively small total fundamental pressure; the reflection coefficients for the calculated harmonics for the two waves are not close to -1 so when they are added, large amplitudes remain. This is almost certainly a problem with the mathematical representation of the sound field as the sum of forward and backward waves, and not a real physical phenomenon, as such waves do not strictly exist in a highly reactive field with infinite phase speed (it is not a precision problem as the summation of the forward and backward waves gives the 'correct' linear solution). Further measurements of distortion over a narrow range of frequencies near the cut-off of a horn would be necessary to prove whether this phenomenon is 'real' or a product of badly conditioned mathematics.

Figure 5.6 shows the levels of fundamental, 2nd, 3rd and 4th harmonics necessary at the throat of the horn above to give sinusoidal pressure waveforms at the mouth over a range of pressure levels at a frequency of 1kHz. It can clearly be seen that the distortion rises with increasing level such that an increase in mouth pressure level of 3dB results in an increase in throat fundamental of approximately 3dB, an increase in throat 2nd harmonic of approximately 6dB, an increase in throat 3rd harmonic of approximately 9dB and an increase in throat 4th harmonic of approximately 12dB. The maximum mouth sound pressure level shown (170dB) is just below that which produces a shock-wave within the horn at this frequency.

5.5.2 Experimental Verification of Model.

Figure 5.7 shows the results of the experimental verification of the model described in section 5.4 in tabular form; the same results are shown graphically in figure 5.8. The tabular results show the amplitude and phase of the measured mouth harmonics, the amplitude of the measured throat harmonics and the amplitude of the predicted throat harmonics when the measured mouth harmonics are used to generate the starting waveform in the model. The graphical results show only a comparison of the predicted and measured throat harmonic amplitudes. Results are shown for throat fundamental levels of 140, 150 and 160 dB SPL at a number of 'spot' frequencies from 200Hz to 5kHz.

It can be seen from the results that good agreement exists between the measured and predicted 2nd harmonic throat levels but that the agreement is not very good for 3rd harmonic levels. Figure 5.6 shows that a 3dB increase in the level of the

fundamental gives rise to approximately 6dB rise in 2nd harmonic and approximately 9dB rise in 3rd harmonic level. The comparisons between the predicted and measured harmonics show differences in the levels of the fundamentals of up to 5dB, particularly at the frequency extremes. These differences, which may be due to errors in the linear modelling of the horn (eg. beaming (see chapter 4), or to measurement tolerances and accuracy, could be responsible for some of the differences between measured and predicted 2nd and 3rd harmonics; any differences between the fundamentals will give rise to twice as much difference in 2nd harmonic levels and three times as much difference in third harmonic levels. Thus up to 15dB variation in 3rd harmonic levels could be expected from consideration of the fundamental levels.

Figure 5.8c shows the results for a throat fundamental level of 160dB SPL; the measured third harmonic levels are between 15 and 20dB higher than those predicted. This peculiarly 'bad' result cannot be explained using the above argument as the fundamentals are at worst only 3dB different. According to the manufacturers, the microphone used develops approximately 3% (-30dB) of 3rd harmonic distortion at 160dB. The predicted levels of 3rd harmonic lie between 35 and 45dB below the fundamental; considerably lower than the distortion limit of the microphone. Figure 5.8c shows the measured 3rd harmonic levels to be between 27 and 30dB below the fundamental, so it is reasonable to assume that these levels are due to microphone distortion. It is possible that the microphone 3rd harmonic distortion is also comparable in level to that of the horn at the lower drive levels, which could explain the differences between the predictions and measurements for the third harmonics. This would depend upon the relative rates of increase in distortion with level and frequency for the microphone and the horn.

On the whole, the experimental verification can be considered successful, especially when the above points regarding errors are taken into account. It can be concluded therefore, that confidence can be had in the capability of the model to predict the degree of non-linearity present in finite length acoustic horns where strong standing wave fields and phase dispersion may be present.

5.6 PRACTICAL USES FOR THE MODEL

The prediction of the input waveform necessary to achieve a desired output waveform has many practical uses; in ultrasonic medical treatments for example, where a high level transient sound waveform of a specific shape may be desirable as an output from a horn; a thorough analysis of the model output could lead to the development of a 'pre-distortion black-box' using digital signal processing techniques to correct the distortion in loudspeaker horns. In the form described above however, the model has limited practical use when applied to horn loudspeaker design and analysis. The capability to predict the distortion present in the radiated field when a 'perfect' driver is attached to a horn is of much greater importance here. As stated in section 5.2, a direct solution of the 'time-forward problem', where a given input results in a calculated output, is not possible at finite levels in real horns, due to the lack of linear superposition between the radiated and reflected sound waves. This led to the model being developed to solve the 'time-backwards problem' where a given output at the mouth of a horn (which, it is assumed, can be characterised by a linear radiation impedance), results in a calculated input at the throat. In an attempt to solve the time-forwards problem, the model was extended to include iteration around the time-backwards solution in the form of a negative feedback loop. The following section contains a description of how this iteration was implemented.

5.6.1 Iteration to a Time-Forwards Solution.

When the model is given a sinusoidal starting waveform as the output at the mouth of a horn, the time-backwards solution yields a set of harmonics that would need to be present at the throat (input) of the horn to give the sinusoid as output. To iterate towards a time-forwards solution, these harmonics (all except the fundamental) are propagated *linearly* back to the mouth, phase inverted and added to the original starting waveform to define a new starting waveform. When this new starting waveform is used, the time-backwards solution yields a new set of harmonics at the throat with levels very much lower than when the original starting waveform was used. This process is repeated until the throat waveform is a sinusoid, or at least until the harmonics have reduced to an acceptably low level. The last-used starting waveform is then the output from the horn when the waveform at the throat is a sinusoid. As yet, the model has been programmed to iterate towards a sinusoidal throat waveform only, but any desirable waveform can be programmed by filtering the harmonics in the feedback loop. In practice, if a sufficient number of elements are used to describe the horn, the residual throat harmonics can be reduced to below

-100dB with reference to the fundamental in just four iterations. Figure 5.9 shows the levels of the throat harmonics for a typical horn after 0, 1, 2, 3 and 4 iterations for a fundamental frequency of 1kHz and a level of 140dB at the mouth.

It was intended to experimentally verify the time-forward solution by using the highly linear driver mentioned in section 5.4 to generate a sinusoidal throat waveform and to measure the radiated sound field. When this was attempted however, measurements of the pressure waveform at the throat of the small axisymmetric horn showed harmonic levels much higher than the output from the driver would suggest. The high harmonic levels were due to the presence of distortion in the reflected wave which had been propagated in a non-linear manner to the mouth of the horn and back again. This led to the conclusion (dilemma?) that the only horns which can be used to verify the time-forward solution using this method, are those which do not produce a standing-wave field; ie. those for which a much simpler model will suffice! In practice, the time-forward solution could be verified by using a pure pressure or velocity source at the throat to 'force' either the pressure or the velocity waveform (but not both) to remain sinusoidal; this immediately excludes all loudspeaker compression drivers as they are designed to have mechanical impedances as closely matched to the horn throat as possible to maximise electroacoustic efficiency; a compression driver will therefore only deliver a low-distortion output if driving into a linear impedance. The value of a time-forward finite amplitude model for loudspeaker horns is therefore questionable and may be restricted to qualitative comparisons between designs, rather than accurate predictions of the distortion performance of real loudspeakers.

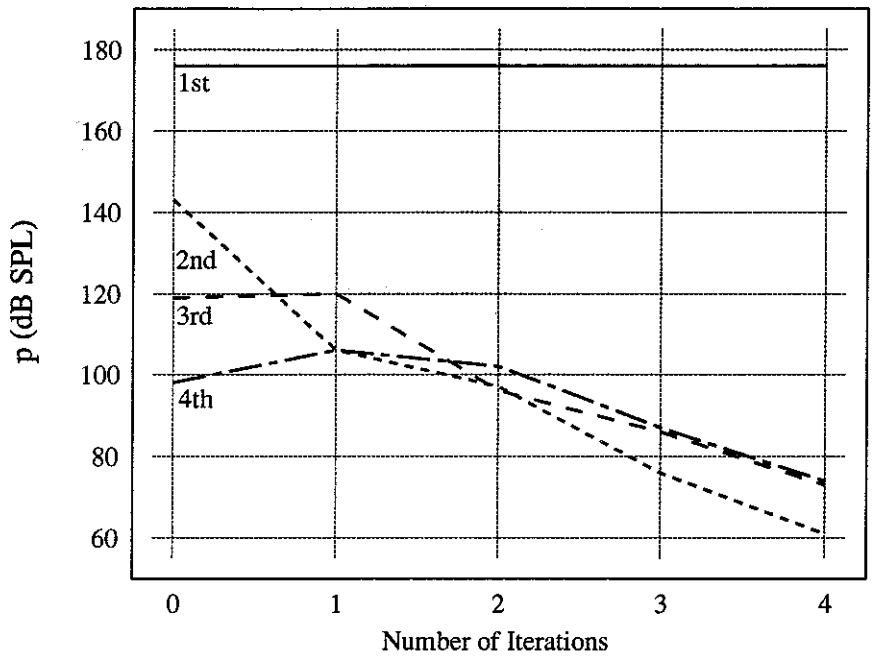

Figure 5.9 Sound Pressure Level of Harmonics at the Throat of a Horn as a Function of the Number of Iterations Towards a Time-Forwards Solution.

5.7 MEASUREMENT OF HARMONIC DISTORTION PRODUCED BY HORN / DRIVER COMBINATIONS

As stated in section 5.1, the distortion produced by a horn / driver combination can be due to non-linearity in the mechanical / electro-mechanical system of the driver, volumetric changes of the various cavities in the driver, or propagation distortion within the horn flare. Because of the reasons outlined in section 5.6.1, the effects of these various non-linearities on the output of the horn cannot easily be separated. For example, the non-linearity in the flare of a horn is dependent to some extent upon the output impedance of the driver, the motion of the driver diaphragm is dependent upon the linearity of the throat impedance etc; although each part of the system may be investigated individually, the distortion in the output from the horn cannot generally be predicted from the 'sum' of the individual non-linearities.

A comparison between the harmonic distortion in the output from a horn system and that predicted by the propagation distortion model, with a 'perfect' pressure source at the throat, may give a quantitative measure of the relative importance of this form of

distortion in the presence of others. An experiment was carried out on two typical horn / driver combinations: The Reflexion Arts horn / Emilar EK175 driver (sample 5 in appendix 5) and the JBL 2370 horn / JBL 2426 driver (sample 16 in appendix 5). This experiment involved the measurement of the harmonic distortion produced by the horn systems over a range of frequencies and drive-levels in the far-field at 3m distance in the large anechoic chamber at ISVR. The equivalent pressures at the mouth of the Reflexion Arts horn were calculated from the far-field pressures using directivity data (see chapter 4) and these pressures were used in the starting waveforms for the model. Figure 5.10 shows the measurements of the harmonic distortion for both horn systems and the theoretical distortion for the Reflexion Arts system in tabular form. The physical dimensions and directivity data were not available for the JBL system but the measured results are included to show that those for the Reflexion Arts system are not atypical.

		Total Pressure (dB SPL)		Measured Harmonics (dB re 1st)			Theoretical Harmonics (dB re 1st)		
Loudspeaker system	*f* (Hz)	*p* (3m)	*p* (m'th)	2nd	3rd	4th	2nd	3rd	4th
Reflexion Arts	1k	85	110	-50	-55	-76	-49	-84	-119
	3k	"	106	-49	-65	-73	-43	-73	-106
	5k	"	104	-38	-54	-71	-38	-67	-96
"	1k	95	120	-40	-53	-68	-39	-69	-97
	3k	"	116	-40	-55	-61	-33	-57	-80
	5k	"	114	-29	-48	-71	-28	-51	-70
"	1k	105	130	-28	-32	-45	-30	-53	-76
	3k	"	126	-29	-52	-57	-23	-41	-57
	5k	"	124	-20	-36	-51	-18	-33	-46
JBL	1k	85	-	-42	-44	-60			
	3k	"	-	-43	-36	-49			
	5k	"	-	-41	-37	-61			
"	1k	95	-	-41	-49	-55			
	3k	"	-	-35	-53	-67			
	5k	"	-	-29	-55	-			
"	1k	105	-	-26	-41	-58			
	3k	"	-	-27	-43	-55			
	5k	"	-	-19	-37	-60			

Figure 5.10 Measured and Theoretical Harmonic Distortion of Horn / Driver Combinations.

It can be seen in figure 5.10 that the levels of harmonic distortion produced by the two horn systems are very similar and that both produce a 'worst' case of about 10% 2nd harmonic distortion at a frequency of 5kHz and a sound pressure level of 105dB at 3m. It should be noted here that these horn systems were not being driven near to their limits and that very few non-horn mid-range loudspeakers are capable of reproducing sine-waves at these levels at all.

The measured 2nd harmonic distortions are clearly of the same order as those predicted for propagation non-linearity alone, with an increase in distortion with increasing frequency and level which is characteristic of propagation non-linearity. The measured third and forth harmonics are however very different to those for the propagation non-linearity alone, and although there is a general rise in these harmonics with increasing level, there is little evidence of a rise with increasing frequency. On the whole, the measured third and forth harmonic distortions are higher than those due to propagation non-linearity alone. Propagation non-linearity produces mainly second harmonic distortion with the levels of the higher harmonics falling rapidly with increasing order. Most loudspeaker drive-units produce 2nd and 3rd harmonic distortion in about equal quantities, with the highest levels at low frequencies. It appears from these data that, in general, the 2nd harmonic distortion produced by the horn systems is due to propagation non-linearity, and the higher harmonics are due to driver non-linearities. The propagation non-linearity model described above is therefore a useful tool in the investigation and design of horn loudspeakers for use in high quality systems.

Chapter 6
THE LISTENING TEST

6.1 INTRODUCTION

Horn loudspeakers, particularly those used in systems where high quality sound reproduction is required, have been the subject of debate for a number of years. The use of horns for public address applications, where high electro-acoustic efficiency and good directivity control are of paramount importance, is almost universally accepted as good practice; in fact in many cases there are no alternatives. However where it is necessary for these useful horn properties to take second place to high sound quality, for instance in home hifi equipment or studio monitor systems, the use of horn loudspeakers is questionable. The controversy about the use of horns in these systems is generally confined to the mid-range of frequencies (500Hz to 10kHz); the use of horn loudspeakers for the reproduction of low frequencies is often totally impractical due to sheer size limitations, and for very high frequencies, horns seem to be acceptable to most people. Opinions on the perceived sound quality of such systems are generally polarised on two extremes. On the one hand there are people for whom horn loudspeakers are capable of the very highest sound quality with an "immediacy" or "clarity" unobtainable with other systems. On the other hand there are people who actively dislike the reproduction of sound over horn loudspeakers and claim that horns have a characteristic sound, often described as "honky" or "quacky", which allows a horn to be identified as a horn. To attempt to clarify this situation, a blind listening test was set up allowing listeners to directly compare horns with other horns and with direct radiating loudspeakers.

6.2 DESCRIPTION OF LISTENING TEST

6.2.1 The Objectives of the Test.

A wide selection of horn loudspeakers designed to operate in the mid frequency range was made available, along with a selection of equivalent direct radiating loudspeakers. As most of these units were not capable of reproducing the entire audio frequency range, it was decided that the test could not aim to compare the absolute sound quality of the loudspeakers without 'filling in' the rest of the frequency range. It was thought impractical to attempt to interface, both physically and electro-acoustically, such a wide variety of mid-range units with the rest of a loudspeaker system and, as a result, it was decided to limit the test to establishing differences or similarities between the loudspeakers in the mid frequency range only.

A blind listening test was therefore designed to answer three questions:

a) Do horns sound different from each other?
b) Do horns sound different from direct radiators?
c) If the answers to a and b are affirmative, is the difference between horns and direct radiators in general greater than the difference between horns?

6.2.2 Experimental technique.

Ideally, the listening test would involve many different loudspeakers, many different test signals and a large number of auditioning subjects. Each subject would then compare the reproduction of each signal by each loudspeaker with that of every other loudspeaker, with the order of presentation arranged so as to minimise bias (using a 'latin square' arrangement for example). If this were attempted however, the test would take a prohibitive amount of time so some compromise in experimental technique was necessary.

The physical properties of the loudspeakers that were likely to be responsible for any 'horn sound' were largely unknown, so it was important that as many different mid-range horn loudspeakers as possible were included in the test, along with some direct-radiating loudspeakers; a large number of test loudspeakers was therefore unavoidable. Also largely unknown was whether any particular type of signal would highlight the differences or similarities between the loudspeakers, so a reasonable number of different test signals was also considered important. Finally, in order that the results of the test be statistically significant, a reasonable number of test subjects would be required. With these requirements in mind, it was decided that each test loudspeaker would only be compared with four 'reference' loudspeakers chosen as typical examples of their kind, thereby allowing a reasonable number of loudspeakers, signals and subjects to be tested within practical time limitations.

6.2.3 The Test Set-Up.

There are many parameters that can affect the perceived sound quality of a loudspeaker. In order to extract meaningful information from the results of the test, many of these parameters had to be eliminated, or at least their effect minimised. A number of precautions were taken to enable this simplification to be made:

♦ As the effect of a loudspeaker's directivity on sound quality is very 'room dependent', to carry out the test in any ordinary room would bias the results in a very complicated and almost unquantifiable manner. To overcome this problem, the test was set up in the large anechoic chamber at ISVR.

♦ It is well known that the level at which a sound is reproduced has a large effect on the perceived sound quality. The sensitivities of the loudspeakers under test covered a range of about 25dB, so a means of adjusting the amplifier gain individually for each loudspeaker had to be incorporated in the set-up. At first it appeared as if the gain for each loudspeaker would have to be set for each different sound, as two loudspeakers adjusted to reproduce the same level on one sound would not reproduce the same level on another. As well as being logistically very difficult, this matching of levels for individual sounds was considered undesirable as the reproduction of different sounds at different levels can be considered to be an important part of the characteristic sound of a loudspeaker; to attempt to remove these differences between the loudspeakers would therefore bias the test results. The gain settings were thus adjusted so that all of the loudspeakers reproduced band-limited pink noise at the same level.

♦ To ensure, as far as possible, that each loudspeaker reproduced the same bandwidth, fourth order (24dB per octave) filters at 1kHz (high pass) and 6kHz (low pass) were introduced into the signal path.

♦ Finally an acoustically transparent and visually opaque curtain was erected between the loudspeakers and the listener to eliminate the all too common "I see, therefore I hear" phenomenon.

Figure 6.1 shows the listening test arrangement. To ensure that every listener sat on-axis to every loudspeaker, only one listener took the test at a time; this also removed the temptation for a listener's comments or actions to influence the judgement of another. The loudspeakers were arranged in a circular arc subtending 60 degrees around a swivel chair. As sitting in an anechoic chamber can be disconcerting to some people, and for other safety reasons, the experimenter was present in the chamber at all times behind a foam wall which permitted verbal and eye contact with the subject.

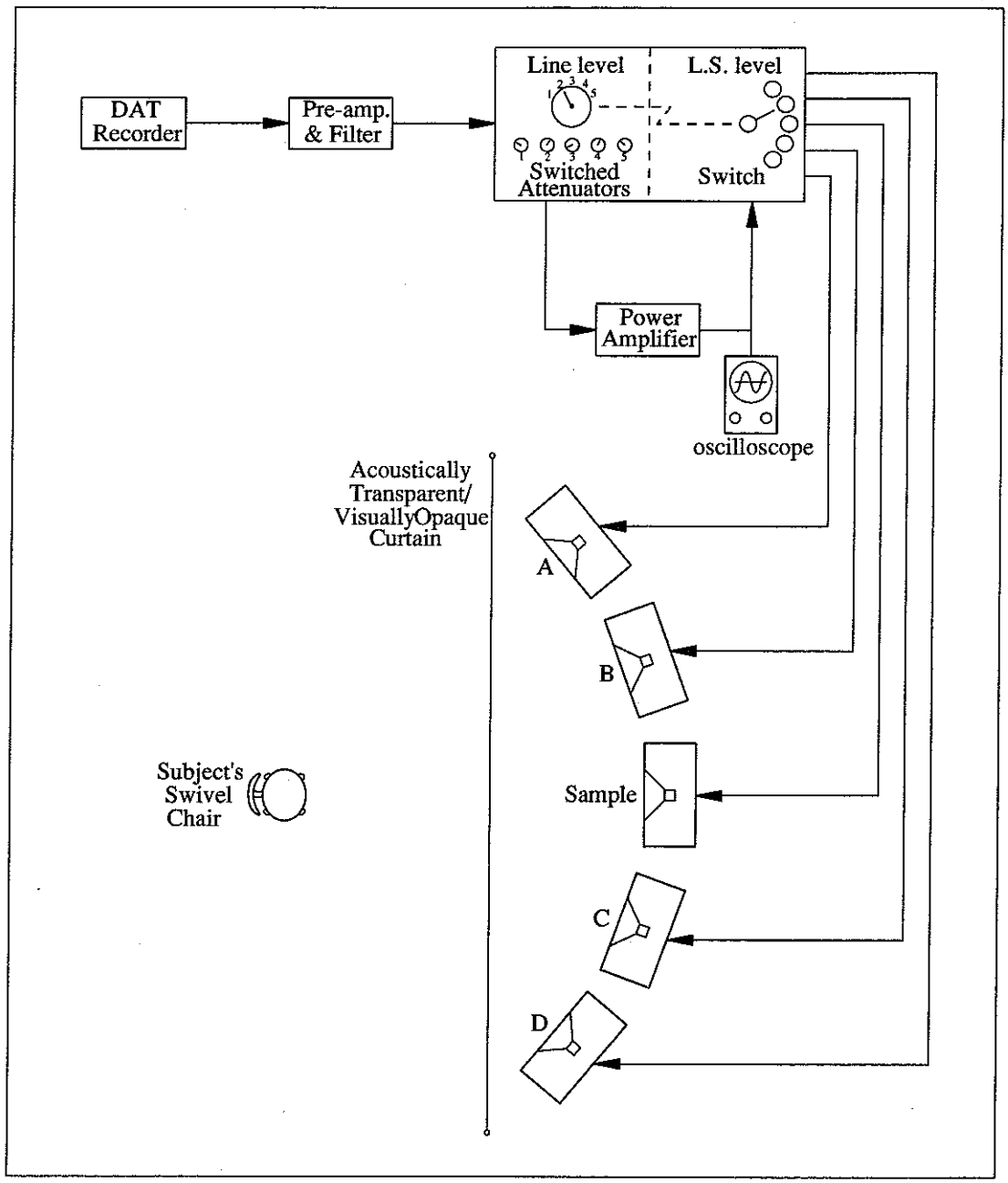

Figure 6.1 Listening Test Set-Up in Anechoic Chamber.

6.2.4 The Loudspeakers Under Test.

A total of 20 loudspeakers were made available for the test; these included 14 compression driver / horn combinations, 4 direct radiating cone loudspeakers, a dual concentric horn and an electrostatic loudspeaker. The electrostatic, a direct radiating cone, a compression driver / horn combination and a dual concentric horn were chosen as the four references and were labelled A to D respectively. At any one time, five loudspeakers were set up for listening, and were arranged behind the curtain in the following order from left to right: A, B, Sample, C and D. The term

'Sample' herein refers to the particular loudspeaker under test. A full list of all of the loudspeakers tested, including the references, is contained in appendix 5.

Amongst the 16 test loudspeakers were two 'experiment controls'; loudspeakers for which the results were thought to be known prior to the test. These were included to give an indication of the accuracy of the test result data. One of the controls, sample 6, was a direct radiating cone loudspeaker which was nominally identical to reference B; the expected result was therefore 100% similarity with reference B. The other control, sample 3, was a direct radiating cone loudspeaker which was designed to operate over a lower frequency range than that of the test; the expected result for this control was 'no similarity' with any of the references. The results for the rest of the samples were expected to lie somewhere between these 'similar' and 'non-similar' controls.

6.2.5 The Test Signals.

To avoid listeners being distracted by any preferences for the sound of any particular loudspeakers, it was considered important that the signals used in the test should contain as little information content as possible. This ruled out speech and music, which would probably have been the most relevant signals, but many of the transient and steady state aspects of these were represented by nine signals, two synthetic and seven recorded 'live' sounds. One second of each signal was sampled and repeatedly recorded onto digital audio tape for three minutes with short gaps between each repetition. Two repetitions were played through each loudspeaker in the following order: Sample, A, Sample, B, Sample, C, Sample, D, Sample, A, ... etc until the subject had made a decision. At any time, the subject could request that any comparison be repeated or omitted via verbal communication with the experimenter. A list of the signals used, along with brief descriptions and replay levels are contained in appendix 6.

6.2.6 The Test Equipment.

Throughout the setting up of the test, great care was taken to ensure that conditions were as near identical for all loudspeakers and all listeners as was practical. The leads running from the switch box to the loudspeakers were all of the same length, and were rated at 15A. The switch box itself was tailor-made for the test and was split into two sections; one for the line level signals with six separate gain controls linked to a six-way switch and input and output buffers, and the other for the loudspeaker level signals with a six-way switch, rated at 10A, which was ganged to

the low level switch. An Amcron Straight Line One pre-amplifier coupled to a Crown DC300 power amplifier was used to drive the loudspeakers and provide overall gain control. The band-pass filter was the upper-mid-range section from a four-way active crossover system with turn-over points at 1kHz and 6kHz and 24dB per octave slopes. A Sony DC1000 DAT recorder was used as the signal source, providing rapid indexing to the start of each signal. Care was taken to minimise noise in the set-up by avoiding earth loops and ensuring the presence of adequate signal levels at all stages.

6.2.7 The Subjects.

In all, twenty people were kind enough to act as listening subjects. They included mostly people from the professional audio industry, along with some lay people and some academics, with ages ranging from late teens to middle age. It was decided that it was not necessary to screen the subjects through hearing tests as the opinions of people with a range of hearing ability were considered desirable. On average, a complete test took about four hours, and as quite a high degree of concentration was required, subjects were given frequent opportunities for breaks. Many of the subjects could not afford the time to complete a whole test, so those loudspeakers that they missed were covered by another person. Twelve complete tests were therefore split amongst the twenty subjects.

6.2.8 The Questionnaire.

Figure 6.2 shows the format of the questionnaire that each subject was asked to fill out. It consisted of five columns, marked A, B, C, D and NONE, and for each sample loudspeaker, nine rows marked 1-9. Four such sheets comprise a complete questionnaire to cover the sixteen sample loudspeakers. For each sample loudspeaker, and for each of the nine, numbered sounds, the subject was asked to tick the column for the reference loudspeaker, A, B, C or D, that sounded most similar to the sample loudspeaker. More than one column could be ticked and the NONE column could be ticked when none of the references were judged to sound similar to the sample. The interpretation of the word 'similar' was left up to the individual subject. As little 'briefing' was given to the subjects as was possible to avoid any pre-conditioning of a subject's opinions (an interesting result of the test was finding out what people mean when they say "different" or "similar" in the context of this test and to what extent people differ in this respect). The 'tick boxes' were large enough for short comments to be written about a comparison if the subject desired, indeed, such additional information was welcomed. Each subject,

even those who were finishing off another person's test, was given a 'clean' questionnaire so that at no time did any subject have access to a previous subject's comments or results.

Subjective Test 1 : Audible Similarity

For each sample, tick the box for the loudspeaker considered to sound closest to the sample. More than one box may be ticked and short comments can be added if considered necessary.

SIGNAL	A	B	C	D	NONE
Sample 1					
1					
2					
3					
4					
5					
6					
7					
8					
9					
Sample 2					
1					
2					
3					
4					
5					
6					
7					
8					
9					
Sample 3					
1					
2					
3					
4					
5					
6					
7					
8					
9					
Sample 4					
1					
2					
3					
4					
5					
6					
7					
8					
9					

Figure 6.2 Format of Listening Test Questionnaire.

6.3 LISTENING TEST RESULTS

Twelve complete tests were carried out by twenty subjects, each test contained information on sixty four comparisons for nine sounds; a total of nearly seven thousand comparisons and nearly nine thousand possible ticks! Clearly, to present all of these data separately within these notes would be impractical, so for reasons of neatness a breakdown of the data will be presented. Figure 6.3 shows a table of the total number of ticks from all twelve tests for each comparison, including any 'half ticks' or those with comments showing reservations along side them. Figure 6.4 shows the same data, but with half ticks etc given half a mark. Finally, figure 6.5 shows just the unambiguous ticks. The various comments made by subjects about the comparisons will not be itemised here, but will be discussed along with the data analysis.

	Sample 1					Sample 2					Sample 3					Sample 4				
Signal	A	B	C	D	None	A	B	C	D	None	A	B	C	D	None	A	B	C	D	None
1	-	4	4	7	1	2	5	4	2	-	-	9	2	6	-	-	8	-	3	2
2	-	5	3	4	3	1	5	2	1	2	-	3	3	4	3	-	8	2	2	3
3	-	6	4	6	1	-	8	2	1	1	4	2	2	2	5	1	8	-	4	1
4	-	7	1	3	6	1	4	-	-	7	2	1	-	-	9	-	7	-	1	4
5	1	5	3	4	5	1	5	-	-	5	1	-	1	-	9	-	7	-	-	5
6	-	6	1	4	3	-	7	2	2	3	1	3	1	2	5	-	8	1	3	4
7	-	6	-	5	6	-	7	1	1	5	2	-	-	-	9	-	9	-	-	3
8	-	7	1	7	-	1	9	1	3	1	-	5	1	5	4	-	8	-	3	2
9	-	4	-	6	3	-	9	-	1	-	2	3	-	2	8	-	4	-	5	4

	Sample 5					Sample 6					Sample 7					Sample 8				
Signal	A	B	C	D	None	A	B	C	D	None	A	B	C	D	None	A	B	C	D	None
1	1	7	4	5	-	1	13	2	6	-	2	9	4	2	-	-	3	2	8	1
2	-	9	4	2	1	-	10	1	2	3	2	7	2	-	2	-	1	-	6	3
3	-	6	4	6	1	-	13	3	5	-	2	6	7	2	2	1	5	3	7	2
4	-	6	1	4	6	-	13	-	1	1	1	3	-	2	7	-	3	1	3	6
5	-	5	2	3	5	-	14	-	2	-	-	4	3	3	7	-	1	1	3	7
6	-	7	4	5	2	-	13	2	4	1	-	8	6	-	2	-	5	4	4	4
7	-	4	1	3	7	2	14	1	2	-	1	3	1	3	7	-	-	1	2	9
8	-	9	2	3	3	1	13	2	3	1	3	7	5	2	-	-	3	2	5	5
9	-	5	-	6	5	-	14	-	3	-	-	6	2	2	3	-	2	1	5	5

	Sample 9					Sample 10					Sample 11					Sample 12				
Signal	A	B	C	D	None	A	B	C	D	None	A	B	C	D	None	A	B	C	D	None
1	1	8	5	2	3	-	11	1	1	-	3	8	3	-	2	-	7	4	5	-
2	-	6	4	1	3	-	10	2	-	1	2	5	7	1	2	1	2	3	4	3
3	-	5	9	4	1	-	8	6	4	1	2	9	6	-	-	-	6	8	1	-
4	-	2	1	2	10	-	6	-	1	8	2	4	2	1	8	-	3	4	1	6
5	-	2	-	1	9	-	8	1	2	5	2	7	3	2	5	1	3	2	1	6
6	-	7	3	3	4	-	6	2	3	3	-	9	4	2	2	-	3	6	-	3
7	-	4	2	3	7	-	7	2	2	4	3	3	3	2	8	1	1	4	2	5
8	1	6	2	2	5	-	9	1	3	2	-	7	3	2	3	2	3	7	-	1
9	-	3	5	3	3	-	6	-	4	1	1	8	1	2	1	-	2	7	3	2

	Sample 13					Sample 14					Sample 15					Sample 16				
Signal	A	B	C	D	None	A	B	C	D	None	A	B	C	D	None	A	B	C	D	None
1	2	6	1	3	2	1	5	2	6	2	1	9	2	3	-	3	2	7	-	2
2	3	5	3	-	1	2	5	5	2	1	2	8	2	2	2	3	8	7	1	1
3	4	5	7	3	1	3	3	7	1	1	1	5	6	1	2	1	2	7	1	2
4	1	-	4	-	9	3	-	3	1	7	2	-	2	1	8	4	1	1	-	7
5	3	1	2	1	9	2	-	4	1	7	3	1	4	2	7	-	2	1	1	7
6	3	3	3	1	2	2	1	2	-	6	-	3	3	1	7	1	6	7	1	1
7	3	-	4	-	8	2	1	2	1	5	3	-	2	1	7	2	2	-	-	9
8	3	1	6	2	2	3	-	9	-	1	3	1	5	-	5	3	-	7	1	2
9	3	-	5	1	4	-	1	8	-	3	1	2	6	-	4	-	3	6	1	3

Figure 6.3 Listening Test Results: Overall Total Numbers of Ticks.

	Sample 1					Sample 2					Sample 3					Sample 4				
Signal	A	B	C	D	None	A	B	C	D	None	A	B	C	D	None	A	B	C	D	None
1	-	4	4	6	1	2	5	4	2	-	-	9	1.5	5	-	-	7.5	-	3	2
2	-	5	3	3.5	3	1	5	2	1	2	-	2	2	3.5	3	-	7.5	1.5	1.5	3
3	-	6	4	6	1	-	8	2	1	1	3	1.5	2	2	5	1	8	-	4	1
4	-	5.5	0.5	3	6	0.5	3.5	-	-	7	1	0.5	-	-	9	-	6.5	-	1	4
5	0.5	3	2.5	3.5	5	1	4.5	-	-	5	0.5	-	1	-	9	-	6.5	-	-	5
6	-	6	1	4	3	-	6.5	2	2	3	0.5	2	1	2	5	-	7	0.5	2	4
7	-	4.5	-	4.5	6	-	5.5	1	1	5	1	-	-	-	9	-	8	-	-	3
8	-	6.5	1	7	-	1	8.5	1	3	1	-	4.5	1	5	4	-	8	-	2.5	2
9	-	4	-	5	3	-	9	-	1	-	1	1.5	-	1	8	-	3.5	-	4	4

	Sample 5					Sample 6					Sample 7					Sample 8				
Signal	A	B	C	D	None	A	B	C	D	None	A	B	C	D	None	A	B	C	D	None
1	0.5	7	4	5	-	1	13	2	4	-	1.5	9	3.5	1.5	-	-	3	2	7	1
2	-	8	4	2	1	-	9.5	1	1.5	3	1.5	7	2	-	2	-	1	-	5.5	3
3	-	5.5	4	5.5	1	-	13	2.5	5	-	1.5	6	7	2	1.5	1	5	3	7	1.5
4	-	4.5	0.5	3.5	6	-	12.5	-	1	1	1	2.5	-	1.5	7	-	2.5	1	3	5.5
5	-	3.5	1.5	2.5	5	-	14	-	1.5	-	-	3	2	2.5	7	-	1	0.5	2.5	7
6	-	6.5	3.5	4	2	-	13	1	3	1	-	7.5	5.5	-	2	-	5	3.5	3.5	4
7	-	2.5	0.5	3	7	1.5	14	1	1.5	-	0.5	2	1	2	7	-	-	0.5	2	9
8	-	8.5	2	2.5	3	0.5	13	1.5	2.5	1	3	6	5	1.5	-	-	2.5	2	4	5
9	-	4.5	-	5	5	-	14	-	2	-	-	6	2	2	3	-	2	1	5	5

	Sample 9					Sample 10					Sample 11					Sample 12				
Signal	A	B	C	D	None	A	B	C	D	None	A	B	C	D	None	A	B	C	D	None
1	0.5	7	4.5	1.5	3	-	11	1	1	-	2.5	7	3	-	2	-	6.5	3.5	4	-
2	-	5.5	3	1	3	-	9.5	2	-	1	1.5	5	5.5	0.5	2	0.5	1.5	3	3.5	3
3	-	4.5	7.5	3.5	1	-	8	5	3	1	2	8.5	6	-	-	-	5.5	8	1	-
4	-	1	0.5	1.5	10	-	4.5	-	1	8	1.5	2.5	1.5	1	8	-	2	3.5	1	6
5	-	2	-	1	9	-	7	1	2	5	1.5	5.5	2.5	2	5	1	2	2	1	6
6	-	6.5	2	2.5	4	-	6	1.5	2.5	3	-	8	4	2	2	-	3	5.5	-	3
7	-	3.5	1.5	2.5	7	-	6.5	1.5	2	4	2	2.5	2	2	8	0.5	1	3.5	1.5	5
8	0.5	5.5	2	1.5	5	-	8	0.5	2.5	2	-	7	3	2	3	2	3	7	-	1
9	-	2.5	5	3	3	-	4.5	-	4	1	1	7.5	1	1.5	1	-	1.5	6.5	2.5	2

	Sample 13					Sample 14					Sample 15					Sample 16				
Signal	A	B	C	D	None	A	B	C	D	None	A	B	C	D	None	A	B	C	D	None
1	1.5	6	1	3	2	1	5	1.5	5	2	1	9	2	3	-	3	2	6.5	-	2
2	2.5	5	3	-	1	2	5	4	2	1	2	7.5	2	2	2	3	8	6.5	0.5	1
3	4	4.5	7	3	1	2.5	2.5	6.5	1	1	1	5	6	1	2	1	2	7	1	2
4	1	-	3	-	9	2	-	1.5	0.5	7	1.5	-	1	1	8	3	1	1	-	7
5	1.5	0.5	1.5	0.5	9	2	-	3	0.5	7	2	1	3	2	7	-	1.5	1	0.5	7
6	3	3	3	1	2	1.5	1	1.5	-	6	-	3	3	1	7	1	6	6.5	1	1
7	2.5	-	3	-	7.5	1.5	1	1	0.5	5	2.5	-	1	1	7	1	1.5	-	-	9
8	3	1	6	1.5	2	2.5	-	8.5	-	1	2.5	1	4	-	5	3	-	6.5	1	2
9	3	-	4.5	1	4	-	0.5	7.5	-	3	1	2	4.5	-	4	-	2.5	5.5	0.5	3

Figure 6.4 Listening Test Results: Weighted Ticks.

	Sample 1					Sample 2					Sample 3					Sample 4				
Signal	A	B	C	D	None	A	B	C	D	None	A	B	C	D	None	A	B	C	D	None
1	-	1	2	4	1	-	2	4	1	-	-	3	1	1	-	-	6	-	2	1
2	-	2	1	3	3	-	4	2	1	2	-	-	1	2	3	-	6	-	-	2
3	-	3	-	4	1	-	7	1	-	1	1	-	1	1	4	-	6	-	2	1
4	-	2	-	1	4	-	3	-	-	5	-	-	-	-	8	-	5	-	-	4
5	-	1	1	2	2	1	4	-	-	4	-	-	1	-	9	-	6	-	-	4
6	-	5	-	3	3	-	4	-	1	2	-	1	1	1	5	-	3	-	-	3
7	-	1	-	2	4	-	3	1	-	2	-	-	-	-	9	-	7	-	-	2
8	-	4	-	5	-	-	5	-	1	-	-	2	-	2	4	-	6	-	1	2
9	-	3	-	3	3	-	9	-	1	-	-	-	-	-	5	-	1	-	2	4

	Sample 5					Sample 6					Sample 7					Sample 8				
Signal	A	B	C	D	None	A	B	C	D	None	A	B	C	D	None	A	B	C	D	None
1	-	3	2	2	-	-	6	-	-	-	-	5	1	-	-	-	1	-	4	1
2	-	5	1	1	1	-	7	-	-	3	-	5	2	-	2	-	1	-	5	3
3	-	2	1	4	1	-	8	-	-	-	-	3	2	-	1	-	1	1	3	1
4	-	1	-	1	4	-	11	-	-	1	1	2	-	1	5	-	1	1	2	4
5	-	2	1	2	4	-	12	-	-	-	-	1	-	1	4	-	1	-	2	6
6	-	2	1	2	1	-	8	-	-	1	-	3	2	-	1	-	2	1	1	3
7	-	-	-	2	6	-	10	-	-	-	-	-	-	-	4	-	-	-	2	8
8	-	6	-	1	2	-	9	-	-	1	1	1	2	-	-	-	1	1	1	3
9	-	3	-	3	3	-	11	-	-	-	-	4	1	1	3	-	2	-	3	4

	Sample 9					Sample 10					Sample 11					Sample 12				
Signal	A	B	C	D	None	A	B	C	D	None	A	B	C	D	None	A	B	C	D	None
1	-	3	2	-	-	-	9	-	-	-	-	3	1	-	2	-	3	2	1	-
2	-	3	2	-	2	-	7	-	-	1	1	1	3	-	2	-	1	2	3	2
3	-	-	4	-	-	-	3	2	-	1	-	3	2	-	-	-	3	5	-	-
4	-	-	-	1	8	-	2	-	-	5	-	-	-	-	6	-	-	1	1	5
5	-	1	-	-	9	-	4	-	-	3	-	1	-	-	2	1	-	1	-	6
6	-	2	-	-	3	-	4	1	1	2	-	4	1	-	1	-	2	4	-	3
7	-	-	-	1	5	-	5	-	1	3	-	-	-	-	4	-	-	3	-	4
8	-	2	-	1	3	-	4	-	1	1	-	4	-	1	3	1	2	5	-	1
9	-	-	4	2	2	-	3	-	4	1	1	6	-	-	1	-	-	5	2	1

	Sample 13					Sample 14					Sample 15					Sample 16				
Signal	A	B	C	D	None	A	B	C	D	None	A	B	C	D	None	A	B	C	D	None
1	-	4	-	1	2	-	2	-	3	1	-	6	1	1	-	2	1	4	-	1
2	1	5	2	-	1	-	3	1	1	1	-	4	-	-	2	-	3	-	-	-
3	1	1	2	-	1	1	1	3	1	1	1	2	3	-	2	1	-	6	-	2
4	-	-	1	-	7	-	-	-	-	5	1	-	-	1	6	2	-	-	-	6
5	-	-	-	-	7	1	-	1	-	5	-	-	1	1	5	-	1	1	-	7
6	3	2	3	-	2	1	1	1	-	5	-	1	1	-	7	-	3	4	-	-
7	2	-	1	-	4	1	1	-	-	5	2	-	-	1	5	-	1	-	-	7
8	3	-	4	-	2	1	-	6	-	1	1	1	3	-	4	2	-	5	-	2
9	2	-	3	1	3	-	-	6	-	3	1	1	2	-	3	-	2	4	-	2

Figure 6.5 Listening Test Results: Unambiguous Ticks.

6.4 ANALYSIS OF RESULTS

The analysis of the listening test data was divided into four parts. First, the data was studied in its 'raw' form, with conclusions drawn from consideration of the number of ticks entered for each sample loudspeaker and for each sound. Second, statistical analysis was performed on the data and conclusions drawn from the results. Third, statistical analysis was performed on measurements taken of the voltage/pressure transfer functions (on-axis frequency response) of the sample loudspeakers and on recordings of the test. The results of these analyses were then compared to the results from the listening test data analyses. Finally, further analyses of the transfer functions and listening test data were performed, to attempt to correlate the listening test results with the physical properties of the loudspeaker samples. The first analysis was carried out independently by two people and discussion was deferred until conclusions had been reached; this was thought desirable as any conclusions that were common to both analyses could then be considered more objective and less the result of preconceptions or bias.

6.4.1 Experiment Control Samples.

First, the results for the 'similar' and 'non-similar' controls had to be studied to determine their effectiveness as controls. Figures 6.3, 4 & 5 show sample 6 to have 70% of all ticks, 72% of the weighted ticks and 93% of the unambiguous ticks entered in the 'B' column. These results show a strong tendency towards the expected result of 100% similarity with reference B and appear to indicate that the 'similar' control was effective. The results for sample 3, show 43% of all ticks, 49% of the weighted ticks and 72% of the unambiguous ticks to be entered in the 'NONE' column, with the rest of the ticks distributed fairly evenly among the four references. These results appear to indicate that subjects, on the whole, were undecided as to whether sample 3 was similar or not to any of the references. There is a tendency here towards the expected result of no similarity with any reference; the 'non-similar' control appears to have been fairly effective, although not as effective as the 'similar' control.

The above quoted figures for the percentage of ticks entered in a particular column serve only as a guide to the confidence that an experimenter can have in the controls. Statistical analysis was therefore performed on the test data to calculate numbers to indicate confidence in the controls.

6.4.2 Statistical Analysis.

In order to calculate the confidence in the results for the controls, a 'null hypothesis' was chosen to which the results could be compared. This null hypothesis was: *That the results were due to pure chance or guesswork on the part of the subjects.* If the hypothesis were true, all of the columns would, if enough subjects were used, carry equal numbers of ticks; if it were not true, a bias to one or more columns would be evident. The confidence in the null hypothesis was calculated for each column and for each signal from the listening test data in terms of a percentage. The confidence in the result for any particular column for each of the signals is then merely: (100% - the confidence in the null hypothesis). Details of the analysis used are contained in appendix 7. The confidence in the results for the two controls are shown in figures 6.6 and 6.7.

	Total (%)					Weighted (%)					Unambiguous (%)				
Signal	A	B	C	D	None	A	B	C	D	None	A	B	C	D	None
1	-	100	-	58	-	-	100	-	-	-	-	100	-	-	-
2	-	100	-	-	-	-	100	-	-	-	-	100	-	-	30
3	-	100	-	22	-	-	100	-	22	-	-	100	-	-	-
4	-	100	-	-	-	-	100	-	-	-	-	100	-	-	-
5	-	100	-	-	-	-	100	-	-	-	-	100	-	-	-
6	-	100	-	-	-	-	100	-	-	-	-	100	-	-	-
7	-	100	-	-	-	-	100	-	-	-	-	100	-	-	-
8	-	100	-	-	-	-	100	-	-	-	-	100	-	-	-
9	-	100	-	-	-	-	100	-	-	-	-	100	-	-	-

Figure 6.6 Confidence in Results for 'Similar' Control (Sample 6 vs Reference B).

	Total (%)					Weighted (%)					Unambiguous (%)				
Signal	A	B	C	D	None	A	B	C	D	None	A	B	C	D	None
1	-	100	-	87	-	-	100	-	67	-	-	94	-	-	-
2	-	-	-	25	-	-	-	-	30	30	-	-	-	39	90
3	25	-	-	-	67	-	-	-	-	67	-	-	-	-	97
4	-	-	-	-	100	-	-	-	-	100	-	-	-	-	100
5	-	-	-	-	100	-	-	-	-	100	-	-	-	-	100
6	-	28	-	-	93	-	-	-	-	97	-	-	-	-	99
7	-	-	-	-	100	-	-	-	-	100	-	-	-	-	100
8	-	67	-	67	25	-	25	-	67	25	-	-	-	-	78
9	-	-	-	-	100	-	-	-	-	100	-	-	-	-	100

Figure 6.7 Confidence in Results for 'Non-similar' Control (Sample 3).

It can be seen from figure 6.6 that the confidence in the 'similar' control, ie the result that sample 6 is similar to reference B, is 100% for every signal regardless of the way in which the ticks are interpreted. As indicated by a study of the raw test data,

the 'similar' control is clearly demonstrated to be effective. The results for the 'non-similar' control (figure 6.7) show the confidence in the result that sample 3 is not similar to any of the references to be signal dependent. Good confidence (100%) is shown for signals 4, 5, 7 & 9, fair confidence (67-99%) for signals 3 & 6, and poor confidence (0-78%) for signals 1, 2 & 8. On the whole, the 'non-similar' control has worked reasonably well, although not as well as the 'similar' control. The increased spread in results for the 'non-similar' control compared to the 'similar' control, can be explained by reference to the original questionnaires and any comments contained within them. An individual subject's use of the NONE column depended, to a large extent, on their interpretation of the word 'similar' and is a result of the lack of pre-conditioning of the subjects prior to the test. Some subjects used the NONE column seldom, if at all, preferring to choose the reference(s) that was 'closest' to the sample; sometimes all four references were ticked in preference to 'NONE'. Other subjects used the NONE column when none of the references sounded 'close' to the sample. This may at first appear to be a weakness in the test procedure but, as a similar spread of opinion and interpretation is likely to occur in a real-life situation, it does in fact serve to reinforce any positive results that may have been apparent (the 'similar' control above for example). The effect that this spread has on the results can be seen by comparing the confidence in the results for the total number of ticks with those for the weighted ticks and for the unambiguous ticks in figure 6.7. As discrimination against 'half ticks', ticks with comments showing reservations or ticks in more than one column increases, the confidence in the results 'crystallises' towards a single column. It may be concluded therefore, that from a study of the results for the two experiment controls, the confidence in a result indicating a similarity is likely to be higher than one indicating no similarity due to a spread in the interpretation of 'similar' by the subjects, and that because of this spread, any near unanimous, positive results can be believed.

The statistical analysis carried out on the controls proved to give a useful indication of the absolute value of a given number of ticks entered in a column taking into account the numbers of ticks entered in the other columns. Because of this, it was thought useful to calculate the confidence in all of the results using the same analysis as for the controls. The resultant numbers, expressed as a percentage will, throughout these notes, be termed 'Similarity Confidence Indices'. Each calculated result can be interpreted as a number between 0 and 100% expressing either; the similarity of the reference to the sample for the particular signal, or more literally; the confidence in the result that the reference is similar to the sample in the

reproduction of that signal. The similarity confidence indices for all of the results are shown in figures 6.8, 9 & 10 with those above 90% in underlined **bold**. These figures correspond to the raw data shown in figures 6.3, 4 & 5.

	Sample 1 (%)					Sample 2 (%)					Sample 3 (%)					Sample 4 (%)				
Signal	A	B	C	D	None	A	B	C	D	None	A	B	C	D	None	A	B	C	D	None
1	-	25	25	**97**	-	-	67	25	-	-	-	**100**	-	87	-	-	**100**	-	-	-
2	-	67	-	25	-	-	**95**	-	-	-	-	-	-	25	-	-	**100**	-	-	-
3	-	87	24	87	-	-	**100**	-	-	-	25	-	-	-	67	-	**100**	-	25	-
4	-	**96**	-	-	87	-	73	-	-	**100**	-	-	-	-	**100**	-	**100**	-	-	73
5	-	22	-	-	22	-	**95**	-	-	**95**	-	-	-	-	**100**	-	**100**	-	-	**93**
6	-	**91**	-	25	-	-	**99**	-	-	-	-	28	-	-	**93**	-	**99**	-	-	25
7	-	87	-	64	87	-	**99**	-	-	67	-	-	-	-	**100**	-	**100**	-	-	28
8	-	**98**	-	**98**	-	-	**100**	-	-	-	-	67	-	67	25	-	**100**	-	-	-
9	-	25	-	**91**	-	-	**100**	-	-	-	-	-	-	-	**100**	-	25	-	67	25

	Sample 5 (%)					Sample 6 (%)					Sample 7 (%)					Sample 8 (%)				
Signal	A	B	C	D	None	A	B	C	D	None	A	B	C	D	None	A	B	C	D	None
1	-	**96**	24	64	-	-	**100**	-	58	-	-	**100**	24	-	-	-	-	-	**100**	-
2	-	**100**	25	-	-	-	**100**	-	-	-	-	**99**	-	-	-	-	-	-	**99**	30
3	-	87	24	87	-	-	**100**	-	22	-	-	60	85	-	-	-	22	-	85	-
4	-	87	-	24	87	-	**100**	-	-	-	-	-	-	-	**99**	-	-	-	-	**91**
5	-	67	-	-	67	-	**100**	-	-	-	-	24	-	-	**96**	-	-	-	28	**100**
6	-	85	-	22	-	-	**100**	-	-	-	-	**99**	89	-	-	-	64	24	24	24
7	-	25	-	-	**98**	-	**100**	-	-	-	-	-	-	-	**98**	-	-	-	-	**100**
8	-	**100**	-	-	-	-	100	-	-	-	-	**96**	64	-	-	-	-	-	67	67
9	-	66	-	89	66	-	**100**	-	-	-	-	**91**	-	-	-	-	-	-	67	67

	Sample 9 (%)					Sample 10 (%)					Sample 11 (%)					Sample 12 (%)				
Signal	A	B	C	D	None	A	B	C	D	None	A	B	C	D	None	A	B	C	D	None
1	-	**96**	22	-	-	-	**100**	-	-	-	-	**99**	-	-	-	-	**97**	25	66	-
2	-	**91**	25	-	-	-	**100**	-	-	-	-	64	**96**	-	-	-	-	-	25	-
3	-	22	**99**	-	-	-	**96**	60	-	-	-	**100**	87	-	-	-	**90**	**100**	-	-
4	-	-	-	-	**100**	-	**90**	-	-	**100**	-	24	-	-	**99**	-	-	25	-	**91**
5	-	-	-	-	**100**	-	**99**	-	-	66	-	85	-	-	22	-	-	-	-	**91**
6	-	**96**	-	-	24	-	**91**	-	-	-	-	**100**	24	-	-	-	28	**98**	-	28
7	-	25	-	-	**97**	-	**98**	-	-	25	-	-	-	-	**96**	-	-	25	-	67
8	-	89	-	-	66	-	**100**	-	-	-	-	**98**	-	-	-	-	-	**99**	-	-
9	-	-	67	-	-	-	**99**	-	75	-	-	**100**	-	-	-	-	-	**99**	-	-

	Sample 13 (%)					Sample 14 (%)					Sample 15 (%)					Sample 16 (%)				
Signal	A	B	C	D	None	A	B	C	D	None	A	B	C	D	None	A	B	C	D	None
1	-	**91**	-	-	-	-	66	-	89	-	-	**100**	-	-	-	-	-	**99**	-	-
2	28	**93**	28	-	-	-	67	67	-	-	-	**99**	-	-	-	-	**96**	84	-	-
3	-	22	84	-	-	-	-	**98**	-	-	-	67	**90**	-	-	-	-	**99**	-	-
4	-	-	25	-	**100**	-	-	-	-	**99**	-	-	-	-	**100**	25	-	-	-	**99**
5	-	-	-	-	**100**	-	-	25	-	**99**	-	-	24	-	**96**	-	-	-	-	**100**
6	28	28	28	-	-	-	-	-	-	**99**	-	-	-	-	**99**	-	89	**97**	-	-
7	-	-	25	-	**100**	-	-	-	-	**95**	-	-	-	-	**99**	-	-	-	-	**100**
8	-	-	**91**	-	-	-	-	**100**	-	-	-	-	67	-	67	-	-	**99**	-	-
9	-	-	67	-	25	-	-	**100**	-	28	-	-	**91**	-	25	-	-	**91**	-	-

Figure 6.8 Similarity Confidence Indices: Total Numbers of Ticks.

	Sample 1 (%)					Sample 2 (%)					Sample 3 (%)					Sample 4 (%)				
Signal	A	B	C	D	None	A	B	C	D	None	A	B	C	D	None	A	B	C	D	None
1	-	25	25	**90**	-	-	67	25	-	-	-	**100**	-	67	-	-	**100**	-	28	-
2	-	67	-	-	-	-	**95**	-	-	-	-	-	-	30	30	-	**100**	-	-	28
3	-	87	24	87	-	-	**100**	-	-	-	-	-	-	-	67	-	**100**	-	25	-
4	-	67	-	-	**91**	-	30	-	-	**100**	-	-	-	-	**100**	-	**99**	-	-	75
5	-	-	-	-	67	-	77	-	-	**97**	-	-	-	-	**100**	-	**99**	-	-	**95**
6	-	**91**	-	25	-	-	**91**	-	-	-	-	-	-	-	**97**	-	**99**	-	-	25
7	-	25	-	25	**91**	-	**93**	-	-	**93**	-	-	-	-	**100**	-	**100**	-	-	30
8	-	**91**	-	**99**	-	-	**100**	-	-	-	-	25	-	67	25	-	**100**	-	-	-
9	-	73	-	**93**	28	-	**100**	-	-	-	-	-	-	-	**100**	-	30	-	75	75

	Sample 5 (%)					Sample 6 (%)					Sample 7 (%)					Sample 8 (%)				
Signal	A	B	C	D	None	A	B	C	D	None	A	B	C	D	None	A	B	C	D	None
1	-	**97**	25	66	-	-	**100**	-	-	-	-	**100**	-	-	-	-	-	-	**99**	-
2	-	**100**	25	-	-	-	**100**	-	-	-	-	**100**	-	-	-	-	-	-	**98**	30
3	-	67	25	67	-	-	**100**	-	22	-	-	87	**96**	-	-	-	64	-	**96**	-
4	-	25	-	-	**91**	-	**100**	-	-	-	-	-	-	-	**100**	-	-	-	30	**95**
5	-	30	-	-	**95**	-	**100**	-	-	-	-	-	-	-	**99**	-	-	-	-	**100**
6	-	**90**	-	25	-	-	**100**	-	-	-	-	**99**	67	-	-	-	67	-	-	25
7	-	-	-	28	**100**	-	**100**	-	-	-	-	-	-	-	**100**	-	-	-	-	**100**
8	-	**100**	-	-	-	-	**100**	-	-	-	-	**90**	67	-	-	-	-	-	25	67
9	-	25	-	67	67	-	**100**	-	-	-	-	**91**	-	-	-	-	-	-	67	67

	Sample 9 (%)					Sample 10 (%)					Sample 11 (%)					Sample 12 (%)				
Signal	A	B	C	D	None	A	B	C	D	None	A	B	C	D	None	A	B	C	D	None
1	-	**98**	25	-	-	-	**100**	-	-	-	-	**99**	-	-	-	-	**91**	-	25	-
2	-	**93**	28	-	28	-	**100**	-	-	-	-	67	67	-	-	-	-	30	30	30
3	-	25	**98**	-	-	-	**99**	64	-	-	-	**99**	89	-	-	-	67	**100**	-	-
4	-	-	-	-	**100**	-	25	-	-	**100**	-	-	-	-	**100**	-	-	28	-	**98**
5	-	-	-	-	**100**	-	**98**	-	-	67	-	67	-	-	67	-	-	-	-	**98**
6	-	**91**	-	-	25	-	**98**	-	-	28	-	**99**	25	-	-	-	30	**95**	-	30
7	-	-	-	-	**99**	-	**91**	-	-	25	-	-	-	-	**99**	-	-	30	-	**97**
8	-	67	-	-	67	-	**100**	-	-	-	-	**98**	-	-	-	-	-	**99**	-	-
9	-	-	67	-	-	-	78	-	78	-	-	**100**	-	-	-	-	-	**99**	-	-

	Sample 13 (%)					Sample 14 (%)					Sample 15 (%)					Sample 16 (%)				
Signal	A	B	C	D	None	A	B	C	D	None	A	B	C	D	None	A	B	C	D	None
1	-	**91**	-	-	-	-	67	-	67	-	-	**100**	-	-	-	-	-	**91**	-	-
2	-	**95**	30	-	-	-	67	25	-	-	-	**98**	-	-	-	-	**97**	60	-	-
3	-	-	85	-	-	-	-	**98**	-	-	-	67	**90**	-	-	-	-	**99**	-	-
4	-	-	-	-	**100**	-	-	-	-	**100**	-	-	-	-	**100**	28	-	-	-	**100**
5	-	-	-	-	**100**	-	-	28	-	**100**	-	-	-	-	**98**	-	-	-	-	**100**
6	28	28	28	-	-	-	-	-	-	**100**	-	-	-	-	**99**	-	**90**	**90**	-	-
7	-	-	28	-	**100**	-	-	-	-	**99**	-	-	-	-	**100**	-	-	-	-	**100**
8	-	-	**91**	-	-	-	-	**100**	-	-	-	-	73	-	**93**	28	-	**98**	-	-
9	28	-	73	-	73	-	-	**100**	-	30	-	-	75	-	75	-	-	**97**	-	30

Figure 6.9 Similarity Confidence Indices: Weighted Ticks.

	Sample 1 (%)					Sample 2 (%)					Sample 3 (%)					Sample 4 (%)				
Signal	A	B	C	D	None	A	B	C	D	None	A	B	C	D	None	A	B	C	D	None
1	-	-	-	78	-	-	37	**97**	-	-	-	**94**	-	-	-	-	**100**	-	-	-
2	-	-	-	30	30	-	78	-	-	-	-	-	-	39	**90**	-	**100**	-	-	-
3	-	29	-	78	-	-	**100**	-	-	-	-	-	-	-	97	-	**100**	-	-	-
4	-	37	-	-	**97**	-	29	-	-	**99**	-	-	-	-	**100**	-	**98**	-	-	78
5	-	-	-	39	39	-	78	-	-	78	-	-	-	-	**100**	-	**99**	-	-	77
6	-	**95**	-	30	30	-	**97**	-	-	37	-	-	-	-	**99**	-	**90**	-	-	**90**
7	-	-	-	37	**97**	-	**90**	-	-	39	-	-	-	-	**100**	-	**100**	-	-	-
8	-	78	-	**98**	-	-	**100**	-	-	-	-	-	-	-	78	-	**100**	-	-	-
9	-	30	-	30	30	-	**100**	-	-	-	-	-	-	-	**100**	-	-	-	37	**97**

	Sample 5 (%)					Sample 6 (%)					Sample 7 (%)					Sample 8 (%)				
Signal	A	B	C	D	None	A	B	C	D	None	A	B	C	D	None	A	B	C	D	None
1	-	85	37	37	-	-	**100**	-	-	-	-	**100**	-	-	-	-	-	-	**98**	-
2	-	**99**	-	-	-	-	**100**	-	-	30	-	**98**	-	-	-	-	-	-	**98**	30
3	-	-	-	78	-	-	**100**	-	-	-	-	**90**	39	-	-	-	-	-	**90**	-
4	-	-	-	-	**98**	-	**100**	-	-	-	-	-	-	-	**98**	-	-	-	-	78
5	-	-	-	-	78	-	**100**	-	-	-	-	-	-	-	**98**	-	-	-	-	**100**
6	-	39	-	39	-	-	**100**	-	-	-	-	**90**	39	-	-	-	37	-	-	85
7	-	-	-	-	**100**	-	**100**	-	-	-	-	-	-	-	**100**	-	-	-	-	**100**
8	-	**100**	-	-	-	-	**100**	-	-	-	-	-	41	-	-	-	-	-	-	**90**
9	-	30	-	30	30	-	**100**	-	-	-	-	78	-	-	30	-	-	-	30	78

	Sample 9 (%)					Sample 10 (%)					Sample 11 (%)					Sample 12 (%)				
Signal	A	B	C	D	None	A	B	C	D	None	A	B	C	D	None	A	B	C	D	None
1	-	**94**	41	-	-	-	**100**	-	-	-	-	**90**	-	-	39	-	**90**	39	-	-
2	-	85	37	-	37	-	**100**	-	-	-	-	-	85	-	37	-	-	-	29	-
3	-	-	**100**	-	-	-	**90**	39	-	-	-	**94**	41	-	-	-	29	**99**	-	-
4	-	-	-	-	**100**	-	37	-	-	**100**	-	-	-	-	**100**	-	-	-	-	**100**
5	-	-	-	-	**100**	-	**97**	-	-	85	-	-	-	-	38	-	-	-	-	**100**
6	-	41	-	-	**94**	-	78	-	-	-	-	**98**	-	-	-	-	-	78	-	30
7	-	-	-	-	**100**	-	**98**	-	-	30	-	-	-	-	**100**	-	-	85	-	**97**
8	-	39	-	-	**90**	-	**98**	-	-	-	-	78	-	-	29	-	-	**98**	-	-
9	-	-	78	-	-	-	29	-	78	-	-	**100**	-	-	-	-	-	**99**	-	-

	Sample 13 (%)					Sample 14 (%)					Sample 15 (%)					Sample 16 (%)				
Signal	A	B	C	D	None	A	B	C	D	None	A	B	C	D	None	A	B	C	D	None
1	-	**97**	-	-	37	-	39	-	**90**	-	-	**100**	-	-	-	-	-	78	-	-
2	-	**98**	-	-	-	-	**90**	-	-	-	-	**98**	-	-	39	-	**99**	-	-	-
3	-	-	41	-	-	-	-	85	-	-	-	-	29	-	-	-	-	**100**	-	-
4	-	-	-	-	**100**	-	-	-	-	**100**	-	-	-	-	**100**	-	-	-	-	**100**
5	-	-	-	-	**100**	-	-	-	-	**100**	-	-	-	-	**100**	-	-	-	-	**100**
6	30	-	30	-	-	-	-	-	-	**99**	-	-	-	-	**100**	-	85	**97**	-	-
7	37	-	-	-	**97**	-	-	-	-	**100**	-	-	-	-	**99**	-	-	-	-	**100**
8	30	-	78	-	-	-	-	**100**	-	-	-	-	30	-	78	-	-	**98**	-	-
9	-	-	30	-	30	-	-	**100**	-	30	-	-	37	-	85	-	-	78	-	-

Figure 6.10 Similarity Confidence Indices: Unambiguous Ticks.

6.4.3 Statistical Analysis of Listening Test Recordings and Measurements.

At the end of the listening test, each of the signals was played through each of the loudspeakers in turn and recorded onto digital tape via a measurement microphone placed at the average position of a subject's head. The recorded time waveforms were then transferred onto a computer. Voltage / pressure transfer functions (on-axis frequency response), measured for each of the loudspeakers using a dual-channel FFT analyser, were also transferred to the computer.

Direct comparison between the time waveforms for different samples and references proved difficult and was thus restricted to qualitative, eye-ball assessment only. An important property of a time waveform, and one for which comparisons are possible, is its frequency spectrum. Figure 6.11 shows the spectra of each of the nine source signals. The spectra for each of the signals reproduced by the loudspeakers were calculated using FFT techniques and stored for comparison with other spectra; the spectra of each signal, reproduced by each sample, were compared to the equivalent spectra reproduced by the four reference loudspeakers using a mean squared error technique described in appendix 8. The result of these comparisons, is shown in figure 6.12. The numbers shown have arbitrary units with a high number representing a close similarity, and a low number, a large difference. Note that in these results, the NONE column has been replaced by an ABSOLUTE column which refers to comparison with the source signal. The result for the most similar reference in each case is shown in underlined **bold**.

6.4.4 Further Analysis of Listening Test Recordings and Measurements.

In an attempt to find relationships between the test results and the physical characteristics of the sample loudspeakers, the measured transfer functions for the samples were analysed in detail. Figures 6.13F to 13.16 show the measured transfer functions for the band-pass filter and the test loudspeakers.

Figure 6.11 Frequency Spectra of Source Signals (through filter):

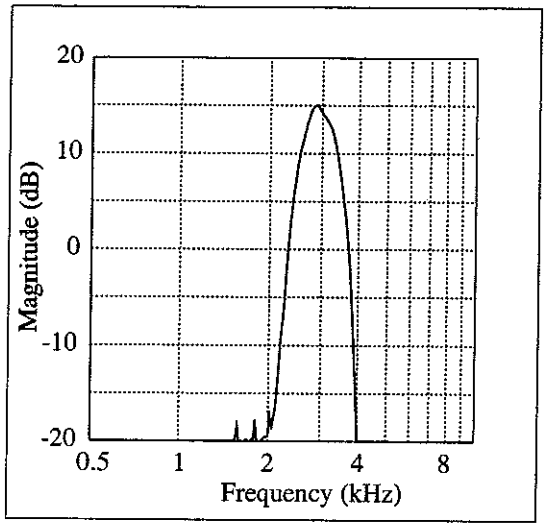

Fig. 6.11.1 "Chirp"

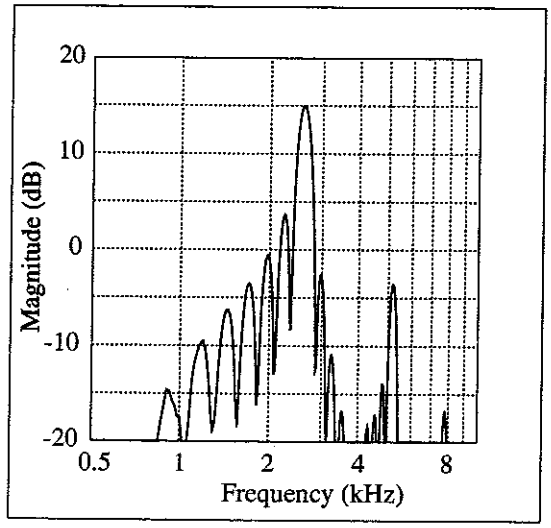

Fig. 6.11.2 "Burst"

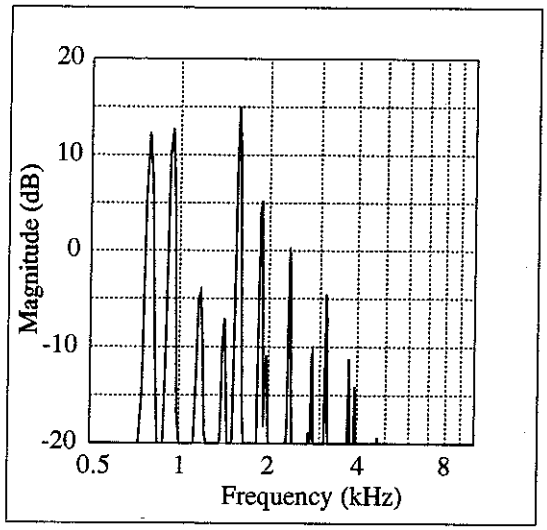

Fig. 6.11.3 "Flute Notes"

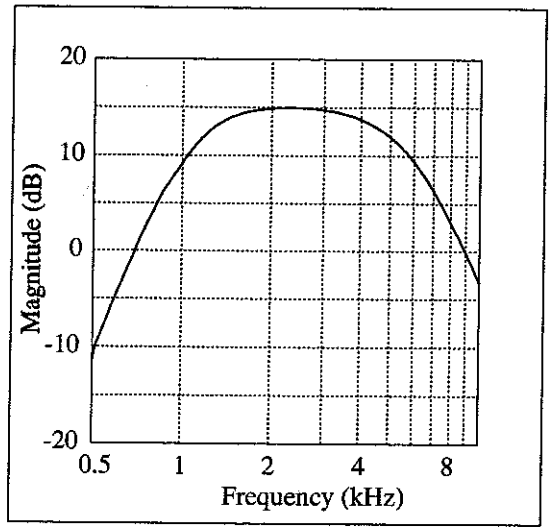

Fig. 6.11.4 "White Noise"

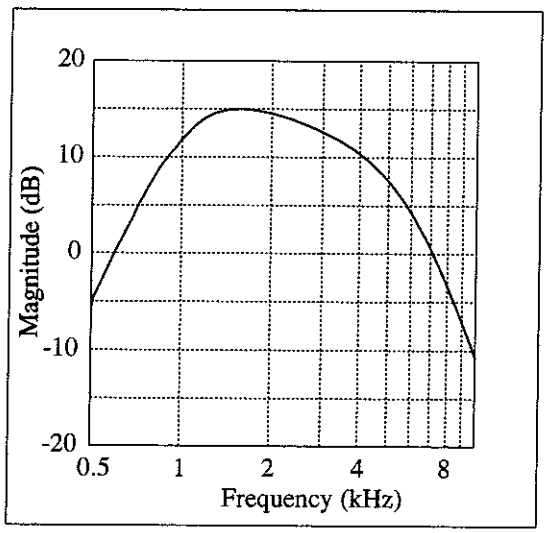

Fig. 6.11.5 "Pink Noise"

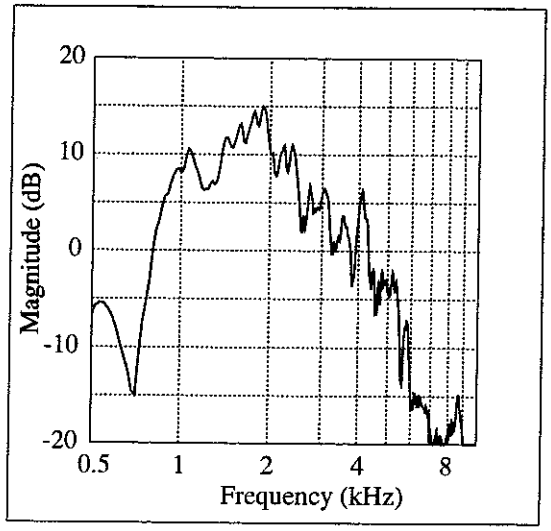

Fig. 6.11.6 "Slamming Book"

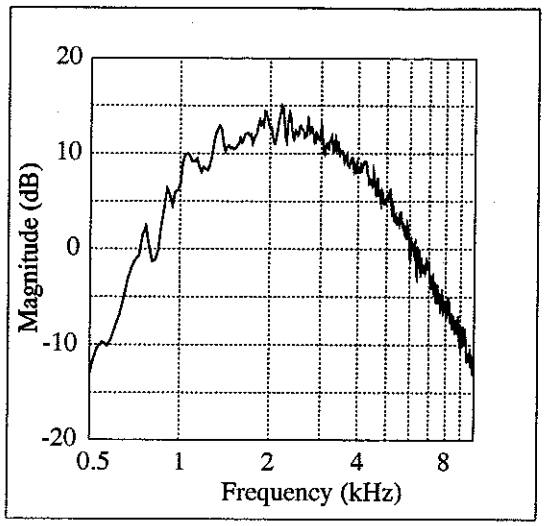

Fig. 6.11.7 "Waterfall"

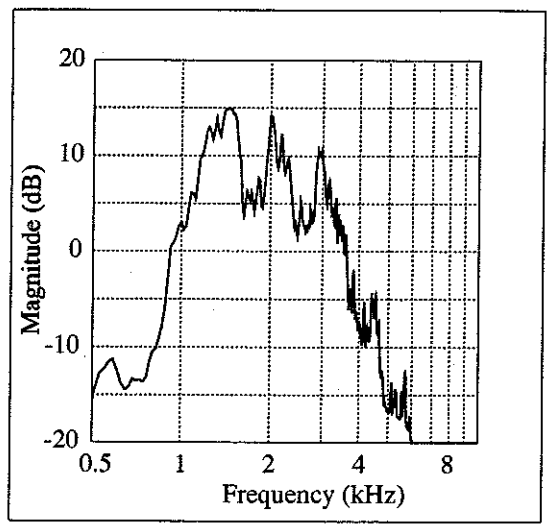

Fig. 6.11.8 "Statue Impact"

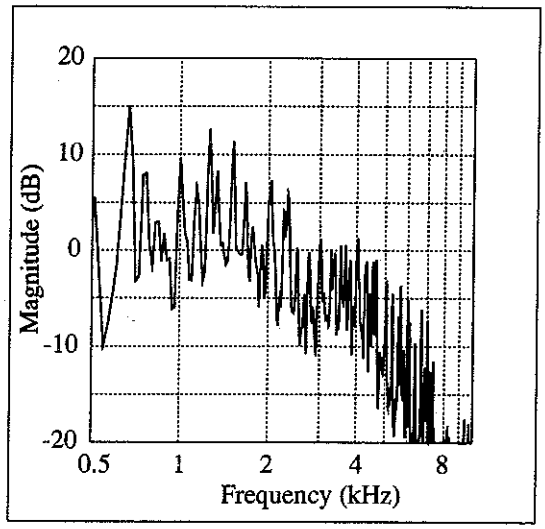

Fig. 6.11.9 "Guitar Chord"

	Sample 1					Sample 2					Sample 3					Sample 4				
Signal	A	B	C	D	Abs.	A	B	C	D	Abs.	A	B	C	D	Abs.	A	B	C	D	Abs.
1	56	**125**	36	46	93	**82**	72	26	77	93	**76**	54	21	69	62	37	**51**	32	31	46
2	45	**81**	51	41	95	34	**42**	31	25	50	22	26	21	**40**	24	33	**39**	27	24	40
3	16	24	23	**28**	23	24	**36**	32	28	42	**38**	32	29	25	49	19	**35**	25	30	28
4	24	**44**	37	27	43	17	**30**	20	18	30	17	16	18	**21**	18	18	**39**	28	22	35
5	22	**42**	32	26	37	20	**34**	24	19	36	21	22	21	**26**	26	17	**36**	26	21	29
6	26	**46**	36	25	45	22	**39**	30	22	41	22	25	24	**29**	31	18	**37**	28	22	29
7	24	**47**	38	26	46	18	**33**	23	18	33	18	19	19	**25**	21	17	**38**	29	20	32
8	32	**61**	37	26	54	31	**43**	31	24	52	21	26	21	**31**	27	25	**41**	30	23	36
9	18	**34**	30	26	29	19	**33**	23	19	35	**24**	21	20	22	28	16	**34**	27	21	27

	Sample 5					Sample 6					Sample 7					Sample 8				
Signal	A	B	C	D	Abs.	A	B	C	D	Abs.	A	B	C	D	Abs.	A	B	C	D	Abs.
1	49	**94**	38	46	78	50	**97**	37	42	69	63	**119**	32	56	105	75	**101**	31	91	159
2	41	**67**	49	35	86	45	**94**	47	38	104	41	**61**	40	40	69	50	**71**	48	55	64
3	16	23	23	**25**	24	23	**67**	27	36	40	32	**40**	**40**	26	69	18	26	27	**36**	27
4	24	**44**	37	26	51	24	**68**	31	31	54	26	**42**	34	27	52	37	32	30	**39**	35
5	22	**41**	35	24	43	21	**66**	32	30	47	25	**40**	38	23	53	28	**35**	31	32	37
6	25	**44**	40	24	48	23	**71**	36	32	49	26	**41**	**41**	23	54	34	**43**	32	32	45
7	23	**46**	39	24	50	23	**72**	34	30	53	26	**43**	36	25	52	**37**	36	31	**37**	39
8	33	**52**	42	23	60	27	**66**	32	32	50	33	**41**	39	23	57	38	**56**	36	31	61
9	18	**34**	**34**	24	32	20	**62**	29	30	45	22	37	**39**	23	44	21	29	**32**	31	29

	Sample 9					Sample 10					Sample 11					Sample 12				
Signal	A	B	C	D	Abs.	A	B	C	D	Abs.	A	B	C	D	Abs.	A	B	C	D	Abs.
1	44	**54**	42	53	55	62	**110**	29	42	85	48	**67**	28	34	61	56	**81**	31	39	73
2	**46**	45	43	29	52	50	**70**	38	37	80	**41**	40	37	23	55	**63**	54	43	30	65
3	17	20	**24**	21	23	26	**39**	36	30	50	28	**37**	36	25	58	35	26	**65**	23	55
4	27	27	**35**	20	31	25	**44**	36	30	50	25	**43**	32	24	62	28	33	**39**	24	37
5	24	25	**30**	19	28	23	**44**	36	28	50	28	**39**	35	21	65	33	31	**43**	21	45
6	26	25	**30**	18	30	25	**47**	39	29	53	30	**39**	**39**	22	66	36	34	**46**	21	55
7	27	27	**34**	20	31	25	**46**	36	29	51	26	**43**	35	23	62	30	34	**41**	23	44
8	32	26	**37**	17	33	30	**48**	34	30	56	**41**	40	40	22	72	**47**	34	43	20	61
9	20	24	**33**	19	26	21	**41**	37	28	45	27	**36**	32	21	65	26	29	**46**	22	38

	Sample 13					Sample 14					Sample 15					Sample 16				
Signal	A	B	C	D	Abs.	A	B	C	D	Abs.	A	B	C	D	Abs.	A	B	C	D	Abs.
1	49	**71**	32	34	60	79	**118**	32	52	127	44	**68**	32	34	53	73	**138**	33	58	132
2	54	**60**	49	32	98	55	**67**	61	37	88	49	**59**	39	42	65	60	**73**	45	38	100
3	34	30	**53**	24	62	22	25	**33**	28	34	39	30	**51**	24	54	37	**38**	35	27	78
4	30	32	**39**	29	40	**36**	32	**36**	31	43	26	29	**35**	27	33	40	**44**	32	33	62
5	33	32	**47**	23	46	32	36	**39**	28	50	29	32	**40**	23	42	32	**42**	33	27	61
6	35	35	**50**	24	55	39	**41**	**41**	30	64	30	35	**43**	24	47	36	**39**	33	27	59
7	31	34	**42**	26	44	**38**	36	**38**	31	51	27	32	**36**	26	38	39	**44**	33	31	63
8	43	35	**49**	22	58	45	**54**	43	28	82	34	**37**	**37**	24	49	35	**48**	32	28	56
9	28	30	**49**	24	39	26	33	**38**	28	41	25	30	**41**	23	36	26	**41**	32	26	54

Figure 6.12 Waveform Spectral Similarity (arbitrary units).

Figure 6.13 Transfer Functions of Test Loudspeakers:

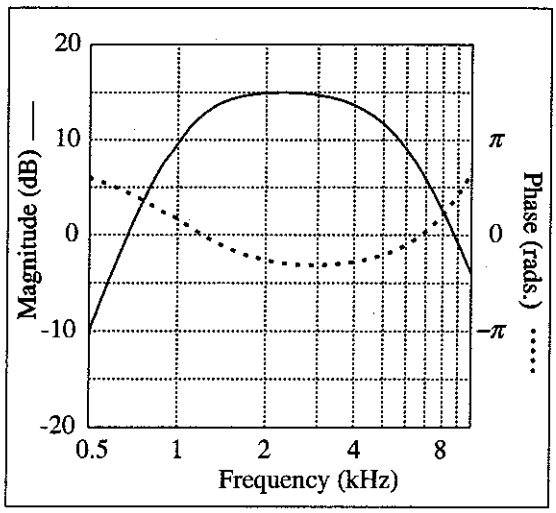

Fig. 6.13F Bandpass Filter Response.

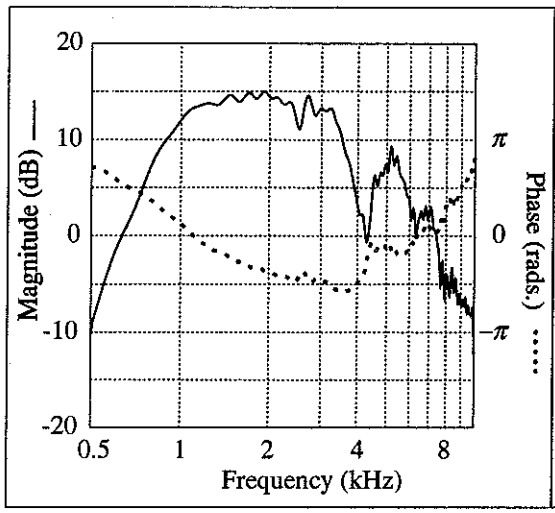

Fig. 6.13A Reference A.

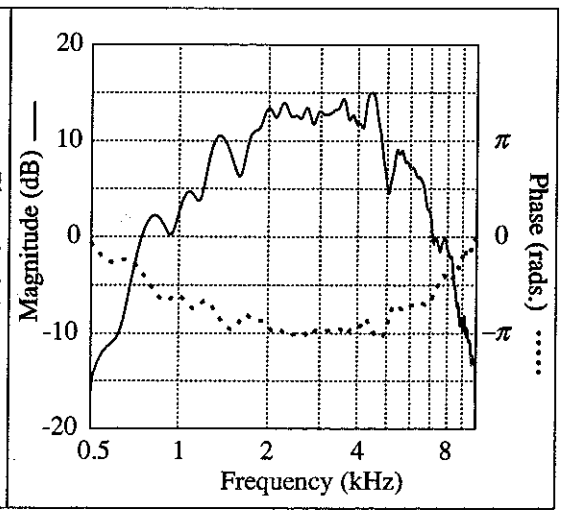

Fig. 6.13B Reference B.

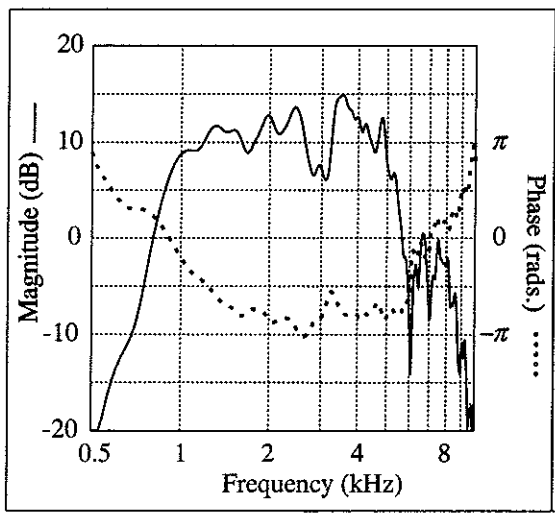

Fig. 6.13C Reference C.

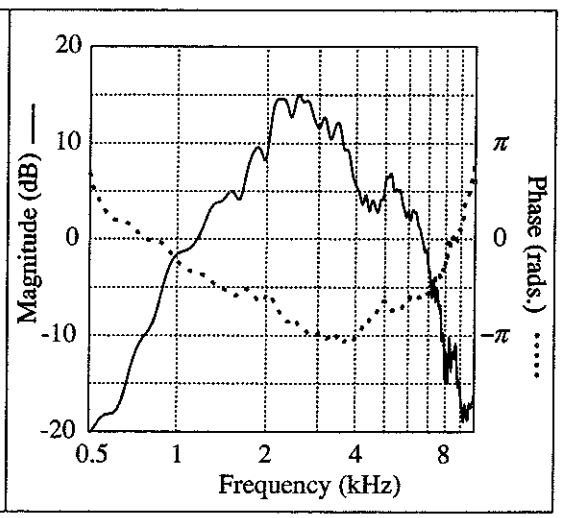

Fig. 6.13D Reference D.

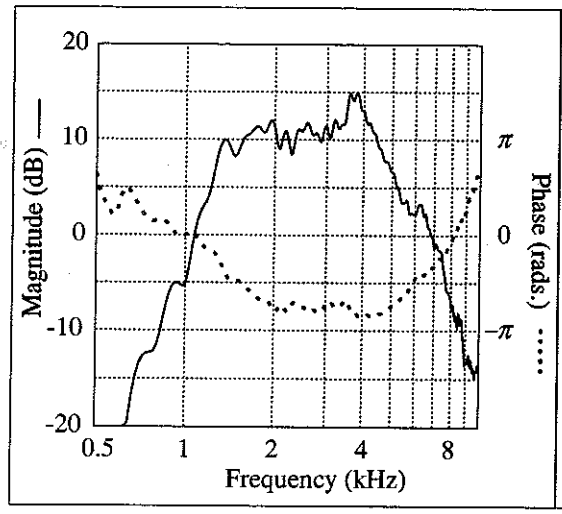

Fig. 6.13.1 Sample 1

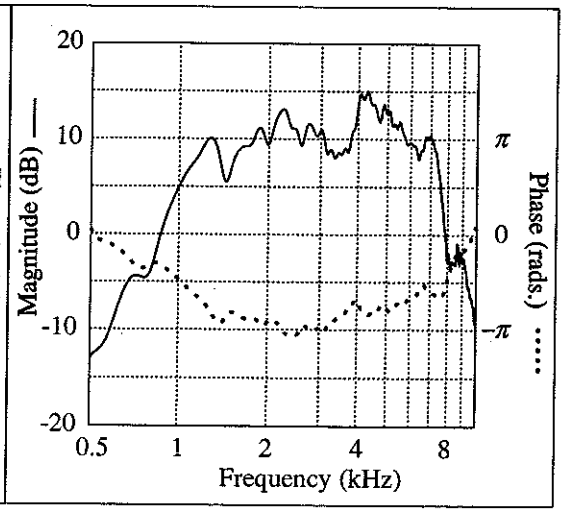

Fig. 6.13.2 Sample 2

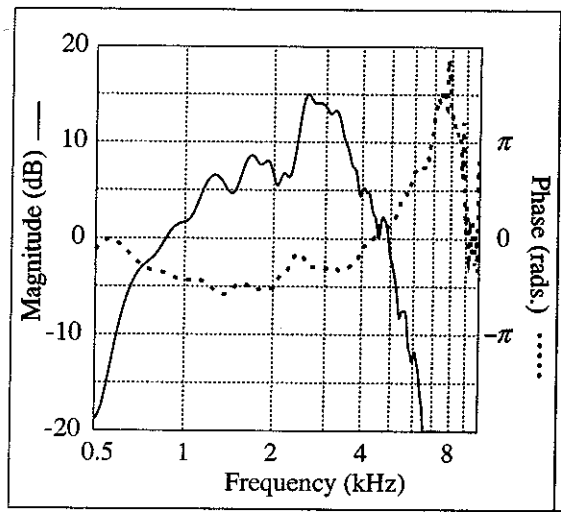

Fig. 6.13.3 Sample 3

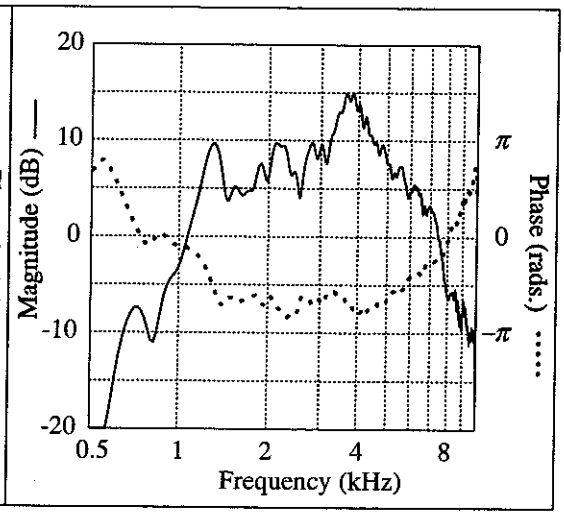

Fig. 6.13.4 Sample 4

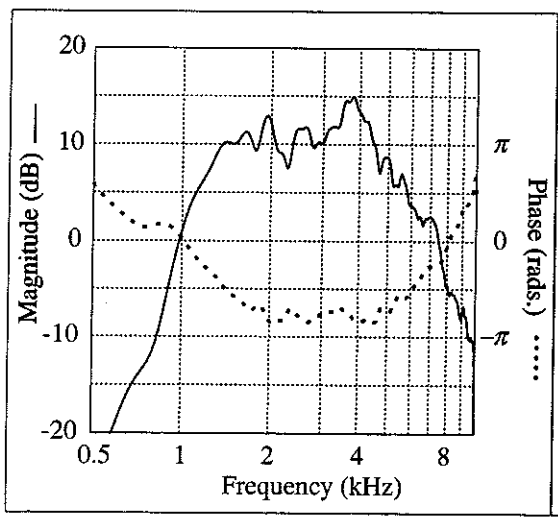

Fig. 6.13.5 Sample 5

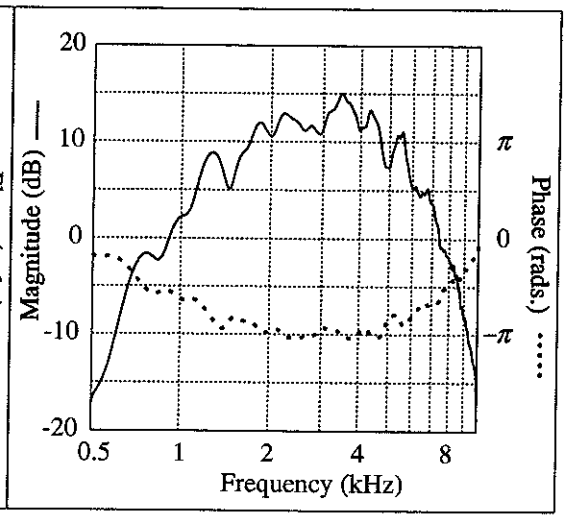

Fig. 6.13.6 Sample 6

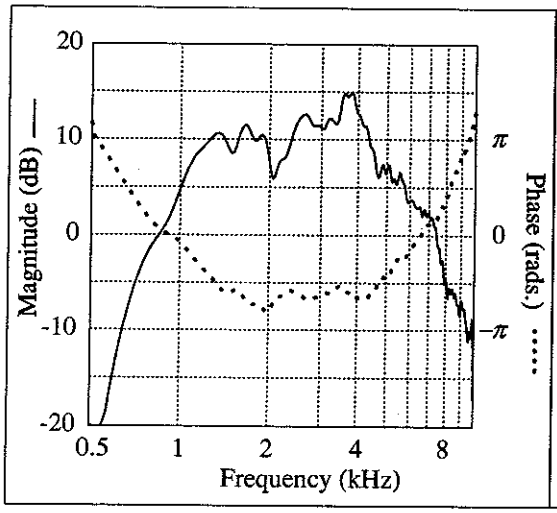

Fig. 6.13.7 Sample 7

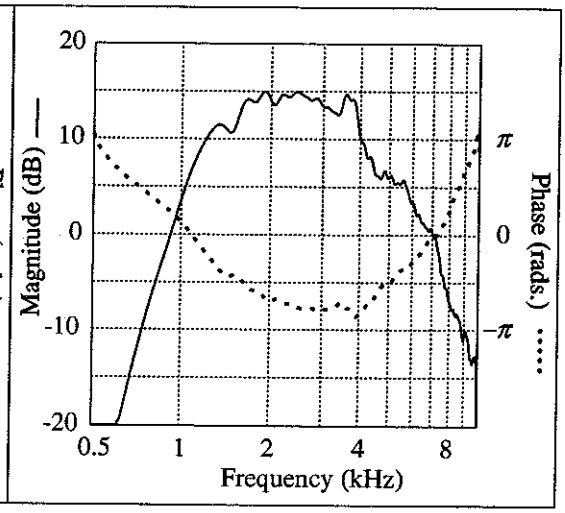

Fig. 6.13.8 Sample 8

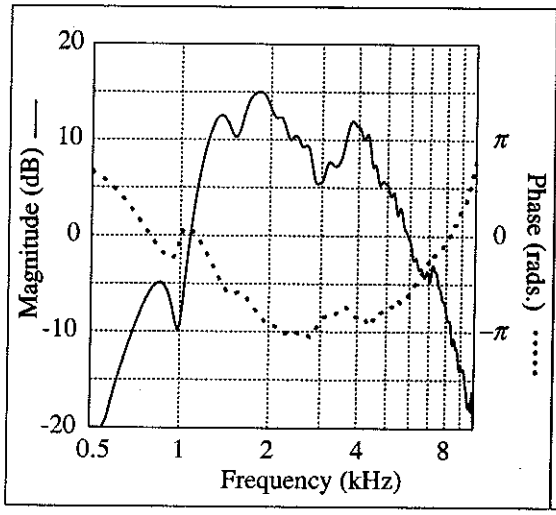

Fig. 6.13.9 Sample 9

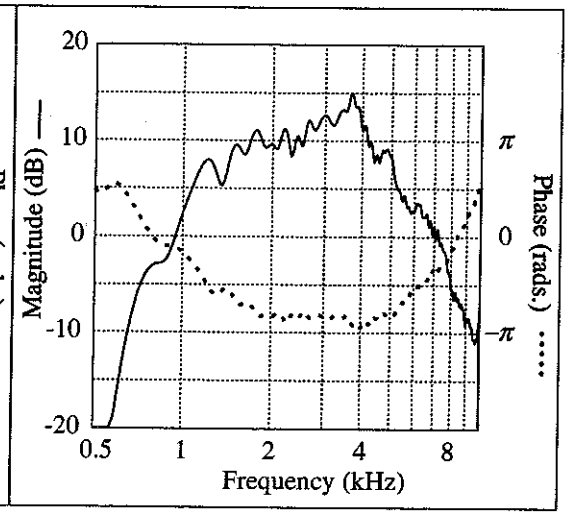

Fig. 6.13.10 Sample 10

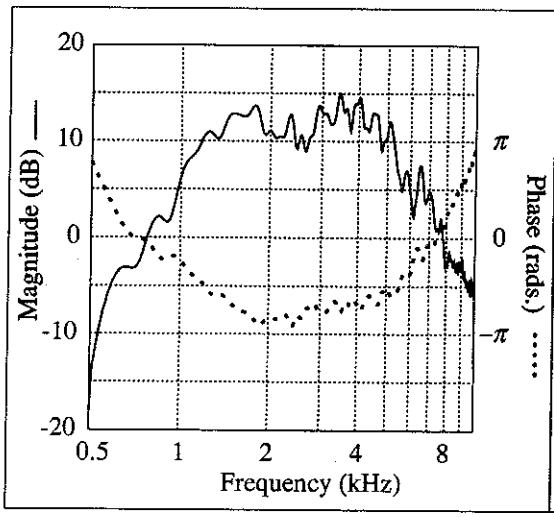

Fig. 6.13.11 Sample 11

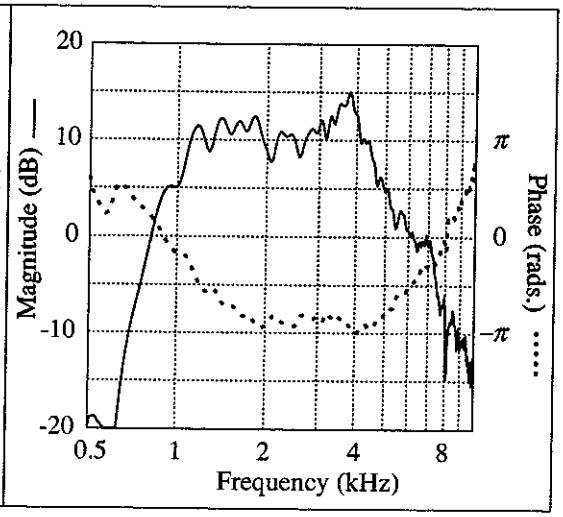

Fig. 6.13.12 Sample 12

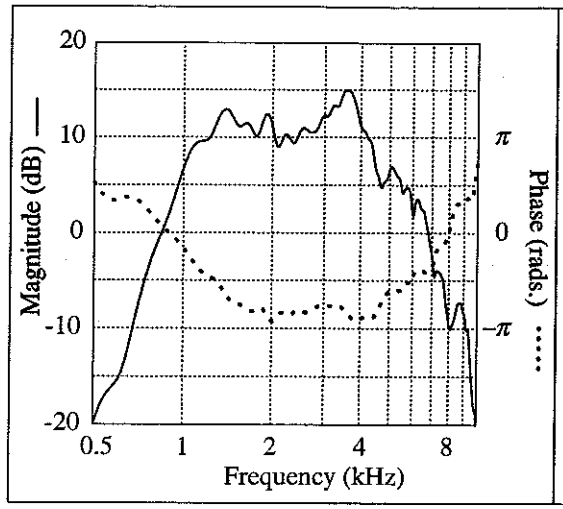

Fig. 6.13.13 Sample 13

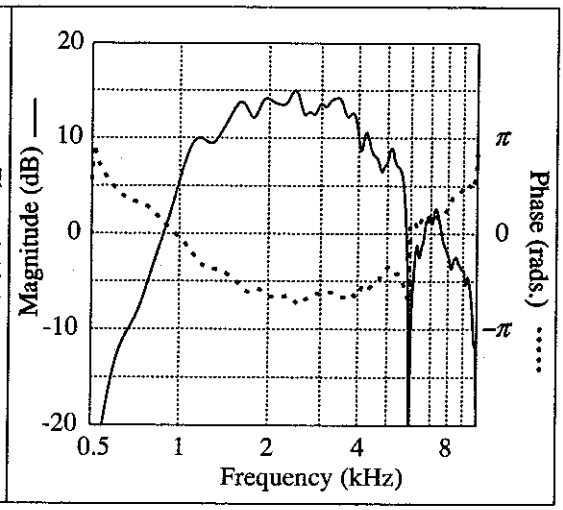

Fig. 6.13.14 Sample 14

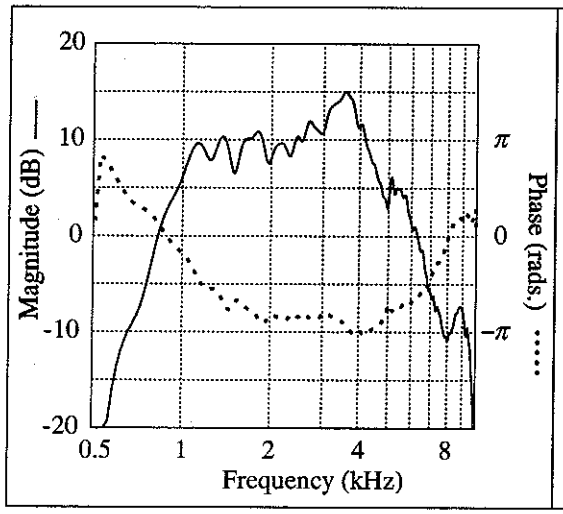

Fig. 6.13.15 Sample 15

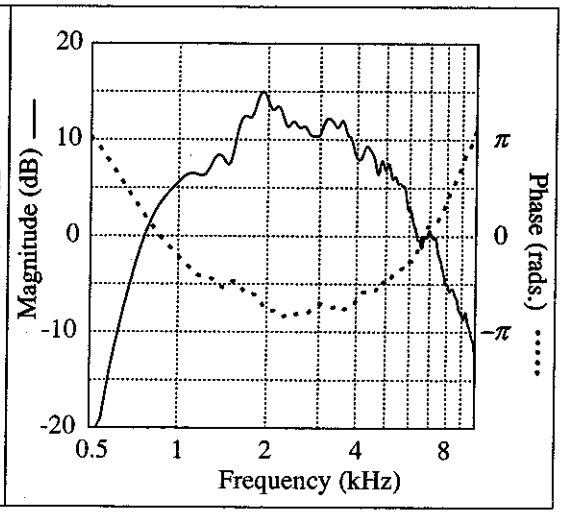

Fig. 6.13.16 Sample 16

6.5 DISCUSSION OF RESULTS

6.5.1 Analysis of 'Raw' Listening Test Data.

This preliminary analysis involves a detailed study of the listening test results shown in 'condensed' form in figures 6.3, 4 & 5. As mentioned in section 6.4, the analysis was conducted independently by two people, with discussion deferred until conclusions had been reached. This was considered necessary as analysis of this nature requires much interpretation of trends and patterns. Any conclusions that are common to both analyses are likely to be more reliable than those for either individual analysis. The results below are drawn from careful consideration of both sets of analyses, with emphasis placed on those results where agreement is strong.

The results for the experimental controls, samples 6 and 3, are discussed in detail in section 6.4. These controls, as well as helping to validate the test results, were expected to define a range of results from 'similar' to 'non-similar' over which the results for the rest of the samples would lie. A scale of similarity can be set up between the two control extremes such that results close to those for control sample 6 can be considered 'similar' and results close to control sample 3, 'non-similar'. Using this scale, some observations can be made from a study of the 'raw' test results shown in figures 3 to 5:

One obvious result is that more ticks have been entered in the reference B column than in any other column, and very few ticks have been entered in the reference A column. As reference A operates on a totally different principle from all other loudspeakers in the test† (all of the other loudspeakers, whether direct radiating or horn, operate on a moving-coil principle), the result that it has been judged not to sound similar to any of the samples (except some similarity with sample 13) is perhaps not surprising. This will be discussed in more detail when the measurements are considered. Reference B has been used as the mid-range driver in many studio monitoring systems; its popularity for use in these systems may be due to the broad similarity to a wide range of other loudspeakers evident from these results.

Other clearly defined results indicate that samples 2, 4 & 10 are similar to reference B: Samples 1 & 5 are fairly similar to both references B & D: Sample 12 is similar to reference C: Sample 8 is quite similar to reference D: Sample 9, like the 'non-similar' control, is similar to none of the references:

---

† *Note: Ref. A: Quad Electrostatic. Ref. B: Audax cone. Ref. C: Fostex Horn. Ref. D: Tannoy horn.*

Samples 7, 11, 13, 14, 15 & 16 all show some similarity with references B, C & D, with sample 13 also showing some similarity with reference A and sample 16, more similarity with reference C.

Considering the test signals† individually, it is clear that signals 4, 5 & 7 (see appendix 6) gave rise to many ticks being entered in the 'NONE' column. These signals are all wide-band noise type signals, and this result seems to indicate that this type of signal is the most critical for showing differences between loudspeakers. The consistency in the strongly similar results, for example those for the 'similar' control, across the range of test signals indicates that conclusions drawn from these positive results are very probably signal independent; if this were not the case, the results of the test would be much less valid. As with the results in general, the negative, non-similar results, such as those for the 'non-similar' control, show more variation across the range of test signals.

6.5.2 Analysis using Similarity Confidence Indices results.

Figures 6.8, 9 & 10 show the results for the 'similarity confidence indices' which correspond to the 'raw' data of figures 6.3, 4 & 5. The relevance of these indices is discussed in section 6.4.2 and the method of calculation described in detail in appendix 7.

The most obvious benefit of using these indices over studying the 'raw' data is that for each individual result (eg. sample 2, signal 3, reference B) the number of ticks entered in the other columns is taken into acount in the result, so that if equal numbers of ticks are entered into all columns, the confidence in the result for all of the columns is zero. Thus an ambiguous result consisting of a spread of ticks, recieves low confidence, and a strong positive result showing a clear preference for one column, high confidence. This benefit is clear when the spread of results between considering all ticks, weighted ticks and unambiguous ticks is compared with that for the 'raw' data; the three sets of figures agree to a much greater degree.

From figures 6.8, 9 & 10, all of the observations made above are in agreement except the following: the similarity between sample 5 and reference D is not as strong as that to reference B: There is some similarity between sample 9 and references B & D: samples 7 & 11 show quite strong similarity with reference B:

† *Note:* *Signal 1: Chirp.* *Signal 2: Tone burst.* *Signal 3: Flute notes.* *Signal 4: White noise.* *Signal 5: Pink noise.* *Signal 6: Slamming book* *Signal 7: Waterfall.* *Signal 8: Impact.* *Signal 9: Guitar chord.*

there is not much confidence in the similarity between sample 13 and reference A.

Additional results that can be obtained from the figures are as follows:
Signals 1, 4, 5 & 7 have large numbers of high confidence results (84% - 96% of possible), indicating that the subjects were in agreement over the similarity or otherwise of the samples when these signal were used: Signal 9 has a low number of high confidence results (56% of possible), indicating a spread in the opinions of the subjects over the similarity or otherwise of the samples when this signal was used.

6.5.3 Comparison between Listening Test Results and Measurements.

The objective of this comparison is to discover whether the listening test results can be explained in terms of the similarity, or otherwise, between the frequency spectra of the reproduced test signals. This will be the case if the characteristic sound of the loudspeaker samples in the test is due entirely to 'on-axis frequency response', and does not depend upon phase response or nonlinearity (the test was conducted under anechoic conditions so directivity should not be a factor). The 'root mean squared error' technique used for comparing the spectra is described in detail in appendix 8. Figure 6.12 shows the 'waveform spectral similarity' for each of the samples compared to each of the references, for each signal. An 'absolute' column is also present which compares the spectra with those of the original signals, thus giving an indication of the absolute spectral accuracy of a sample in the reproduction of each of the signals. The numbers given have arbitrary units but have been scaled to roughly agree with the similarity confidence indices above.

The spectral comparison for the 'similar' control, sample 6 vs reference B, shows high numbers indicating that there is a lot of similarity between the spectra of sample 6 and reference B for all signals. The comparison for the 'non-similar' control, sample 3, shows low numbers indicating dissimilarity between the spectra of sample 3 and the spectra of all of the references, for all signals (with the exception of signal 1). The numbers for signal 1 are generally higher than those for the other signals due to the narrow bandwidth of this signal leading to less possibility for error between spectra.

Comparison between the spectral similarity results (figure 6.12) and the similarity confidence indices (figures 6.8 - 10) shows good agreement. An indication of the degree of correlation between the results can be demonstrated by comparing references that show similarity confidence indices with a value of over 90% with

references that shows the highest spectral similarity, for each sample, for each signal. The number of 'correct' results amounts to:-

63 out of a possible 91† comparisons using the total numbers of ticks (69%).
61 out of a possible 77† comparisons using the weighted ticks (79%).
52 out of a possible 63† comparisons using the unambiguous ticks (82.5%).

Clearly this agreement between the listening test results and the comparisons between the spectra of the signals reproduced by the test loudspeakers indicates that a large part, but not all, of the sound of the test loudspeakers can be described in terms of their on-axis, amplitude frequency response. This finding is in accordance with those of other researchers (for example, see Toole [37] and Gabrielsson [38]). The samples for which good agreement was evident are samples 2, 4, 5, 6 and 10 and those for which poor agreement is evident are samples 8, 14 and especially 16. The signals for which good agreement is evident are signals 3, 4, 5, 6 and 7 and those for which poor agreement is evident are signals 1, 2, 8 and 9.

The key to the disparity between the listening test results and the spectral comparisons may lie in the phase response of the loudspeakers. Figures 6.13A to 13.16 show the measured transfer functions for each of the loudspeakers. It can be seen that the phase response of reference B is quite different from those of references A, C and D. Sample 16 will be used as an example to attempt to explain differences between the listening test results and the spectral comparisons. A comparison between figure 6.13.16 and figures 6.13A to 13D shows the amplitude response of sample 16 to be most similar to reference B. This result is borne out by the spectral similarity results that show sample 16 to be most similar to reference B for all nine signals. The listening test results however, show sample 16 to be similar to reference C for signals 1, 3, 6, 8 & 9, similar to no references for signals 4, 5 & 7 and similar to reference B only for signal 2. Figure 6.13.16 shows that sample 16 has a phase response similar to references C and D. The amplitude response of sample 16 is unlike that of reference D, so the listening test results for sample 16 may be explained using a combination of the amplitude and phase responses.

6.5.4 General Answers to the Questions Posed in Section 6.2.1.

The listening test was designed to answer the three questions listed in section 6.2.1. In the text below, the test results are studied in a general manner in an attempt to give broad answers to these questions.

† *Note: Comparison is only possible for those results for which a similarity confidence index of greater than 90% exists.*

Question a) Do horns sound different from each other?

Thirteen of the 16 sample loudspeakers and 2 of the references are horns, giving a total of 26 horn / horn comparisons for each of the 9 signals. The number of unambiguous ticks for all of these comparisons totals 272; giving an average of 10.5 ticks per loudspeaker comparison or an average of 1.16 ticks per signal. If this average is compared with 9.11 ticks per signal for the similar control, and 0.53 ticks per signal for the non-similar control, it is clear that in this test, in general the horns do not sound similar to each other. Of the 234 horn / horn comparisons, only 14 (6%) showed a similarity confidence index of over 90% (unambiguous ticks). When it is considered that 11 of the 13 horn loudspeaker samples were driven by the same driver, the wide spread in the results for these samples shows that horns do sound significantly different from each other.

Question b) Do horns sound different from direct radiators?

Although reference A is a direct radiating loudspeaker, being an electrostatic, it is not at all representative of the vast majority of direct radiators in use so the results for reference A will not be included in this discussion. The horn / direct radiating comparisons that will be considered here do not include the controls and are the 13 sample horns vs reference B and the direct radiating sample (2) vs references C & D; a total of 15 comparisons. The number of unambiguous ticks for these comparisons totals 270; giving an average of 18 ticks per loudspeaker comparison or 2 ticks per signal. Again, comparison with the results for the two controls shows that in this test, in general, the horns do not sound very similar to the direct radiators. The similarity confidence index results show 34 of the 135 (25%) horn / direct radiating comparisons to have greater than 90% confidence; indicating that some similarity exists between the sound of the horns and that of the direct radiators (particularly reference B).

Question c) Is the difference between horns and direct radiators greater than the difference between horns?

A comparison between the answers to questions a & b shows that there is more difference between horns than there is between horns and direct radiators. However, it must be borne in mind that most of the 'similar' results mentioned in answer to question b were for comparison between the samples and reference B; as mentioned

in section 6.5.1, the reproduction of sound through reference B appears to be more representative than that of the other three references of the reproduction through a wide variety of loudspeakers, so this result is perhaps not surprising. It can be concluded though that no evidence exists from the results of this listening test to show that horns in general sound more different from direct radiating loudspeakers than they do from each other.

6.5.5 Discussion of the Results for Individual Loudspeaker Samples.

In this section, the results for each loudspeaker sample are discussed in turn, with reference to the physical properties of the loudspeakers and to the analysis of the measured on-axis transfer functions.

Figures 6.14A to 14.16 show a form of power cepstra, derived from the transfer functions of each of the reference and sample loudspeakers. The plots are calculated from the log-amplitude of the transfer functions after deconvolution of the bandpass filter and subsequent corrective filtering. Details of the method used are contained in appendix 9. These power cepstra are useful for separating out parts of a signal (or response) that are time-separated from the main signal (or response), such as reflections or echos. The presence of such a reflection in a response would show as comb-filtering on a transfer function plot and as a 'spike' displaced along the 'x-axis' (units of time) on a cepstrum plot, allowing it to be easily identified. A study of the power cepstra of the loudspeakers can be useful for finding the physical cause of some of the response irregularities that they may possess.

Sample 1: Vitavox exponential horn.

The results in figures 6.3 to 10 show this sample to sound most similar to both reference B, a direct radiating cone, and reference D, a horn. The signals for which it was chosen as being most similar to reference B are the white noise (4) and the slamming book (6), and the signals for which it was chosen as being most similar to reference D are the chirp (1) and the guitar chord (9). Almost equal similarity between the two references was evident for the impact (8). Signals 1 & 9 are both tonal in nature, signals 4 & 6 contain no tonal information and signal 8 contains a mix of tonal and transient information, so it appears as if this sample sounds more like reference B when reproducing wide-band, non-tonal sounds (noise or transient) and more like reference D when reproducing tonal sounds. The exceptions to this are the pink noise (5) waterfall (7, noise-like), and flute (3, tonal) signals for which little similarity was evident to any particular reference. Comparisons between the

transfer function measurements (figs. 6.13) show this sample to have an amplitude response that is most similar to that of reference B (fig. 6.12) but a phase response that is most like reference D.

Figure 6.14.1 shows the power cepstrum for this sample. The most notable feature is the presence of a distinct 'echo' at about 1.8ms. This horn / driver combination has a length from diaphragm to mouth of approximately 340mm, so a wave reflected from the mouth, back down the horn will be radiated about 1.8ms after the original wave, giving rise to the 'echo'. This mouth reflection is responsible for the narrow-band response irregularities evident in figure 6.13.1.

Sample 2: JBL 5" direct radiating cone.
The results (figs. 6.3 to 10) show this sample to sound similar to reference B for all nine signals. A comparison between the measured transfer functions of this sample and reference B (figs. 6.13) shows them to be similar in both amplitude and phase, which explains good agreement between the similarity confidence index results and the spectral similarity on all signals.

Sample 3: JBL 10" direct radiating cone.
This sample was included in the test as the 'non-similar' control. The results (figs. 6.3 to 10) show it not to sound similar to any of the references for signals 2 to 9 but to sound similar to reference B for signal 1. Figure 6.13.3 shows that the transfer function of this sample is dominated by a rapid tail-off above 3.5kHz, due to it having been designed for operation below 2kHz. Figure 6.11.1 shows that signal 1 (chirp) has a spectrum that is concentrated around 3kHz and is thus largely unaffected by this tail-off.

Sample 4: AX1 low flare-rate axisymmetric horn.
The results for this sample (figs. 6.3 to 10) show a very strong resemblance in sound to reference B, a direct radiator, with similarity confidence index results of greater than 90% evident for signals 1 to 8, regardless of how the questionnaire ticks were interpreted. Despite being fitted with a similar driver, this sample does not sound similar to reference C on any signal. Figure 6.14.4 shows the power cepstrum for this sample. The plot is dominated by a very strong reflection at about 1.4ms which is undoubtedly due to reflection from the small horn mouth which is approximately 230mm from the driver diaphragm. The effect of this reflection on the transfer function of this sample can be seen as large peaks and troughs in figure 6.13.4. The

height and position of these peaks are similar to those in the transfer function of reference B (figs. 6.13), and the reason for this similarity can be seen in the power cepstrum for reference B (fig. 6.14B) which shows a strong reflection at about 1.1ms. Other peaks in the power cepstra of the two loudspeakers coincide at about 2.1 and 3.7ms. Although the phase response of this sample is more similar to references C & D than to reference B, the strong similarity in amplitude response to reference B is responsible for their similar sound.

Sample 5: Reflexion Arts horn.

The similarity confidence index results for this sample (figs. 6.8 to 10) show quite a wide spread between the results for different signals and for different interpretations of the questionnaire ticks. Overall, the sample sounds more similar to reference B for signals 1, 2, 6 & 8 than to the other references, with some similarity to reference D for signals 3 & 9. Signals 3 (flute) & 9 (guitar) both contain a lot of information at frequencies below 1kHz (figs. 6.11) and a comparison between the transfer function for this sample and that of reference D (figs. 6.13) shows that both loudspeakers have a fall in response below this frequency. When reproducing signals with little information in these lower frequencies (signals 1, 2, 6 & 8), this sample sounds more similar to reference B, and for wide-band signals (signals 4, 5 & 7), it sounds similar to none of the references.

Sample 6: Son Audax 7" direct radiating cone.

This sample was included in the test as the 'similar' control. It is nominally identical to reference B, being from the same production batch. As mentioned in section 6.4.1, the results show this sample to sound similar to reference B with similarity confidence indices of 100% for all nine signals regardless of how the questionnaire ticks were interpreted; in all, more than 70% of all of the ticks for this sample were entered in the 'B' column. A comparison between the transfer functions for this sample and reference B (figs. 6.13) shows small differences which are more apparent from a comparison of their power cepstra (figs. 6.14). These small differences, along with a less than 100% listening test result, show that even two nominally identical drive-units do not measure or sound identical. The measurements and test results do show however that this sample and reference B are more similar than any other two loudspeakers in the test.

Sample 7: Reflexion Arts horn without 'lips'.

This sample was included in the test to see if a change in the mouth termination of a "generally well-liked" horn would significantly alter its sound characteristics. As

can be seen from both the test results (figs. 6.3 to 10) and the measured transfer functions (figs. 6.13) for samples 5 & 7, the sound of this horn has been only subtly changed by the removal of the mouth 'lips'. Under other than anechoic or free-field listening conditions, it is expected that the difference in sound of this horn with or without 'lips' would be less subtle due to changes in directivity.

Sample 8: AX2 rapid flare-rate axisymmetric horn.
The results for this sample (figs. 3 to 10) show a strong similarity to reference D for signals 1 (chirp), 2 (burst) & 3 (flute) with a slight similarity to reference B for signal 6 (book). Little similarity to any reference is evident for all other signals. The power cepstrum for this sample (fig. 6.14.8) shows a series of reflections at about 0.3ms intervals which die away rapidly with time up to about 2ms, indicating reflections from the interface between the driver and horn (approximately 50mm from diaphragm) rather than in the horn itself. The absence of reflections at longer times shows that there is little reflection from the mouth of this horn. This power cepstrum plot bears some resemblance to that for reference D, but is unlike that of any other sample.

Sample 9: Yamaha sectoral horn.
The test results for this sample (figs. 6.3 to 10) show it to sound similar to reference B for signals 1, 2, & 6, and similar to reference C for signal 3. Little similarity to any reference is evident for the other signals. Figure 6.13.9 shows the transfer function for this sample to be very uneven, with large, wide-band peaks and troughs throughout its response. The power cepstrum for this sample (fig. 6.14.9) shows the presence of a severe reflection at about 0.4ms followed by another, less severe reflection at about 1.8ms. This horn has a rapid change in cross-sectional shape and flare-rate at a distance of about 70mm from the diaphragm which is probably responsible for the strong early reflection and the uneven response. The later reflection is a horn mouth reflection (diaphragm to mouth distance 350mm). From these plots, it is surprising that this sample shows any similarity to any of the references, although the peaks in the transfer function do coincide in frequency with those in the transfer functions of references B & C, and the power cepstrum for reference B (fig. 6.14B) shows quite a strong reflection at about 0.5ms. The spectral similarity results (fig. 6.12) show that this sample is not very similar to any of the references, although it is most similar to reference C for six of the nine signals, which indicates very poor agreement between the measurements and listening test

results. Comments made by some subjects about this sample indicate that this horn has a "strange" or "odd" sound.

Sample 10: Fostex wooden sectoral horn.
The results for this sample (figs. 6.3 to 10) indicate a strong resemblance in sound to the direct radiating reference B, with similarity confidence indices of greater than 90% for all signals, if the total number of questionnaire ticks are counted, and all except signals 4, 6 & 9, if only unambiguous ticks are counted. Some similarity with reference D is evident for signal 9 (guitar). The transfer function for this sample (fig. 6.13.9) shows an amplitude response that is similar to, although smoother than, that for reference B (fig. 6.13B), and the spectral similarity results show strong similarity with reference B for all signals. The phase response for this sample is most similar to that for reference D, which may explain the similarity with this reference for signal 9.

Sample 11: JBL axi-symmetric horn.
The results for this sample (figs. 6.3 to 10) indicate that it sounds similar to reference B for signals 1, 3, 8 & 9, with some similarity to reference C for signal 2 (burst). The transfer function for this sample (fig. 6.13.11) shows similarity in overall shape with that for reference B, as is indicated by the spectral similarity results (fig. 6.12), but quite severe comb-filtering can be seen throughout the response. The power cepstrum plot (fig. 6.14.11) for this sample shows a strong reflection at about 1.9ms, indicative of a poor mouth termination; this is responsible for the comb filtering evident in figure 6.13.11. This horn is similar in size and shape to sample 4, but has a 'slant plate' fitted over the horn mouth to improve directivity. As the mouth reflection appears to be stronger for this sample than that for sample 4, it can be concluded that the slant-plate is responsible for the poor mouth termination.

Sample 12: Altec sectoral horn.
The listening test results for this sample (figs. 6.3 to 10) show similarity with reference C for signals 3, 6, 8 & 9, and similarity with reference B for signal 1. The spectral similarity results (fig. 6.12) agree very closely with these results, indicating that the similarities are amplitude response dominated. The transfer function for this sample (fig. 6.13.12) can be seen to be broadly similar to, but smoother than, that for reference C. However, reference C has a large dip in response at about 3kHz which is not present in the response for this sample. As signal 1 has a spectrum which is concentrated around 3kHz, this may explain the similarity to reference B for this

signal. The similarity of this sample to reference C in both the listening test results and the measurements is not surprising as they are very similar in size and shape to one another, both being very long with diaphragm to mouth distances of about 500mm. The power cepstrum for this sample (fig. 6.14.12) shows only slight evidence of a mouth reflection at about 3ms. This is to be expected as the mouth of this horn is large compared to the wavelengths considered. This sample was identified by one subject as a horn.

Sample 13: Altec multicellular horn.

The results for this sample (figs. 6.3 to 10) show a wide spread, with similarity to reference B for signals 1 & 2 and similarity to reference C for signal 8. The results for the remaining signals being either spread amongst the references or entered in the 'NONE' column. This sample was one of a very few samples in the test to show any clear similarity to reference A, the electrostatic. The reason for this may lie in the smoothness of the transfer functions for the loudspeakers. The transfer function for this sample (fig. 6.13.13) is very similar in shape to that for the other Altec horn, sample 12 (fig. 6.13.12), but is smoother, and the listening test results show that they sound quite different. A comparison between the power cepstra of the two samples (figs. 6.14.12 & 14.13), shows sample 12 to have more late reflections than this sample, which are responsible for the less smooth response. The transfer function for reference A (fig. 6.13A) is exceptionally smooth up to about 3.5kHz, unlike the other three references and most of the samples. Signals 1 & 2 do not contain much information below 2kHz, which may explain the similarity with reference B. Like sample 12, this horn has a large mouth and the power cepstrum for this sample (fig. 6.14.13) shows only very slight evidence of mouth reflections at an expected 3.5ms. Good agreement between the listening test results and the spectral similarity results (fig. 6.12) is found for this sample.

Sample 14: Starr gramophone horn.

This sample was included in the test for curiosity and amusement. Interestingly, despite its pre-war, non-loudspeaker design and folded shape, not one of the test subjects thought it sounded odd or bad, in fact one subject actually commented that it sounded "nice" (the test was of course 'blind') but it was identified by some subjects as a horn. The results for this sample (figs. 6.3 to 10) show similarity with reference C for signals 3, 8 & 9, and similarity with reference D for signal 1. The transfer function for this sample (fig. 6.13.14) is remarkably smooth up to 6kHz, where a deep, but narrow, dip is present. Like sample 13, this sample showed slight similarity with reference A.

Sample 15: Vitavox sectoral horn.

The results for this sample show similarity with reference B for signals 1 & 2, and similarity with reference C for signal 3. Very little similarity with any of the references is evident for the other signals. The results for this sample are similar to those for sample 13 except for a weaker similarity with reference A. The transfer function (fig. 6.13.15) is also similar to, but not as smooth as, that for sample 13, as is the power cepstrum (fig. 6.14.15). Physically, this horn is similar in shape and size to sample 12 and reference C. Some subjects noticed a metallic "ring" from this sample on signals 2 and 6, and some also identified it as a horn.

Sample 16: JBL bi-radial horn.

The results for this sample show similarity with reference C for signals 1, 3, 6, 8 & 9, and similarity with reference B for signal 2. In common with many of the samples, the results for the wide-band noise signals (4, 5 & 7) show little similarity with any of the references. As mentioned in section 6.5.3, there is very little agreement between the listening test results and the spectral similarity results for this sample. This disparity is explained in section 6.5.3 in terms of the phase responses of the loudspeakers, although it is unclear why the phase response of this loudspeaker should appear to be more dominant than it is for the other samples.

Figure 6.14 Power Cepstra of Test Loudspeakers:

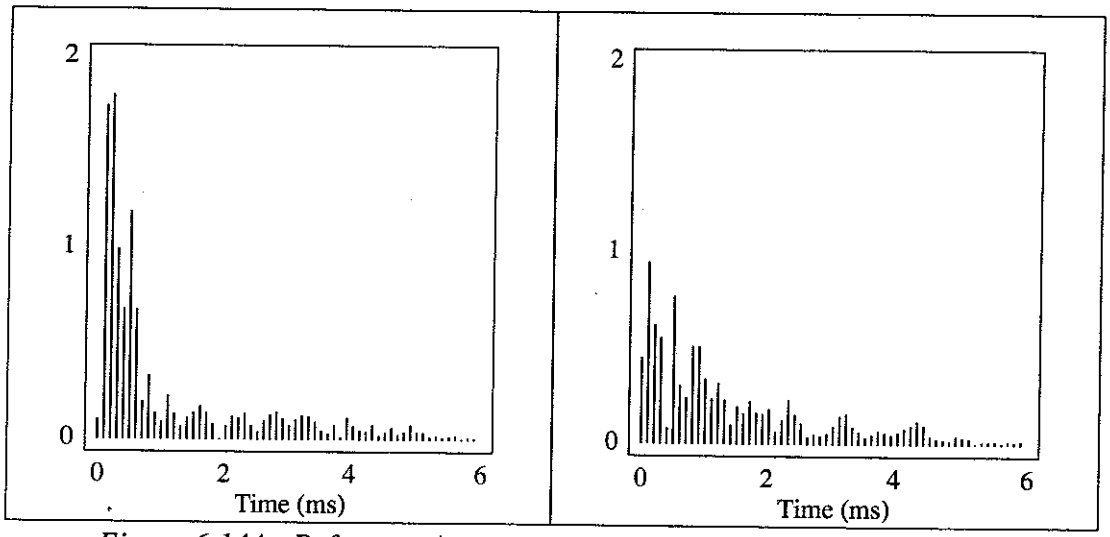

Figure 6.14A Reference A

Figure 6.14B Reference B

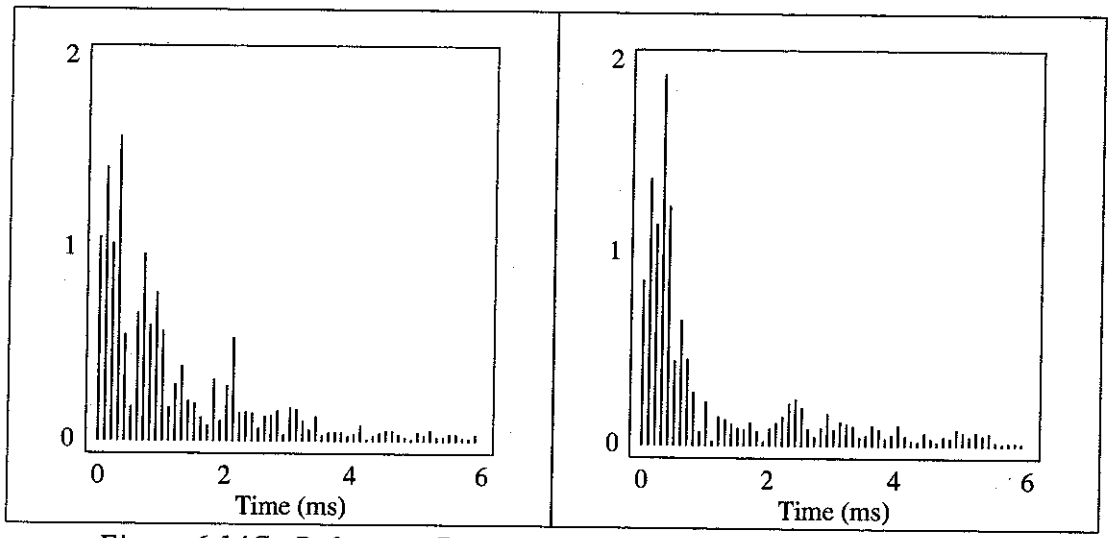

Figure 6.14C Reference C

Figure 6.14D Reference D

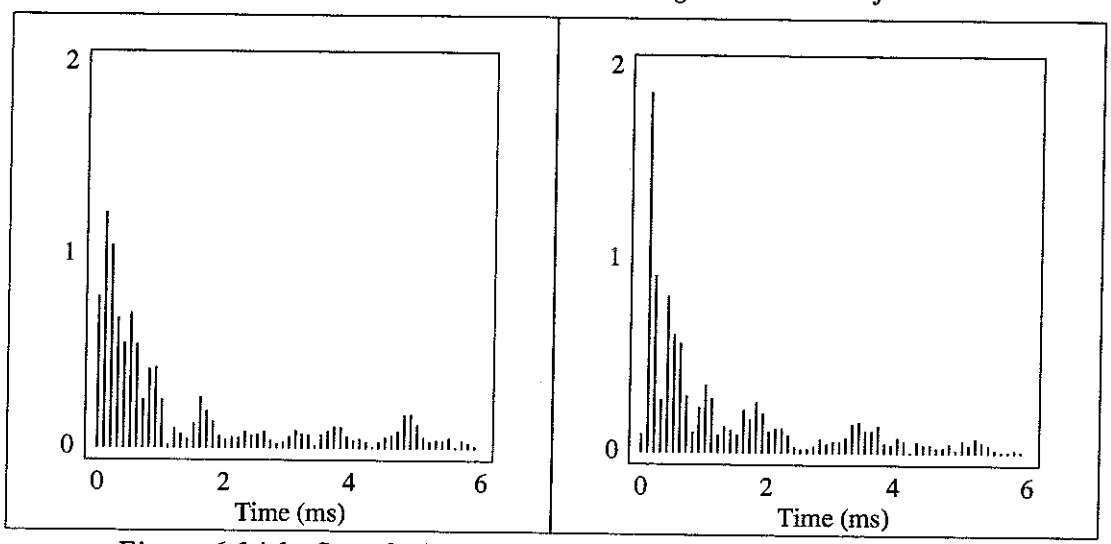

Figure 6.14.1 Sample 1

Figure 6.14.2 Sample 2

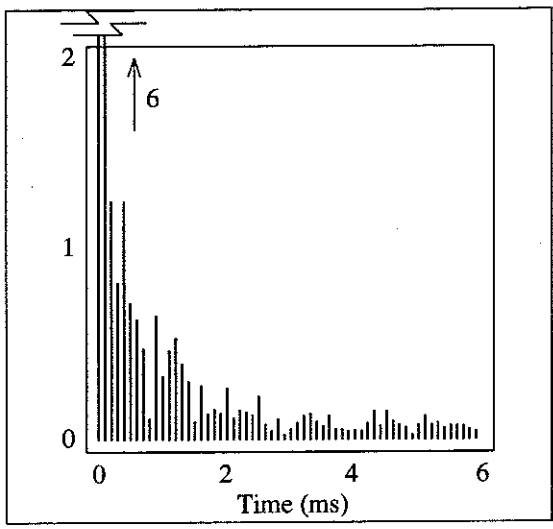

Figure 6.14.3 Sample 3

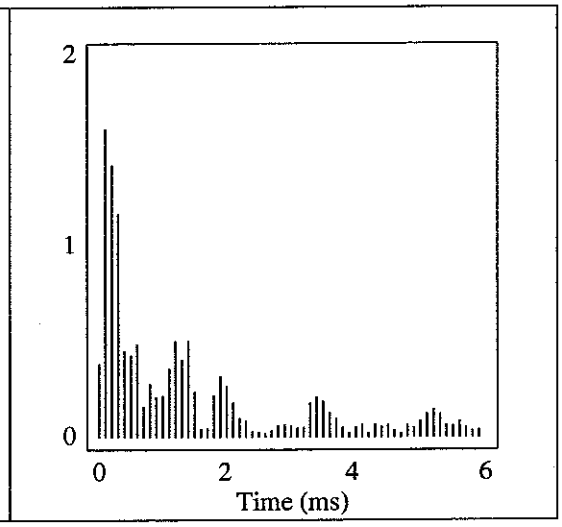

Figure 6.14.4 Sample 4

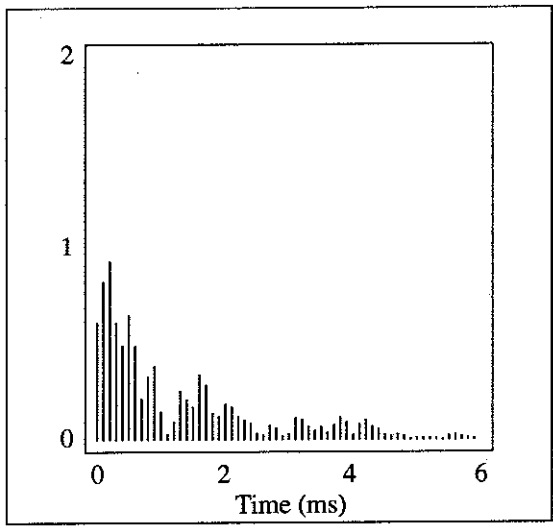

Figure 6.14.5 Sample 5

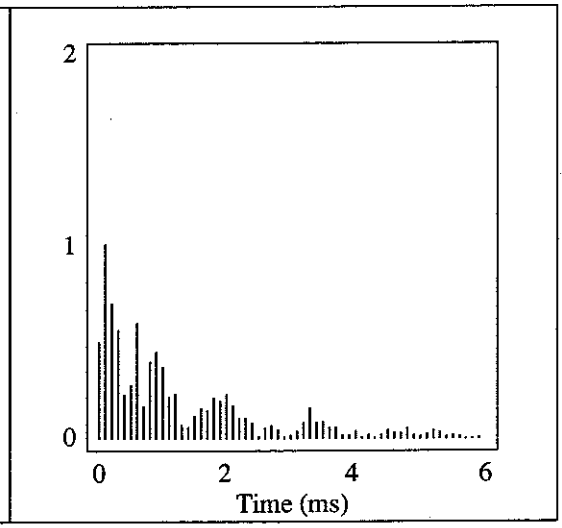

Figure 6.14.6 Sample 6

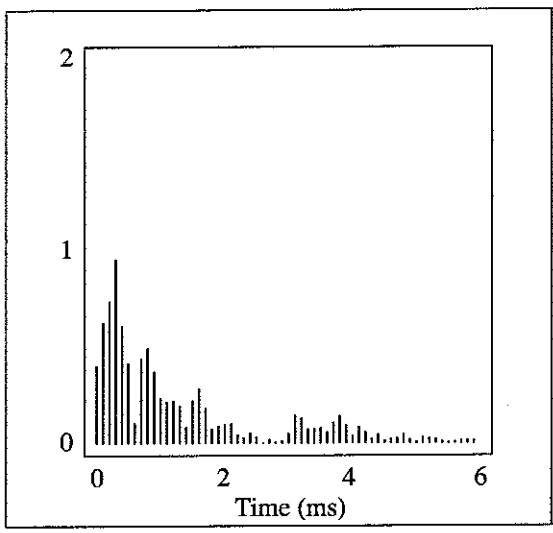

Figure 6.14.7 Sample 7

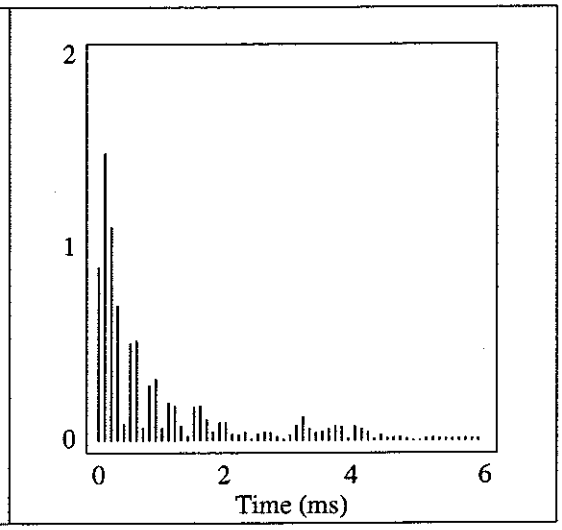

Figure 6.14.8 Sample 8

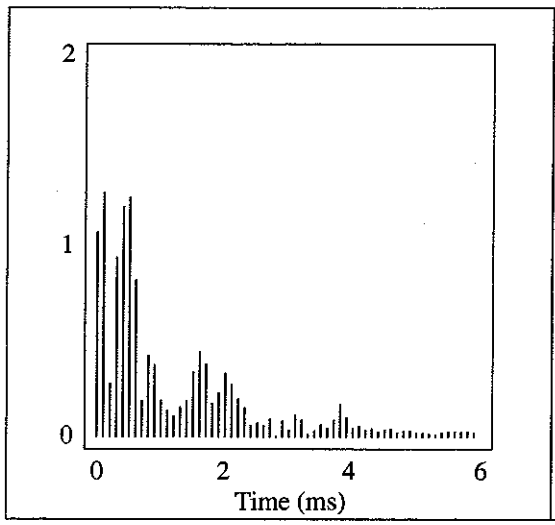

Figure 6.14.9 Sample 9

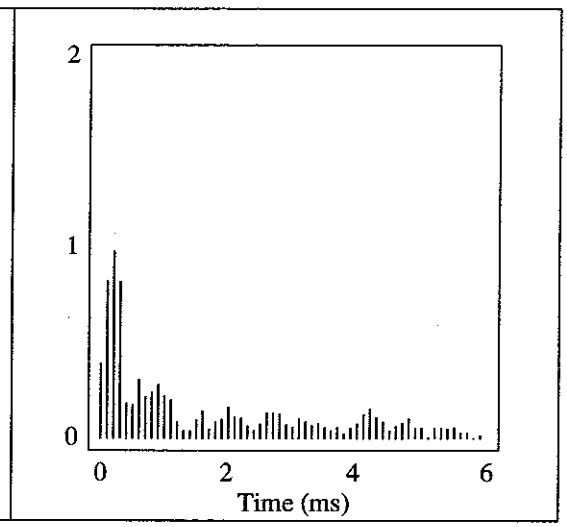

Figure 6.14.10 Sample 10

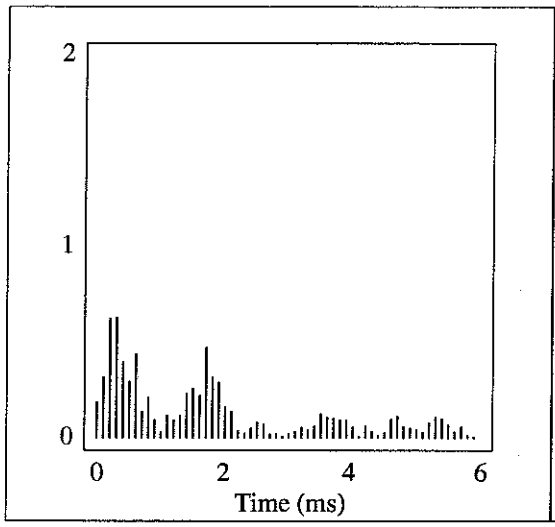

Figure 6.14.11 Sample 11

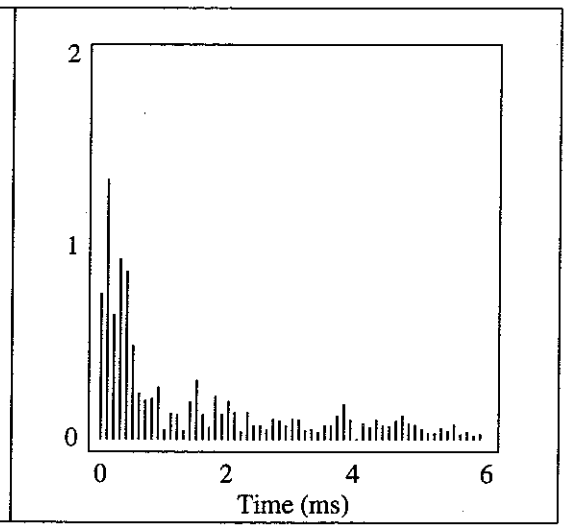

Figure 6.14.12 Sample 12

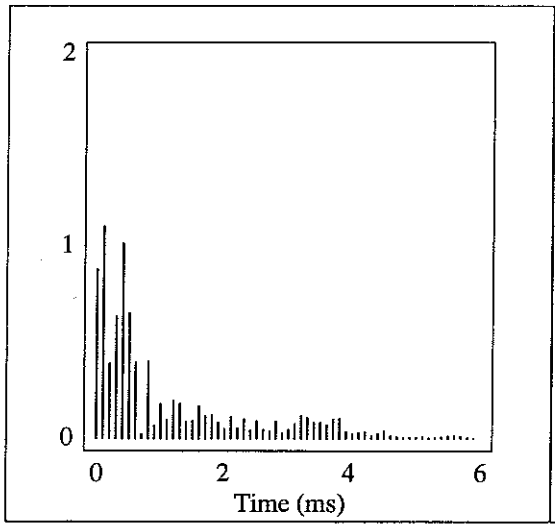

Figure 6.14.13 Sample 13

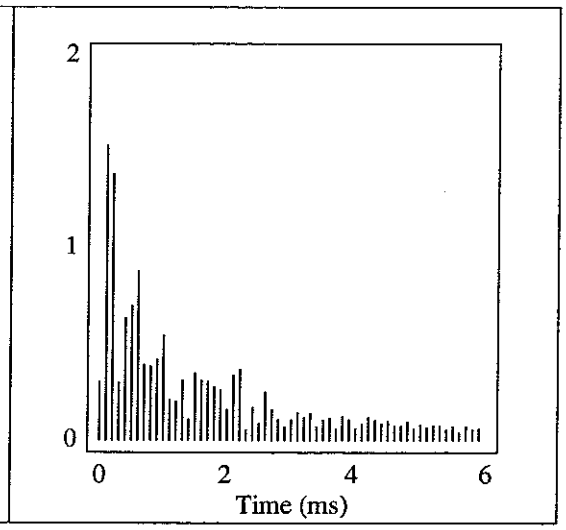

Figure 6.14.14 Sample 14

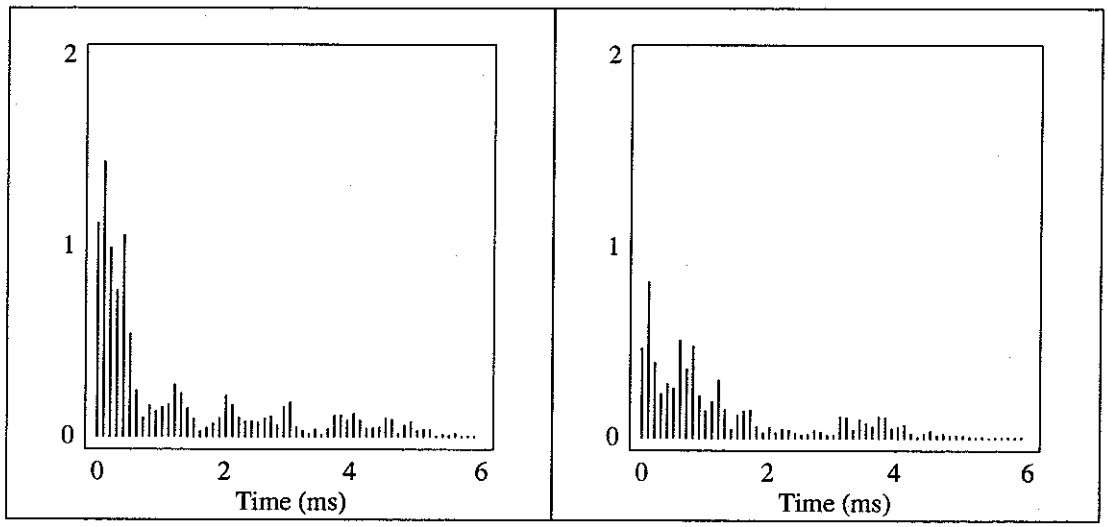

Figure 6.14.15 Sample 15 *Figure 6.14.16 Sample 16*

6.5.6 General Discussion of Results.

In section 6.5.4 it was found that in general, the similarity between the horn loudspeakers in the test and the direct radiating loudspeakers was at least as strong as the similarity between different horns driven by similar, or even the same, driver. The horn samples appear to polarise more or less into two different sounds; some having a strong similarity with the direct radiating reference B, and little or no similarity with the horn reference C, and others having a similarity to reference C, and little similarity with reference B. Figure 6.15 shows the horn samples grouped according to which reference they sound most similar to.

Those samples marked * showed particularly strong similarity to the reference. All of the horn samples were fitted with the same Emilar driver with the exception of sample 11 which was fitted with a similar Emilar driver, and sample 16 which was fitted with a JBL driver. Reference C was fitted with a third Emilar driver.

From figure 6.15, it is clear that horn length plays an important part in deciding which of the two references a particular horn is more similar to; horns with diaphragm to mouth lengths of less than 340mm sound similar to reference B and those with lengths greater than 400mm sound similar to reference C which is also a long horn. The exceptions to this rule are samples 8, 9 & 10:–

Sample 8, the AX2 axisymmetric horn showed overall similarity with reference D, with little similarity to references A, B or C. The main difference between this horn and the other short horns is the high flare-rate, giving the horn a higher cut-off

frequency and also an almost total lack of mouth reflections. Sample 9, the Yamaha sectoral horn showed some similarity with both references B & C, but measurements indicate a very uneven frequency response and the sample was generally considered to sound "strange". This horn differs from the other short horns in having an abrupt change in flare-rate and cross-sectional shape part way along the flare, giving rise to the response aberrations and probably the 'strange' sound. Sample 10, the wooden Fostex sectoral horn also has a change in cross-section and flare-rate, but the flare in the horizontal plane after the change is extremely rapid (included angle 140 degrees), leading to a very wide, almost semicircular mouth. It appears as if the sound of this horn is dictated by the short throat section of the horn, the rest of the flare acting more or less as 'lips' for controlling directivity.

Sample No.	Manufacturer / Type	Flare Material	Flare-rate	Length (mm)	Mouth Size
Horns with similarity to reference B					
Ref. B	Son Audax direct radiator	-	-	-	-
1	Vitavox exponential	aluminium	medium	340	medium
4	AX1 axisymmetric*	glassfibre	low	230	small
5	Reflexion Arts	glassfibre	medium	330	medium
7	Reflexion Arts - no lips	glassfibre	medium	240	medium
10	Fostex sectoral*	wood	high	440	large
11	JBL axisymmetric	aluminium	low	250	small
Horns with similarity to reference C					
Ref. C	Fostex sectoral	aluminium	medium	500	large
12	Altec sectoral*	aluminium	medium	530	large
13	Altec multicellular	aluminium	low/med	600	large
14	Starr gramophone	wood	low	650	medium
15	Vitavox sectoral	aluminium	medium	450	large
16	JBL bi-radial*	composite	medium	400	medium
Others					
8	AX2 axisymmetric	glassfibre	high	230	medium
9	Yamaha sectoral	aluminium	medium	350	medium

Figure 6.15 Horn Loudspeaker Samples Grouped According to Similarity.

The polarisation in sound between the short horns and the long horns may be explained by considering the time interval between a signal and any changes that may be imparted on the signal by the loudspeaker. Reflections from the mouths of the short horns are radiated between about 1ms to 2ms after the signal has been

radiated, and those from the long horns about 2ms to 4ms after the signal. It appears from the transfer function for reference B (fig. 6.13B) and from the spectral similarity results (fig. 6.12), that the various resonances and reflections in the direct radiating cone, give rise to irregularities in the transfer function that are of a similar nature to those due to reflections in the short horns. The mouth reflections in the long horns are generally less severe than those of the short horns as the mouth is larger; this can be seen from the generally smoother transfer functions for the longer horns. From the various comments made by the subjects both orally during the test, and on the questionnaires, it is clear that the longer horns can be more reliably identified as horns. Only one short horn, sample 11, was ever identified as a horn, but then only by one 'golden eared' professional sound engineer. Two possible reasons for this are: a) because of similar response irregularities, the short horns are mistaken for direct radiating cone loudspeakers, and b) because the reflections from the long horns occur after a longer delay, they are more audible. These hypotheses agree with the observation that of the two horns in the test that produce negligible mouth reflections, samples 8 & 13, neither was ever identified as a horn, and the short horn, sample 8 did not sound like the direct radiating reference B.

Little or no evidence exists from the results of this listening test that horn flare construction material, flare-rate or shape (sectoral, exponential etc) have much effect on the on-axis sound of a horn under anechoic or free-field listening conditions. It is expected however that under reflective or reverberant listening conditions the directivity properties of a horn, controlled by the shape and size of flare, will affect the perceived sound quality.

6.6 SUMMARY & CONCLUSIONS

A blind listening test, based on perceived sonic similarity, has been set up under anechoic conditions to investigate similarities, or otherwise, in perceived sound quality between a selection of horn and direct radiating loudspeakers. The test was designed to answer three questions: Do horns sound different from each other? Do horns sound different from direct radiators? And is the difference between horns and direct radiators greater than the difference between horns?

Sixteen sample loudspeakers, comprising thirteen horns and three direct radiators were compared with four reference loudspeakers. The reference loudspeakers were a

direct radiating electrostatic, a direct radiating cone, a sectoral horn and the high frequency horn from a two-way dual concentric loudspeaker. Source material consisted of nine test signals comprising a mix of simple synthesized and natural sounds which were digitally recorded and band limited to between one and six kiloHertz. A switching box, consisting of a six-way line-level switch with individual gain controls ganged to a six-way loudspeaker switch, provided sensitivity matching and permitted rapid switching between the loudspeakers. Twenty subjects completed questionnaires in which they were asked to decide which of the four reference loudspeakers sounded most similar to each of the sample loudspeakers, for each of the signals.

The test results were studied in a 'raw', 'number of ticks' manner and initial conclusions drawn. Statistical analysis was performed on the test results leading to a set of 'similarity confidence indices' representing the confidence in the result that the two loudspeakers sound similar in the reproduction of that signal.

Measurements were taken of the transfer function between the voltage applied to the band-pass filter and the sound pressure at the subject head position for each of the loudspeakers and recordings were made of the reproduction of each signal through each loudspeaker. This measured data was used to compare the spectra of the reproduced signals using a mean-squared-error technique, for each of the loudspeaker comparisons leading to a set of numbers representing 'waveform spectral similarity'. The transfer functions were analysed using cepstral analysis techniques in an attempt to find physical reasons for the similarity or otherwise in the sound of one loudspeaker with another.

Two experimental controls were included in the test. One of the sample loudspeakers was nominally identical to one of the references, providing a 'similar' control, and a 'non-similar' control was provided by a loudspeaker that was designed to operate outside the frequency range of the test. Both controls appeared to work well with the similar control achieving 100% similarity confidence for all signals and the non-similar control, similarity with none of the references for eight of the nine signals. The similarity or otherwise between the other sample and reference loudspeakers were judged on a scale set by these two results.

A comparison between the similarity confidence index and waveform spectral similarity results yielded 70 - 80% agreement when comparing those references with

similarity confidence indices of over 90% with those that showed the highest spectral similarity, for each sample loudspeaker, for each signal.

Answers to the three questions above were concluded from the test results and can be summarised as follows:

♦ Horns do sound different from each other, even when fitted with the same driver.

♦ Some similarity exists between the sound of the horns and the sound of the direct radiators.

♦ No evidence exists that horns in general sound more different from direct radiators than they do from each other.

The test results and measurements for each of the sample loudspeakers are discussed in turn and a set of conclusions are reached based on these discussions. These conclusions can be summarised as follows:

♦ Little similarity was evident between the sample loudspeakers and the electrostatic reference A.

♦ The horn samples appear to polarise into two different sounds; strong similarity with reference B, a direct radiating cone, or with reference C, a sectoral horn.

♦ The polarisation appears to be dependent upon the length of the horn, with horns of less than 340mm between diaphragm and horn mouth sounding similar to the direct radiator reference, and those with more than 400mm length sounding similar to the horn reference (a 'long' horn).

♦ The various reflections and resonances in the cone of the direct radiator give rise to irregularities in the transfer function that are similar to those due to the mouth reflections in the short horns.

♦ The longer horns were more reliably identified as horns by the test subjects than the short horns.

♦ The two horns having minimal mouth reflections, one long and one short, were not identified as horns and did not sound similar to the direct radiating reference.

Chapter 7
DISCUSSION

7.1 INTRODUCTION

In order to reliably reproduce music and speech at the high levels required in a modern recording studio, a monitor loudspeaker system requires horn loaded drive-units to be used for the upper mid- and high frequency ranges. Although much has been written about the use of horns for public address applications, little literature is available on the perceived sound quality of horns and their use in systems where high quality sound reproduction is important. When horns that have been designed primarily for public address are used in studio monitors, listeners have reported a characteristic horn 'sound' which allows a horn to be identified by sound alone. The objective of this research project is to find the physical cause of this characteristic sound, initially by comparing objective measurements of the behaviour of horns with models of idealised horn behaviour, and finally via a subjective listening test. No attempt is made to model the horn using sophisticated numerical techniques; the use of simpler models being preferred as these generally give more insight into the physics of horn behaviour.

7.2 MODELS OF IDEALISED HORN BEHAVIOUR

Traditional horn design and analysis is centered around the one-parameter horn equation ("Webster's Horn Equation", equation (2.1)). This equation describes the sound field within a tapered waveguide as a function of axial position, and thus takes no account of the cross-sectional shape of the waveguide. The horn equation can only be solved analytically for horns having area profiles of a few special shapes; thus the equation cannot be directly applied to horns of arbitrary shape. Most of the horns made available for testing do not have area profiles for which the horn equation has analytical solutions, so numerical methods are required. The development of a semi-numerical model is described in chapter 2. This model splits a horn of arbitrary shape into small exponential elements, within which the horn equation can be solved analytically. The model is used to find out to what extent horns with a variety of cross-sectional shapes and area profiles can be modelled in a one-parameter manner.

An attempt to explain the physics of one-parameter horn behaviour using the concept of a 'stretching pressure', resulted in the extension of the model to take into account the cross-sectional shape of a horn. A set of empirical rules are derived from

measurements of the shape of the wavefronts at the mouth of a variety of horns and these are then used to estimate the area of the wavefronts in any horn from the shape of the horn walls. These 'assumed' wavefront areas are used in the extended one-parameter model in place of the cross-sectional areas. The measurements of the distribution of pressure across the mouths of five horns (figures 4.1.2 to 4.1.4) show that these wavefront shape approximations are valid. In chapter 3, the measured throat impedances of a selection of horns are compared with those predicted using the extended one-parameter model. The agreement is good, showing that this aspect of the behaviour of a horn can be modelled using the one-parameter horn equation, provided the areas of the wavefronts within the horn are taken into account. The most significant feature of both the measured and theoretical results is the effect that reflections from discontinuities, either at the mouth or within the flare, can have on the throat impedance; these reflections have a 'comb-filtering' effect on the power-frequency response of a horn / driver combination, the severity of which is dependent upon the damping properties of the driver.

Agreement between the theoretical and measured transfer impedances and axial pressure distributions is not good for some of the horns however, indicating that the field within these horns cannot be described by a one-parameter model. Several reasons for this non-one-parameter behaviour are put forward in chapter 4. One of the horns has stiffening pillars within the flare which upset the free propagation of the wavefront from the throat to the mouth. The pillars are seen to have a gross effect on the far-field radiation of the horn, which exhibits very poor horizontal directivity control. Another horn suffers resonant wall vibration at the horn mouth which upsets the distribution of pressure at the mouth but only affects the far-field radiation at angles far off-axis. A third horn has truncated mouth 'lips' which set up interference patterns between the radiating wave and the reflection from the mouth discontinuity. These interference patterns or 'modes' do not affect the horizontal directivity of the horn but they do give the horn poor vertical directivity control.

Although, in some circumstances, directivity control may not be important, if the horn is used with a driver having a smooth power frequency response, the on-axis frequency response of the combination is dependent upon the directivity characteristics in all planes; for example, a narrowing of the vertical directivity pattern at a certain frequency will result in a peak in the on-axis frequency response at that frequency. This argument can be extended to include the overall frequency response of the combination. Many compression drivers have a power frequency

response that reduces with increasing frequency above the diaphragm / suspension resonant frequency, and if such a driver is coupled to a 'constant directivity' horn, the resultant on-axis frequency response of the combination will fall off at the same rate and electrical equalisation is required. To offset this, some horns are designed to have a directivity pattern that steadily narrows as frequency is increased which gives the combination a 'flat' on-axis frequency response. On-axis frequency responses of combinations of horns and drivers in chapter 4 show that it is necessary to match the power frequency response of the driver with the directivity pattern of the horn if electrical equalisation, which may result in headroom / overload problems, is to be avoided. It is also important to match the flare-rate at the throat of the horn to that of the exit from the driver, as a discontinuity here can affect the power frequency response of the combination.

The one-parameter model is further extended in chapter 5 with the inclusion of the non-linear effects of producing finite-amplitude sound waves. In order to take into account the reflections from any flare discontinuities, this model can only work in a 'time-backwards' manner; thus the 'input' waveform required at the throat of a horn is calculated in order to give a specified 'output' at the mouth of the horn. Comparison between the model output and measured data shows that the finite-amplitude model is a valid one. The model predicts a severe increase in non-linearity when the frequency of excitation is at the cut-off frequency of the horn. It is not clear whether this phenomenon is real, or whether it is a product of badly conditioned mathematics. If it is a real phenomenon, horns with multiple sections having different flare-rates may suffer high distortion over a wider bandwidth than those having the same flare-rate along the length of the horn. Further experimental investigation is necessary before a satisfactory conclusion can be drawn.

An approximation to a 'time-forwards' solution is possible using iteration around the model in a form of 'negative feedback' loop. This time-forwards solution is only correct if the source at the throat of the horn is either a pure pressure source or a pure velocity source. To maximise electro-acoustic efficiency, loudspeaker horn compression drivers have mechanical impedances that are of the same order as the acoustic impedance seen by the diaphragm, so they are neither velocity or pressure sources. The time-forwards model therefore has limited practical value in the modelling of loudspeaker horns.

Comparisons between the harmonic distortion due to the propagation of finite-amplitude waves predicted by the model and measurements of that generated by two different horn / driver combinations indicates that finite-amplitude propagation distortion within the horn flare is probably the cause of most of the second harmonic distortion generated by the horn systems, and that the third and higher order harmonics are probably generated within the driver. Although the measured levels of distortion generated by the two horn systems are quite high, the maximum levels generated in the test (105dB SPL continuous sinewave at 3m anechoic) are beyond the capability of most direct-radiating loudspeakers, but were well within the capabilities of the horn systems. At more moderate levels the distortion figures are comparable with those generated by a high quality direct-radiating loudspeaker. Clearly, the characteristic horn sound is not due to non-linear distortion.

7.3 SUBJECTIVE TESTING

In order to find out which of the physical horn characteristics investigated affect the perceived sound quality of a horn, and which, if any, are responsible for the characteristic horn sound, a series of listening tests were planned. These tests were to include comparisons between different mid-range loudspeakers to find out which sounded alike, and driving a non-horn loudspeaker with signals that have been convolved with the impulse response of various typical horn characteristics to see which would make it sound like a horn. The convolution test was not attempted due to lack of time; the comparison test was more ambitious than at first planned. The convolution test is suggested here as a worthwhile future project, but the results from the comparison test were fairly conclusive and serve the purposes of this project.

Subjects taking part in the test were asked which of four reference loudspeakers sounded most similar to the loudspeaker sample under test when reproducing each of nine simple sounds. The test was repeated for sixteen loudspeaker samples, which include a mix of direct-radiating and horn loudspeakers. The test was conducted 'blind', in an anechoic chamber, with all of the loudspeakers mounted on identical baffles behind a visually opaque / acoustically transparent screen. Conclusions are drawn from comparisons between the listening test results, the measured on-axis frequency response of the loudspeakers and the physical properties of the horns in the test. The horn samples were seen to polarise towards similarity with one of two of the reference loudspeakers; one a horn and the other a direct-radiating

loudspeaker. Further analysis reveals that, in general, 'long' horns sound like horns and 'short' horns sound like direct radiating loudspeakers. It appears that reflections from the mouth of a horn are responsible for the 'horn sound', and that the response aberrations due to the reflections from the mouth of short horns are similar to those present in direct-radiators. The reflections from the mouth of the longer horns are generally less severe than those from the short horns, but the ear may be more sensitive to these as the time delay between the 'direct' and 'reflected' signals is longer. The effect can be demonstrated simply if one talks through a short tube, and then a longer one. The voice may sound strange with the short tube, but the presence of the tube is more obvious with the longer tube.

7.4 A NEW HORN FOR STUDIO MONITOR LOUDSPEAKERS

Horn type 5 in the measurements, the large axi-symmetric (AX2), was designed to possess as smooth a throat impedance characteristic as possible within reasonable size constraints. The measured throat impedance for this horn (figure 3.5.5b) shows that this was achieved, with very little evidence of reflections from the horn mouth or anywhere else in the flare. This performance is a result of the rapid flare and circular cross-sectional shape giving only a very slight discontinuity between the flare at the mouth and a flat baffle. The penalty for having such a rapid flare is that the cut-off frequency of the horn is much higher than that for most comparably sized horns. Although this high cut-off frequency raises the low-frequency bandwidth limit of the horn, the throat impedance measurements show that the cut-off is very gradual in comparison with the other horns, so in practice the horn can be used down to, or below the cut-off frequency. The transfer impedance and axial pressure distribution measurements for the AX2 horn (figures 3.6.5 and 3.7.5) show close agreement with the one-parameter predictions, indicating that this horn behaves in an essentially one-parameter manner. This conclusion is borne out by the measurements of the pressure distribution across the horn mouth; very little transverse pressure variation is evident over the entire frequency range of the measurements, except for that responsible for the curvature of the wavefronts.

Prior to the measurement of the directivity properties of the horns, the TAD TD2001 compression driver mentioned in chapter 4 was made available. It was decided that this driver would be suitable for the directivity measurements as it is specified as having a flat power response over a wide bandwidth. The directivity characteristics

for the AX2 horn (figure 4.3.5) are very controlled and because of this, and the smooth throat impedance, the on-axis frequency response in combination with the TAD driver (figure 4.7) is very flat and smooth from 1kHz up to beyond 20kHz. Clearly, this horn / driver combination is very suitable for use in studio monitoring systems; it has a very smooth frequency response at all angles on- and off-axis, and the bandwidth is such that a high frequency driver would no longer be necessary.

The AX2 horn in combination with an Emilar EK175 driver was sample 8 in the listening test. The results show that this loudspeaker did not sound very much like either the horn or the direct-radiating reference due to the absence of mouth reflections. A discontinuity between the flare at the exit from the driver and that at the throat of the horn, and the falling power response of the driver, gave this combination an un-even frequency response; the AX2 / TAD combination would have been a useful loudspeaker to include in the test but the TAD driver was not made available until after the test was completed. A comparison between the frequency response of the AX2 / TAD combination on-axis and at 10 degrees off-axis (figures 4.7 and 4.8) shows that a ripple of about ± 2dB in the on-axis response is due to a diffraction problem from the edge of the circular mouth. Further research is required to find the most effective way of reducing this problem; suggestions include a ring of soft material covering the edge and a 'rippled', non-axisymmetric termination to the mouth.

A prototype monitor loudspeaker system, consisting of two fifteen inch diameter direct-radiating drive-units and one AX2 / TAD TD2001 horn combination per cabinet, has been constructed by Philip Newell (see section 1.1) and fitted in a recording studio which, conveniently, was being built at the time of this research project. All listeners to the system, many of whom are 'golden eared' professional sound engineers, were impressed by the quality of sound reproduction, considering this system to be significantly "better" than previous ones.

The objectives of the research project have been achieved. The reason for the wide variety of shapes and sizes of available mid-range horns has been explained, the probable causes of the characteristic 'horn sound' have been pinpointed, and a prototype horn has been designed, built and tested that fulfils the requirement for a high-quality, efficient and robust mid-range loudspeaker that does not sound like a horn.

Chapter 8
CONCLUSIONS

The objective of this research project is to investigate the measurable physical properties of mid-range horn loudspeakers intended for use in studio monitoring systems, and the relationship that these may have to the perceived quality of sound reproduction.

The conclusions drawn from objective measurements on a variety of horns are as follows:-

- A one-parameter model can be used to predict the throat impedance of horns of any arbitrary shape, including those with rapid flare and rectangular cross-section, provided the shape of the wave-fronts within the horn are taken into account.
- The wave-fronts within axi-symmetric horns take the form of 'flattened spherical caps' and can be approximated by an average of the plane cross-section and a spherical cap normal to the horn walls.
- The wave-fronts within rectangular horns take the form of circular arcs normal to the horn walls.
- Horns in which the acoustic field can be described in a one-parameter manner perform better than those having behavioural characteristics which departs from this ideal.
- Obstructions and discontinuities within or at the mouth of a horn flare can upset the free propagation of acoustic waves within the flare and out to the far-field, and are thus deemed undesirable features of a horn for studio monitoring applications.
- Much of the second harmonic distortion generated by horn / driver combinations could be due to non-linear propagation within the flare.
- The levels of distortion generated by a well designed horn loudspeaker are comparable to those characteristic of conventional direct-radiating loudspeakers, and significantly higher distortions are only generated when a horn is producing sound power outputs beyond the capabilities of most non-horn loudspeakers.
- Non-linear propagation within a horn flare is not responsible for a characteristic horn sound.

The conclusions drawn from listening test results are as follows:-

- The horn samples appear to polarise into two different sounds; strong similarity with reference B, a direct radiating cone, or with reference C, a sectoral horn.
- The polarisation appears to be dependent upon the length of the horn, with horns of less than 340mm between diaphragm and horn mouth sounding similar to the direct radiator reference, and those with more than 400mm length sounding similar to the horn reference (a 'long' horn).

- The various reflections and resonances in the cone of the direct radiating loudspeaker give rise to irregularities in the frequency response function that are similar to those due to the mouth reflections in the short horns.
- The longer horns were more reliably identified as horns by the test subjects than the short horns.
- The two horns having minimal mouth reflections, one long and one short, were not identified as horns and did not sound similar to the direct radiating reference.

General conclusions:-

- Reflections from the mouth of horns greater than about 350mm long are responsible for the characteristic horn sound, and that horns having lengths shorter than this tend not to sound like horns.
- A loudspeaker with the high electro-acoustic efficiency of a horn / compression driver combination without a characteristic 'horn sound' can, and has been designed.

Chapter 9
REFERENCES AND BIBLIOGRAPHY

9.1 REFERENCES

[1] P. R. Newell, "Studio Monitoring Design", Studio Sound, December 1986.

[2] E. Eisner, "Complete Solutions of the 'Webster' Horn Equation", J. Acoust. Soc. Am., **41**(4) part 2, 1967.

[3] D. Bernoulli, "Physical, Mechanical and Analytical Researches on Sound and on the Tones of Differently Constructed Organ Pipes", Mém. Acad. Sci. (Paris) 1762, p431.

[4] J. L. Lagrange, "New Researches on the Nature and the Propagation of Sound", Misc. Taurinensia (Mélanges Phil. Math., Soc. Roy. Turin) 2, No.2, p11, 1760/1.

[5] J. W. Strutt; Lord Rayleigh, "On the Propagation of Sound in Narrow Tubes of Variable Section", Phil. Mag. Ser. 6, 31, p89, 1916.

[6] A. G. Webster, "Acoustical Impedance and the Theory of Horns and of the Phonograph", Proc. Natl. Acad. Sci. (US) 5, p 275, 1919.

[7] W. M. Hall, "Comments on the Theory of Horns", J. Acoust. Soc. Am., **3**, p552, 1932.

[8] V. Salmon, "Generalized Plane Wave Horn Theory", J. Acoust. Soc. Am., **17**(3), p199, 1946.

[9] V. Salmon, "A New Family of Horns", J. Acoust. Soc. Am., **17**(3), p212, 1946.

[10] D. B. Keele, Jr., "Optimum Horn Mouth Size", presented at the 46th Convention of the Audio Engineering Society (preprint no. 933), 1973.

[11] E. Geddes and D. Clark, "Computer Simulation of Horn-Loaded Compression Drivers", J. Audio Eng. Soc., **35**(7/8), p 556, 1987.

[12] E. R. Geddes, "Acoustic Waveguide Theory", J. Audio Eng. Soc., **37**(7/8), p554, 1989.

[13] A. F. Stevenson, "General Theory of Electromagnetic Horns", J. App. Phys., **22**(12), p1447, 1951.

[14] A. F. Stevenson, "Exact and Approximate Equations for Wave Propagation in Acoustic Horns", J. App. Phys., **22**(12), p1461, 1951.

[15] A. H. Benade and E. V. Jansson, "On Plane and Spherical Waves in Horns with Nonuniform Flare 1. Theory of Radiation, Resonance Frequencies, and Mode Conversion", Acustica, **31**, p79, 1974.

[16] R. J. Alfredson, "The Propagation of Sound in a Circular Duct of Continuously Varying Cross-Sectional Area", J. Sound Vib., **23**(4), p433, 1972.

[17] S. Morita, N. Kyouno and S. Sakai, "Acoustic Radiation of a Loudspeaker by the Finite Element Method - A Consideration of the Acoustic Characteristics of Horns", J. Audio Eng. Soc., **28**(7/8), p484, 1980.

[18] N. Kyouno, S. Sakai, S. Morita, T. Yamabuchi and Y. Kagawa, "Acoustic Radiation of a Horn Loudspeaker by the Finite Element Method - Acoustic Characteristics of a Horn Loudspeaker with an Elastic Diaphragm", J. Audio Eng. Soc., **30**(12), p896, 1982.

[19] T. F. Johansen, "An Integral Equation Method to Solve the Nonhomogeneous Nuemann Problem for Thin Objects", presented at the Nordic Acoustical Meeting, Tampere, 1988.

[20] U. R. Kristiansen and T. F. Johansen, "The Horn Loudspeaker as a Screen Diffraction Problem", J. Sound Vib., **133**(3), p449, 1989.

[21] T. F. Johansen, "Implementation and Use of a Numerical Technique for Studies of Directional Properties of the Sound Radiation from Horn Loudspeakers", PhD thesis, University of Trondheim, Norway, 1991.

[22] K. R. Holland, F. J. Fahy, C. L. Morfey and P. R. Newell, "The Prediction and Measurement of the Throat Impedance of Horns", Proceedings of the Institute of Acoustics, **11**(7), Reproduced Sound 5, 1989.

[23] K. R. Holland, F. J. Fahy and C. L. Morfey, "Prediction and Measurement of the One-Parameter Behaviour of Horns", J. Audio Eng. Soc., **39**(5), p315, 1991.

[24] P. M. Morse, "Vibration and Sound", McGraw-Hill, New York, 1948.

[25] H. F. Olson, "Elements of Acoustical Engineering", Chapman and Hall, London, 1940.

[26] D. B. Keele, Jr., "What's So Sacred about Exponential Horns?", presented at the 51st Convention of the Audio Engineering Society (preprint no. 1038), 1975.

[27] M. Long, "Constant Directivity", Sound and Video Contractor, December 1983.

[28] P. G. A. H. Voigt, British Patents No.s 278,098 (1927), 351,209 (1930), 404,037 (1934), 435,042 (1935).

[29] J. Merhaut, "Impulse Measurement of Acoustic Impedance", J. Audio Eng. Soc., **37**(5), p343, 1989.

[30] F. J. Fahy, "Rapid Method for the Measurement of Sample Acoustic Impedance in a Standing Wave Tube", Letter to Editor, J. Sound Vib., **97**(1) p168, 1984.

[31] H. Levine and J. Schwinger, "On the Radiation of Sound from an Unflanged Circular Pipe", Phys. Rev. **73**, p383, 1948.

[32] K. R. Holland, F. J. Fahy and P. R. Newell, "Axi-Symmetric Horns for Studio Monitor Systems", Proceedings of the Institute of Acoustics, **12**(8), Reproduced Sound 6, 1990.

[33] M. R. Schroeder, "Models of Hearing", Proceedings of the IEEE, **63**(9), 1975.

[34] K. R. Holland and C. L. Morfey, "A Model of Finite Amplitude Sound Propagation in Horns",
Proceedings of the Institute of Acoustics, **12**, Acoustics 90, 1990.

[35] K. R. Holland and C. L. Morfey, "Finite Amplitude Sound Propagation in Waveguides of Variable Area", Presented at the 12th International Symposium on Nonlinear Acoustics, Texas, 1990.

[36] F. G. Pla and G. Reethof, "Effects of Attenuation, Dispersion, and High Sound Pressure Levels on Acoustic Wave Distortion in Horns", presented at the 116th Meeting of the Acoustical Society of America, Honolulu, 1988.

[37] F. E. Toole, "Loudspeaker Measurements and Their Relationships to Listener Preferences: Parts 1 & 2", J. Audio Eng. Soc., **34**, 1986.

[38] A. Gabrielsson, B. Lindstrom and T. Ove, "Loudspeaker Frequency Response and Perceived Sound Quality", J. Acoust. Soc. Am., **90**(2), 1991.

9.2 Bibliography

This section contains a list of publications on the subject of horns encountered during this project that are not specifically referred to in the text and are not included in the bibliography in reference [2].

H. Fletcher et al, "Discussion of Function and Design of Horns for Loudspeakers", 1924, reprint: J. Audio Eng. Soc., **26**(3), p130, 1978.

C. R. Hanna, "Theory of the Horn Type Loudspeaker",
J. Acoust Soc. Am., **2**, p150, 1930.

H. F. Olson and F. Massa, "A Compound Horn Loudspeaker",
J. Acoust Soc. Am., **8**, p48, 1936.

P. W. Klipsch, "A Low Frequency Horn of Small Dimensions",
1941, reprint: J. Audio Eng. Soc., **27**(3), p141.

R. H. Smith, "A Distributed Source Horn", Audio Engineering, January 1951.

B. H. Smith, "An Investigation of the Air Chamber of Horn Type Loudspeakers",
J. Acoust Soc. Am., **25**, p305, 1953.

B. N. Locanthi, "Application of Acoustically Terminated Tube for Measurement of Horn Loudspeaker Driver Characteristics", J. Acoust Soc. Am., **47**, p79, 1970.

B. N. Nagarhar and R. D. Finch, "Sinusoidal Horns",
J. Acoust Soc. Am., **50**, p23, 1971.

E. A. G. Shaw, "Acoustic Horns with Spatially Varying Density or Elasticity,"
J. Acoust Soc. Am., **50**, p830, 1971.

J. R. Gilliom, "Optimising Horn Loudspeaker System Performance",
J. Audio Eng. Soc., **21**(9), p748, 1973.

J. L. Peube and J. Chasseriaux, "Non-Linear Acoustics in Ducts with Varying Cross Section", J. Sound Vib., **27**, p533, 1973.

R. N. Baldock, "Horn Loudspeaker Design", Wireless World, **80**(1468): p497, 1974.

J. K. Hilliard, "Historical Review of Horns used for Audience Type Sound Reproduction", J. Acoust Soc. Am., **59**, p1, 1976.

C. A. Henricksen, "Ultimate Performance of Wide Range, High Frequency Compression Drivers", J. Audio Eng. Soc., **24**(8), p639, 1976.

E. C. Wente and A. L. Thuras, "A High Frequency Receiver for Horn Type Loudspeakers", J. Audio Eng. Soc., **26**(3), p139, 1978.

C. A. Henricksen and M. S. Ureda, "The Manta-Ray Horns", J. Audio Eng. Soc., **26**(9), p629, 1978.

M. Leach Jr. "On the Specification of Moving Coil Drivers for Low Frequency Horn Loaded Loudspeakers", J. Audio Eng. Soc., **27**(12), p950, 1979.

T. Zamorski and R. Wyrzkowski, "Approximate Methods for the Solution of the Equation of Acoustic Wave Propagation in Horns", Archives of Acoustics, **6**, p237, 1981.

L. M. B. C. Campos, "Some General Properties of the Exact Acoustic Field in Horns and Baffles", J. Sound Vib., **95**, p177, 1984.

J. Kergomard, "General Equivalent Electrical Circuits for Acoustic Horns", J. Audio Eng. Soc., **36**(12), p948, 1988.

T. Shindo et al, "Calculation of Sound Radiation from an Unbaffled, Rectangular Cross-Section Horn Loudspeaker using Combined Analytical and Boundary Element Methods", J. Audio Eng. Soc., **38**(5), 1990.

APPENDICES

APPENDIX 1

Derivation of Webster's Horn Equation:

$$\frac{1}{c_o^2}\frac{\partial^2 p}{\partial t^2} - \frac{\partial^2 p}{\partial x^2} - \left\{\frac{1}{S}\frac{dS}{dx}\right\}\frac{\partial p}{\partial x} = 0$$

and its Solution for an Exponential Area Profile

Consider a thin element of a flaring horn of thickness δx and cross-sectional area S. The volume of the element $V_1 = S\delta x$. (A.1.1)

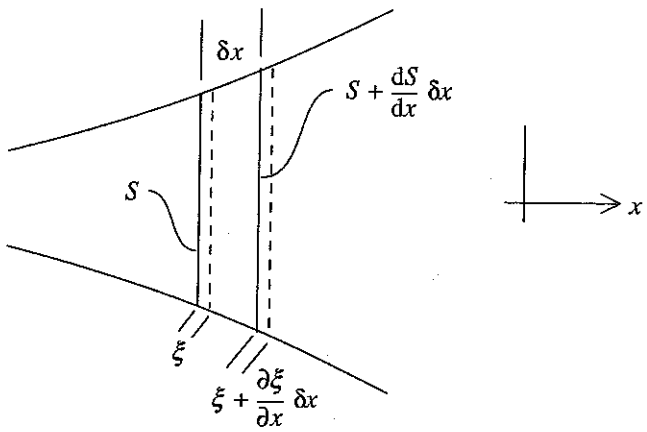

If the element is displaced along the horn axis by a small amount ξ, the volume of the element

$$V_2 = S\delta x + \left(S + \frac{dS}{dx}\delta x\right)\left(\xi + \frac{\partial \xi}{\partial x}\delta x\right) - S\xi$$

$$= S\delta x + S\xi + S\frac{\partial \xi}{\partial x}\delta x + \xi\frac{dS}{dx}\delta x + \frac{dS}{dx}\frac{\partial \xi}{\partial x}\delta x^2 - S\xi \quad ,$$

and ignoring higher powers of δx:

$$V_2 = S\delta x + \left(S\frac{\partial \xi}{\partial x} + \xi\frac{dS}{dx}\right)\delta x \quad ,$$

thus:

$$V_2 = S\delta x + \frac{\partial (S\xi)}{\partial x}\delta x \quad . \qquad \text{(A.1.2)}$$

From continuity considerations, the acoustic pressure

$$p = -\rho_o c_o^2 \left(\frac{V_2 - V_1}{V_1}\right) \quad . \qquad \text{(A.1.3)}$$

Substitution of equations (A1.1) and (A1.2) into (A1.3) gives

$$p = -\rho_o c_o^2 \frac{1}{S\delta x}\left(S\delta x + \frac{\partial(S\xi)}{\partial x}\delta x - S\delta x\right) = -\frac{\rho_o c_o^2}{S}\frac{\partial(S\xi)}{\partial x} \quad .$$

Differentiating twice with respect to time,

$$\frac{\partial^2 p}{\partial t^2} = -\frac{\rho_o c_o^2}{S}\frac{\partial}{\partial x}\left(S\frac{\partial^2 \xi}{\partial t^2}\right) \quad . \tag{A.1.4}$$

From momentum considerations,

$$\frac{\partial u}{\partial t} = -\frac{1}{\rho_o}\frac{\partial p}{\partial x} \quad ,$$

therefore,

$$\frac{\partial^2 \xi}{\partial t^2} = -\frac{1}{\rho_o}\frac{\partial p}{\partial x} \quad . \tag{A.1.5}$$

Substituting equation (A.1.5) into (A.1.4) gives

$$\frac{\partial^2 p}{\partial t^2} = -\frac{\rho_o c_o^2}{S}\frac{\partial}{\partial x}\left(-\frac{S}{\rho_o}\frac{\partial p}{\partial x}\right) \quad ,$$

thus:

$$\frac{1}{c_o^2}\frac{\partial^2 p}{\partial t^2} - \frac{\partial^2 p}{\partial x^2} - \left\{\frac{1}{S}\frac{dS}{dx}\right\}\frac{\partial p}{\partial x} = 0 \quad . \tag{A.1.6}$$

This equation, known as 'Webster's Horn Equation', describes the sound field within a waveguide which has a cross-sectional area that is a function of distance along the axis ($S = S(x)$).

For an exponential horn, the cross-sectional area is defined by

$$S(x) = S(0)e^{mx} \quad ,$$

the multiplying factor in the right-most term of equation (A.1.6) then becomes

$$\frac{1}{S(x)}\frac{dS(x)}{dx} = m \quad ,$$

where m is independent of axial position and is known as the flare-rate of the horn. Substituting in equation (A.1.6) gives

$$\frac{1}{c_o^2}\frac{\partial^2 p}{\partial t^2} - \frac{\partial^2 p}{\partial x^2} - m\frac{\partial p}{\partial x} = 0 \quad ,$$

and assuming harmonic time dependence,

$$-k^2 p - \frac{\partial^2 p}{\partial x^2} - m\frac{\partial p}{\partial x} = 0 \quad , \tag{A.1.7}$$

The pressure field within the horn takes the form

$$\hat{p} = \hat{A}e^{\hat{\gamma}x} \quad , \tag{A.1.8}$$

where $\hat{A}$ is the amplitude of the pressure wave at $x = 0$, and $\hat{\gamma}$ is a complex propagation coefficient. Substitution of equation (A.1.8) into (A.1.7) yields

$$- k^2\hat{A}e^{\hat{\gamma}x} - \hat{\gamma}^2\hat{A}e^{\hat{\gamma}x} - \hat{\gamma}m\hat{A}e^{\hat{\gamma}x} = 0 \quad ,$$

thus:

$$\hat{\gamma}^2 + \hat{\gamma}m + k^2 = 0 \quad ,$$

and

$$\hat{\gamma} = \frac{-m \pm \sqrt{m^2 - 4k^2}}{2} = a \mp b \quad .$$

The two solutions for $\hat{\gamma}$ represent forward and backward travelling waves which, under most conditions will both be present. A general solution for the pressure field within an exponential horn is thus:

$$\hat{p} = \hat{A}e^{\hat{\gamma}^+} + \hat{B}e^{\hat{\gamma}^-} \quad ,$$

where $\hat{A}$ and $\hat{B}$ represent the amplitudes of the forward and backward travelling waves respectively at $x = 0$. When $k > m/2$,

$$\hat{\gamma}^+ = a + ib \quad \text{and} \quad \hat{\gamma}^- = a - ib \quad , \tag{A.1.9}$$

and when $k < m/2$,

$$\hat{\gamma}^+ = a + b \quad \text{and} \quad \hat{\gamma}^- = a - b \quad , \tag{A.1.10}$$

the choice of sign for b being made such that the amplitudes of the waves tend to zero as x tends to infinity; the real part of the propagation coefficient thus represents an attenuation with increasing area necessary for the conservation of energy, and the imaginary part represents a phase shift with distance. The phase speed,

$$c_{ph} = \frac{\omega}{b} = \frac{kc_o}{b} \quad ,$$

thus when $k > m/2$,

$$\frac{c_{ph}}{c_o} = \frac{k}{b} = \frac{1}{\sqrt{1 - m^2/4k^2}} \quad ,$$

which takes the form shown in figure A.1.1. This figure shows that waves within an exponential horn are dispersive. The frequency at which $k = m/2$ is known as the 'cut-off' frequency of the horn. Below this frequency, only a rapidly decaying, non-propagating field is possible, and at high frequencies, the phase speed approaches that of c_o.

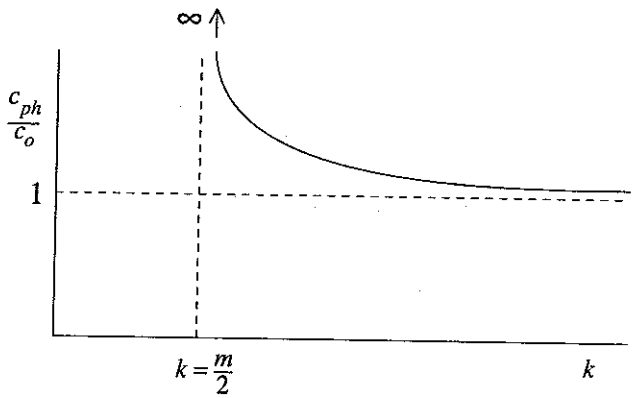

Figure A.1.1 Normalised Phase Speed of Waves in an Exponential Horn.

APPENDIX 2

Derivation of the Reflection Coefficient Form of the Horn Wave Equation:

$$\frac{d\hat{R}_p(x)}{dx} = 2ik\hat{R}_p(x) + \frac{1}{2}\left(1 - \hat{R}_p(x)^2\right)\frac{d}{dx}\ln\left(\frac{S}{\rho_o c_o}\right)$$

Starting with the one-dimensional momentum equation for simple harmonic time dependence:

$$i\omega\hat{q} = \frac{-S}{\rho}\frac{\partial\hat{p}}{\partial x} \quad , \tag{A.2.1}$$

and the definition of specific acoustic impedance:

$$\hat{Z} = \frac{\hat{p}S}{\rho_o c_o \hat{q}} \quad , \tag{A.2.2}$$

from equations (A.2.1) and (A.2.2),

$$\frac{1}{\hat{p}}\frac{\partial\hat{p}}{\partial x} = \frac{-ik}{\hat{Z}} \quad , \tag{A.2.3}$$

where k is the acoustic wave number (ω/c_o). From the one-dimensional continuity equation for simple harmonic time dependence:

$$\frac{-i\omega\hat{p}S}{\rho_o c_o^2} = \frac{\partial\hat{q}}{\partial x} \quad , \tag{A.2.4}$$

and from equation (A.2.2),

$$\frac{\partial\hat{q}}{\partial x} = \frac{\partial\hat{p}}{\partial x}\left(\frac{S}{\rho_o c_o\hat{Z}}\right) + \hat{p}\,\frac{\partial}{\partial x}\left(\frac{S}{\rho_o c_o\hat{Z}}\right) \quad ,$$

substitution yields

$$\frac{\partial\hat{p}}{\partial x}\left(\frac{S}{\rho_o c_o\hat{Z}}\right) + \frac{\hat{p}}{\hat{Z}^2}\left\{\hat{Z}\frac{d}{dx}\left(\frac{S}{\rho_o c_o}\right) - \left(\frac{S}{\rho_o c_o}\right)\frac{d\hat{Z}}{dx}\right\} = \frac{-i\omega\hat{p}S}{\rho_o c_o^2} \quad ,$$

which reduces to

$$-ik\hat{Z}^2 = \hat{Z}\left(\frac{1}{\hat{p}}\frac{\partial\hat{p}}{\partial x}\right) + \hat{Z}\left\{\frac{d}{dx}\ln\left(\frac{S}{\rho_o c_o}\right)\right\} - \frac{d\hat{Z}}{dx} \quad . \tag{A.2.5}$$

Substitution of equation (A.2.3) in (A.2.5) yields

$$-ik\hat{Z}^2 = -ik + \hat{Z}\left\{\frac{d}{dx}\ln\left(\frac{S}{\rho_o c_o}\right)\right\} - \frac{d\hat{Z}}{dx} \quad ,$$

therefore

$$\frac{d\hat{Z}}{dx} = ik\left(\hat{Z}^2 - 1\right) + \hat{Z}\left\{\frac{d}{dx}\ln\left(\frac{S}{\rho_o c_o}\right)\right\} \quad . \tag{A.2.6}$$

Now,

$$\hat{Z} = \frac{1 + \hat{R}_p}{1 - \hat{R}_p} \quad \text{and} \quad \frac{d\hat{Z}}{dx} = \frac{2}{\left(1 - \hat{R}_p\right)^2} \frac{d\hat{R}_p}{dx} \quad ,$$

where $\hat{R}_p$ is the compex pressure reflection coefficient (= $\hat{R}_p(x)$). Substitution in equation (A.2.6) yields

$$\boxed{\frac{d\hat{R}_p(x)}{dx} = 2ik\hat{R}_p(x) + \frac{1}{2}\left(1 - \hat{R}_p(x)^2\right) \frac{d}{dx} \ln\left(\frac{S}{\rho_o c_o}\right)} \quad .$$

APPENDIX 3

Details of the Measured Horns

Horn type 1: Small axi-symmetric (AX1).

This horn is of glassfibre construction and is axi-symmetric. It has a throat diameter of 25.4mm and an exponential area profile with a cut-off frequency of about 350Hz. The flare is 180mm long and the mouth is 80mm in diameter. The truncation of the flare at the small mouth results in a gross discontinuity which was designed, using the one-parameter model (chapter 2), to allow mouth reflections to be studied.

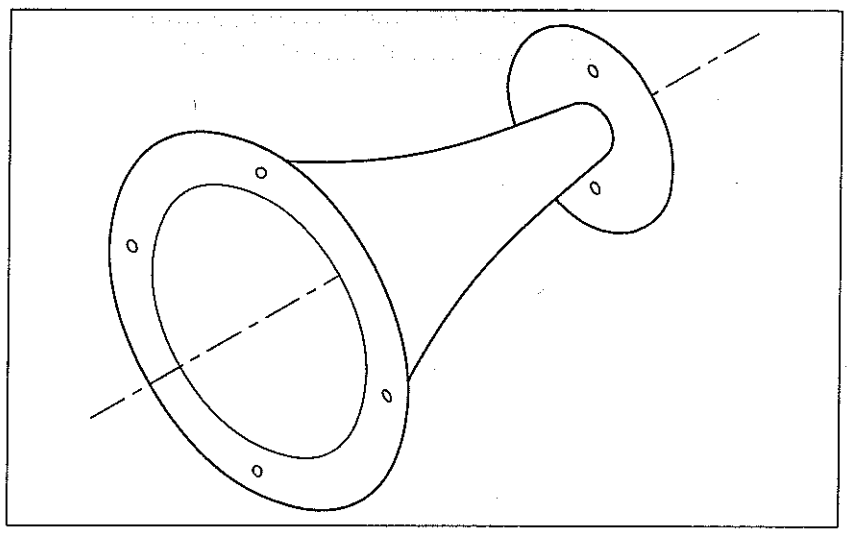

Figure A.3.1 Horn Type 1

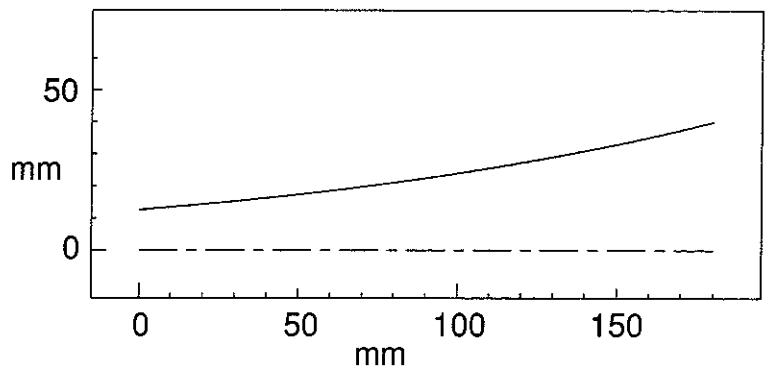

Figure A.3.2 Wall Profile for Horn Type 1

Horn type 2: Reflexion Arts Rectangular.

This horn is constructed of mineral-loaded glassfibre with bonded stiffeners running from the throat to the baffle flange. It has a circular throat of 25.4mm diameter and a flare that smoothly opens out to a rectangular mouth which is 570mm wide and 60mm high at the baffle flange. The mouth has curved 'lips' which are shorter than circular arcs normal to the horn walls with a maximum mouth height of 80mm at the centre, giving the horn an overall length of 280mm. The flare in the horizontal plane is very rapid and that in the vertical plane is straight-sided. This horn has been used in a successful range of studio monitoring systems.

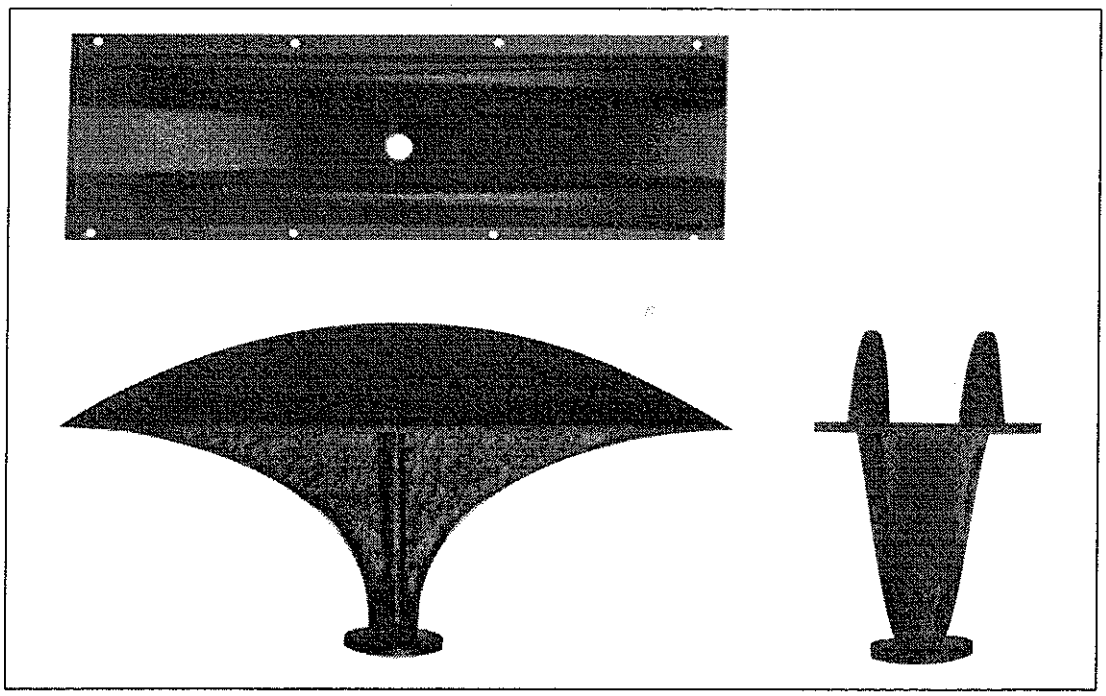

Figure A.3.3 Horn Type 2

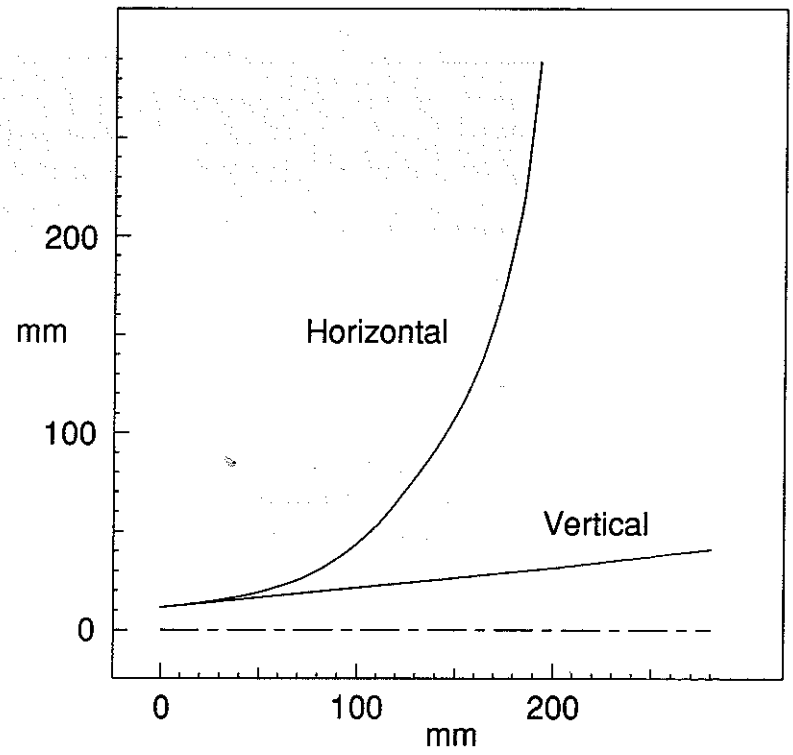

Figure A.3.4 Wall Profile for Horn Type 2

Horn Type 3: Vitavox Rectangular.

This horn is of cast aluminium construction. It has a circular throat of 25.4mm diameter and, apart from a rapid expansion for about 1mm at the throat, a flare that smoothly opens out to a rectangular mouth which is 390mm wide and 150mm high at the edge of circular arc 'lips'. The 'lips' are slightly shallower than circular arcs normal to the horn walls. Two straight, vertical 'waveguide' slats are extend from the mouth of the horn to approximately 100mm down the flare, dividing the mouth into three sections. The horizontal and vertical flares are both roughly exponential in shape and the horn has an overall length of 290mm.

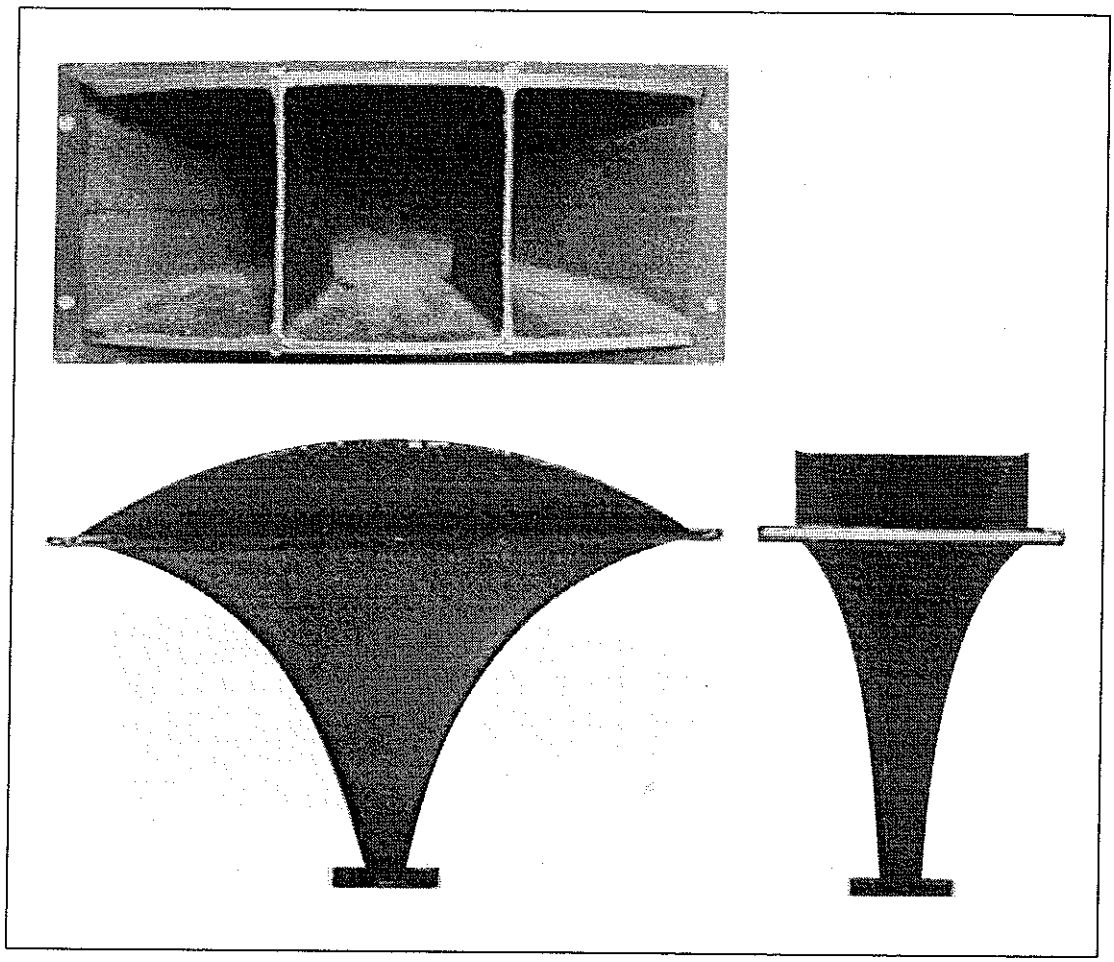

Figure A.3.5 Horn Type 3

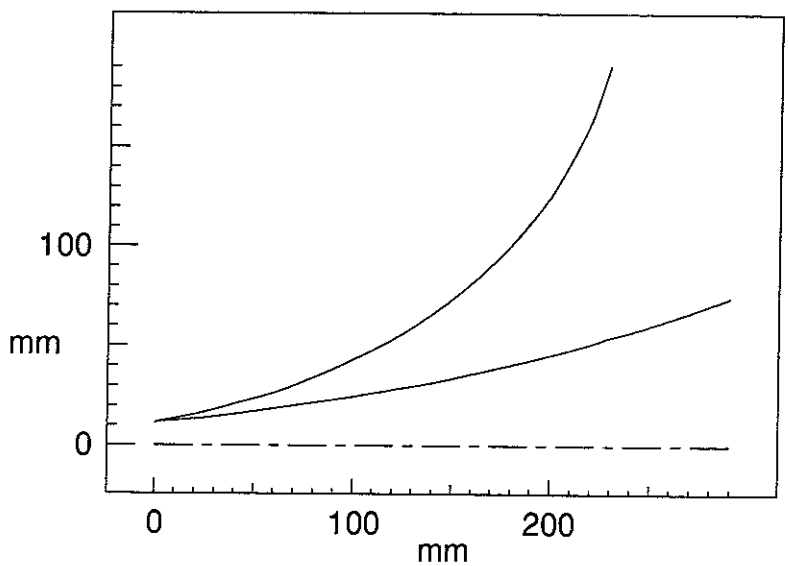

Figure A.3.6 Wall Profile for Horn Type 3

Horn Type 4: Fostex Sectoral (H351).

The horn is of cast aluminium construction with bracing from a throat adaptor flange to the baffle flange, and also in the centre of the mouth 'lips'. The adaptor has a circular throat of 25.4mm diameter and a straight-sided flare in both planes. The interface between the adaptor and the horn flare has a square cross-section, and the horn flare opens out rapidly to a straight-sided horizontal flare and contracts before flaring in the vertical plane. Three vertical pillars of approximately 10mm diameter are present near the adaptor flange to further brace the top and bottom walls. The mouth has a width of 490mm and a height of 150mm at the edge of 'lips' that are circular arcs normal to the horn walls, giving the horn and adaptor an overall length of 450mm.

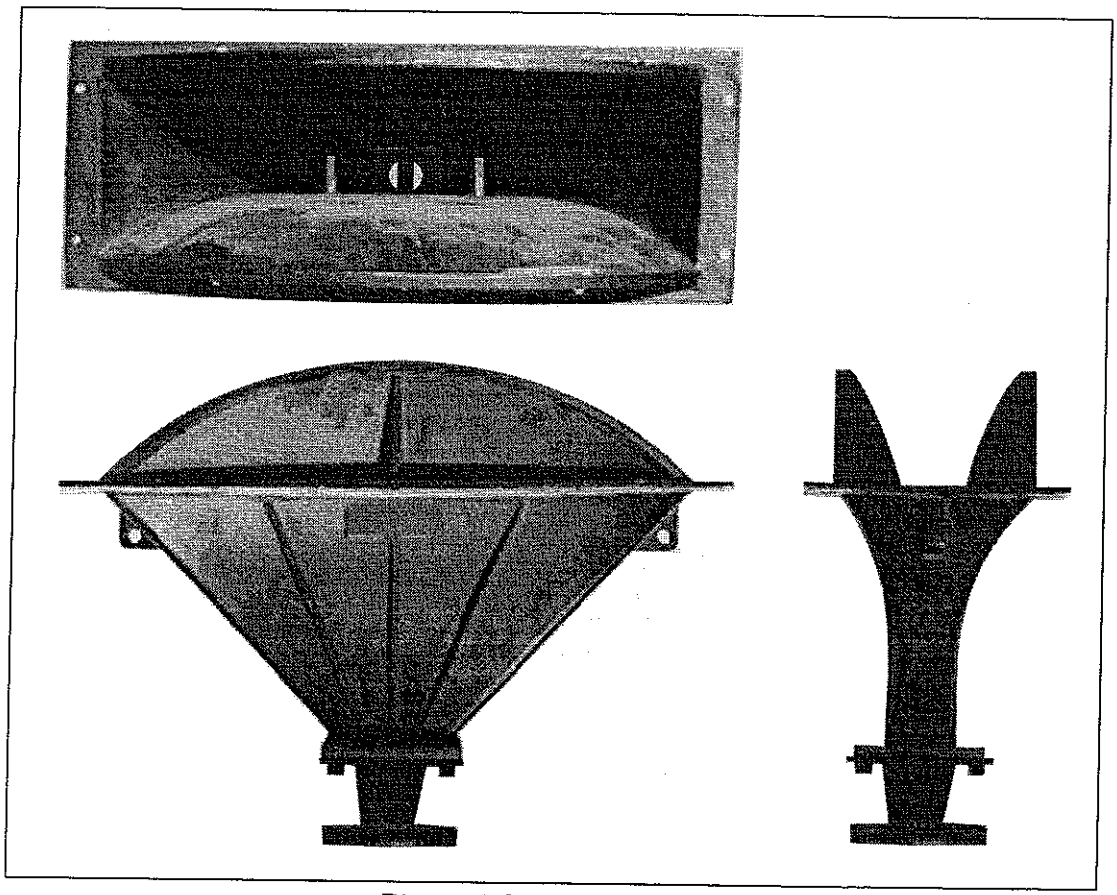

Figure A.3.7 Horn Type 4

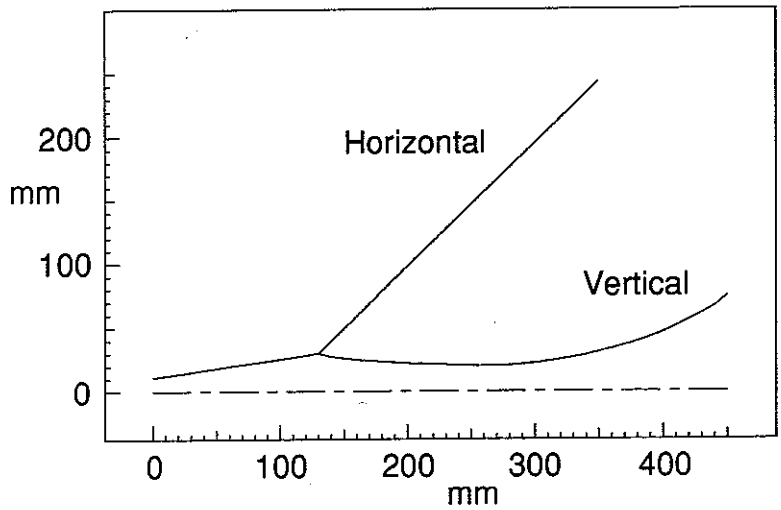

Figure A.3.8 Wall Profile for Horn Type 4

Horn Type 5: Large Axi-symmetric (AX2).

This horn is of glassfibre construction and is axi-symmetric. The circular throat has a diameter of 25.4mm and the flare is approximately exponential with a theoretical (plane-wave assumed) cut-off frequency of 730Hz. The horn is 180mm long and terminates in a mouth of 280mm diameter. This horn was designed, using the one-parameter model, to have as smooth a throat impedance characteristic as possible by flaring relatively rapidly, thus avoiding a flare discontinuity at the mouth.

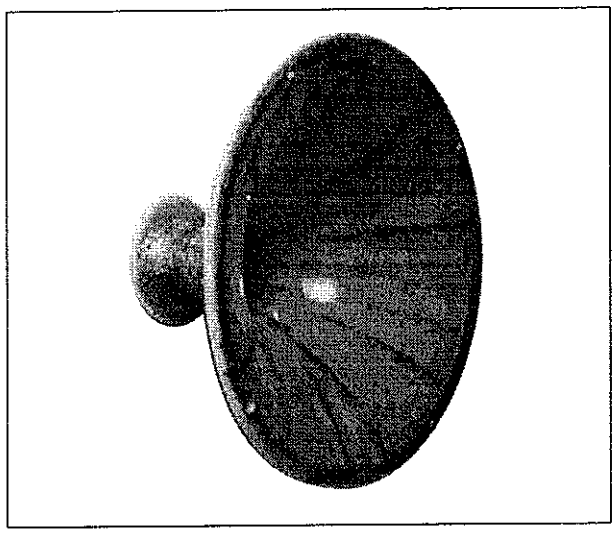

Figure A.3.9 Horn Type 5

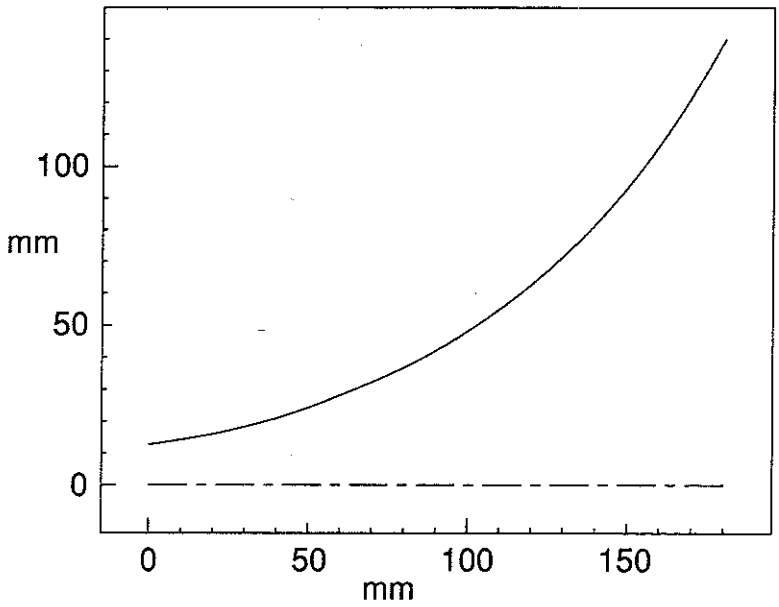

Figure A.3.10 Wall Profile for Horn Type 5

APPENDIX 4

The Derivation of the Impedance Measurement Equation:

$$\hat{Z} = i\left\{\frac{\sin(kl_2) - \hat{T}\sin(kl_1)}{\hat{T}\cos(kl_1) - \cos(kl_2)}\right\}$$

Consider a length of rigid-walled tubing terminated at axial distance $x = 0$, by a normalised acoustic impedance $\hat{Z}$:

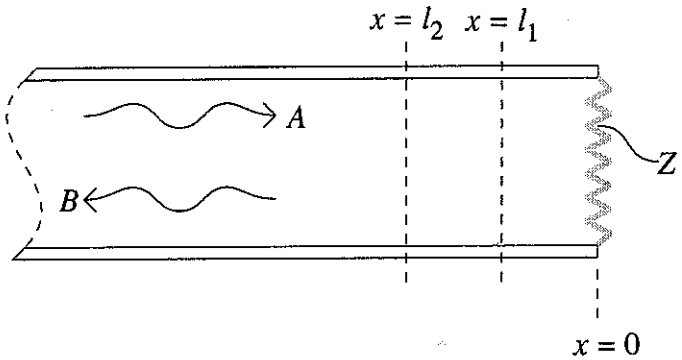

Any acoustic pressure field within the tube at frequencies below the cut-off of the first cross-mode of the tube (dictated by $ka = 1.83$, where a is the radius of the tube) can be expressed as the sum of a forward propagating wave of amplitude A, and a backward propagating wave of amplitude B, thus:

$$\hat{p}(x) = \hat{A}e^{ikx} + \hat{B}e^{-ikx} \quad .$$

The acoustic pressure $\hat{p}_1$ at a position $x = l_1$ within the tube is then

$$\hat{p}(l_1) = \hat{A}e^{ikl_1} + \hat{B}e^{-ikl_1} \quad ,$$

and similarly at $x = l_2$,

$$\hat{p}(l_2) = \hat{A}e^{ikl_2} + \hat{B}e^{-ikl_2} \quad .$$

The transfer function $\hat{T}$ between the pressures at the two points is then

$$\hat{T} = \frac{\hat{p}_2}{\hat{p}_1} = \frac{\hat{A}e^{ikl_2} + \hat{B}e^{-ikl_2}}{\hat{A}e^{ikl_1} + \hat{B}e^{-ikl_1}} \quad .$$

Rearranging:

$$\hat{B} = \hat{A}\left\{\frac{\hat{T}e^{ikl_1} - e^{ikl_2}}{e^{-ikl_2} - \hat{T}e^{-ikl_1}}\right\} \quad . \qquad \text{(A.4.1)}$$

The normalised acoustic impedance $\hat{Z}$ at $x = 0$ can be written

$$\hat{Z} = \frac{\hat{p}(0)}{\rho c \hat{u}(0)} = -ik \frac{\hat{p}(0)}{\partial \hat{p}(0)/\partial x} = \frac{\hat{A} + \hat{B}}{\hat{A} - \hat{B}} \quad . \tag{A.4.2}$$

Substitution of equation (A.4.1) in (A.4.2) yields

$$\hat{Z} = \left\{ \frac{e^{-ikl_2} - \hat{T}e^{-ikl_1} + \hat{T}e^{ikl_1} - e^{ikl_2}}{e^{-ikl_2} - \hat{T}e^{-ikl_1} - \hat{T}e^{ikl_1} + e^{ikl_1}} \right\} \quad ,$$

which, using the identities

$$2\cos(x) = e^{ix} + e^{-ix} \quad \text{and} \quad 2i\sin(x) = e^{ix} - e^{-ix} \quad ,$$

becomes

$$\hat{Z} = i \left\{ \frac{\sin(kl_2) - \hat{T}\sin(kl_1)}{\hat{T}\cos(kl_1) - \cos(kl_2)} \right\}$$

This equation expresses the normalised acoustic impedance at a position within a tube in terms of the transfer function between the acoustic pressures at two known positions within the tube.

APPENDIX 5

Details of the Loudspeakers in the Listening Test

Reference A. Quad Electrostatic Loudspeaker (early type).
Full-range electrostatic loudspeaker consisting of three separate radiating panel areas for low, mid & high frequencies.

Reference B. Son Audax PR17 / HR100 / 1AK7.
Mid-range direct radiating paper-cone loudspeaker of nominally 7" (178mm) diameter.

Reference C. Fostex H351 / HA21 Horn / Emilar EK175 Driver (no.3†).
Large sectoral horn of cast aluminium construction, coupled to a compression driver with an aluminium diaphragm of nominally 2" (51mm) diameter and a plastic phase-plug. This horn is horn type 4 described in appendix 3.

Reference D. High Frequency Horn Section of a Tannoy 'Puma' Dual-Concentric loudspeaker.
Axisymmetric horn using paper cone of low frequency driver as the outer part of the horn. The diaphragm and phase plug of the driver are both aluminium.

Sample 1. Vitavox Exponential Horn / Emilar EK175 Driver (no.1†).
Medium sized exponential horn of cast aluminium construction coupled to a compression driver similar to reference C above. This horn is horn type 3 described in appendix 3.

Sample 2. JBL 2105.
Mid-range direct radiating paper-cone loudspeaker of nominally 5" (127mm) diameter.

Sample 3. JBL 2121.
Lower mid-range direct radiating paper-cone loudspeaker of nominally 10" (254mm) diameter. This sample was designed to operate over a lower frequency range than that of the test and was included as a 'non-similar' experimental control.

---

† Note: Three Emilar EK175 compression drivers were used in the test. These have been labelled nos. 1, 2 & 3.

Sample 4. AX1 Horn / Emilar EK175 Driver (no.1).
Short axisymmetric horn of glassfibre construction with a low flare-rate and small horn mouth. Compression driver as sample 1 above. This horn is horn type 1 described in appendix 3.

Sample 5. Reflexion Arts horn / Emilar EK175 Driver (no.1).
Medium sized horn constructed of mineral-loaded glassfibre. Horn flare is rectangular in cross-section with a smooth, rapid exponential horizontal flare and a shallow, straight-sided vertical flare. Compression driver as sample 1 above. This horn is horn type 2 described in appendix 3.

Sample 6. Son Audax PR17 / HR100 / 1AK7.
This sample is nominally identical to reference B, originating from the same production batch, and is included as a 'similar' experimental control.

Sample 7. Reflexion Arts horn without lips / Emilar EK175 Driver (no.1).
As sample 5 but with the mouth 'lips' sawn off flush with the mounting flange.

Sample 8. AX2 horn / Emilar EK175 Driver (no.1).
Short axisymmetric horn of glassfibre construction with a rapid flare-rate terminating in a medium sized mouth. Compression driver as sample 1 above. This horn is horn type 5 described in appendix 3.

Sample 9. Yamaha horn / Emilar EK175 Driver (no.1).
Medium sized sectoral horn of cast aluminium construction. Compression driver as sample 1 above.

Sample 10. Fostex H320 horn / Emilar EK175 Driver (no.1).
Large sectoral horn of laminated wood construction with near semi-circular horizontal flare. Compression driver as sample 1 above.

Sample 11. JBL 2307 horn with JBL 2308 slant-plate / Emilar EK175 Driver (no.2).
Short axisymmetric horn similar to sample 4 but of cast aluminium construction and fitted with horizontal slant-plates at the mouth. Compression driver similar to sample 1 above but with different mounting arrangements.

Sample 12. Altec Sectoral horn / Emilar EK175 Driver (no.1).
Large sectoral horn of cast aluminium construction. Compression driver as sample 1 above.

Sample 13. Altec 806C horn / Emilar EK175 Driver (no.1).
Large multicellular horn with eight individual flares of sheet aluminium construction joined to a single throat via a cast aluminium manifold. Compression driver as sample 1 above.

Sample 14. Starr "Singing Throat" horn / Emilar EK175 Driver (no.1).
Folded Gramophone horn of sheet / solid wood construction. Compression driver as sample 1 above.

Sample 15. Vitavox Sectoral horn / Emilar EK175 Driver (no.1).
Large sectoral horn of cast aluminium construction. Compression driver as sample 1 above.

Sample 16. JBL 2370 horn / JBL 2426 Driver.
Medium sized bi-radial horn of composite plastic construction and flat front. Compression driver has titanium diaphragm and exponential phase-plug.

APPENDIX 6

Details of the Signals Used in the Listening Test

Overall Test Level: L_{eq} = 71dB.

Signal 1. Chirp.
Enveloped swept sinusoid. Frequency swept from 2kHz to 4kHz with a '½(1-cos)' envelope. Peak replay level 71dB SPL.

Signal 2. Tone Burst.
Ten cycles of 2.5kHz sinusoid. Peak replay level 80dB SPL.

Signal 3. Flute Notes.
Two flute notes recorded anechoically using a Brüel & Kjær measurement microphone. Peak replay level 65dB SPL.

Signal 4. White Noise.
A one-second burst of white noise. Peak replay level 69dB SPL.

Signal 5. Pink Noise.
A one-second burst of pink noise. Peak replay level 66dB SPL

Signal 6. Slamming Book.
The slamming shut of a heavy book recorded anechoically using a Brüel & Kjær measurement microphone. Peak replay level 80dB SPL.

Signal 7. Waterfall.
Small stream waterfall recorded using a Knowles electret microphone. Peak replay level 71dB SPL.

Signal 8. Impact.
The impact of a peach stone on a 25ft high square-section steel statue recorded using a Knowles electret microphone. Peak replay level 76dB SPL.

Signal 9. Guitar Chord.
The chord 'open E', strummed on an acoustic guitar recorded anechoically using a Brüel & Kjær measurement microphone. Peak replay level 61dB SPL.

APPENDIX 7

Calculation of Similarity Confidence Indices

The analysis below is based on the null hypothesis:

The results are due to pure chance or guesswork on the part of the subjects.

If this hypothesis were true, all columns would, if enough subjects were used, carry equal numbers of ticks. The confidence that the null hypothesis is correct (one-tailed) is calculated thus:

$$P = \sum_{r=n}^{N} \left(\frac{N!}{r!(N-r)!} \right) p^r q^{(N-r)} \quad ,$$

where
N is the sum of the ticks entered in all columns,
n is the number of ticks entered in the column of interest,
p (= $^1/_5$) is the probability that a tick will be entered in the column of interest and
q (= $^4/_5$) is the probability that a tick will not be entered in the column of interest.

The percentage confidence that the null hypothesis is wrong, or in this case the similarity confidence index, is then

$$\textit{Similarity Confidence Index} = (1\text{-}P) \times 100\% \quad .$$

This figure is calculated for each sample, for each reference column, for each signal.

APPENDIX 8

Calculation of Waveform Spectral Similarity

Two methods were used to obtain the spectra of the reproduced signal waveforms: first, the spectra of the recorded waveforms were calculated directly using FFT techniques, and second, the source signals were convolved with the measured transfer functions of the loudspeakers. The two methods yielded very close results and the latter method is favoured because of better signal-to-noise performance only. The spectra obtained contain 512 linearly spaced lines up to a maximum frequency of 10kHz.

Various different ways of comparing the spectra were tried. These included all combinations of both linear ($V(f)$), power ($V^2(f)$) and logarithmic (dB) spectra with linear (512 lines) and logarithmic (third, sixth and twelfth octave bands) frequency spacing. The results from each method were compared to the listening test results and the method that yielded the best agreement, which was linear spectra ($V(f)$) with linear frequency spacing, was chosen.

In order to calculate the difference between two spectra, the mean levels need to be matched. To achieve this, the total error between the two spectra is calculated thus:

$$C = \frac{\sum_{n=1}^{N} S_1(n)}{\sum_{n=1}^{N} S_2(n)} \quad ,$$

where $S_1(n)$ and $S_2(n)$ are the linear spectra ($V(f)$) at frequency n and N is the number of frequency points.

One of the spectra is then multiplied by this total error to remove any broadband level differences. The root-mean-squared-error between the two spectra is then calculated:

$$E = \frac{1}{N}\sum_{n=1}^{N} \sqrt{\left(S_1(n) - S_2(n)\right)^2} \quad .$$

The waveform spectral similarity is calculated from this figure by inverting, normalising with respect to the average spectral level and scaling the root-mean-squared-error for comparison with the similarity confidence indices:

$$Waveform\ Spectral\ Similarity = 10 \times \frac{\frac{1}{N}\sum_{n=1}^{N} S_1(n)}{E}$$

This figure is calculated for each sample, in comparison with each reference and the source signals, for each signal.

APPENDIX 9

Calculation of Power Cepstra of Listening Test Loudspeakers

The power cepstrum of a transfer function is the Fourier Transform of the log of the amplitude of the transfer function. The power cepstrum is useful for pin-pointing the physical cause of any irregularities in the amplitude response such as reflections etc. A reflection can be difficult to identify in the frequency domain, as it shows as comb filtering, but on the cepstral plot, such a reflection would show as a single spike displaced along the time axis which can be more easily identified. The transfer functions of the test loudspeakers shown in figures are all band-limited by the filter, so the power cepstra would be dominated by the low and high frequency roll-offs, thus masking any differences between them. To overcome this problem, the filter response is removed from the transfer functions by deconvolution. To eliminate the effect of any response irregularities outside the pass-band of the filter, the resultant log-amplitude responses are normalised to an average level of 0dB and weighted by the amplitude response of the filter. To illustrate this, figure A.9.1 shows how the log-amplitude response of reference B is processed prior to calculation of the power cepstrum. The power cepstra for the listening test loudspeakers are calculated from these resultant amplitude responses using FFT techniques.

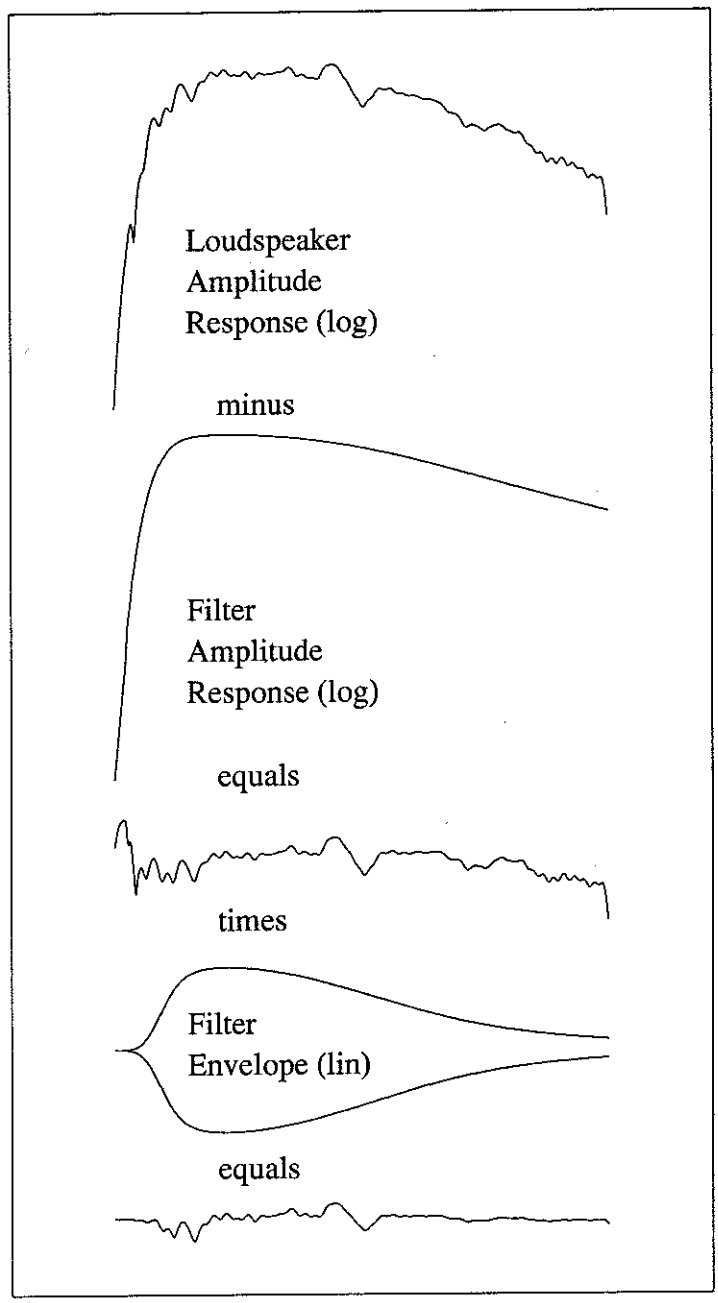

Figure A.9.1 Diagrammatic Representation of Processing of Loudspeaker Transfer Function Prior to Calculation of Power Cepstrum